Spectral Characterization of a Complete Equatorial Sample of 615 K Dwarfs

by

Hodari-Sadiki Hubbard-James

Under the Direction of Todd J. Henry Ph.D.

A Dissertation Submitted in Partial Fulfillment of the Requirements for the Degree of

Doctor of Philosophy

in the College of Arts and Sciences

Georgia State University

2023

ABSTRACT

We present the results of a spectroscopic study to determine the stellar properties, activity levels, space motions, and ages of the nearest K dwarfs. The targeted stars are members of RKSTAR (RECONS K Star) Survey that includes ∼5000 K dwarf primaries within 50 pc. An initial study established a benchmark calibration set of 35 K dwarfs with known ages of 20 Myr to 5 Gyr and high resolution (R=80000) spectra acquired on the CHIRON echelle spectrometer on the SMARTS 1.5m telescope at CTIO. Two known spectral indicators of activity and youth — the Hα absorption line (6562.8 Å) and the Li I resonance line (6707.8 Å) — showed strong trends in the training set. A sample of 615 K dwarfs within 33 parsecs and found between declinations +30° and −30° has now been observed with CHIRON and analyzed relative to the stars in the benchmark calibration set. Surprisingly, it appears that as many as ∼8% of these K dwarfs have spectroscopic features indicating that they are young and/or active. As expected, Galactic UVW space motions indicate that most of the stars fall into the thin (80%) and thick (20%) disk populations, with a single outlier, HD 134439, which is a known halo star. Overall, we find a set of metal poor K dwarfs with [Fe/H]values of −0.5 dex or less that account for 4% of the population in the solar neighborhood.

Empirical SpecMatch has been used to measure stellar properties for this sample of K dwarfs: temperatures range from 3600–5500 K, metallicities range from $-0.6 <$ [Fe/H]$<$ +0.55, and rotational velocities ($v \sin i$) range from less than 10 km/s to more than 50 km/s. Surface gravity values ($\log g$ values) have also been determined, although they are less reliable than the other quantities. Cross-matching with NASA's Exoplanet Archive reveals that only 42 exoplanet host stars are among our sample, highlighting the limited focus on mid and late-type K dwarfs (Teff $<$ 4800 K) in large exoplanet surveys. As a result of this work, we have identified 500 K dwarfs that are calm host stars worthy of detailed efforts to detect terrestrial planets. This work will serve as a key resource for assessing host star suitability

for exoplanet habitability.

INDEX WORDS: Late-type stars, Stellar activity, Stellar age, Solar neighborhood, Spectroscopic binary stars, Surveys

Spectral Characterization of a Complete Equatorial Sample of 615 K Dwarfs

by

Hodari-Sadiki Hubbard-James

Committee Chair: Todd J. Henry

Committee: Douglas R. Gies

Eric E. Mamajek

Russel J. White

Electronic Version Approved:

Office of Graduate Studies

College of Arts and Sciences

Georgia State University

August 2023

DEDICATION

This dissertation and all of my scientific endeavors are dedicated to my mother, Donna Richards, for her unwavering love, financial and personal sacrifices, and lifelong support in pursuing my dream to become a scientist. To my wife, Yoshika Hubbard-James, who has been my constant source of love, support, and inspiration throughout this journey. To my son, DaHee-Sadiki Hubbard-James, who was born during my graduate studies and has symbolized my personal and academic growth throughout the program. And to my brother, Andrey Brevett, who has always encouraged me and shared my triumphs and challenges.

ACKNOWLEDGMENTS

I would like to begin by acknowledging the dedicated work of Roberto Aviles and Rodrigo Hinojosa in executing the telescope observations. I also extend my gratitude to my colleagues at RECONS: Todd Henry, Wei-Chun Jao, Leonardo Paredes, Eliot Vrijmoet, Andrew Couperus, Aman Kar, D. Xavier Lesley, Sebastián Carrazco-Gaxiola, Tim Johns, and Madison LeBlanc. Their invaluable contributions have significantly enriched this project and my personal growth as a graduate student. I further wish to recognize the support and guidance provided by the staff of Georgia State's Physics & Astronomy Department, specifically Russel White, Azmain Nisak, Bokyoung Kim, and Ben McGimsey.

The progression and completion of my academic journey were significantly enabled by financial support from Georgia State University, and the Southern Regional Education Board (SREB). The Provost's Dissertation Fellowship from Georgia State University and the SREB Dissertation Year Award provided essential financial assistance and facilitated the advancement of my research. Additionally the continued financial support from Georgia State's Physics & Astronomy Department has served as the bedrock for my success.

This work, supported by the National Science Foundation (NSF) through grant AST-1910130, benefited greatly from the tireless efforts of the SMARTS Consortium and the NSF's National Optical-Infrared Astronomy Research Laboratory (NOIRLab) in maintaining the SMARTS/CTIO 1.5-m telescope and CHIRON spectrograph.

Lastly, I wish to acknowledge the wealth of data that underpinned this research. We made

extensive use of data from the European Space Agency's (ESA) Gaia mission, processed by the Gaia Data Processing and Analysis Consortium (DPAC), as well as data products from the Two Micron All Sky Survey (2MASS), funded by the NSF and NASA. I also appreciate the accessibility of the SIMBAD database and the VizieR catalog access tool, both operated by the Center de Donnees astronomiques de Strasbourg in France.

TABLE OF CONTENTS

LIST OF TABLES

LIST OF FIGURES

CHAPTER 1

Introduction: The Importance of Characterizing the Closest K Dwarfs

1.1 Goldilocks Stars: What Are K Dwarfs and Why Are They Special?

Dear reader, as we embark on this scholarly adventure together, I invite you to join me in uncovering the secrets of the often-overlooked K dwarf stars. Situated between the hotter and more massive G dwarfs and the cooler, less massive M dwarfs, K dwarfs are stars in the main-sequence phase of their evolution that may hold the key to unlocking our understanding of habitable worlds beyond our Solar System.

K dwarfs are characterized by surface temperatures ranging from 3930 to 5270 K and masses between 0.59 and 0.88 solar masses (Henry & McCarthy 1993; Gray & Corbally 2009; Pecaut & Mamajek 2013). In observational terms, these stars have *Gaia* Early Data Release 3 (EDR3) absolute BP magnitudes of $M_{BP} = 5.9$–9.6 and colors of BP–$K = 2.0$–4.0. Although cooler and slightly less massive than the Sun, a G2 dwarf star, K dwarfs are particularly appealing candidates for exoplanet surveys because their lifespans are longer than for G-type dwarfs.

According to the REsearch Consortium On Nearby Stars (RECONS; `www.recons.org`), K stars constitute approximately 12% of all stars in the solar neighborhood, while G stars only account for 5% (Henry et al. 2006, 2018). Despite their potential of as hosts of habitable planets, K dwarfs have been largely overlooked in previous exoplanet surveys, which have predominantly targeted either brighter F and G-type dwarfs or smaller M dwarfs (Arney 2019; Richey-Yowell et al. 2019). The more massive stars have been targeted primarily

because they offer more photons than K dwarfs, resulting in higher signal-to-noise observations. The less massive M dwarfs have been targeted because planets of a given size and mass create observable effects that are more easily detected than for K dwarfs with larger sizes and masses. In particular, K dwarfs with temperatures below 4800 K (spectra types K3V–K9V), have been overlooked by previous exoplanet surveys. As illustrated in Figure 1.1 for stars within 25 parsecs (pc), there are more G and M dwarfs with reported planets than for K dwarfs. This is not because K dwarfs don't have planets, but because they have not been surveyed as extensively as G and M dwarfs.

Ongoing radial velocity surveys such as the RECONS K Star (RKSTAR) survey (Paredes et al. 2021; Hubbard-James et al. 2022) and the K Dwarfs Orbited By Habitable Exoplanets (KOBE) experiment Lillo-Box et al. (2022) are specifically targeting K dwarfs within 50 pc of Earth. Promising early results indicate that ∼25% of nearby K dwarfs have companions that are Jupiter-sized or larger (including stellar, brown dwarf, and jovian planets) orbiting within a few AU of the star, and that approximately half of nearby K dwarf systems may contain habitable zone planets (Kunimoto & Matthews 2020; Paredes et al. 2021; Lillo-Box et al. 2022). A closer look at the types of companions orbiting K dwarfs indicates that only ∼4% of K dwarfs have jovian planets (Gaidos et al. 2013). Although that assessment included only 110 stars, the takeaway is that there is plenty of room for terrestrial planets. To bolster their image as targets worthy of scrutiny, Cuntz & Guinan (2016) found that early-type K dwarfs are likely to be the most likely places to find habitable planets with life. In addition, Arney (2019) discussed a potential *K Dwarf Advantage* for detecting bio-

signatures in the atmosphere of directly imaged exoplanets. The discovery of more liquid water habitable zone planets orbiting K dwarfs would be particularly significant to testing this theory.

A critical aspect in evaluating the enchanting environments of individual planets is the age of the celestial guardian, the star it orbits. The question arises: is the star young, adolescent, or mature? Much like a story unfolding, stellar youth is often characterized by dramatic events such as elevated ultraviolet luminosity, chromospheric flares, and a general increase in stellar activity, all factors linked to the magnetic dynamo at the star's core (Davenport et al. 2019). Young and active K dwarfs, akin to cosmic teenagers, are less likely to provide a stable environment for life to flourish (Segura et al. 2010). This leads us to seek post-adolescent hosts with low levels of stellar activity, which are preferred for exoplanet surveys (Luger et al. 2015; Arney 2019) not only because they may be better hosts for life, but because many measurements are easier to make and interpret. Therefore, accurate measurements of fundamental stellar properties, activity, and age are crucial in determining the habitability of these exoplanets.

In this celestial quest, my dissertation has embarked on the journey of measuring these values, targeting 615 of the nearest K dwarfs. This treasure trove of data will significantly advance our understanding of potential habitable worlds beyond our Solar System, unveiling the hidden realms where life might thrive.

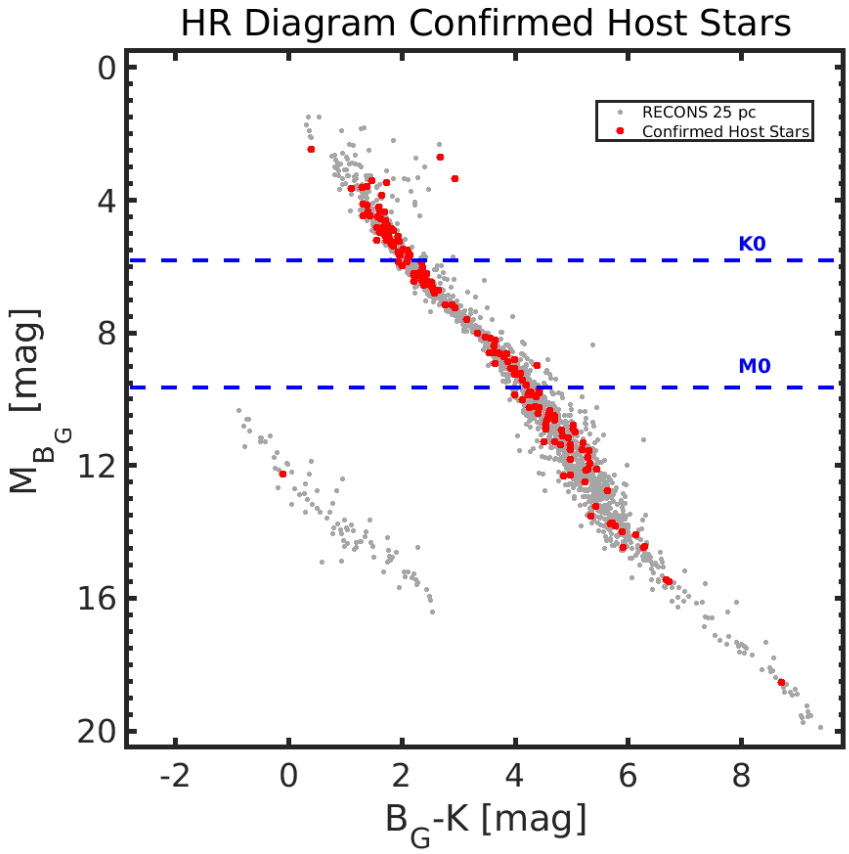

Figure 1.1 HR diagram displaying the RECONS sample of stars within 25 pc (grey dots), with confirmed exoplanet hosts as of April 17, 2023 from the NASA Exoplanet Archive highlighted in red. Dashed blue lines indicate K0 and M0 dwarf stars' absolute B_G boundaries. Magnitude information is obtained from *Gaia* DR3 ($BP = B_G$) and 2MASS ($K_s = K$). Absolute B_G magnitudes were derived using *Gaia* DR3 parallax measurements.

1.2 Stellar Age & Activity

Stellar age is a crucial parameter for understanding the evolution and properties of stars and their surrounding planets, as well as the formation and evolution of galaxies. The most precise age measurement for a star to date is that of the Sun, which has been measured to be approximately 4.6 billion years old by both Bahcall et al. (1995) and Bonanno et

al. (2002). This age was determined using the decay of radioactive isotopes in meteorites, which are thought to have formed from the same material as the early Solar System (Bahcall et al. 1995; Soderblom 2010). However, because it is not currently feasible to obtain a similar age measurement for other stars, determining reliable stellar ages is a challenging task. Age estimates of other stars are less accurate and rely on measuring stellar activity, semi-fundamental properties, or using model-derived inferences (Soderblom 2010; Soderblom et al. 2014).

For late type stellar G-, K-, & M-types, several methods have been proposed to estimate their ages. One such method is lithium depletion, which has been used in several studies, including Skumanich (1972); White et al. (2007); Lopez-Santiago et al. (2010); Binks & Jeffries (2014); Hubbard-James et al. (2022). Another method involves kinematic motions in the Galaxy, as highlighted in Nordström et al. (2004), Lopez-Santiago et al. (2010) and Mamajek & Bell (2014). A third method involves gyrochronology and/or stellar rotation studies, such as those of Skumanich (1972); Brandt & Huang (2015); Gossage et al. (2018); Curtis et al. (2020).

In addition to measuring the ages of K dwarfs, it is also important to understand their activity levels, as they are known to undergo significant changes as they age (West et al. 2008; Richey-Yowell et al. 2019). Thus, activity measurements can be used as proxies of direct age determinations, albeit with appropriate *caveats* about the accuracy of such estimates. Observable characteristics are driven by magnetic activity in K dwarfs, and the magnetic activity is driven by a dynamo mechanism that is linked to the star's rotation rate and

convective properties (Barnes 2003, 2007). As a K dwarf ages, it undergoes a process known as magnetic braking, which causes it to lose angular momentum and slow down its rotation. This process is due to the star's magnetic field interacting with its stellar wind, causing a transfer of angular momentum from the star to its surrounding environment. Thus, measuring the activity levels of K dwarfs can provide insights into their ages and their underlying physical processes.

One way to measure the activity of K dwarfs is through chromospheric emission, which is caused by heating in the outer atmosphere of the star by magnetic field lines. This emission can be measured using various diagnostic lines, such as the Ca II H&K lines at 3968.47 Å and 3933.66 Å, the Hα line at 6562.8 Å, and the Ca II infrared triplet at approximately 8497.6, 8542.1, and 8662.1 Å (Montes & Martin 1998). Several studies have used Hα emission to estimate the ages of K dwarfs, e.g., West et al. (2008). Isaacson & Fischer (2010) used Ca II H&K and Hα emission to study the activity and rotation of K dwarfs in the Kepler field, concluding that chromospherically quiet K dwarfs are well-suited for radial velocity searches for exoplanets due to their reduced stellar jitter.

1.3 Stellar and Kinematic Properties of K Dwarfs

A suite of stellar attributes are worth considering when evaluating K dwarfs for habitable worlds. These fall generally into two broad categories. The stars themselves present effective temperatures, metallicities, surface gravities, rotation rates, and activity/age indicators, all of which may factor into the environments presented to orbiting planets. In addition, a

star's UVW motion through our Milky Way Galaxy provides clues about how long it has existed, and thus, its age. Here we briefly outline each of these attributes, all of which will be determined for ∼600 of the closest K dwarfs using high-resolution spectroscopy and comparison techniques in the work presented here.

Effective temperature ($T_{\rm eff}$) is a vital factor in determining a star's habitable zone because it sets the distance range from the star where planets can maintain liquid water on their surfaces (Kasting et al. 1993). Planets that are too close to a star will have their water evaporate, while water on planets that are too far away will freeze.

Metallicity ([Fe/H]), which refers to the amount of heavy elements in a star's atmosphere, has been suggested to play a crucial role in planet formation (Fischer & Valenti 2005; Luck & Heiter 2006). Some studies suggest that higher metallicity stars may be more likely to host planets, and that multi-planet systems are more common around high metallicity stars (Fischer & Valenti 2005). However, the relationship between metallicity and planet formation is still an active area of research, and there may be other factors involved, e.g., *which types of planets* can form under various circumstances (Boley et al. 2021). With the continued discovery of new exoplanets, there is a need for more research to understand fully the role of metallicity and other factors in planet formation.

Surface gravity ($\log g$) is a critical parameter for estimating a star's age and evolutionary history. A low surface gravity indicates that the star is young and has not yet reached the main sequence or has evolved off it (Siess et al. 2000).

Projected equatorial velocity ($v \sin i$) can be used because of its link to a star's activity level; generally, faster spinning stars exhibit more activity, which can affect the habitability of any planets in its system.

Activity/Age indicators (Li, Hα, Ca II) Lithium is destroyed over time in stars like K dwarfs that have convective envelopes, so the strength of the Li 6708 Å line can be used as an age stopwatch[1] for K dwarfs, at least for ages up to 200–300 Myr for early-type K dwarfs (Soderblom 2010; Soderblom et al. 2014; Hubbard-James et al. 2022). High levels of stellar activity can be detected via emission in the Hα and Ca II lines in K dwarfs, indicating that hotter and more expansive chromospheres. These events can strip a planet's atmosphere or damage its surface, rendering it uninhabitable (Brandt & Huang 2015; Cuntz & Guinan 2016).

UVW space motions can be used to understand the kinematic properties of K dwarfs and place them in the timeline of the Milky Way's life. *UVW* velocities are measured in the Galactic coordinate system and are derived via proper motions in Right Ascension and Declination, combined with a star's gamma velocity, which is its motion along the line of sight, i.e., its radial velocity. *UVW* space motions, combined with its Right Ascension, Declination, and parallax, place a star in the Milky Way and provide its three-dimensional vector motion in the Galaxy (Johnson & Soderblom 1987). In addition, *UVW* space motions describe the velocity components of the star relative to the local standard of rest of our Sun, and can be used to trace a star's origin and evolution (Binney & Tremaine 1987), sometimes placing a star into a moving group or cluster, thereby providing information

[1]Stopwatches are particularly useful for measuring shorter increments of time.

about its formation and age (Montes et al. 2001). Furthermore, UVW space motions can also indicate when K dwarfs do not have matching motions in the Galaxy, suggesting that they may have originated from the Galactic halo or thick disk (Nordström et al. 2004).

Overall, combining kinematic data with other stellar parameters, such as effective temperature and metallicity, can provide a more comprehensive picture of a K dwarf's habitability potential and increase the chances of finding life in the Universe.

1.4 Habitability of Planets Orbiting K Dwarfs

Assessing the habitability of exoplanets orbiting late-type stars is integral to the search for life. K dwarf stars provide a wide range of liquid water habitable zones (hereafter, simply HZ), with early K-type stars ranging from 0.7–1.3 AU and later types from 0.1–0.4 AU (Kopparapu et al. 2013; Cuntz & Guinan 2016). These separations allow exoplanets orbiting K stars to have longer orbital periods of 50–200 days compared to planets in similar HZs orbiting much cooler M dwarfs. Larger separations mean weaker tidal effects and decreases the possibility of tidal locking, which may or may not be an issue for habitable environments on planets (see, e.g., Tarter et al. 2007), but at least in the case of K dwarfs allows orbiting planets to experience discrete periods of daylight and darkness (Cuntz & Guinan 2016). This starlight variation may be important to the preservation of liquid water on a rocky exoplanet's surface (Kopparapu et al. 2013; Arney 2019).

Pragmatically, the architecture of K dwarf planetary systems could constitute the optimal configuration for detecting biosignatures by direct imaging. Arney (2019) made numerical

simulations that show that both oxygen (O_2) and methane (CH_4) could be observed together in the atmosphere of exoplanets orbiting K-type hosts. The presence of both molecules implies a chemical imbalance in the planet's atmosphere, for which there are few explanations other than the discovery of a biosignature. More recently, Quanz et al. (2022) predict that a HZ planet orbiting a K7 dwarf within 30 pc will provide a separation of 10 milliarcseconds, which is sufficient for the next generation of space-based interferometers, such as the LIFE mission slated to launch in 2025, to observe exoplanet atmospheres directly. This significant prediction would allow for habitability studies in K dwarf planetary systems without transiting exoplanets (Quanz et al. 2022).

Stellar activity produces X-rays, extreme UV radiation, and flares that can ionize and heat the upper atmospheres of exoplanets (Kasting et al. 1996). Stellar radiation from the host star therefore plays a critical role in determining the habitability of exoplanets. X-rays ($\lambda < 100$ Å) and extreme UV ($\lambda = 100$ Å–910 Å) radiation can heat the upper atmosphere, leading to atmospheric degradation and hydrodynamic escape (Lammer et al. 2009; Luger et al. 2015). While increasing planetary mass reduces atmospheric escape, losing large quantities of essential elements, such as hydrogen, can be detrimental to habitability (Seager 2010; Tian 2015). Furthermore, high amounts of extreme UV can harm cell structures, limiting the spread of life on the surface of a potentially habitable planet (Tian 2015; Lillo-Box et al. 2022). Critically, Nunez et al. (2022) showed that most K dwarfs in the Hyades (with age ∼650 Myr) are X-ray unsaturated, indicating that within 1 Gyr, K dwarfs have "settled down" into hospitable hosts for planets.

Far-UV (λ = 1200–1700 Å) and near-UV (λ = 1700–3200 Å) photon energies drive a HZ planet's photochemistry (Kasting et al. 1996; Lammer et al. 2007; Miguel et al. 2015; Rugheimer et al. 2015). FUV radiation is important in the photodissociation of important molecules found in planetary atmospheres, such as H_2O, CO_2, and CH_4 (Segura et al. 2010; Cuntz & Guinan 2016). Such UV photons can produce abiotic O_2 and O_3 in a planetary atmosphere, thereby confounding the search for genuine biosignature signals (Segura et al. 2010; Rugheimer et al. 2015; Harman et al. 2015). While some theorize that this UV photochemistry is a potential source of primordial compounds (Ehrenfreund et al. 2002), it is widely accepted that long durations of UV excess can harm life on planetary surfaces and lead to the erosion of planetary atmospheres (Tian 2009; Erkaev et al. 2013; Miguel et al. 2015).

In this study, we measured chromospheric activity in over 600 nearby K dwarfs using the Hα and Ca II spectral lines, which exhibit emission in the presence of activity (Hubbard-James et al. 2022). Chromospheric activity measured at optical wavelengths in late-type stars has been previously linked to increased X-ray and UV flux levels (Walkowicz & Hawley 2009; Youngblood et al. 2017; Melbourne et al. 2020). Particularly relevant to our study, although we use a line in the near-infrared Ca II triplet, Youngblood et al. (2017) demonstrated that the Ca II K line at 3933 Å can be used to predict FUV and NUV emission lines (including Lyα & Mg II) and X-ray flux for M dwarfs. Meanwhile, Melbourne et al. (2020) linked Hα luminosity and Ca II H&K S and R′HK indices to UV line luminosity for M dwarfs. Therefore, our work in evaluating chromospheric activity for stars in our sample has the

potential to provide important data on the habitable conditions around hundreds of the nearest stars that may, in fact, be among the best hosts for habitable worlds.

1.5 Dissertation Guide: Overview of Chapters

This dissertation focuses on the investigation of 615 K dwarf stars using high-resolution spectra to determine their fundamental stellar properties, activity levels (as a proxy for age), and kinematic characteristics. The research is organized into the five following Chapters, each serving a distinct purpose in the study.

Chapter 2 details the process of constructing a volume-limited and volume-complete sample of the K dwarf stars used in this study. This selection process is crucial for ensuring the accuracy and reliability of our findings, as it strikes a balance between having a sufficient number of stars for statistical significance and being manageable within a reasonable duration for a PhD project. The volume-complete aspect allows us to make reliable statements about statistical probabilities for different classes of K dwarfs.

Chapter 3 describes the methods employed for data acquisition, reduction, and analysis used to derive the stellar characteristics. This Chapter delves into the various tools, techniques, and algorithms utilized to process and examine the collected data for the selected K dwarf stars. The methodology presented here is crucial for ensuring the accuracy and reliability of the results. Comparisons to previous efforts are included to verify our techniques.

Chapter 4 describes a benchmark study that serves as the foundation for identifying young and active K dwarfs. This study establishes a metric for differentiating between var-

ious K dwarf groups such as metal-poor/metal-rich, active/inactive, and young/old. These classifications allow us to uncover general properties and correlations among K dwarfs.

Building upon the foundation laid by the previous Chapters, Chapter 5 presents the results of the comprehensive analysis of the complete sample of 615 K dwarf stars. Utilizing the refined metrics derived from Chapter 4, this Chapter offers insights into the activity, age, and fundamental properties of nearby K dwarfs, as well as their kinematic behavior.

Finally, Chapter 6 serves as a conclusion to this dissertation. It discusses the overall results and findings, emphasizing their significance and relevance to the broader field of astronomy. Moreover, this Chapter highlights the study's limitations and suggests potential avenues for future research, paving the way for continued exploration and understanding of K dwarf stars. This Chapter also includes an account of additional experiences during the research process, such as contributions as the CHIRON Data Manager for the CTIO/SMARTS 1.5m telescope, which expanded research options for multiple institutions and researchers.

CHAPTER 2

Defining the Sample of K Stars

2.1 Overview of the RECONS K STAR (RKSTAR) Project

The RKSTAR (RECONS K STAR) Project aims to survey the ∼5,000 nearest K dwarfs within 50 parsecs of the Sun, based on *Gaia* DR2 parallax measurements and updates in subsequent *Gaia* data releases. To study this sample comprehensively, RECONS is conducting four systematic surveys of these K dwarfs. Three of these surveys are for stellar companions (and in the case of the Radial Velocity Survey, brown dwarf and planetary companions as well), while the fourth is a characterization survey that is the subject of this thesis. Here we outline all four surveys.

The **Wide Field Survey** investigates stellar companions with separations greater than approximately 1″, utilizing *Gaia* data (Gaia Collaboration et al. 2018, 2022) and cataloged companions from, for example, the Washington Double Star (WDS) Catalog (Mason et al. 2001). To date, the Wide Field Survey has identified nearly 500 stellar companions, with about 80 being new discoveries, with separations extending out to roughly 4,000 AU (Shea et al. 2023).

The **Speckle Survey** uncovers stellar companions ranging from 0.5 to 100 AU, thereby spanning distances similar to the scale of our Solar System. The primary instruments used are optical speckle cameras on 4m to 8m class telescopes, most notably the Differential Speckle Survey Instrument (Horch et al. 2009, 2021). This survey has detected over 160 stellar companions, with approximately 90 being new discoveries, with the majority of stellar

companions found orbiting within 15 AU of the K dwarfs (Henry et al. 2022).

The **Radial Velocity Survey** uses the CHIRON high-resolution spectrograph on the SMARTS 1.5m telescope at CTIO to reveal companions orbiting K dwarfs that are stars, brown dwarfs, and jovian exoplanets orbiting within 3 AU. This survey has resulted in the discovery of several new planets and dozens of stellar companions (Paredes et al. 2021). This survey is complemented by long-term work by others reporting companions with stars and brown dwarf companions, as well as planets down to terrestrial masses.

The **Characterization Survey**, which is the main focus of this work, utilizes CHIRON spectra to determine the activity levels, ages, stellar properties, and kinematic motions of the sample of K stars within 50 parsecs. For this study we target two distinct samples of K dwarfs — a primary sample of 615 field stars within 33 pc in the equatorial region of the sky selected from the RKSTAR sample, and a benchmark comparison sample of 35 stars with reliable estimated ages (Hubbard-James et al. 2022).

2.2 Defining K Dwarfs in the RKSTAR Sample

To define the RKSTAR sample, we carefully assessed the regions in color and luminosity on the HR Diagram where dividing lines between the G/K and K/M spectral types are found. Our goal was to create a comprehensive sample that accurately represents K-type stars. These boundaries were established based on extensive spectroscopic surveys, particularly Gray & Corbally (2009), which provided classifications for hundreds of nearby stars within 40 parsecs on a uniform system. For the G/K boundary, we used Gray & Corbally (2009), while

for the K/M boundary, we used the same source supplemented with RECONS classifications.

To determine the blue and red limits of the K dwarf sequence, we matched spectral types from these datasets to nearby, well-vetted, companion-free members of the RECONS 25 pc sample. This allowed us to map K dwarf spectral types to *Gaia* DR2 $B_G - R_G$ colors from the Gaia Collaboration et al. (2018), using presumably single stars unaffected by stellar companions. This approach ensures that our sample accurately represents the K dwarf population. Initially, we selected K dwarfs with $B_G - R_G$ colors between 1.01–1.89 and an additional constraint of M_{BG} ranging from 5.30–9.90, in order to exclude evolved stars and white dwarfs.

However, after reviewing prior research by the RECONS group and Eric Mamajek's spectral notes[1], we decided to use $B_G - K$ colors that provided a more extended color baseline and higher fidelity in separating similar stars, effectively creating a rubric of more precise estimates of effective stellar temperatures. This choice further refines our sample and enhances the reliability that we have true K dwarfs in our sample. We gathered K values for our sample stars from the 2MASS survey (Skrutskie et al. 2006). Ultimately, we adopted the following parameters for K dwarfs in our final RKSTAR sample: $B_G - K$ colors between 2.00 and 4.00, and M_{BG} values ranging from 5.30 to 9.90.

2.3 Using *Gaia* to Create the Equatorial Sample of 615 K Dwarfs

Among the approximately 5,000 K dwarf systems in the full 50 pc sample — defined as having a K dwarf primary along with any additional lower-mass stellar, brown dwarf, or planetary

[1] `http://www.pas.rochester.edu/~emamajek`

Table 2.1 Summary of the Sample Selection Process for the 615 K Dwarfs

Selection Step	**Number of K Dwarfs**
Initial list (May 2018, *Gaia* DR2)	687
Excluded due to updated parallaxes (*Gaia* DR3)	−22
Removed due to secondary status	−26
Removed due to $B_G - K$ color	−24
Final Primary Sample	**615**

companions — this work focuses on systems located within 33.3 pc, selected using a cutoff in parallax of 30 mas, and situated in the equatorial sky band, ranging from DEC +30° to −30°. This approach results in a volume-limited and (nearly) volume-complete sample. In May 2018, an initial list of 687 K stars was selected based on *Gaia* DR2 parallax measurements and photometry (Gaia Collaboration et al. 2016, 2018). This list was later updated using parallax data from the recent *Gaia* Data Release 3 (DR3), leading to the exclusion of 22 K dwarf systems that were beyond the distance cutoff of 33.3 pc (Gaia Collaboration et al. 2022). Upon closer inspection, an additional 26 K dwarfs that are secondaries to earlier spectral type stars or white dwarfs (see below) were removed. Finally, another 24 stars were removed that fall outside our $B_G - K$ color cutoffs. Table 2.1 provides a summary of the sample selection process for the thesis sample. This leaves a primary sample of 615 K dwarf systems, which are plotted in Figure 2.1. Here the left panel illustrates the sky distribution mapping the "bow tie" configuration that depicts the declination and distance cutoffs, whereas the right panel is the more traditional polar plot. Note the increase in population density with increasing distance in both plots due to the projection of larger

volumes onto the two dimensional maps representing cross-sectional cuts through space.

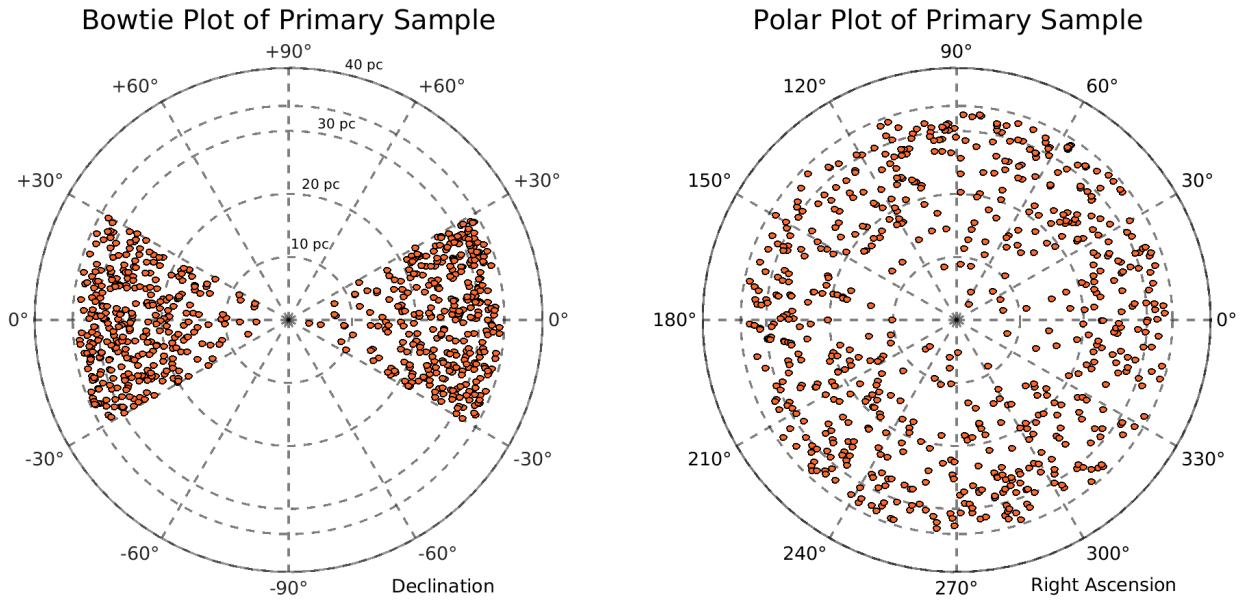

Figure 2.1 Left: Bow Tie Plot displaying declination (Dec) (theta direction) and distance (radial direction) for the primary sample of 615 K dwarfs. Right: Polar Plot illustrating right ascension (R.A.) (theta direction) and distance (radial direction) for the primary sample of 615 K dwarfs. R.A. and Dec positions are based on J2000 coordinates, while distance values were derived from *Gaia* DR3 parallax measurements. Note that the population density increases at greater distances because larger volumes of space are being sampled and plotted in these cross-sectional views.

A list of all stars in the primary sample, along with their positions, proper motions, parallax, and photometry, can be found in Appendix A. An observational HR diagram is shown in Figure 2.2, in which the 615 sample stars are highlighted with orange triangles. In addition to the large group of stars falling along the stellar main sequence, populations of young and/or unresolved multiple stars are evident above the main sequence, and a modest sample of presumably old, low metallicity, subdwarfs are seen below the main sequence.

Sample refinement remains ongoing, as parallaxes may be subject to minor changes in

future *Gaia* Data Releases, and new K dwarfs are likely to be added because *Gaia* DR2 and DR3 may not have provided astrometric solutions in systems that are short period binaries exhibiting astrometric perturbations. Some additional stars will likely be removed to ensure only the inclusion of systems with K dwarf primaries. For example, if additional white dwarfs are discovered, those systems will be excluded from the sample because the white dwarf progenitor originally had a greater mass and was the primary star. It is important to note that systems with white dwarf primaries are valuable for age determination, so they will still be considered for age calibration work but will not be included in the statistics for K dwarf samples and their companions.

This comprehensive sample of K dwarf systems has the potential to significantly contribute to our understanding of various astrophysical processes, such as star formation history, stellar evolution, and the occurrence of exoplanets around K dwarfs. Key to many of the facets of the RKSTAR effort are the possibilities to answer *statistical questions about stars in the solar neighborhood based on a volume-limited, volume-complete sample*, such as "What fraction of K dwarfs are young and/or active?" and "What fraction of K dwarfs are old halo stars?" Furthermore, the high-quality data obtained from the CHIRON spectrograph enables precise measurements of stellar parameters that are used to refine our knowledge of these systems and their implications for broader astrophysical research. All 615 K dwarfs present in the equatorial 33.3 pc sample have been observed at least once using the CHIRON spectrograph since June 2017. Additionally, 35 K stars from nearby (less than $\sim$50 pc) moving associations and open clusters have also been observed using CHIRON to serve as

benchmarks for age and activity estimates of our primary sample. This benchmark sample is described in the next section, §2.4.

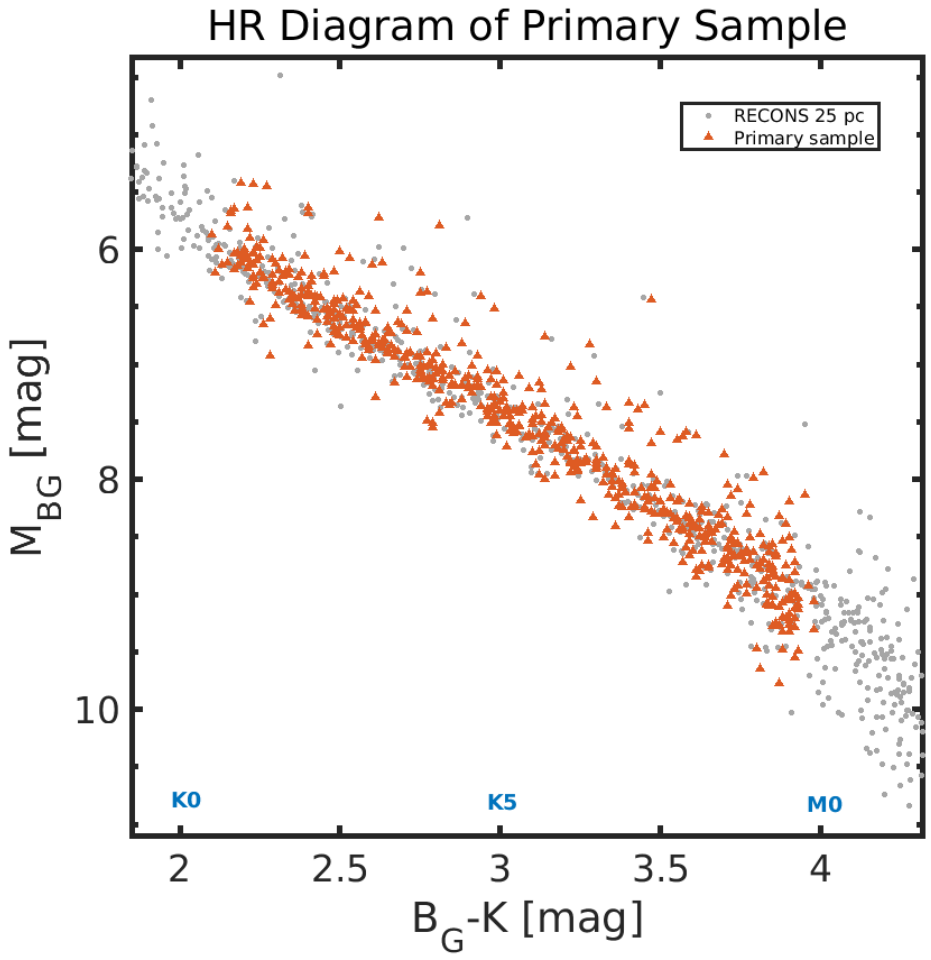

Figure 2.2 HR diagram displaying the RECONS sample of stars within 25 pc (grey dots), with 615 primary sample K dwarfs in the equatorial 33.3 pc sample denoted by orange triangles. There is a clear sequence of young and/or unresolved multiple stars above the set of main sequence stars. Also note the presence of a modest set of subdwarfs along the lower envelope of the main sequence. Magnitude information is obtained from *Gaia* DR3 ($BP = B_G$, updated from the original DR2 list) and 2MASS ($K_s = K$). Absolute B_G magnitudes were derived using *Gaia* DR3 parallax measurements (again, updated from the DR2 values). **Guidelines for spectral types are given along the x-axis.**

2.4 Benchmark Sample of K Dwarfs

A supplementary benchmark sample of ∼100 K dwarfs with age estimates was created to provide measurements of various spectral features and space motions that can be used as guidelines for the larger sample of 615 K dwarfs. These stars were taken from moving groups, associations, or clusters, plus a handful of field stars within 25 pc that have ages determined via isochrone fitting. Table 2.2 lists the various subsets used to construct this benchmark sample and the estimated ages of each group. The four associations utilized here are the β Pictoris moving group (β Pic, age ∼20 Myr), the Tucana-Horologium association (Tuc-Hor, ∼40 Myr), the AB Doradus moving group (AB Dor, ∼120 Myr), and the Hyades cluster (∼750 Myr). The small set of field K dwarfs within 25 pc have age estimates made via model isochrone fits and have ages of 0.3–5.7 Gyr. References for the ages assigned to the groups and individual stars are noted at the end of Table 2.2.

K dwarf members of the β Pic, Tuc-Hor, and AB Dor groups were identified using Bell et al. (2015)'s *bona fide* membership list, and confirmed through Gagne et al. (2018)'s web-based BANYAN Σ code[2], in combination with *Gaia* DR2 parallax, proper motion, and radial velocity data. This yielded a larger sample of K dwarfs than Gagne et al. (2018)'s work, which listed *bona fide* members before the *Gaia* DR2 release. Hyades membership was determined using K dwarfs in Gagne et al. (2018)'s *bona fide* list with all 47 stars checked using BANYAN Σ and updated *Gaia* DR2 data.

An additional seven stars were selected based on their radial velocity variations (RVV) in

[2]BANYAN Σ -http://www.exoplanetes.umontreal.ca/banyan/

Table 2.2 Moving Groups (M.G.), Associations(Assoc.), and Clusters providing K dwarfs for the Benchmark Sample.

Group Name	RA (J2000)	DEC (J2000)	Distance (pc) [a]	Age	Members [b] [c]	K dwarfs	Observed
β Pic M.G.	∼14 30	∼ −42 00	∼30	∼20 Myr[d]	97	19	11
Tuc-Hor Assoc.	∼02 36	∼ −52 03	∼40	∼40 Myr[d]	176	18	10
AB Dor M.G.	∼05 28	∼ −65 26	∼33	∼120 Myr[d]	84	24	8
Hyades Cluster	∼04 26	∼ +15 52	∼42	∼750 Myr[d]	177	47	10
Field K Dwarfs	Various	Various	< 25	0.3–5.7 Gyr	...	10	5
o^2 Eri	04 15 16.3	−07 39 10	5	4.3 Gyr[e]	...	...	...
HD 50281	06 52 18.1	−05 10 25	9	1.9 Gyr[f]	...	...	...
20 Crt	11 34 29.5	−32 49 53	10	4.6 Gyr[e]	...	...	...
PX Vir	13 03 49.7	−05 09 43	22	0.3 Gyr[g]	...	...	...
ϵ Ind	22 03 21.7	−56 47 10	4	3.7–5.7 Gyr[h]	...	...	...

[a] distance from *Gaia* EDR3
[b] membership list for β Pic, Tuc-Hor, and AB Dor: Bell et al. (2015)
[c] membership list for Hyades: Gagne et al. (2018)
[d] Gagne et al. (2018)
[e] Mamajek & Hillenbrand (2008)
[f] Luck (2017)
[g] Stanford-Moore et al. (2020)
[h] Feng et al. (2019)

preliminary work carried out by Paredes et al. (2021). RVV stars are particularly intriguing due to their fluctuating radial velocities that can potentially signal the presence of orbiting exoplanets, binary star systems, or high stellar activity. Our detailed investigation into these seven RVV stars promises to provide valuable insights into the nature of their variability. A more comprehensive discussion of all seven RVV stars is presented in §4.2.1 of Chapter 4.

The observational HR diagrams presented in Figure 2.3 help to illustrate the distribution of these stars in luminosity and temperature using the same absolute magnitudes (M_{BG}) and colors ($B_G - K$) used for the survey sample. The left panel provides an overview of stars within 25 pc with the benchmark sample overplotted, while the right panel offers a more detailed view of the K dwarf region. In Figure 2.3's right panel it is apparent that stars of the β Pic moving group (blue points), the youngest sample examined, lie clearly

above the main sequence. As evident in their spectra (described in Chapter 3), these pre-main sequence stars exhibit significant chromospheric activity. They are larger and brighter because they are still settling onto the main sequence, as their outer layers are contracting and their internal temperatures are increasing. With ages of ∼40 Myr, K dwarf members of the Tuc-Hor group (green points) are also noticeably above the main sequence, but are elevated less than β Pic K dwarfs.

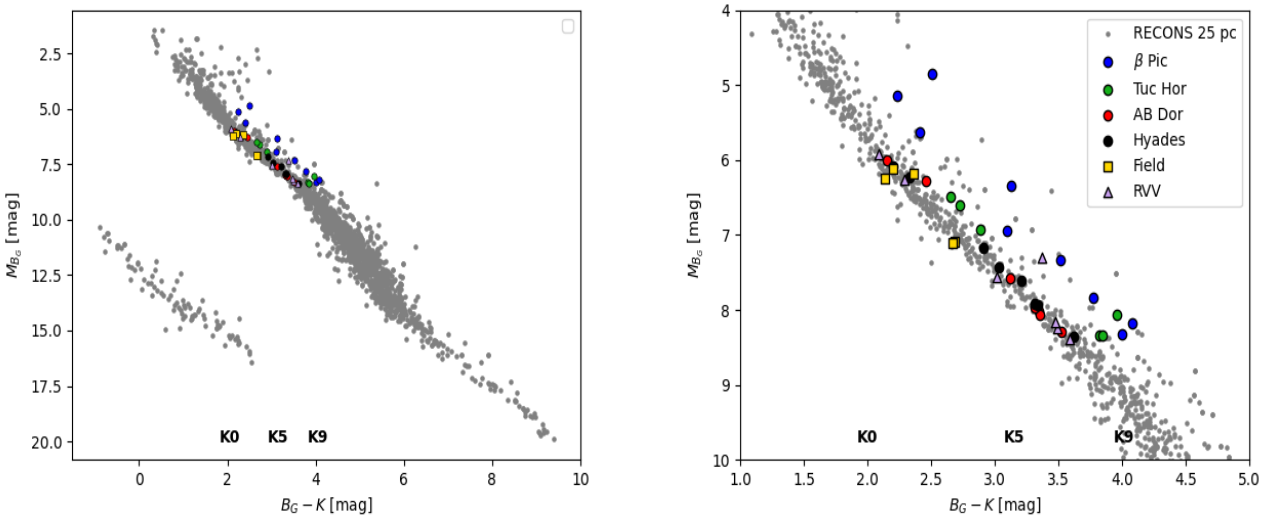

Figure 2.3 Left: HR diagram highlighting the members of the benchmark sample targeted to map spectral features related to age and activity for K dwarfs. Points are color coded as in the legend for β Pic, Tuc-Hor, AB Dor, Hyades, field K dwarfs, and RV variable dwarfs (RVV). Smaller, gray points represent stars in the RECONS 25 pc sample. Right: Zoomed-in view to focus on the stars investigated here, with the same background stars present. Magnitude information is obtained from *Gaia* EDR3 ($BP = B_G$) and 2MASS ($K_s = K$). Absolute B_G magnitudes were derived using *Gaia* EDR3 parallax measurements. **Guidelines for spectral types are given in both panels along the x-axes.**

By ages of ∼120 Myr, members of the AB Dor moving group are found at positions indistinguishable from the main sequence. The Hyades cluster, field stars, and RVV stars all

lie within the distribution of main sequence in the solar neighborhood, with the exception of the dwarf BD+05 2529 (represented by the yellow triangle at $M_{BG} = 7.4$ and $B_G - K = 3.4$), which has recently been found to be a spectroscopic binary (Sperauskas et al. 2019), confirmed via our CHIRON data. Thus, only for ages less than ∼50 Myr can young K dwarfs be identified via their positions on this HR diagram, at least relative to the ensemble of mixed stars in the solar neighborhood.

To date, 44 members of the benchmark sample have been observed using CHIRON, with 35 of these spectra having sufficient signal to noise ratios (SNR) for detailed spectral analysis. The discrepancy between the number of observed and the number of measured spectra mainly stems from the poor SNR achieved for fainter ($V > 12$), usually cooler, stars. The equivalent widths acquired from the set of 35 stars proved to be sufficient for identifying spectral age and activity trends (Hubbard-James et al. 2022).

CHAPTER 3

The Instrument, Observations, Data Reduction, and Analysis

3.1 The Instrument: CHIRON Spectrograph

The instrument used for the spectroscopic observations secured for this research is the CHIRON spectrograph. CHIRON is a stable, high-resolution, cross-dispersed echelle spectrograph designed for the Small and Moderate Aperture Research Telescope System (SMARTS) 1.5-m telescope at Cerro Tololo Inter-American Observatory (CTIO), Chile (Tokovinin et al. 2013). Our standard processing algorithm delivers a set of 59 fixed orders covering the spectral range of 4500–8850 Å[1], effectively discarding shorter wavelengths and the edges of the orders. CHIRON can acquire targets as faint as $V \sim 18$ through a fiber that is 2.7 $''$ in diameter on the sky (Tokovinin et al. 2013; Paredes et al. 2021).

Four instrumental setups are available that provide resolutions ranging from 28,000 to 136,000; details are outlined in Table 3.1. The choice of setup is determined by the scientific goals and the targets' brightnesses. For this work, we utilized CHIRON's slicer mode, which attains a resolution of R = 80,000 and offers minimal light loss with a fast 14-second CCD readout per image. CHIRON offers two wavelength calibration options: a ThAr comparison lamp and an iodine cell. In this study, we used the ThAr lamp for wavelength calibration, as it provides sufficient lines in the spectral orders needed for our science.

[1]The reduced spectral range is a consequence of our standard data processing algorithm, which trims ∼350 Å from the blue end of each spectrum (Tokovinin et al. 2013). Note that the full spectral range, 4150–8850 Å can be reclaimed by using different processing methods.

Table 3.1 Modes available for observing with CHIRON

Mode	Binning	Resolving Power	Relative Efficiency	# orders
Fiber	4×4	27,400	1.0	62
Slicer	3×1	79,000	0.82	59
Slit	3×1	95,000	0.25	62
Narrow	3×1	136,000	0.1	62

3.2 Observations using the CHIRON Spectrograph

All spectroscopic data used in this study were obtained during the period from June 2017 to March 2022 . Each visit to a target consisted of acquiring a single exposure, with a duration of 900 seconds for stars with Johnson V magnitudes brighter than 10.99 and 1800 seconds for stars with Johnson V magnitudes fainter than or equal to 11.00. The exposure times were carefully chosen to ensure a signal-to-noise ratio (SNR) in the spectra greater than 25 near a wavelength of 6740Å (see below), which is crucial for reliable analysis. In order to maintain the quality of the data, targets whose spectra had an SNR below 25 were placed on a re-observation list because the measurement of equivalent widths (EW) for spectral features of interest is known to be less reliable at lower SNR levels. Therefore, these targets were re-observed with longer exposure times of either 1200 or 1800 seconds to enhance the SNR values and ensure more accurate measurements.

To calibrate the wavelength scale, each observation was followed by a single ThAr lamp exposure with a duration of 0.4 seconds. This allowed for precise wavelength calibration of the acquired spectra. In addition, two sets of calibration frames, including biases and quartz lamp flat-fields, were taken before and after each observing night. One set was captured

in the afternoon before nighttime operations began, while the other was obtained after all observations for the night had been completed. These calibration frames played a crucial role in the data reduction process, enabling accurate calibration and reduction of the acquired spectra.

A summarized version of the full Table of observations, including the relevant information from Appendix C, is shown below as Table 3.2 for convenient reference. Please consult the full Table in Appendix C for a comprehensive list of all spectra used in the final analysis for this dissertation.

Table 3.2: List of Spectra Used in the Final Analysis

RKS ID	R.A.	Decl.	V	Date & Time of Obs	Exp. Time	SNR
...	hh mm ss	dd mm ss	mag	UTC	s	...
RKS0000+1659	00 00 48.1	+16 59 17	8.8	2021−12−06 0:34:29	900	88
RKS0001−1656	00 01 25.8	−16 56 54	10.8	2018−12−01 0:59:52	900	31
RKS0007−2349	00 07 32.5	−23 49 07	8.7	2020−12−14 1:22:54	900	71
RKS0012+2142	00 12 33.5	+21 42 48	11.8	2021−08−13 7:17:31	1200	29
RKS0012+2705	00 12 04.0	+27 05 56	8.7	2018−11−08 2:21:41	900	63
.....	.....	.....	...	.....	...	..
RKS2353+2901	23 53 08.5	+29 01 05	9.8	2018−08−16 6:25:28	900	45

Continued on next page

Table 3.2 −− *Continued from previous page*

RKS ID	R.A.	Decl.	V	Date & Time of Obs	Exp. Time	SNR
...	hh mm ss	dd mm ss	mag	UTC	s	...
RKS2355+2211	23 55 26.5	+22 11 35	8.8	2017−07−11 9:41:29	900	60
RKS2358+0949	23 58 19.8	+09 49 50	8.3	2021−08−17 6:37:07	900	84
RKS2359−2602	23 59 13.6	−26 02 55	8.7	2017−06−29 10:25:57	900	50
RKS2359+0639	23 59 47.7	+06 39 50	8.9	2018−09−29 5:01:24	900	41

3.3 CHIRON Data Reduction

The CHIRON data reduction process, carried out by the RECONS team at Georgia State University in Atlanta, involves a series of important steps to convert raw observational data into usable, calibrated spectra. Tokovinin et al. (2013) and Paredes et al. (2021) describe the CHIRON reduction process, which uses a custom data reduction pipeline written in IDL. This pipeline generates calibrated spectra with either 59 spectral orders when slicer mode is used or 62 orders for the other operational modes.

The process begins with bias correction and flat-fielding of each spectrum. In this initial stage, quartz lamp exposures are used as flat fields to remove electronic readout noise and adjust for individual pixels' sensitivities. After this stage, cosmic rays that could distort the data are carefully detected and removed from the spectrum. Next, the profile order extraction

takes place, which relies on an extraction algorithm that is part of the REDUCE package, as presented in Piskunov & Valenti (2002). The output of this process is a spectrum with extracted orders. The final step involves matching each spectrum, now with the extracted orders, with the closest ThAr calibration frame in time, typically taken immediately after the science exposure to match the position of the telescope. This allows for the determination of the wavelength solution for each order.

Although the process might seem lengthy, the entire progression from raw data acquisition to the delivery of fully processed and usable data products can be completed within a single day. However, it is more typical for data to be made available in batches every two weeks. Notably, the execution of the CHIRON pipeline, overseen by members of the RECONS team, has enabled the reduction and distribution of spectra to numerous research teams for over a thousand nights from 2017–2023.

3.4 Post-Pipeline Data Processing

3.4.1 Signal-to-Noise Ratio Calculation

Once the basic pipeline reductions are completed, the signal-to-noise ratio (SNR) per pixel is calculated for order 40 of each spectrum which spans 6705 to 6780 Å using the method described in Tokovinin et al. (2013). Spectra with a SNR less than 25 are excluded from the analysis, as their equivalent width measurements tend to be unreliable for the spectral features of interest. The SNR per pixel is calculated using the formula:

$$\mathrm{SNR} = \frac{N_{\mathrm{ph}}}{\sqrt{N_{\mathrm{ph}} + KR^2}} \tag{3.1}$$

where N_{ph} represents the number of stellar photons per spectral pixel collected during the exposure time, $R = 5.5$ denotes the CCD readout noise in electrons, and K signifies the number of binned pixels across the order. In the 3×1 slicer mode, $K = 9$ and the pixel size is approximately 0.0197 Å at a wavelength of 5500 Å. For comparison, in the fiber mode with 4×4 binning, $K = 2.5$ (assuming optimum extraction), and the spectral pixel is four times larger. This formula, provides an estimation of the SNR per extracted spectral pixel, taking into account the number of stellar photons, readout noise, and the pixel binning across the order. It allows for the quantification of the signal strength relative to the noise level, providing a measure of the quality of the acquired spectra.

3.4.2 Blaze Correction

The blaze function is a measure of the varying intensity along a spectral order across the chip due to the optical elements that disperse the light. The result is that the central portions of each of the 59 orders have higher SNR than the edges. The blaze function maps this changing response and is applied to flatten spectra before radial velocities, equivalent widths, and stellar properties can be measured. To calculate the blaze function and flatten an order of the spectrum, we fit a 7th-order polynomial generated using Matlab's fit function[2] to the continuum after masking major absorption features, such as the Na I doublet (at 5890

[2] `https://www.mathworks.com/help/curvefit/fit.html`

& 5896 Å) for order 28 and Hα line (at 6563 Å) for order 38. The original unmasked spectral order is divided by the blaze function fit to obtain a flattened and normalized spectrum. An example of the result of this process is shown in Figure 3.1 for order 40, which spans a wavelength range of 6705–6780 Å and includes the Li I line at 6708 Å.

3.4.3 Velocity Shift

To compare hundreds of spectra of K dwarf stars and to streamline extraction of information from spectral features at specific wavelengths for individual stars, the spectra are shifted to rest wavelengths. The process of shifting spectra to the rest frame is twofold: (1) applying a barycentric velocity correction, which accounts for the Earth's movement around the Solar System's barycenter, and (2) shifting the spectra to zero velocity relative to the Sun by calculating and removing the radial velocity of the star system itself, otherwise known as its γ velocity.

The first step is essential because the Earth's motion causes a significant (up to $\pm$30 km s^{-1}) Doppler oscillation to be present in all spectra. Accurately removing these variations is crucial for deriving the final radial velocities for a targeted star. To complete the barycentric shift, we employ the "`barycorr`" algorithm by Wright & Eastman (2014), which calculates corrections appropriate for radial velocity precisions of at least better than 3 cm s^{-1}, sufficiently precise for the CHIRON velocity precision measured for our K dwarfs at 5–15 m s^{-1}. The three essential ingredients used to compute the correction are: (1) the geographical position of the telescope on Earth, obtained from GPS measurements by Mamajek (2012); (2) the time stamp of the observation, taken as the midpoint of the exposure weighted by

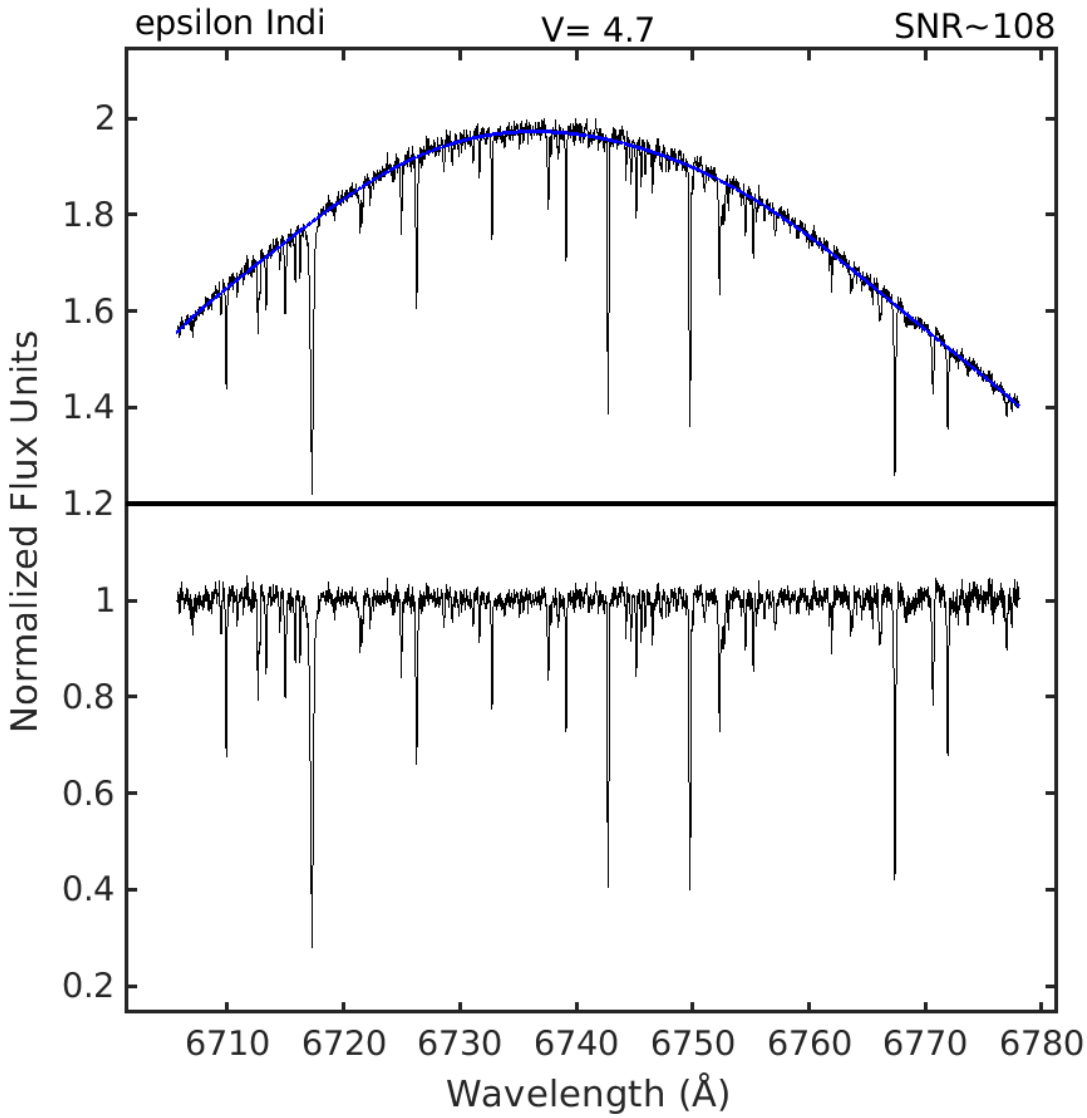

Figure 3.1 Order 40 spectrum (6705 to 6780 Å) of ϵ Indi, obtained in slicer mode (R 80,000) with a S/N $\sim$ 108. Top plot: The normalized spectrum (black) before blaze function removal, featuring a 7th-order polynomial fit (blue) overlaid on the normalized spectrum. Bottom plot: The normalized spectrum after the blaze function removal, displaying a flattened spectrum.

photon counts as measured via CHIRON's exposure meter, saved in the image header under the keyword EMMNWOB; and (3) astrometric information for the target star, including its

RA, DEC, proper motion, and parallax. For each spectrum, a barycentric Julian date in days is acquired, which serves as the time-stamp for the corrected radial velocity. Additionally, a barycentric velocity correction in m s^{-1} is determined and used to obtain the γ velocity measurement at the midpoint of the observation.

In the second step of the process, a synthetic spectrum of K4V spectral type is utilized as the template spectrum for wavelength grid matching; this K4V spectrum is used for all stars in this characterization survey. The template spectrum and the observed spectrum are then cross-correlated to determine the γ velocity using the process described in Paredes et al. (2021). The γ velocity is derived from a standard set of 14 out of the 59 echelle orders produced in slicer mode: orders 10, 12, 13, 16, 17, 18, 20, 21, 22, 23, 24, 27, 30, and 35. Uncertainties for these orders are based on the shapes of the cross-correlation functions (CCFs) and the signal-to-noise (S/N) ratio in each order. The final γ velocity value and its error are computed using the weighted average and standard deviation of the values from the 14 orders. This final value is used not only for wavelength shift but also to compute UVW space motions, as described in Section 3.7.

$$\Delta\lambda = \lambda_0 \times \frac{v}{c} \tag{3.2}$$

For both velocity shifts, the above equation is used to determine the corresponding wavelength shift, where $\Delta\lambda$ represents the wavelength shift, λ_0 denotes the original wavelength, v stands for the velocity shift, and c is the speed of light in a vacuum (approximately 299,792 km/s). After the application of both shifts, each spectrum has now been placed into the

rest frame, as illustrated for order 40 of a spectrum taken of ϵ Indi in Figure 3.2. Having all spectra normalized, flattened (via blaze removal), and shifted to the rest frame is essential for carrying out semi-automated measurements of equivalent widths using the `specutils` package and deriving stellar properties using the Empirical SpecMatch program.

3.5 Measuring Spectral Indicators of Youth & Activity

3.5.1 Line Selection

Four spectral features have been meticulously selected to assess the ages and activity levels of K-dwarf stars — the Na I doublet at 5890 and 5896 Å, Hα at 6563 Å, Li I at 6708 Å, and the Ca II line at 8452 Å. These four features serve as the foundation of our age and activity estimation strategy and have been evaluated for all 657 stars, including the 42 Benchmark stars and 615 Field stars observed in this work. A single spectrum for each star is depicted in Appendix B. This methodology builds upon the work by Montes & Martin (1998) and the "Library of High-Resolution Spectra for Late-Type Stars"[3], as detailed in Montes (2013).

The **Li I resonance line at 6707.8 Å** is a particularly potent age indicator for K dwarfs. It has been well-documented in prior studies (Soderblom et al. 1993; White et al. 2007; Lopez-Santiago et al. 2010; Binks & Jeffries 2014) that lithium depletion in late-type dwarfs acts as a reliable marker of stellar age. This depletion is postulated to occur through a process akin to the proton–proton chain reaction, which results in lithium being destroyed as a young K star transitions onto the main sequence. This reaction yields two helium atoms, along with the release of energy (Soderblom 2010). The observable decrease in the equivalent

[3]Library of Spectra for Cool Stars (Poster 2013)

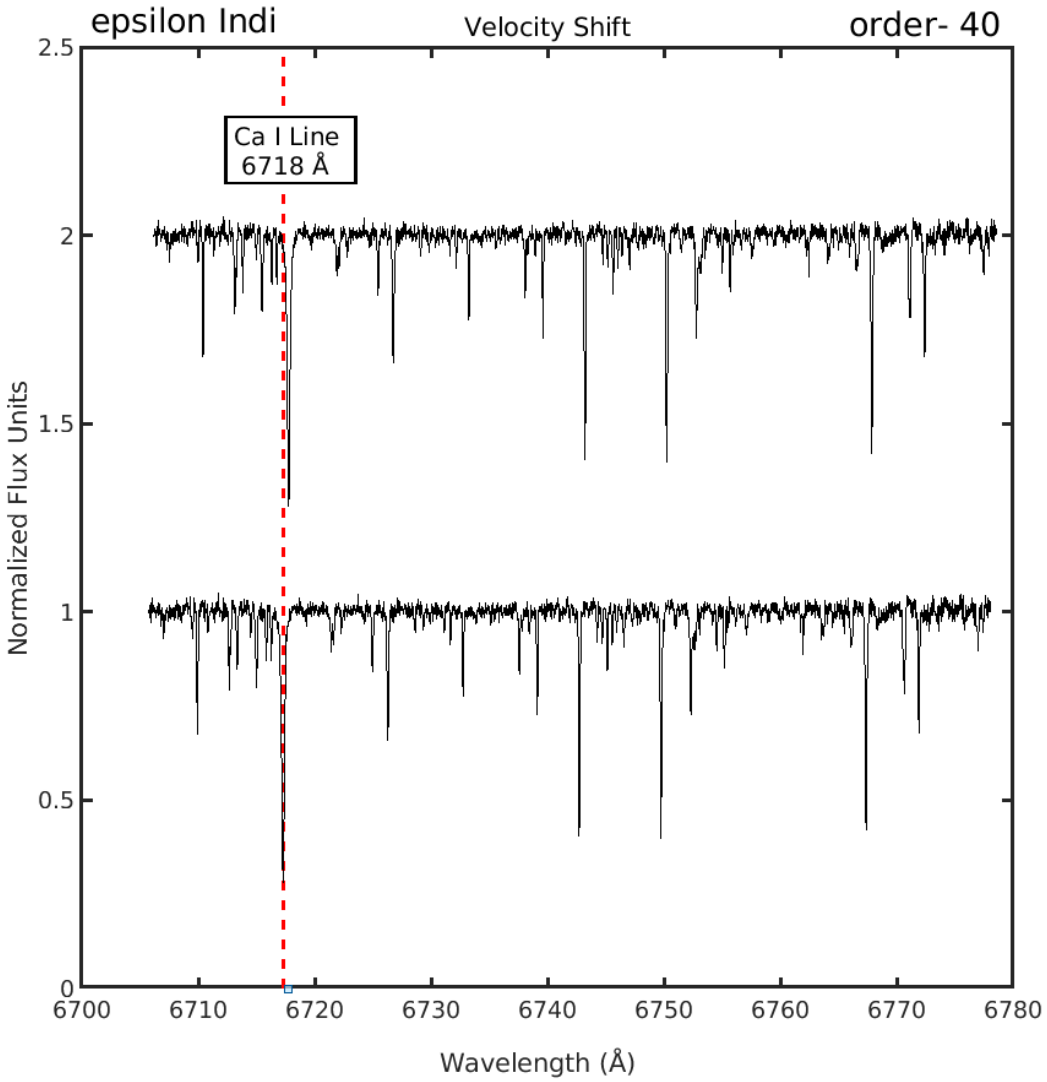

Figure 3.2 Spectrum of order 40 (6705 to 6780 Å) of ϵ Indi taken in slicer mode (R 80,000) at S/N $\sim$ 108. The top plot shows the flattened and normalized spectrum before any velocity shift. The bottom plot shows the spectrum in observer's frame of reference, after the barycentric correction and radial velocity shifts have been applied.

width of the Li I line correlates with an increase in age, making it an invaluable tool in our study. However, using the Li I to determine age has its limitations because a significant portion of lithium is depleted within the first 200 million years (Myr) for late G through

early M-type dwarfs (Soderblom et al. 2014). Moreover, the strength of the Li I 6707.8 line varies with temperature, fading faster for cooler, late-type dwarfs (K8V–M9V) (Riedel et al. 2017) than for earlier-type stars.

To compensate for this limitation and to augment the accuracy of our age estimates, we also incorporate spectral lines caused by stellar activity. The connection between increased chromospheric activity and age in late-type stars has been well-established (Skumanich 1972). We chose spectral lines that fall within CHIRON's spectral range of 4150–8800 Å, and could serve as potential age markers. The **Hα line at 6563 Å** and one line of the **Ca II infrared triplet (IRT) at 8542 Å**[4] were identified as such activity tracers.

Spectral lines indicative of surface gravity have also been suggested as potential age markers for K dwarfs (Soderblom 2010). Younger K dwarfs, with ages less than 100 Myr, are theorized to still be in the contracting phase and possess larger radii, and therefore have lower surface gravities compared to their older main sequence counterparts. The underlying principle driving the lines' shapes is pressure broadening, which depends upon the surface gravity of a star at a particular phase of its lifetime. As stars age and evolve from the pre-main sequence phase onto the main sequence, their atmospheres become compact, causing an increase in internal pressure (Montes et al. 2001). This heightened pressure results in increased atomic collisions and interactions, subsequently causing the spectral absorption features, or 'wings,' to broaden — a characteristic trait of older stars, at least relative to pre-main sequence stars.

[4]The two other lines of the Ca II IRT at 8498 and 8662 Å were disregarded because they are truncated near the edges of orders in CHIRON's slicer mode.

Among these lines, the **Na I doublet lines at 5889.95 and 5895.92 Å** are notably sensitive to pressure broadening and could serve as effective age markers. Specifically, the equivalent width of the Na I doublet feature (EW[Na I D]) is theorized to increase with age (Soderblom 2010). Tracking changes in the equivalent widths of these lines allows an estimation of a star's age and associated surface gravity. However, this method bears an inherent limitation — it is influenced by a star's effective temperature, thereby adding a degree of complexity to age estimations. Despite this, the method has the potential to contribute to understanding the aging and evolution process of K dwarfs.

Table 3.3 Description of Spectral Lines and Measurement Windows

CHIRON Order	**Line**	**Purpose Name**	**Lab λ (Å)**	**EW Window Measurement** (Å)	**Typical Error** (Å)
28	Na I D1	Gravity	5889.9	6.0	0.23
	Na I D2		5895.9	5.0	0.20
38	Hα	Activity	6562.8	2.1	0.07
40	Li I	Age	6707.8	1.4	0.03
	Ca I	Stable[a]	6717.7	NM[b]	NM
58	Ca II IRT[c]	Activity	8542.0	F: 7 C: 2[d]	F:0.25 C:0.10

a Stable: Does not vary significantly with stellar properties.
b NM: Not Measured.
c IRT: Infrared Triplet.
d F and C stand for "Full line" and "Center of Line" respectively.

3.5.2 Equivalent Width Measurements

Our spectroscopic analysis for estimating stellar age and activity involves measuring the Equivalent Widths (EWs) of four key spectral lines: the Na I doublet lines at 5889.95 and

5895.92 Å, the Hα line at 6562.8 Å, the unresolved Li doublet at 6707.8 Å, and the Ca II IRT line at 8542 Å. We carry out these measurements using `specutils`[5], an `Astropy` package designed for spectroscopy (Earl et al. 2020). `specutils` provides the necessary tools for handling, manipulating, and analyzing 1D spectral data.

The methodology adopted in our study designates specific windows for each spectral line, as illustrated in Table 3.3. For the two lines of the Na I doublet feature, we use 6.0 and 5.0 Å windows, respectively. The Hα line is assessed within a 2.1 Å window. In the case of the Li doublet, which is unresolved due to the CHIRON slicer resolution of 80,000, a measurement window of 1.4 Å is employed. A broader window of 7.0 Å is chosen for the middle line of the Ca II IRT line to accommodate its spectral characteristics. To help normalize our measurements and provide a control for stability, we also utilize the Ca I line at 6717.7 Å. This particular line was selected for its stable behavior throughout the spectral range typical of K dwarfs, allowing it to act as a robust point of comparison throughout the spectral analysis.

Figure 3.3 is a demonstration of EW measurements for Hα spectral lines using the `specutils` package in Python. Twenty K dwarf spectra were selected at random to illustrate the methodology. The plot showcases the continuum (horizontal solid line at a flux level of 1), the central line position (vertical solid line), and the measurement windows (five sets of vertical dashed lines). The shaded red area under the continuum level within the measurement window represents the EW of the line. This area was calculated by integrating the area between the continuum level and the curve of the spectral feature between the limits

[5] `specutils` documentation

of the measurement windows.

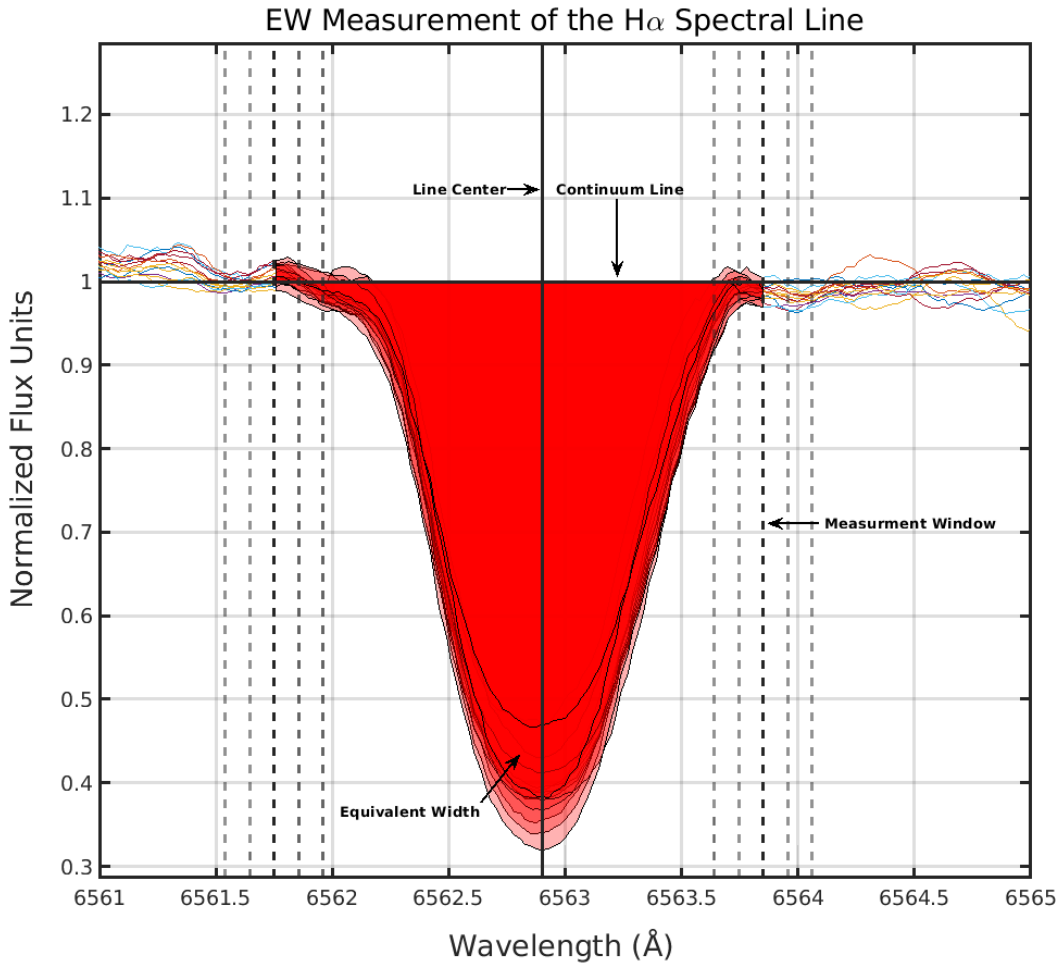

Figure 3.3 Demonstration of Hα EW measurements using `specutils` in Python using twenty randomly selected spectra of K dwarfs. The continuum is shown as a horizontal solid line at flux level 1. The central line position is marked by the vertical solid line at 6562.8 Å. Five sets of dashed lines outline the windows used to provide the EW measurement and its uncertainty. The red shaded area within the window represents the line's EW, calculated by integrating the area between the continuum level and the curved absorption line that falls between window edges.

The equivalent width in `specutils` is computed as follows:

$$EW = \int (1 - \frac{F(\lambda)}{F_c}) d\lambda \tag{3.3}$$

where $F(\lambda)$ is the flux at a wavelength λ and F_c is the continuum flux at the horizontal line. Positive values are assigned for stars with absorption features and negative values are assigned for stars with lines in emission. Notably, for stars with emission lines, the `specutils` package integrates above the continuum line, attributing the appropriate negative value.

Quantifying measurement uncertainties is a crucial component of measuring equivalent widths. We have adopted a systematic approach for this purpose, where we measure each spectral line five times using window widths that deviate by ± 5% and ± 10% from the original size specified in Table 3.3. These alternative widths are outlined with dotted lines in Figure 3.3. The reported EW for each line represents the mean of the five measurements obtained from these varying windows. This strategy, utilized for all lines measured in this study, helps to mitigate potential errors and variability introduced by the pseudo-continuum definition and local spectral features (Skoda et al. 2014). The associated uncertainty is then calculated using the standard deviation of these measurements, offering a reliable estimate of the error. Typical errors for most Field K dwarfs observed in this effort are provided in the final column of Table 3.3.

Modified methodologies are necessary for certain subsets of stars, such as fast spinning and active stars, where spectral characteristics can considerably vary. Rotational broadening, characterized by $v \sin i$, can notably modify spectral line profiles, especially in the case of rapidly rotating stars (Gray 2008). We account for these variations by adjusting the

measurement windows, extending or reducing by the same 5% and 10%, thereby rendering our methodology resilient to such effects. Active stars, exhibiting Hα emission lines instead of absorption features, are handled similarly. These stars often exhibit broad Ca II absorption features akin to inactive stars but with smaller re-emission features in the core of the line. For these instances, we apply the same technique of window variation to compensate for these deviations. This systematic approach, with the help of variable measurement windows, not only assists in addressing the variations due to stellar activity but also contributes to the accurate calculation of uncertainties.

3.5.2.1 Comparison of Specutils and SPLAT-VO Measurements for Na I, Hα, and Ca II

In order to evaluate the effectiveness and reliability of our equivalent width measurements using `specutils`, we compared our results to measurements performed for five stars using `SPLAT-VO` [6] that were published in Hubbard-James et al. (2022) for Na I, Hα, and Ca II. `SPLAT-VO` is a versatile spectroscopic tool used for analysis of low-mass stars and brown dwarfs (Skoda et al. 2014). `SPLAT-VO` applies the ABLINE technique to fit a Gaussian, Lorentzian, or Voigt profile to the absorption feature, depending on user preference, and measures the equivalent width of the line (Skoda et al. 2014). More information about methods used for each line are available in Section 4.2 of Hubbard-James et al. (2022).

We performed the equivalent width measurements using the windows presented in Table 3.3. By comparing the resulting equivalent width measurements, we can validate the consistency and accuracy of the `specutils` measurements. The percentage differences between

[6] `SPLAT-VO` documentation

our `specutils`-derived equivalent width measurements and those obtained using SPLAT are illustrated in Figure 3.4a, 3.4b, and 3.4c, for EW[Na I D], EW[Hα], and EW[Ca II IRT], respectively. For these stars we observed relatively minor differences, generally within 10% and always within 15%, demonstrating that the measurements made by `specutils` are in good agreement with `SPLAT-VO`.

3.5.2.2 Comparison with a Previous Studies for Li I & Hα

Understanding the alignment of our `specutils`-based equivalent width measurements with those obtained in prior research is a critical aspect of our analysis. Therefore, we have referenced two key studies, namely White et al. (2007) and Lopez-Santiago et al. (2010), which have also utilized the spectral lines we are interested in.

As an example of this comparative process, we compared our `specutils`-derived equivalent width measurements of the Li I spectral line in five young K dwarfs with the results reported by White et al. (2007). As illustrated in Figure 3.4d, the differences between our measurements and those reported in the study were less than 15% for each star. This consistency further confirms the reliability of our `specutils`-based measurements. Moreover, we observed that the discrepancies are within the expected measurement uncertainties, which indicates that our results are consistent with this previously published study.

Broadening this comparison to include six K dwarfs from both the studies mentioned above and comparing them with our CHIRON results, we find an average difference of 25 mÅ, with individual differences ranging between 3 to 30 mÅ. Such comparisons bolster our confidence in the EW[Li I] measurements derived from our methodology and help deter-

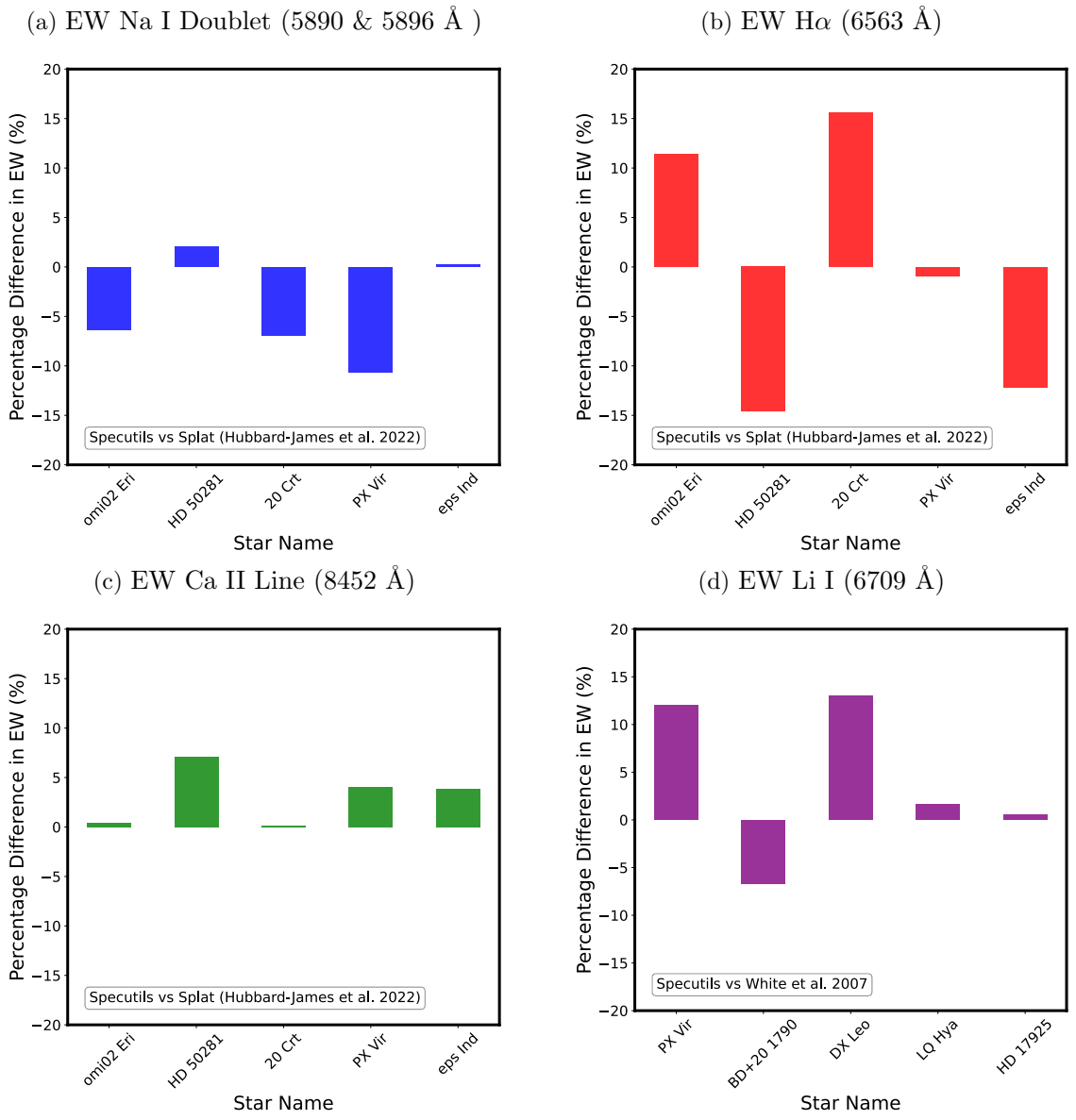

Figure 3.4 Bar plots illustrating the percentage difference between EW measurements of various spectral lines, as derived in this work using Specutils and compared with two reference studies. The differences are shown for Na I D EW (a), Hα EW (b), Ca II IRT EW (c), and Li I EW (d). For (a), (b), and (c), the measurements are compared with those obtained using SPLAT (Hubbard-James et al. (2022)). For (d), the measurements are compared with the results reported by White et al. (2007).

mine a threshold for EW[Li I], set at twice the average difference, i.e., 50 mÅ or 0.05 Å. This threshold accounts not only for the measurement uncertainties but also for potential contamination by the unresolved Fe I line at 6707.44 Å.

The potential for contamination in our spectroscopic measurements is a critical aspect to consider. This contamination can be quantitatively estimated using the method suggested by Soderblom et al. (1993), which states that EW[Fe I 6707.441] = (20(B–V)–3) mÅ. Applying this prescription to K dwarfs, we find the estimated contamination to be around 16 mÅ. Consequently, we have chosen a threshold for EW[Li I] of 50 mÅ, a value that comfortably accommodates both the uncertainties inherent in our measurements and a prudent allowance for potential contamination from Fe I 6707.44 Å. It is important to clarify that we do not explicitly measure the precise contribution of Fe I to our EW[Li I] measurements, nor do we subtract a standard value from our EW[Li I] values.

As an example, we compared our `specutils`-derived equivalent width measurements of the Li I spectral line in five young K dwarfs with the results reported by White et al. (2007). As shown in Figure 3.4d, the differences between our measurements and those reported in the study were less than 15% for each star, further confirming the reliability of our `specutils`-based measurements. We also noticed that the discrepancies are within the expected measurement uncertainties, suggesting that our results are consistent with the previously published study.

To estimate uncertainties in our EW[Hα] and EW[Ca II] measurements, we compared seven of our 42 benchmark stars to the values reported in White et al. (2007) and Lopez-

Santiago et al. (2010). For these measurements, we observed greater variance between our values and those previously published. Typically, our measurements were consistent to approximately 100 mÅ for each feature. This greater variance is not surprising given the time-linked variability of both lines due to stellar activity and the time gaps between previous observations and ours. Despite these differences, the overall agreement in our results with these studies underscores the robustness and reliability of our methodology, affirming our confidence in the analysis and interpretation of our findings.

3.6 Fundamental Stellar Parameters of K Dwarfs

For this study, we employed the Python algorithm Empirical SpecMatch (ESM) (Yee et al. 2017) to derive stellar properties for our primary sample of K dwarfs. The comprehensive results are presented in Table A.3 in Appendix A. ESM extracts fundamental stellar parameters from an input optical spectrum by comparing it with a dense library of high-resolution ($R \sim 55{,}000$), high signal-to-noise (SNR > 100) spectra of 404 calibrator stars. These stars, observed with the High Resolution Echelle Spectrometer (HIRES) on the 10-m Keck telescope in Hawaii, form part of the California Planet Search (CPS). Their parameters, ranging from 3000 to 7000 K in $T_{\rm eff}$, -0.6 to $+0.6$ dex in [Fe/H], 0.1 to 16 solar radii in radius, and F1 to M5 in spectral type, are derived from a variety of methods including interferometry, optical and near-infrared photometry, asteroseismology, and local thermal equilibrium (LTE) spectral synthesis (Yee et al. 2017).

ESM specializes in the optical wavelength range of 5100 to 5800 Å, aligning well with

the CHIRON spectra obtained for this study. This range encompasses the Mg I b triplet lines (5140–5190 Å) suitable for stellar spectral analysis, while avoiding telluric lines found between 6270 to 6310 Å. The ESM algorithm works in a systematic way to deduce stellar parameters. It initiates by accounting for the line-of-sight velocity of the target star and matches the star's spectrum to the wavelength scale of the reference library, especially in the Mg b triplet region (5100-5340 Å). This region acts as a key diagnostic area, with ratios of weak metal lines offering insights for $T_{\rm eff}$, the Mg I b triplet for $\log g$, and different iron lines for [Fe/H]. The algorithm performs a bootstrapping process to align the target spectrum with the reference having the highest median peak. Subsequently, a pairwise match between the target spectrum and each library spectrum is executed. This step includes fitting for $v \sin i$ line broadening and tweaking a cubic spline for continuum level normalization.

ESM finalizes the stellar parameters by interpolating between the library spectra, employing a weighted linear combination of the top five matching spectra; an example is shown for ϵ Indi in Figure 3.5. It uses nonlinear least-squares minimization techniques from Newville et al. (2014) during this phase to reduce the unnormalized χ^2 statistic, as shown in Figure 3.5. The uncertainties provided by ESM arise from the scatter in differences between the algorithm-derived and library values of stellar parameters for the library stars. Within the limited ranges of the characteristics for stars in its library of spectra, ESM is effective for determining characteristics for K dwarfs, with uncertainties that are typically 70-100 K in $T_{\rm eff}$, 0.12 dex in $\log g$, and 0.09 dex in [Fe/H].

While the ESM methodology has proven effective for determining the characteristics of

K dwarfs within its existing spectral library, it is important to consider a limitation that arises in our study. Notably, the spectral library lacks representation in the mid-K dwarf range, particularly from 4200–4800 K with [Fe/H]$>$ 0.2 dex. This gap may lead to potential underestimations of stellar metallicity for some of our sample members. Although this scarcity introduces larger uncertainties in the ESM-derived parameters for this specific spectral range, we still include these stars in our analysis, proceeding with caution when interpreting the results. Despite the challenges posed by this library gap, our results remain comprehensive for early and late K dwarfs. As high-quality spectra for mid-K dwarfs become more accessible in the future, we anticipate a reduction in these uncertainties and an extension of our analysis to fully cover this spectral range.

Our analysis was designed around five spectral regions within this range, chosen to evade regions of increased noise in the CHIRON spectra. These regions, 5340–5400 Å, 5440–5500 Å, 5540–5600 Å, 5640–5700 Å, and 5740–5800 Å, enabled us to derive five independent effective temperature ($T_{\rm eff}$), metallicity ([Fe/H]), and surface gravity ($\log g$) values. These values were averaged to give a final estimate for each star, with errors on each value representing the standard deviations across the five regions.

In Table 3.4, we compare our ESM derived stellar properties for five well known field K dwarfs used as part of our Benchmark study, with the PASTEL catalogue values from Soubiran et al. (2020). PASTEL compiles stellar parameters ($T_{\rm eff}$, [Fe/H], $\log g$) from high-resolution, high signal-to-noise spectral analyses using model atmospheres. Minor discrepancies in $T_{\rm eff}$, [Fe/H], and $\log g$ between our results and those of PASTEL can be attributed

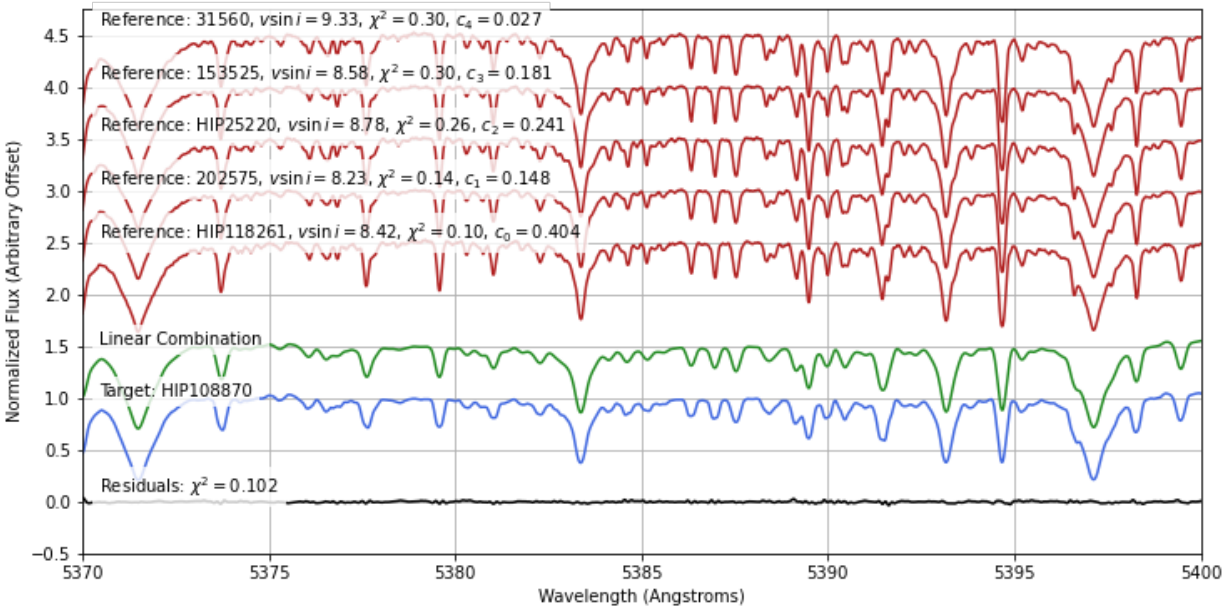

Figure 3.5 Empirical SpecMatch (ESM) is used to match the spectrum of the field K dwarf, ϵ Indi (shown in blue), with five library spectra (depicted in red) and their linear combination (displayed in green) over the spectral range of 5370-5400 Å to extract stellar parameters. This spectral region has many Fe I absorption lines. The residuals, shown in black, indicate a well-fitted match. The properties derived from this process, such as $T_{\rm eff}$, [Fe/H], and $\log g$, correspond closely to the mean values recorded for this star in the PASTEL Catalog by Soubiran et al. (2020). Here we measure $T_{\rm eff}$ = 4617 ± 29 compared to PASTEL's value of 4641 ± 21, [Fe/H]= -0.09 ± 0.03 here to -0.13 ± 0.03 in PASTEL, and $\log g$ = 4.58 ± 0.13 here to 4.29 ± 0.22 in PASTEL.

to differences in model atmospheres, line lists, and stellar physics treatments. These differences fall within the error margins of both methodologies, hence do not significantly affect the interpretation. Thus, despite different methodologies, our results align with PASTEL, affirming ESM's reliability in K dwarf analysis.

Table 3.4 Comparison of Stellar Properties

Name	[1] **E** T_{eff} (K)	[2] **P** T_{eff} (K)	[3] %Δ	**E** [Fe/H] (dex)	**P** [Fe/H] (dex)	%Δ	**E** *log g* (dex)	**P** *log g* (dex)	%Δ
omi02 Eri	5109 ± 32	5133 ± 43	0.5	-0.43 ± 0.02	-0.29 ± 0.01	28	4.49 ± 0.17	4.52 ± 0.02	7
HD 50281	4710 ± 19	4767 ± 31	1.2	0.03 ± 0.02	0.02 ± 0.03	-2	4.54 ± 0.13	4.54 ± 0.08	0
20 Crt	5220 ± 46	5196 ± 23	-0.5	-0.47 ± 0.05	-0.40 ± 0.02	15	4.54 ± 0.12	4.60 ± 0.04	13
PX Vir	5195 ± 52	5174 ± 63	-0.4	-0.12 ± 0.14	-0.08 ± 0.03	8	4.56 ± 0.14	4.55 ± 0.05	-2
eps Ind	4617 ± 29	4641 ± 21	0.5	-0.09 ± 0.03	-0.13 ± 0.03	-10	4.58 ± 0.13	4.54 ± 0.22[4]	9

1 Values derived using Empirical SpecMatch (ESM)
2 Values from the PASTEL Catalog (Soubiran et al. 2020)
3 Percent difference between ESM and PASTEL values.
4 $\log g$ value re-calculated to exclude obvious outlier of 2.87 dex.

3.6.1 Determining Projected Rotational Velocities of K Dwarfs

In our study, we also estimate the projected rotational velocities ($v \sin i$) of the K dwarfs in our sample. We followed the procedure outlined by Nisak et al. (2022), using the widths of the cross-correlation functions to infer $v \sin i$. Our analysis began with the 14 spectral orders referenced for radial velocity computations in Section 3.4.3. These orders were extracted from the spectra of standard stars HD 149661 (for early-K dwarfs), eps Indi (for mid-K dwarfs), and HD 191849 (for late-K dwarfs), and were rotationally broadened using PyAstronomy's rotBroad function. We set the limb-darkening coefficient to $\epsilon = 0.6$, as is typical for optical wavelengths (**??**White et al. 2007).

We measured the Gaussian full width at half maximum (FWHM) from the cross-correlation function of each standard's spectrum. This process was repeated for synthetically generated, rotationally broadened versions of each spectral standard at various $v \sin i$ values. In doing so, we established an empirical relationship between the Gaussian widths of the cross-correlation functions and their corresponding $v \sin i$ values.

Using this relationship, we interpolated $v \sin i$ values for the 615 observed K dwarfs by comparing their measured cross-correlation widths with those of the appropriate spectral standard (early, mid, or late K), determined based on $B_G - K$ color. A relative $v \sin i$ estimate for a primary sample K dwarf was obtained by averaging the $v \sin i$ measurements across all 14 orders, with the standard deviation serving as the uncertainty. Given that the $v \sin i$ values for our field K dwarfs typically fall below 10 km/s, we have only reported measurements exceeding this threshold, in accordance with Hubbard-James et al. (2022).

3.7 Kinematic Analysis of Nearby K Dwarfs

In this section, we outline the kinematic characteristics of the nearby K dwarfs in our sample, specifically, their γ velocities and UVW space motions. These measures are instrumental in gaining a more comprehensive understanding of the stellar movements and affiliations, thereby offering valuable insights for identifying potential memberships to specific moving groups or associations (Hubbard-James et al. 2022).

The γ velocity, otherwise referred to as the systemic radial velocity, characterizes the line-of-sight velocity of a star or a multi-star system. This measure serves as a crucial determinant of a star's relative motion from an observer's perspective. Additionally, monitoring changes in γ velocity over time may unveil the existence of companion stars, brown dwarfs, or exoplanets (Paredes et al. 2021). While these companions might not be directly observable due to close separations and/or low luminosities, nor detected via eclipses or transits, their gravitational influence can affect their primary star's γ velocity. Key to the work presented here, the

systemic radial velocity can offer pivotal clues about a star's affiliation with specific stellar groups or associations. For our comprehensive sample of 615 K dwarfs, we derived γ velocities employing the methodology outlined in Subsection 3.4.3 (Paredes et al. 2021; Wright & Eastman 2014) and present the results in Chapter 5.

We also conducted a UVW space motion analysis. The UVW space motions describe the velocities of stars in a Cartesian coordinate system that aligns with the Milky Way. As illustrated in Figure 3.6, the U-axis is oriented towards the Galactic center, the V-axis coincides with the direction of Galactic rotation, and the W-axis points towards the north Galactic pole. To calculate these motions, we used the *gal_uvw* function from the Python AstroLib libraries. This required inputting each object's celestial coordinates, proper motions, distance (derived from Gaia DR3 parallax), and our computed γ velocity (Gaia Collaboration et al. 2022). The calculations are presented in Tables 4.2 for the benchnark sample & A.2 for the primary sample; note that the solar motion has not been taken into account, so the UVW values presented here remain uncorrected for the local standard of rest (LSR).

As recorded in Table 4.2, the computed γ velocities and UVW space motions play crucial roles in confirming or disputing the membership of individual stars to particular kinematic groups. If a star is a part of a specific moving group or association, we would expect its γ velocity and UVW space motions to be in close alignment with the average values for that group.

In addition to assignments to specific moving groups or clusters for a few stars, the

[7] `http://burro.case.edu/`

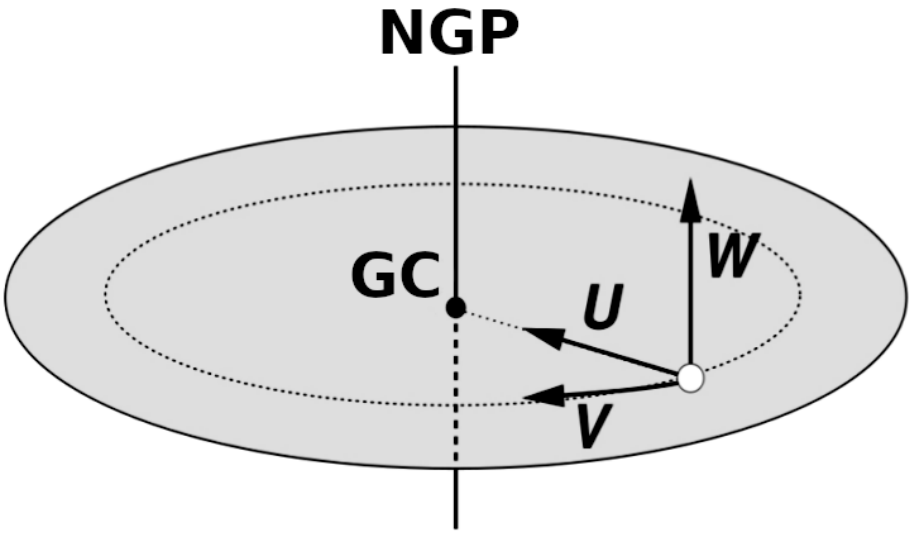

Figure 3.6 Schematic diagram illustrating the UVW space motions in the Galactic coordinate system. The U-axis points towards the Galactic center (GC), the V-axis aligns with the direction of Galactic rotation, and the W-axis points towards the north Galactic pole (NGP). Credit: Chris Mihos [7]

calculated UVW space motions can place stars into various Galactic populations. In the context of the Milky Way, stars are broadly categorized into three populations: the Thin Disk, the Thick Disk, and the Halo, each characterized by distinct kinematic properties.

Thin Disk stars comprise the majority of stars in our Galaxy, including our Sun. This population exhibits relatively small random motions, following nearly circular orbits around the Galactic center, and their velocities have a significant component in the direction of Galactic rotation (positive V velocity).

Thick Disk stars, on the other hand, exhibit somewhat larger random motions, particularly in the direction perpendicular to the Galactic plane (W velocity). They also have broader and more eccentric orbits, which in general cause them to move slower in the direc-

tion of Galactic rotation.

Halo stars are typically old, metal-poor stars, and display larger random velocities than either population of disk stars. Halo stars have highly elliptical, randomly inclined orbits, with no preferred direction of rotation. Their high vertical velocities (W) and high radial velocities (U) set them apart from disk stars.

By examining the UVW velocities, we can infer a star's likely membership to one of these three populations. For instance, stars with high UVW velocities are more likely to belong to the Thick Disk or the Halo, while those with smaller, orderly velocities are likely Thin Disk members. The established kinematic boundaries between these populations are not absolute, but statistical in nature, and this approach to placing ensembles of stars into particular populations provides an invaluable tool for understanding the structure and history of our Galaxy. However, kinematics alone cannot usually definitively determine stellar population membership for individual stars; complementary information such as age and metallicity that can be garnered from spectral analysis methods described in Sections 3.5 and 3.6 must also be considered.

CHAPTER 4

The Benchmark Study: Creating A Spectral Rubric For Identifying The Youngest & Most Active K Dwarfs

4.1 Benchmark Groups: Moving Associations, Clusters, and Nearby Stars with Known Ages

Figures 4.1 and 4.2 show a compilation of K dwarf spectra from all five benchmark groups (see Table 2.2), presented in order of age, with the seven RVV stars in the final set of panels. Within each group, the stellar spectra are arranged based on B_G–K color increasing from top to bottom, effectively hotter to cooler $T_{\rm eff}$. It is clear at first glance that several stars exhibit very broad features indicative of fast rotation, e.g., CD−64 1208, AB Dor, and LO Peg. The specific spectral features highlighted are the Na I doublet highlighted in the far-left plot, the Hα line center left, the Li I region center right, and the Ca II feature in the far-right plot.

There are subtle trends in the Na I doublet feature that are not evident to the eye, but will be discussed below in §4.2. In contrast, an obvious trend is observed for the Hα line, which exhibits core emission or at least partially filled-in line profiles for all of the K dwarfs in β Pic, Tuc-Hor, and AB Dor, but comparatively deep absorption lines typical of older K dwarfs for the Hyades cluster members and the five nearby stars with ages from isochrones. We observe strong Li I absorption lines in all members of β Pic and the hotter members of Tuc-Hor, while the line is generally weak or non-existent in AB Dor and Hyades members. One of the field K dwarfs, PX Vir, shows a strong Li I absorption feature, which is likely why it has been classified in the past as an AB Dor member (Bell et al. 2015). Among the

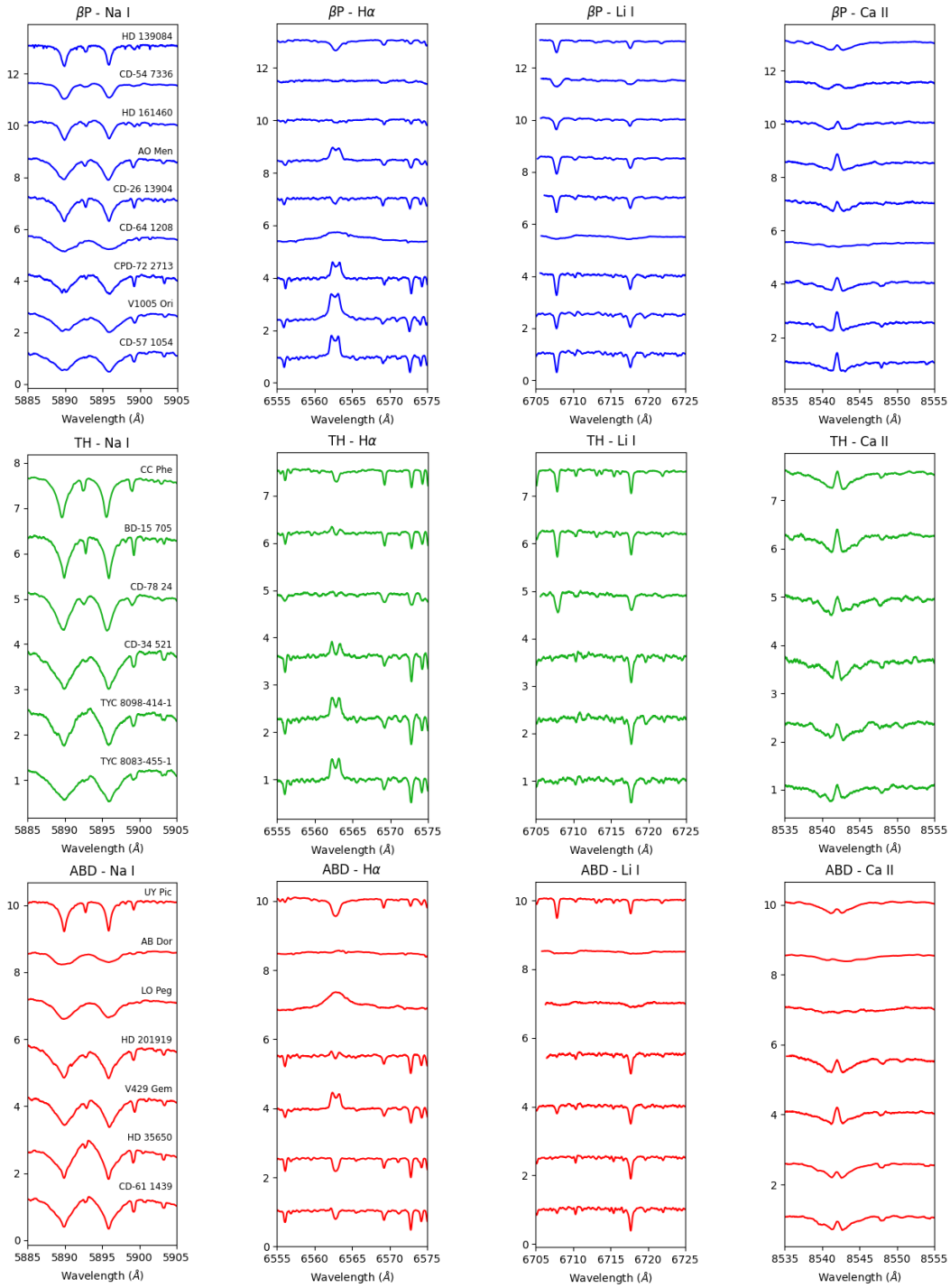

Figure 4.1 Top: Compilation of 9 K dwarf spectra from the β Pic moving group, focusing on the Na I doublet at 5889.95 Å and 5895.92 Å (far left), the Hα line at 6562.8 Å (mid-left), the Li I absorption line at 6707.8 Å (mid-right), and one of the Ca II infrared triplet lines at 8542 Å (far right). Each plot spans 20 Å. Middle: Compilation of 6 K dwarf spectra from the Tuc-Hor association, focusing on the same features. Bottom: Compilation of 7 K dwarf spectra from the AB Dor moving group, focusing on the same features.

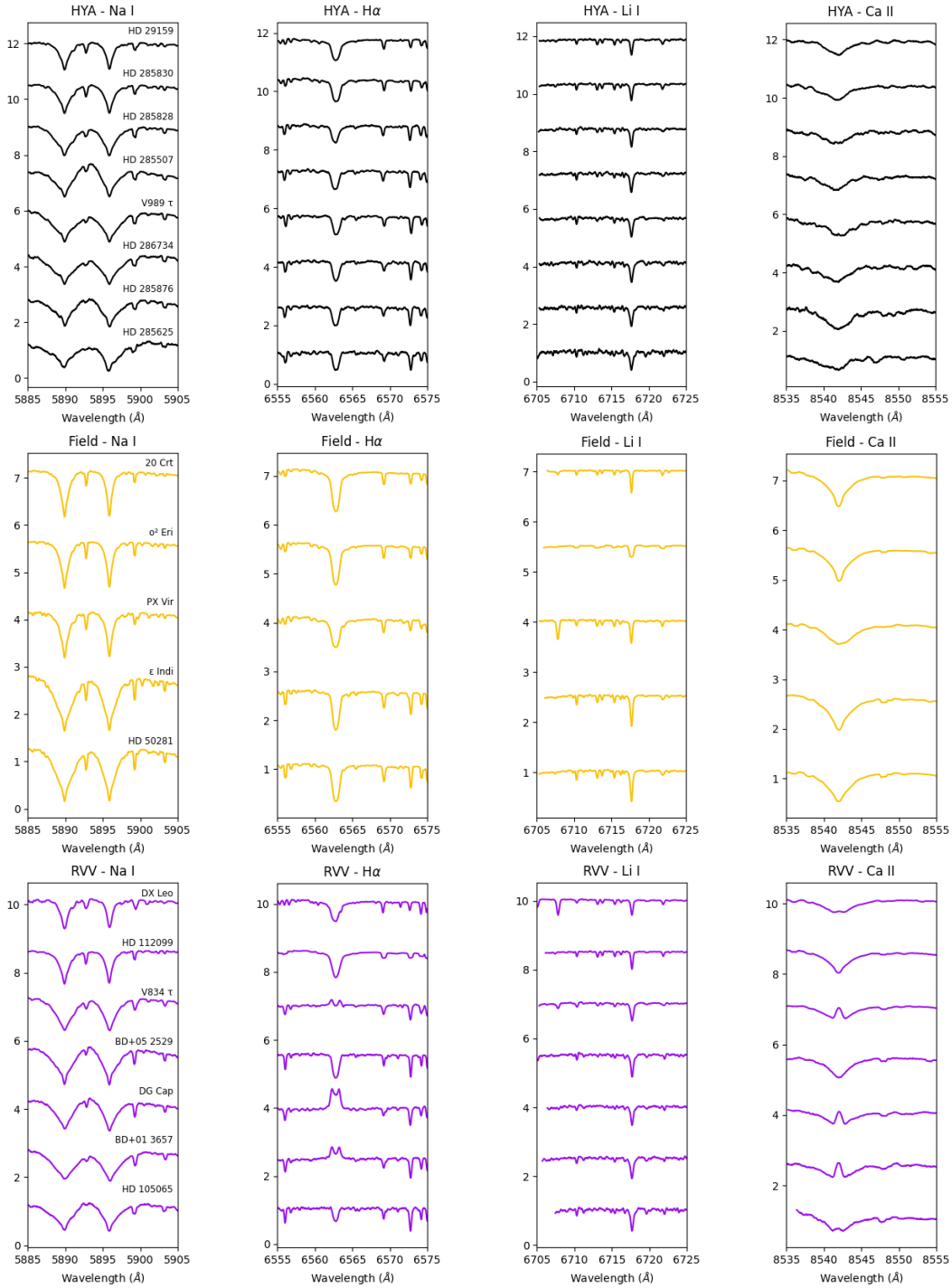

Figure 4.2 Top: Compilation of 8 K dwarf spectra from the Hyades cluster, focusing on the Na I Doublet at 5889.95 Å & 5895.92 Å (far left), the Hα line at 6562.8 Å (mid-left), the Li I absorption line at 6707.8 Å (mid-right), and one of the Ca II infrared triplet lines at 8542 Å (far right). Each plot spans 20 Å. Middle: Compilation of 5 field K dwarf spectra with known ages, focusing on the same features. Bottom: Compilation of 7 field K dwarf spectra for stars that are radial velocity variables (RVV), focusing on the same features.

seven RVV stars, DX Leo and V834 Tau show Li I absorption features. Finally, the Ca II features are generally correlated with Hα — stars with strong Hα emission typically show strong re-emission features in the cores of their Ca II lines.

4.2 Benchmark Sample Spectroscopic Results

Table 4.1 presents spectral parameter results and equivalent widths for the key features for the entire sample separated into the various groups, within which stars are listed in order of Right Ascension. The extracted equivalent widths for Na I, Hα, the Ca II triplet line, and Li I are given, as well as the SNR ratio of the spectra near the Li I feature (computed as described in § 3.4). In combination, the equivalent widths of these spectral features provide trends that can be exploited to reveal previously unrecognized young stars in the solar neighborhood. To that end, we provide a series of plots of the equivalent widths as functions of K dwarf color and age:

Figure 4.3 shows Na I, which can be used to evaluate surface gravity and age, Figure 4.4 includes Hα and Ca II, both of which map activity, and Figure 4.5 shows Li I results that are most directly linked to age.

Figure 4.3(a) reveals subtle trends in the EW[NaID] values when plotted against the colors of benchmark members in the various groups. There is a clear separation between the Hyades and field K dwarfs with isochrone ages compared to stars in the three younger moving groups. This gap is clearest for stars with B_G–K = 2.5–3.5, but fades somewhat at the hotter and cooler ends of the K dwarf temperature sequence. It is important to note

Table 4.1 Spectroscopic Results and Derived Stellar Properties of the 42 Benchmark Sample Stars

Name	Group	T_{eff} (K)	[Fe/H] (dex)	$log\ g$ (dex)	$v \sin i$ ($km\ s^{-1}$)	EW[Na I D] (Å)	EW[Hα] (Å)	EW[CaII] (Å)	EW[Li I] (Å)	SNR *at Li*
V1005 Ori	βP	3944 ± 6	0.02 ± 0.13	4.68 ± 0.14	12.3	5.52	−2.15	1.19	0.31	41
CD-57 1054	βP	3937 ± 10	−0.01 ± 0.12	4.68 ± 0.13	< 10	5.46	−1.29	1.22	0.38	43
AO Men	βP	4641 ± 46	−0.04 ± 0.04	4.56 ± 0.17	17.2	3.76	−0.95	1.10	0.41	48
HD 139084	βP	5333 ± 106	−0.03 ± 0.16	4.52 ± 0.17	16.6	1.81	0.81	1.20	0.28	95
CD-54 7336	βP	5226 ± 84	0.08 ± 0.09	4.42 ± 0.29	35.7	2.17	−0.04	1.03	0.30	46
HD 161460	βP	5293 ± 134	−0.14 ± 0.19	4.55 ± 0.15	19.9	2.13	0.15	0.76	0.32	55
CD-64 1208	βP	NM	NM	NM	> 50	4.63	−2.80	0.66	0.32	68
CD-26 13904	βP	4724 ± 25	−0.10 ± 0.07	4.54 ± 0.16	12.7	3.80	0.16	0.79	0.31	39
CPD-72 2713	βP	4085 ± 34	−0.05 ± 0.14	4.68 ± 0.13	< 10	5.39	−1.06	1.33	0.36	31
CD-78 24	TH	4724 ± 73	−0.18 ± 0.08	4.54 ± 0.19	18.6	3.54	−0.04	0.80	0.27	28
CD-34 52 1	TH	4001 ± 24	−0.11 ± 0.12	4.70 ± 0.13	< 10	5.47	−0.41	1.24	NM	25
CC Phe	TH	4969 ± 25	−0.04 ± 0.02	4.54 ± 0.14	< 10	2.91	0.23	1.33	0.21	51
BD-15 705	TH	4895 ± 32	−0.06 ± 0.04	4.51 ± 0.15	< 10	2.90	−0.17	1.41	0.23	36
TYC 8083-455-1	TH	4024 ± 53	−0.17 ± 0.15	4.69 ± 0.13	< 10	5.06	−0.66	1.47	0.02	23
TYC 8098-414-1	TH	4016 ± 34	−0.07 ± 0.13	4.69 ± 0.13	10.3	6.15	−0.74	1.51	0.02	21
HD 35650	ABD	4191 ± 18	−0.15 ± 0.07	4.67 ± 0.12	9.6	5.67	0.30	1.81	0.01	77
AB Dor	ABD	NM	NM	NM	> 50	2.27	−0.77	1.18	0.27	129
UY Pic	ABD	5248 ± 58	−0.09 ± 0.07	4.53 ± 0.15	12.5	2.01	0.90	1.40	0.26	77
CD-61 1439	ABD	4160 ± 33	−0.14 ± 0.09	4.68 ± 0.12	9.3	5.82	0.16	1.57	0.04	59
V429 Gem	ABD	4314 ± 25	−0.23 ± 0.06	4.66 ± 0.13	12.5	4.65	−0.65	1.39	0.11	39
HD 201919	ABD	4343 ± 31	−0.06 ± 0.18	4.64 ± 0.16	< 10	5.20	−0.08	1.10	0.03	34
LO Peg	ABD	NM	NM	NM	> 50	3.70	−2.90	0.89	0.10	42
HD 285507	HYA	4479 ± 29	0.08 ± 0.02	4.60 ± 0.15	< 10	5.89	0.71	1.51	NM	30
HD 285625	HYA	4068 ± 23	0.12 ± 0.51	4.67 ± 0.14	< 10	6.17	0.55	1.34	NM	21
V989 τ	HYA	4381 ± 11	0.07 ± 0.04	4.64 ± 0.12	< 10	6.01	0.70	1.39	NM	31
HD 286734	HYA	4257 ± 17	−0.04 ± 0.06	4.66 ± 0.13	< 10	6.46	0.64	1.77	NM	27
HD 285828	HYA	4631 ± 33	0.06 ± 0.06	4.57 ± 0.16	< 10	5.03	0.65	1.08	NM	31
HD 285830	HYA	5019 ± 29	0.22 ± 0.08	4.51 ± 0.13	< 10	3.33	0.91	1.90	NM	43
HD 285876	HYA	4258 ± 9	−0.03 ± 0.05	4.66 ± 0.13	< 10	6.29	0.64	2.72	NM	23
HD 29159	HYA	5183 ± 29	0.09 ± 0.07	4.51 ± 0.15	< 10	2.61	0.82	1.26	NM	43
omi02 Eri	Field	5109 ± 32	−0.43 ± 0.02	4.49 ± 0.17	< 10	2.39	1.22	1.73	NM	190
HD 50281	Field	4710 ± 19	0.03 ± 0.02	4.54 ± 0.13	< 10	4.73	0.82	2.13	NM	178
20 Crt	Field	5220 ± 46	−0.47 ± 0.05	4.54 ± 0.12	< 10	2.19	1.31	1.70	NM	72
PX Vir	Field	5195 ± 52	−0.12 ± 0.14	4.56 ± 0.14	< 10	2.35	0.87	1.63	0.15	100
eps Ind	Field	4617 ± 29	−0.09 ± 0.03	4.58 ± 0.13	< 10	4.71	0.85	1.92	NM	116
V834 Tau (2)	RVV	4562 ± 18	−0.19 ± 0.07	4.59 ± 0.01	12.6	4.34	−0.11	1.45	0.06	93
DX Leo (1)	RVV	5283 ± 54	−0.09 ± 0.06	4.52 ± 0.02	10.4	2.06	0.77	1.55	0.18	113
BD+05 2529 (7)	RVV	4226 ± 35	−0.28 ± 0.06	4.68 ± 0.01	< 10	6.04	0.64	1.84	0.01	54
HD 105065 (5)	RVV	4028 ± 32	−0.16 ± 0.20	4.68 ± 0.02	< 10	5.76	0.05	1.09	0.01	39
HD 112099 (6)	RVV	5083 ± 49	−0.12 ± 0.05	4.50 ± 0.15	< 10	2.61	0.94	1.63	0.01	92
BD+01 3657 (4)	RVV	4186 ± 10	−0.19 ± 0.04	4.68 ± 0.01	10.6	5.42	−0.55	−0.11	0.01	41
DG Cap (3)	RVV	4092 ± 49	−0.45 ± 0.06	4.70 ± 0.01	10.5	4.75	−0.85	1.41	0.02	49

EW[NaID]: Equivalent width of the Na I doublet at 5889.95 Å & 5895.92 Å
EW[Hα]: Equivalent width of the Hα line at 6563 Å
EW[CaII]: Equivalent width of the Ca II infrared triplet line at 8542 Å
EW[Li I]: Equivalent width of the Li I line at 6707.8 Å
NM: Not Measured

that we observe no difference between Hyades members and K dwarf field stars with age estimates over 1 Gyr. Figure 4.3(b) shows that no clear trend is observed when EW[NaID] is plotted against estimated stellar age because the spread in temperatures within a group obfuscates the overall differences.

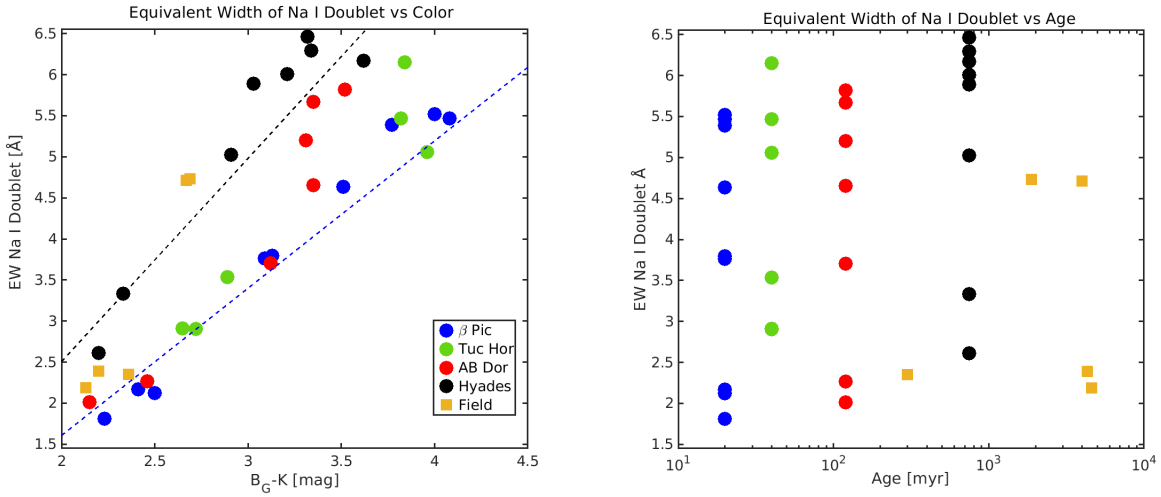

(a) (b)

Figure 4.3 (a) Plot showing the EW[NaID] vs. B_G–K color for the five groups of stars used in the benchmark sample. Cluster trends are indicated by dotted lines of the same color for β Pic and the Hyades. (b) Plot showing the EW[NaID] vs. estimated age for all five benchmark age groups. Points are color coded as shown in plot (a).

Figure 4.4(a) shows EW[Hα] strength vs. color, with negative values indicating emission. There is a boundary between the young and old K dwarfs in the benchmark sample stretching through all temperatures, indicated by a broken black line at an equivalent width value of 0.5 Å. In particular, the yellow squares represent generally old stars, including o^2 Eri, 20 Crt, and ϵ Indi that have ages estimated to be 3.7–4.6 Gyr. The EW[Hα] vs. age comparison illustrated in Figure 4.4(b) shows the steady decrease of Hα emission strength with increasing age for the five benchmark groups. K dwarfs in the younger associations, β Pic, Tuc-Hor,

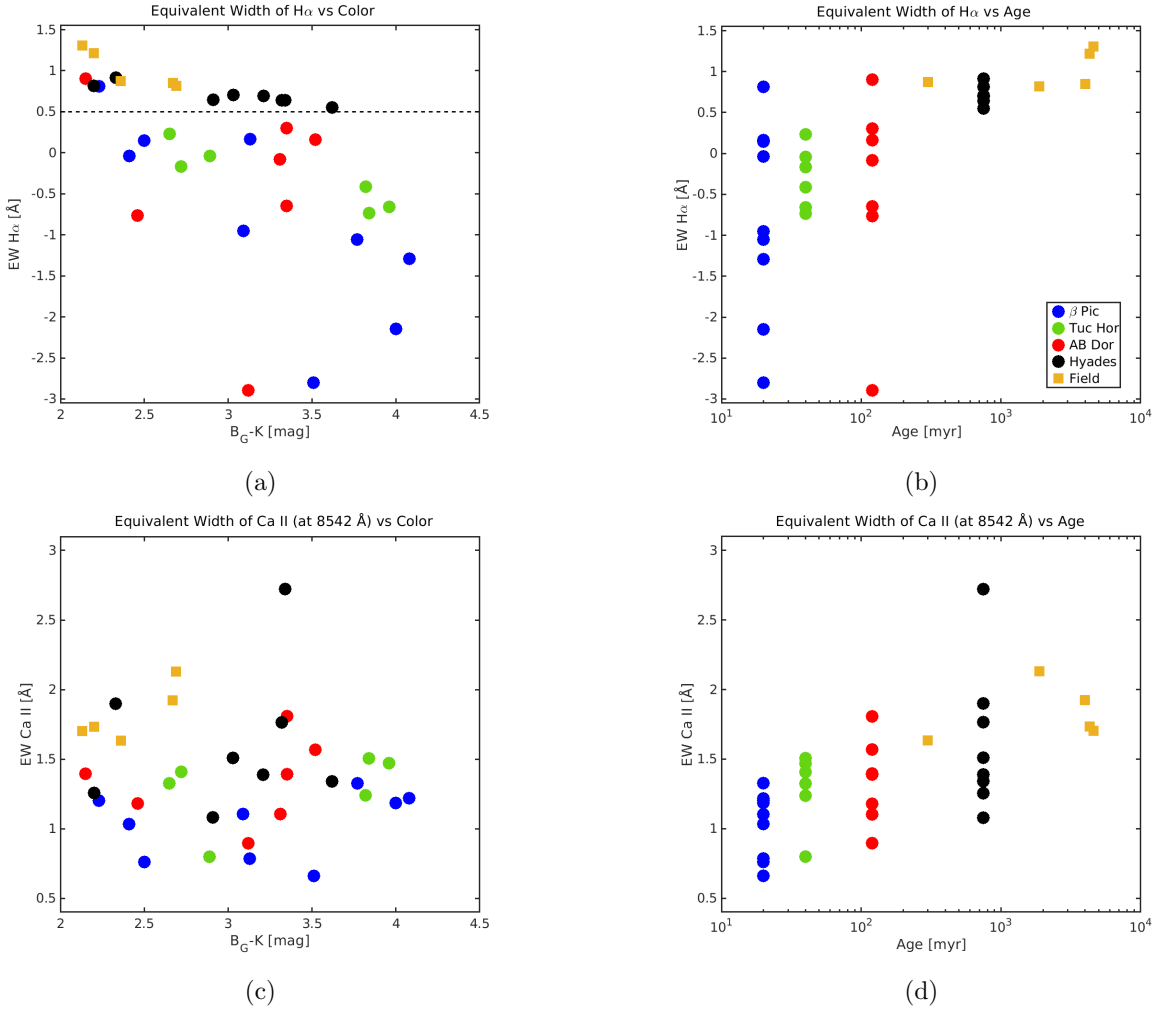

Figure 4.4 (a) Plot showing the EW[Hα] vs. B_G–K color for the five groups of stars in the benchmark sample. The black dotted line at EW = 0.5 Å separates the old and young stars. (b) Plot showing the EW[Hα] vs. estimated ages for all five benchmark age groups. (c) Plot showing the EW[CaII] vs. B_G–K color for the five groups of stars in the benchmark sample. (d) Plot showing the EW[CaII] vs. estimated ages for all five benchmark age groups. Points are color coded as shown in plot (b).

and AB Dor, generally exhibit emission or filled-in line profiles; both cases are visible in the center left plot of Figure 4.1 for all three young moving groups. As stellar age increases, core emission fades, with all of the Hyades and field K dwarfs exhibiting Hα absorption lines

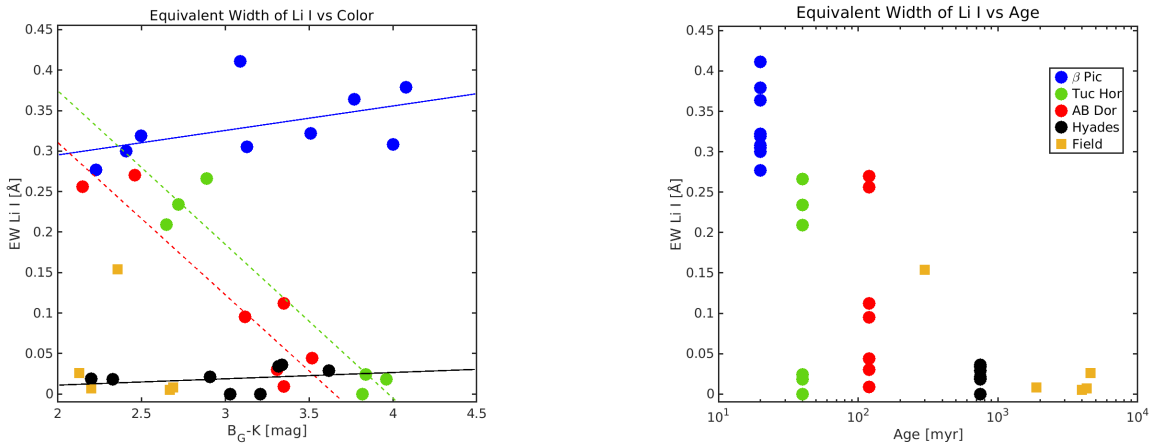

(a) (b)

Figure 4.5 (a) Plot showing the EW[LiI] vs. B_G–K color for the five groups of stars in the benchmark sample. Cluster trends are indicated by lines of the same color. (b) Plot showing the EW[LiI] vs. estimated age for all five benchmark age groups. Points are color coded as shown in plot (b).

(Figure 4.2), corresponding to positive EW[Hα] values.

The bottom two plots in Figure 4.4 outline results for the other chromospheric activity diagnostic investigated, the Ca II line at 8452 Å. Figure 4.4(c) indicates that there is no clear trend for the stars of the benchmark sample when EW[Ca II] is plotted against color. A slight trend is seen when EW[Ca II] is plotted against age in Figure 4.4(d), with EW[Ca II] values generally increasing from younger to older groups. Careful examination of the Ca II line profiles presented in the far-right panels of Figures 4.1 and 4.2 indicates that for Hyades and K field stars there is no core re-emission, whereas effectively all stars in the younger associations show re-emission.

Results for the EW[LiI] diagnostic illustrated in Figure 4.5(a) indicate that all stars in β Pic (blue points and line) show strong Li absorption signatures, regardless of B_G–K color,

while there are trends with color for members of both Tuc-Hor (green points and dotted line) and AB Dor (red points and dotted line). These trends can be seen visually in Figure 4.1, while Figure 4.2 shows that only a single star from the Hyades and K field groups, PX Vir, shows evidence of a Li I feature.

Figure 4.5(b) illustrates the clear trend of Li I absorption strength and age. All nine K dwarfs observed in β Pic exhibit strong Li I absorption, with EW[LiI] values of at least 0.25 Å. There is effectively no overlap between the β Pic values and those of the slightly older Tuc-Hor and AB Dor members, two groups that show similar ranges in EW[LiI] values that are temperature-dependent. As mentioned, all but one of the Hyades and field K dwarfs show no Li I signature, with values measured below what we consider to be our signal threshold of 0.05 Å in the CHIRON spectra. The exception is PX Vir, which has an estimated age of 300 Myr from Stanford-Moore et al. (2020), and shows an EW[LiI] value similar to K dwarfs in the Tuc-Hor and AB Dor groups.

4.2.1 Evaluation of 7 Radial Velocity Variable K Dwarfs

With trends in EW[NaID], EW[Hα], and EW[LiI] established for groups in the benchmark sample, we can now evaluate the seven K dwarfs from our RVV sample using these three spectral diagnostics. The seven stars were chosen based on their variable radial velocity measurements in early sets of CHIRON data. Their RV plots are presented in Figure 4.6, with a K field dwarf, HIP 42074, that shows no variable RV at the CHIRON precision resulting from our observing and reduction protocols, $\sim$10 m/s. Figure 4.2 illustrates the regions around the spectral features for these seven stars.

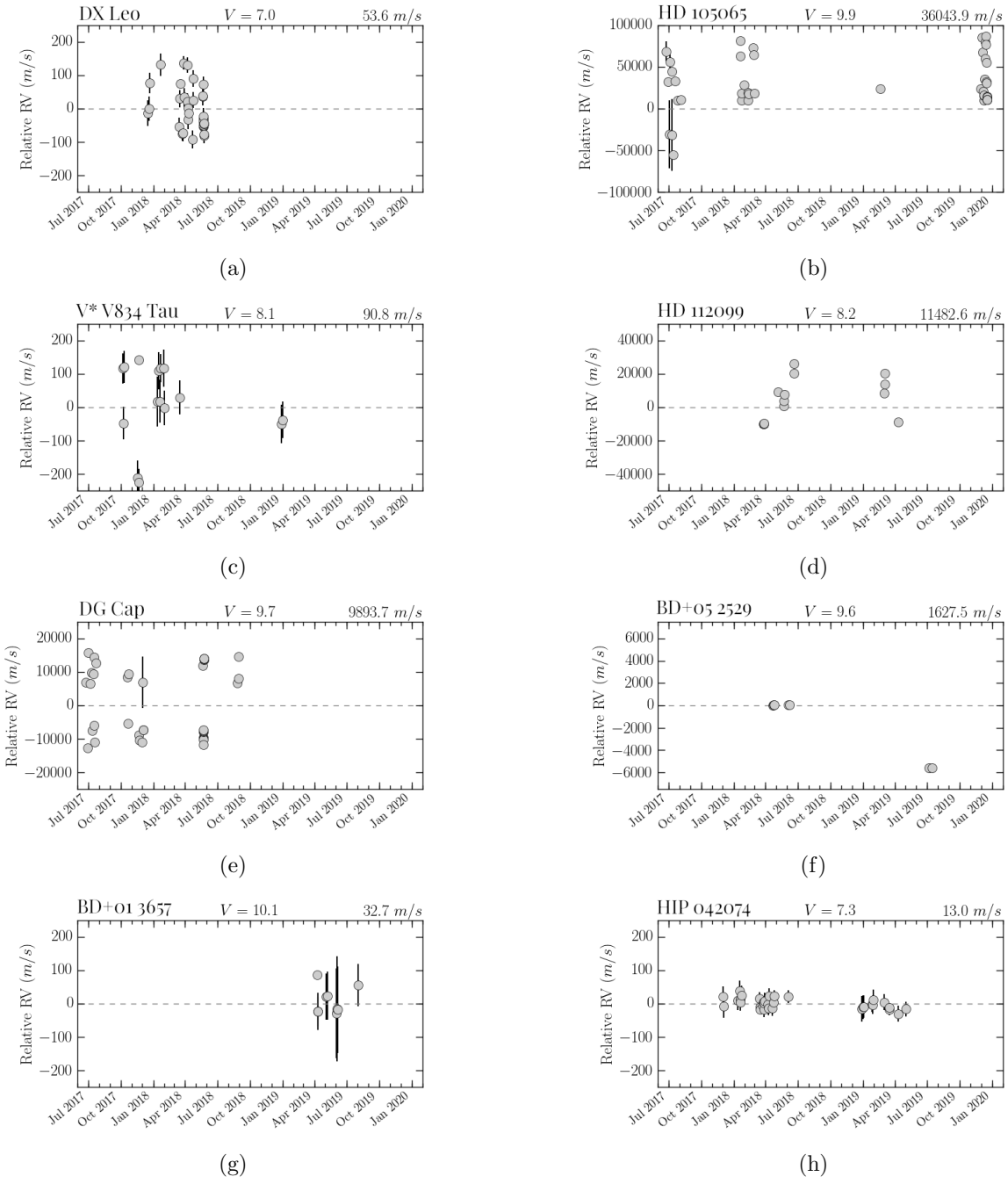

Figure 4.6 Plots showing RV results from CHIRON spectra for the RVV stars DX Leo, V834 Tau, DG Cap, BD+01 3657, HD 105065, HD 112099, and BD+05 2529. HIP 42074 in the bottom right is shown as a non-variable control star.

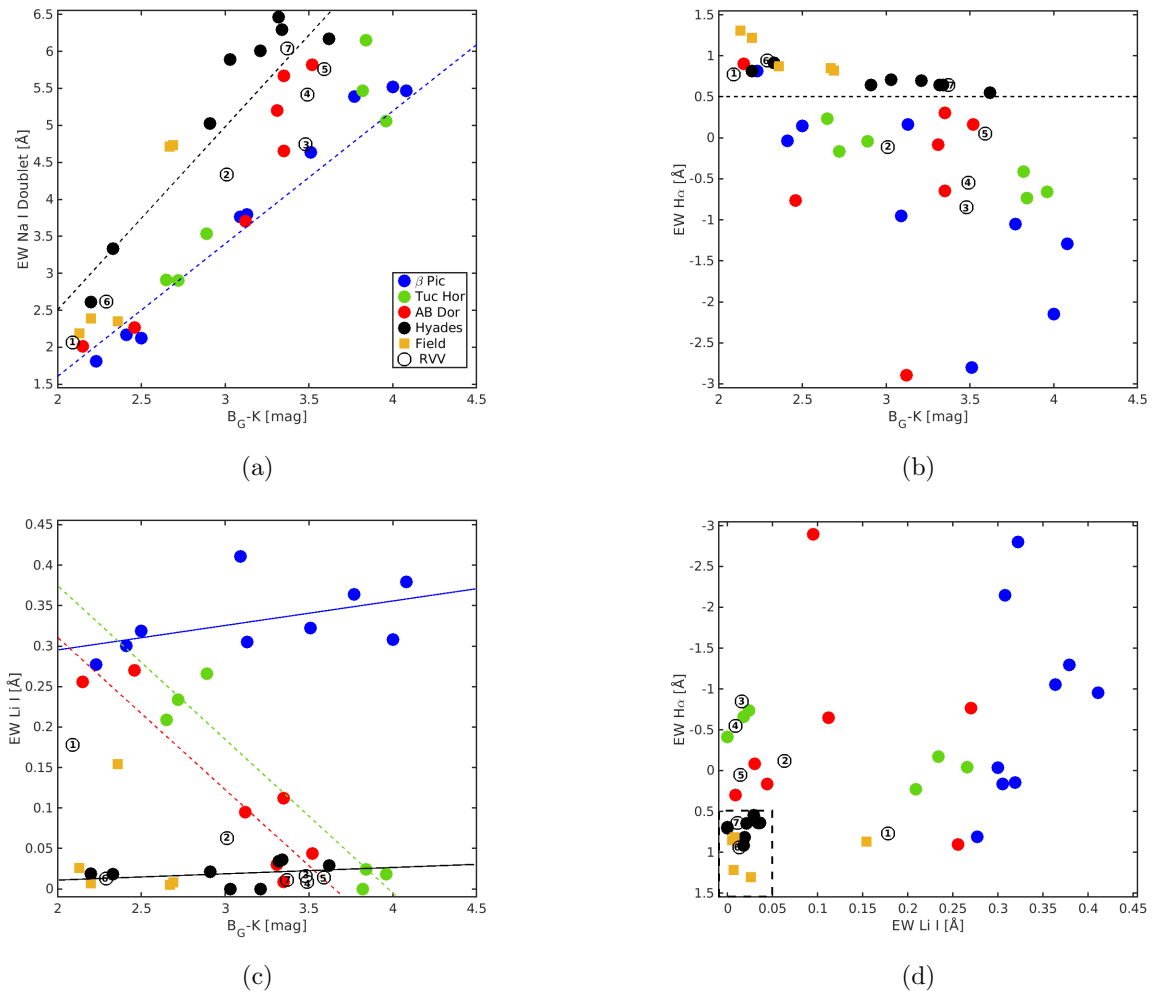

Figure 4.7 Plots placing the 7 RVV stars (encircled numbers) among the set of 35 stars with estimated ages in the benchmark sample: (a) EW[NaID] vs. $B_G - K$ color, (b) EW[Hα] vs. $B_G - K$ color, (c) EW[LiI] vs. $B_G - K$ color, and (d) EW[Hα] vs. EW[LiI], where the dashed black box in the bottom left encloses K dwarfs present in the old locus. Numbered stars: (1) DX Leo, (2) V834 Tau, (3) DG Cap, (4) BD+01 3657, (5) HD 105065, (6) HD 112099, and (7) BD+05 2529.

Figure 4.7 illustrates the locations of the RVV stars, identified with circled numbers, overplotted on the results for the benchmark stars for the three relevant equivalent widths individually and for the combination of EW[Hα] and EW[LiI]. Plot (a) shows where the

RVV K dwarfs fall with respect to the EW[NaID] vs. $B_G - K$ trends that were established for the benchmark sample. Four (numbers 2 through 5) of the seven stars have EW[NaID] values significantly below the Hyades trend line and with $B_G - K \approx 2.5$–3.5. These stars also stand out in plot (b) for Hα, with the same four K dwarfs falling below the activity boundary indicated by a dashed black line. In plot (c), the trend for EW[LiI] vs. $B_G - K$ shows that two RVV stars (① and ②) have EW[LiI] greater than the 0.05 Å threshold set for a significant Li I signal. Both stars have $B_G - K < 3.0$, with ② V834 Tau also standing out in plot (b) as active based on the Hα trend.

Combinations of spectral features are often even more powerful than evaluations of individual lines, so in Figure 4.7 panel (d) we show EW[Hα] vs. EW[LiI] for both the benchmark sample stars and the seven RVV K dwarfs. There is a locus of stars representing the oldest benchmark groups in the lower left box of the plot, with borders set at EW[Hα] = 0.5 and and EW[LiI] = 0.05. K dwarfs from the younger associations radiate from this mature locus, with stars in the youngest cluster, β Pic, being the furthest removed and falling to the right of the plot. In addition to calibrating the methodology we will use on the full sample of more than 600 stars, a key result of this initial effort is that we find five K dwarfs with variable RVs that land outside the old locus, with ① DX Leo being flagged as young based on Li I, ② V834 Tau showing markers of both youth via Li I and activity via Hα, and the three stars ③ DG Cap, ④ BD+01 3657, and ⑤ HD 105065, flagged by Hα as being active. We find that ⑥ HD 112099 and ⑦ BD+05 2529 show no signs of youth or activity, and their radial velocity variations turn out to be caused by companions orbiting in periods of a

few weeks to a few years, for which we confirm previously reported spectroscopic detections. In §4.5.3 we show that (3) DG Cap and (5) HD 105065 are newly identified spectroscopic binaries (type SB1) with close companions orbiting in less than 10 days, and therefore could be young and/or have enhanced emission due to the close companions. In §4.5.3 we discuss all four spectroscopic binaries, and in §4.6 Systems Worthy of Note, we provide additional details for all seven RVV stars.

4.3 Stellar Properties of the Benchmark Sample

Alongside the equivalent widths, we also report the spectral parameter results for our sample in Table 4.1. These include the derived $T_{\rm eff}$, [Fe/H], and $\log g$ values for the 39 K dwarfs in the benchmark sample, obtained using Empirical SpecMatch. However, for the three stars with high rotational velocities - CD-64 1208, AB Dor, and LO Peg - we have not provided any values due to the significant uncertainties associated with them. According to Zuniga-Fernández et al. (2021), the $v \sin i$ values for these stars are reported to be 55.37, 74.97, and 46.28 km s^{-1}, respectively. We have estimated these values to be greater than 50 km s^{-1}.

For all 42 K dwarfs in our sample, we have included $v \sin i$ estimates, though they are limited to a range between 10 km s^{-1} and 50 km s^{-1}. This limitation is a direct result of the derivation process for our $v \sin i$ values, which were obtained from Empirical SpecMatch reference stars used for the benchmark sample. As pointed out by Yee et al. (2017), to maintain the accuracy of spectral line matching, it is necessary to establish a cutoff at 10 km s^{-1}.

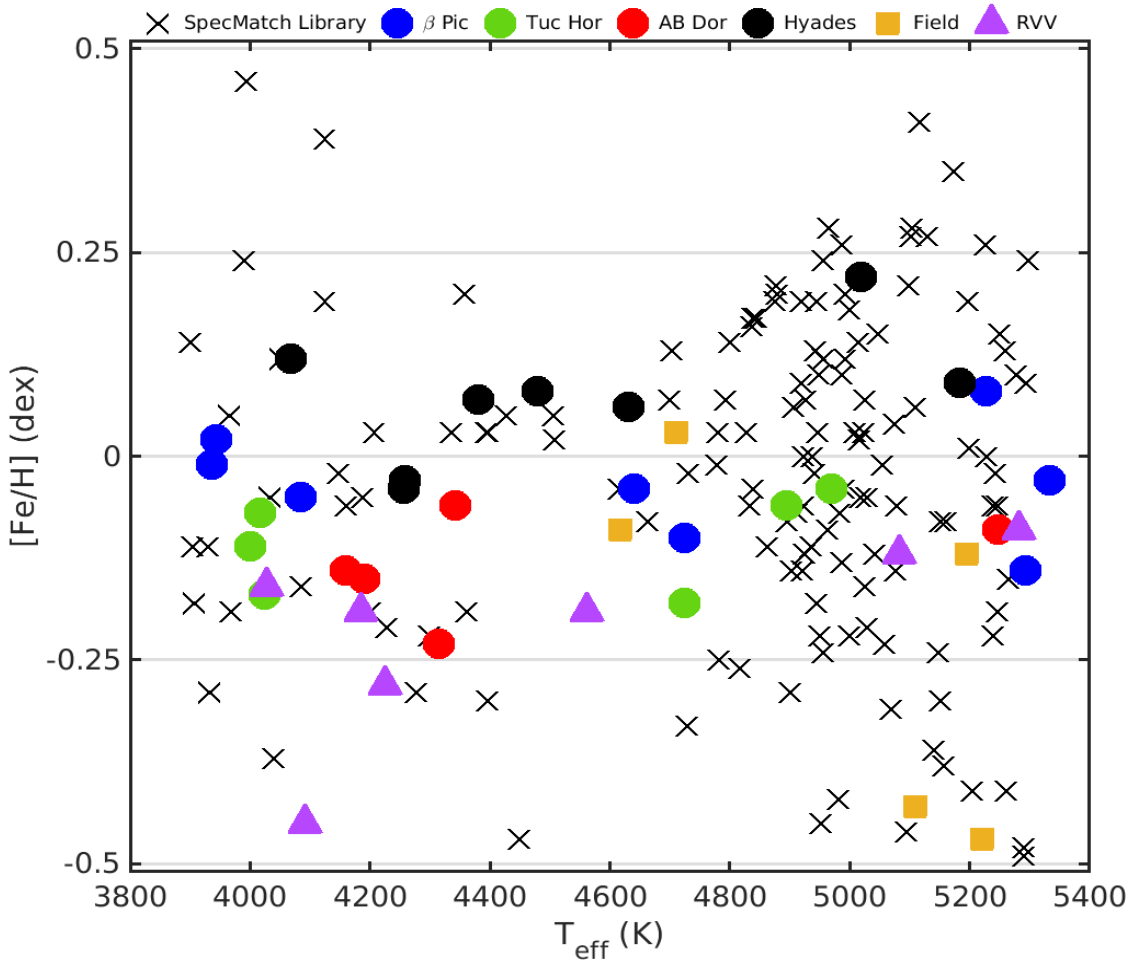

Figure 4.8 [Fe/H] plotted against effective temperature for 39 K dwarfs in our benchmark sample, with 143 stars (black X's) from Yee et al. (2017)'s SpecMatch library shown in the background.

Figure 4.9 illustrates the relationship between the ESM-derived effective temperatures and the $B_G - K$ colors of the stars. A discernible trend can be observed for most of the 42 stars in our sample. However, three significant outliers — CD−64 1208, AB Dor, and LO Peg, which are fast rotators with extremely broad absorption line profiles — compromise the accuracy of the T_{eff} measurements.

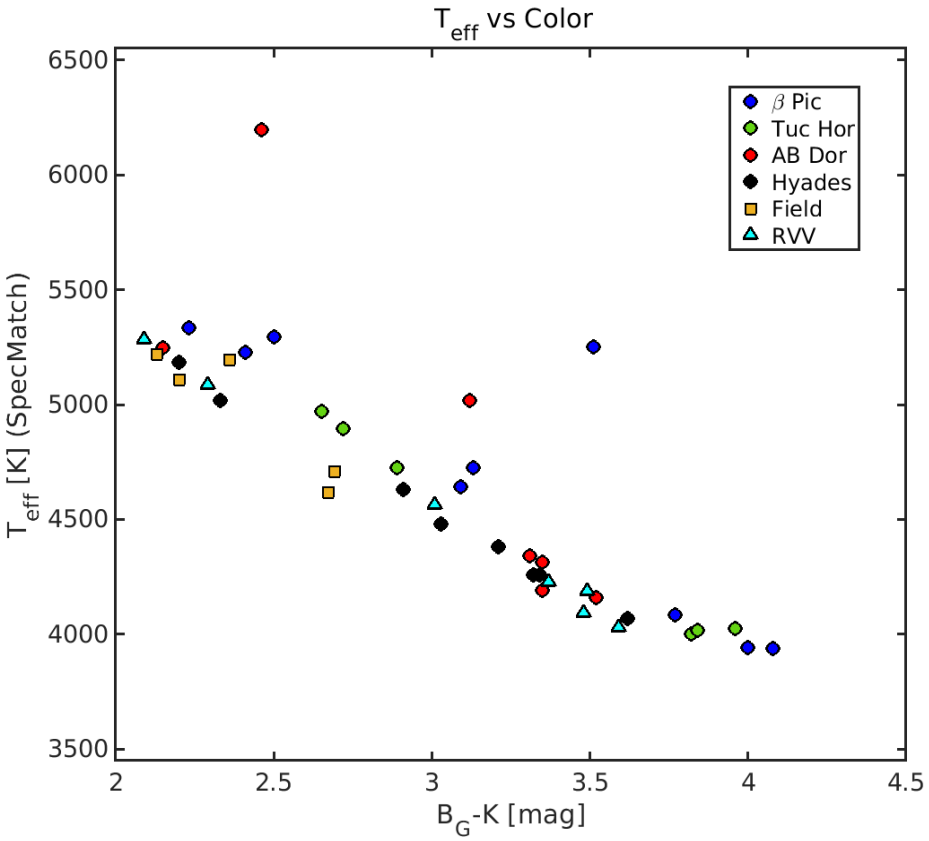

Figure 4.9 Effective temperature derived from ESM is plotted against $B_G - K$ color for all 42 K dwarfs in our Benchmark Sample.

For members of the K field group, we observed negligible differences when comparing our derived $T_{\rm eff}$ values to existing measurements in the literature (Luck 2018; Aguilera-Gomez et al. 2018; Hojjatpanah et al. 2019). Four of the five field K dwarfs are in both papers, and we find that our $T_{\rm eff}$ measurements differ by only 20 K on average. The sequence of temperatures we measure exhibits a smooth correlation with $B_G - K$ color, as shown in Figure 4.9 (recall that the three points off the trend are the fast rotators), a further indication that our temperatures are reliable.

Figure 4.8 depicts a comparison between our derived [Fe/H]values and those of the Empirical SpecMatch library stars. The [Fe/H]values we determined for the four moving associations in our study were benchmarked against values in Viana Almeida et al. (2009) for the β Pic, Tuc-Hor, and AB Dor stars, and against those in Perryman et al. (1998) for Hyades members. Notably, our ensemble averages for each group differed by no more than 30% from the values previously reported for these groups. Our [Fe/H]measurements of individual stars from the K field group align with the values reported by Hojjatpanah et al. (2019) within a range of 11–17%. Further evidence of the consistency between our ESM-derived values and previous determinations is presented in Table 3.4 in §3.6, which compares our values with the compilation from Soubiran et al. (2020). We draw attention to the three relatively metal-poor stars with [Fe/H]< -0.4: o^2 Eri, 20 Crt, and DG Cap. None of these stars belong to a young group, and all appear to offer reliable fits when utilizing ESM.

In regard to overall metallicities, it's worth noting that the Hyades cluster exhibits higher metal richness than the other studied clusters. It's critical, however, to recognize that sparse sections in ESM's library can introduce limitations in our ability to match to gaps in their coverage. The inherent limitations and uncertainties associated with these sparse sections can influence the accuracy of the derived spectral parameters, which necessitates a cautious interpretation of our findings in those areas.

Finally, $\log g$ results were inconsistent for the younger moving groups, β Pic and Tuc-Hor, but reliable for older stars in our sample. As shown in Figure 2.3, younger stars are clearly above the main sequence in the H-R diagram. However, Table 4.1 shows similar $\log g$ values

for K dwarfs of comparable $T_{\rm eff}$ even if they have markedly different ages. The likely reason for similar surface gravity values is that Yee et al. (2017)'s spectral library includes primarily main sequence stars, so the $\log g$ results for young stars reported here should be treated with caution.

4.4 Kinematic Motions of the Benchmark Sample

The UVW space motions for each K dwarf provide important information linking individual stars to the various moving groups and clusters, and can indicate when those stars *do not* have matching motions in the Galaxy. Table 4.2 provides positions, proper motions, and parallaxes for the stars from *Gaia*, their B_G magnitudes and B_G-K colors, our derived γ systemic velocities from the CHIRON spectra and similar measurements from *Gaia*, and the derived UVW space velocities.

Figure 4.10 illustrates the dynamics of the stars in the samples. Panel (a) illustrates the comparison between the measured CHIRON γ velocities and those given in *Gaia*. Stars offset from the 1-to-1 line are multiples with orbits caught at different phases and/or are stars that are young, active, or exhibit rapid rotation, any combination of which can make velocity measurements difficult. Outliers in the benchmark sample are labeled with encircled letters a through k. Stars with mismatched velocities are (a) HD 105065 (mildly active), (b) DG Cap (active), (c) LO Peg (rapid rotator), (d) HD 112099 (close multiple), (e) CD−64 1208 (close multiple and rapid rotator), (f) HD 139084 (close multiple), (g) HD 161460 (close multiple), (h) PX Vir (close multiple), (i) AO Men (young, active), (j) AB Dor (close multiple and

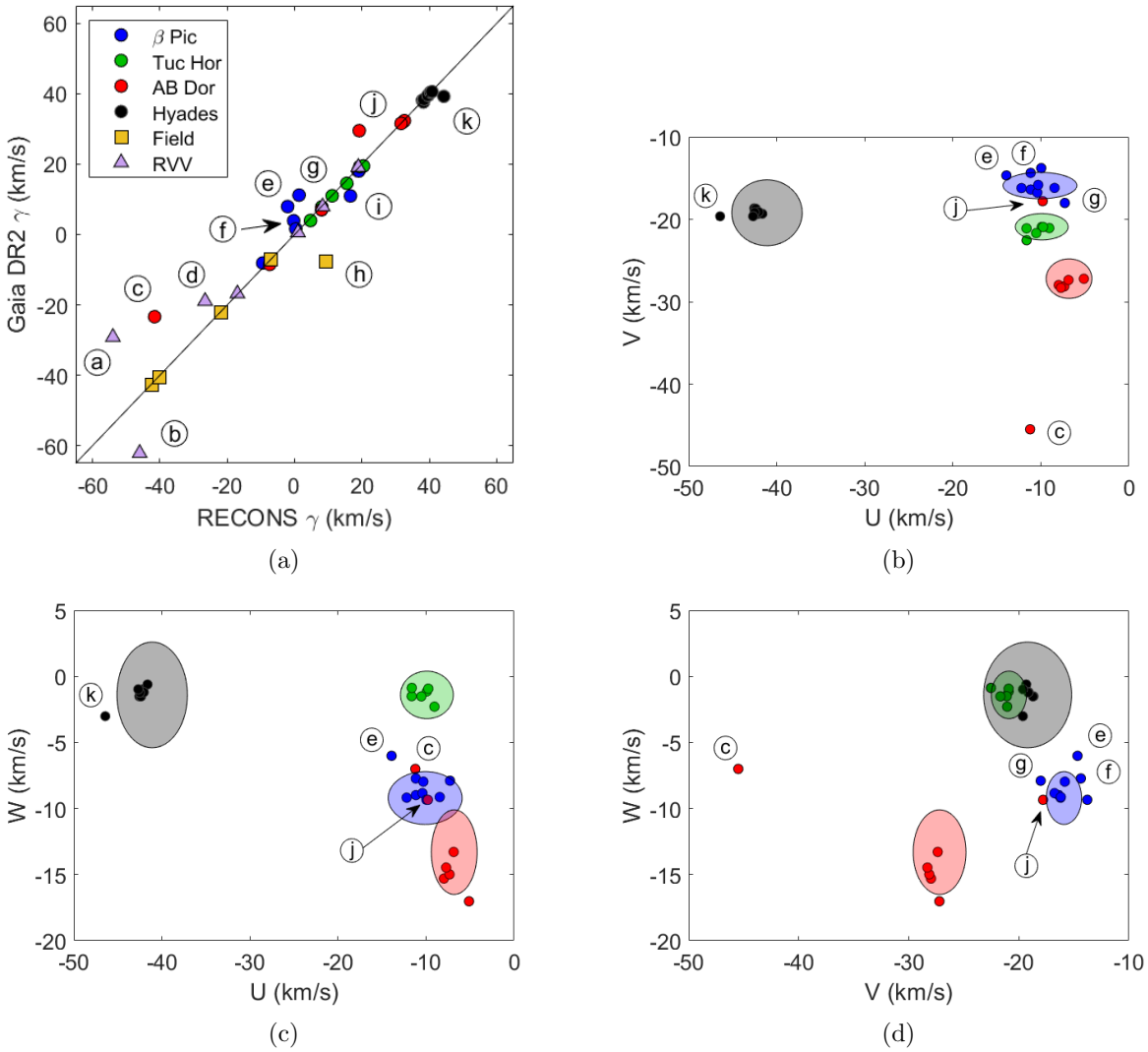

Figure 4.10 Diagrams illustrating the dynamics for members of the four moving groups and clusters used in the benchmark sample: (a) 1-to-1 correlation plot of CHIRON γ velocity vs. *Gaia* γ velocity, where the line represents equal values, (b) Galactic space motions V vs. U, (c) W vs. U, and (d) W vs. V. Points represent members in β Pic (blue circles), Tuc-Hor (green circles), AB Dor (red circles), Hyades (black circles), field K dwarfs (yellow squares), and RVV stars (purple triangles). Ovals represent characteristic UVW velocities for the groups and stars represented by encircled letters are outliers discussed in the text.

rapid rotator), (k) HD 285828 (close multiple). Among these eleven outliers, seven are close multiples included in Table 4.3, which lists all stars in the sample known to have companions (more details in §4.5), explaining the difference in the radial velocity values for these stars.

Panels (b), (c), and (d) in Figure 4.10 illustrate the UVW space motions for stars in the moving groups and clusters. The ovals represent velocities for the four groups as reported in Riedel et al. (2014), where we have doubled the sizes of the value ranges given in order to trace the ellipses. There are six stars represented by encircled letters reported to be members of the groups that fall outside the ellipses. These are six out of seven moving group stars with radial velocity values that are discordant between our measurements and those from *Gaia*.[1] The implications of these offsets is that neither the CHIRON nor *Gaia* measurements may, in fact, represent each system's γ velocity, and only when a radial velocity orbit is determined and the true systemic velocity derived can these stars be placed confidently in their relative groups.

Note that the field star PX Vir has been identified as a member of the AB Dor moving group by Zuckerman et al. (2004). AB Dor group members typically have UVW space motions of $(-7,\ -27,\ -13)$ (Riedel et al. 2014), but our derived measurements for PX Vir $(-3,\ -31,\ -3)$ are significantly different than these values, given errors of less than 1 km/s. However, because PX Vir is a close binary, the offset in UVW may simply be due to measuring the close pair at an epoch with an RV that does not match the AB Dor moving group. Whereas PX Vir's EW[Li I] = 0.15 is consistent with AB Dor K dwarfs, it has EW[Hα] = 0.87, which is a deeper absorption feature than all but one AB Dor member, UY

[1]The seventh star is AO Men and does fall within the oval for β Pic.

Pic. A final comparison can be made using the Ca II feature — UY Pic and all other slow rotators in the AB Dor group show a re-emission feature, but PX Vir does not. Given this ensemble of attributes, we conclude that PX Vir is *not* a member of AB Dor.

Table 4.2: Dynamical and color information for Benchmark sample stars.

Name	†Group	R.A.	Decl.	$\mu_{R.A}$	μ_{Decl}	π	σ_π	B_{Gaia}	B_G−K_S	γ_{REC}	$\sigma_{\gamma_{REC}}$	γ_{Gaia}	U	V	W
...	...	J2000.0	J2000.0	mas yr^{-1}	mas yr^{-1}	mas	mas	mag	mag	km s^{-1}	km s^{-1}	km s^{-1}	km s^{-1}	km s^{-1}	km s^{-1}
(1)	(2)	(3)	(4)	(5)	(6)	(7)	(8)	(9)	(10)	(11)	(12)	(13)	(14)	(15)	(16)
V1005 Ori	βP	04 59 34.8	+01 47 01	39.130	−94.900	40.990	0.013	10.26	4.00	18.832	0.198	18.079	−12.2	−16.2	−9.2
CD-57 1054	βP	05 00 47.1	−57 15 25	35.388	74.113	37.212	0.013	10.33	4.08	19.077	0.105	18.073	−11.1	−16.4	−9.0
AO Men	βP	06 18 28.2	−72 02 41	−7.709	74.412	25.566	0.013	9.91	3.09	16.575	0.435	10.952	−10.4	−16.8	−8.8
HD 139084	βP	15 38 57.6	−57 42 27	−54.602	−92.786	25.829	0.201	8.08	2.23	−0.286	0.483	3.900	−11.2	−14.4	−7.7
CD-54 7336	βP	17 29 55.1	−54 15 48	−5.490	−63.435	14.790	0.014	9.78	2.41	0.360	0.307	1.6*	−8.4	−16.2	−9.1
HD 161460$^\diamond$	βP	17 48 33.7	−53 06 43	−6.730	−57.235	13.053	0.114	9.28	2.50	1.321	0.237	11.189	−7.3	−18.0	−7.9
CD-64 1208	βP	18 45 36.9	−64 51 47	19.891	−154.401	35.158	0.181	9.61	3.51	−2.071	5.739	7.939	−13.9	−14.7	−6.0
CD-26 13904	βP	19 11 44.7	−26 04 08	21.447	−48.196	14.769	0.212	10.50	3.13	−9.465	0.186	−8.1*	−10.0	−13.8	−9.3
CPD-72 2713	βP	22 42 48.9	−71 42 21	94.854	−52.384	27.231	0.011	10.67	3.77	8.006	0.081	7.019	−10.3	−15.8	−8.0
CD-78 24	TH	00 42 20.3	−77 47 39	79.965	−29.881	20.084	0.009	10.42	2.89	11.159	0.531	10.994	−9.0	−21.1	−2.3
CD-34 521	TH	01 22 04.4	−33 37 03	109.930	−57.349	25.904	0.016	11.27	3.82	4.719	0.074	3.985	−9.9	−20.9	−1.1
CC Phe	TH	01 28 08.6	−52 38 19	106.287	−43.149	25.110	0.011	9.49	2.65	8.052	0.054	7.825	−9.7	−20.9	−0.9
BD-15 705	TH	04 02 16.4	−15 21 29	66.103	−26.834	18.282	0.013	10.30	2.72	15.502	0.109	14.553	−11.6	−21.1	−1.5
TYC 8083-455-1	TH	04 48 00.6	−50 41 25	56.404	19.164	17.194	0.023	11.88	3.96	19.331	0.070	19.3*	−11.6	−22.5	−0.9
TYC 8098-414-1	TH	05 33 25.5	−51 17 13	42.970	26.107	18.560	0.012	12.00	3.84	20.448	0.128	19.472	−10.5	−21.7	−1.5
HD 35650	ABD	05 24 30.1	−38 58 10	43.159	−57.276	57.271	0.015	9.27	3.35	32.330	0.057	32.078	−8.0	−28.0	−15.3
AB Dor	ABD	05 28 44.9	−65 26 55	37.554	158.574	67.333	0.441	7.15	2.46	19.191	0.868	29.500	−9.8	−17.8	−9.3
UY Pic	ABD	05 36 56.9	−47 57 53	23.129	−1.134	40.657	0.014	7.96	2.15	32.596	0.157	32.359	−7.3	−28.1	−15.0
CD-61 1439	ABD	06 39 50.0	−61 28 41	−26.991	75.011	45.033	0.012	10.02	3.52	31.617	0.050	31.576	−7.7	−28.3	−14.5
V429 Gem	ABD	07 23 43.5	+20 24 58	−65.642	−230.692	36.086	0.019	10.23	3.35	7.988	0.167	7.066	−5.1	−27.2	−17.0
HD 201919	ABD	21 13 05.2	−17 29 12	79.282	−146.185	26.021	0.016	10.89	3.31	−7.394	0.108	−8.502	−6.9	−27.4	−13.3

Continued on next page

Table 4.2 – *Continued from previous page*

Name	†Group	R.A.	Decl.	$\mu_{R.A}$	μ_{Decl}	π	σ_π	B_{Gaia}	$B_G - K_S$	γ_{REC}	$\sigma_{\gamma_{REC}}$	γ_{Gaia}	U	V	W
...	...	J2000.0	J2000.0	mas yr^{-1}	mas yr^{-1}	mas	mas	mag	mag	km s^{-1}	km s^{-1}	km s^{-1}	km s^{-1}	km s^{-1}	km s^{-1}
(1)	(2)	(3)	(4)	(5)	(6)	(7)	(8)	(9)	(10)	(11)	(12)	(13)	(14)	(15)	(16)
LO Peg	ABD	21 31 01.7	+23 20 07	134.654	−144.889	41.291	0.017	9.50	3.12	−41.571	1.664	−23.355	−11.2	−45.5	−7.0
HD 285507	HYA	04 07 01.2	+15 20 06	124.626	−19.786	22.229	0.017	10.70	3.03	37.912	0.046	38.121	−42.6	−18.7	−1.5
HD 285625	HYA	04 15 10.4	+14 23 54	114.581	−18.388	20.978	0.018	11.75	3.62	38.267	0.051	37.622	−42.1	−19.4	−1.0
V989 τ	HYA	04 23 25.2	+15 45 47	125.173	−26.474	24.134	0.025	10.70	3.21	38.408	0.046	38.423	−41.6	−19.3	−0.6
HD 286734	HYA	04 23 54.4	+14 03 07	115.516	−19.066	23.111	0.019	11.10	3.32	39.637	0.040	39.545	−42.4	−18.7	−1.5
HD 285828	HYA	04 27 25.3	+14 15 38	102.458	−19.956	20.422	0.192	10.62	2.91	44.302	0.042	39.248	−46.4	−19.6	−3.0
HD 285830	HYA	04 27 47.0	+14 25 04	100.550	−19.200	20.353	0.016	9.68	2.33	39.576	0.049	39.592	−42.0	−19.1	−1.2
HD 285876	HYA	04 31 52.4	+15 29 58	105.365	−24.241	21.872	0.016	11.24	3.34	40.315	0.044	40.443	−42.5	−19.1	−1.2
HD 29159	HYA	04 36 05.2	+15 41 02	95.399	−24.022	19.993	0.018	9.57	2.20	40.784	0.052	40.619	−42.7	−19.6	−1.0
o^2 Eri	Field	04 15 16.3	−07 39 10	−2240.085	−3421.809	199.608	0.121	4.61	2.20	−42.325	0.038	−42.621	96.8	−12.4	−41.3
HD 50281	Field	06 52 18.1	−05 10 25	−543.690	−3.515	114.355	0.042	6.80	2.69	−7.057	0.038	−7.204	0.0	12.8	−19.9
20 Crt	Field	11 34 29.5	−32 49 53	−670.230	822.399	104.613	0.028	6.15	2.13	−21.912	0.040	−21.974	−47.5	19.5	12.3
PX Vir	Field	13 03 49.7	−05 09 43	−191.130	−218.730	46.100	0.810	7.87	2.36	9.149	0.074	−7.547	−2.9	−30.9	−3.3
ϵ Indi	Field	22 03 21.7	−56 47 10	3966.661	−2536.192	274.843	0.096	4.91	2.67	−40.096	0.035	−40.504	−80.8	−40.9	2.3
V834 Tau	RVV	04 41 18.9	+20 54 05	−234.261	−254.314	75.687	0.024	8.16	3.01	0.995	0.170	0.546	5.0	−3.5	−20.8
DX Leo	RVV	09 32 43.8	+26 59 19	−147.260	−246.593	55.329	0.021	7.21	2.09	8.309	0.087	7.936	−10.1	−23.3	−5.6
BD+05 2529	RVV	11 41 49.6	+05 08 26	230.643	−469.130	31.762	0.381	9.80	3.37	18.909	0.040	19.141	62.7	−50.2	−0.5
HD 105065	RVV	12 05 50.7	−18 52 31	−15.018	−317.780	43.365	0.092	10.21	3.59	−53.945	0.051	−29.157	1.2	17.8	−61.7
HD 112099	RVV	12 53 54.4	+06 45 46	−231.846	93.538	36.594	0.061	8.44	2.29	−26.576	0.039	−18.923	−36.6	0.7	−20.4
BD+01 3657	RVV	18 22 17.2	+01 42 25	84.197	−19.688	37.864	0.017	10.35	3.49	−16.972	0.088	−16.802	−14.6	−5.8	−12.6
DG Cap	RVV	20 41 42.2	−22 19 20	656.071	−538.708	41.326	0.042	10.08	3.48	−46.001	0.085	−62.133	−68.1	−66.6	−50.3

Notes: (1) object identifier, (2) sample, (3) right ascension, (4) declination, (5) & (6) proper motion, (7) trigonometric parallax, (8) error in trigonometric parallax, (9) *Gaia* EDR3 BP

magnitude = B_{Gaia}, (10) long baseline color, (11) CHIRON γ velocity, (12) error in CHIRON γ velocity, (13) *Gaia* DR2 γ velocity, and (14) U (15) V (16) W space velocity components.

[†]Moving groups located in the second column are denoted by the following:

βP = Beta Pictoris

TH = Tucana-Horologium

ABD = AB Doradus

HYA = Hyades

Field = K Field Star

RVV = RV Variable Star

[*]Measurements obtained from Torres et al. (2006)

[◇]Astrometry obtained from *Gaia* DR2

4.5 Companions

4.5.1 Sweep for Companions to All 42 Benchmark Stars

We have used both *Gaia* EDR3 (Gaia Collaboration et al. 2021) and the Washington Double Star (WDS) Catalog (Mason et al. 2001) to search for and confirm existing companions to the targets in our sample. In all, 16 of the 42 systems are multiples, with details given in Table 4.3. In addition to identifiers and coordinates, we list the parallaxes and errors from EDR3, and the separations (ρ) and position angles (θ) from EDR3 or WDS. To assist in tracking the components, we also provide magnitudes, colors, and spectral types for each component, where available. Note that many potential components listed in WDS have been eliminated using *Gaia* data.

The search for companions in the EDR3 results was conducted using a search radius of $60'$, with an additional constraint of $\pi > 10$ mas, a value representative of the sample given that all of our sample stars are within 100 pc. This yielded a wealth of candidates, which were then winnowed to potential companions worthy of scrutiny by imposing a condition that parallaxes needed to match within ± 0.5 mas, a value that works well to identify true binaries when applied to stars within 100 pc during other RECONS-related surveys. However, for stars in moving groups it is possible that stars with similar π values are not gravitationally-bound companions, but merely members of the same moving association; this is especially evident in the Hyades cluster. To reveal true companions, we adopted a projected physical separation limit of $\leq 10^4$ AU, a conservative value that captures the few widely-separated true companions to stars in the solar neighborhood, but allows for manageable vetting for

possible companions that does not result in overwhelming numbers of false positives. We then consulted the WDS to determine whether or not the EDR3 companions were previously recorded. We also made a comprehensive sweep of all 42 stars in WDS for companions, including stars that may not have had any candidate companions in EDR3. We found that the companions with separations $\rho > 2''$ were generally in both EDR3 and WDS, and those at smaller separations were in WDS only.

4.5.2 Discovery of a Tertiary in the HD 161460 System

During the companion search, we found a previously unreported companion to the known binary, HD 161460, which is a member of β Pic. The third component is a 14^{th} mag star separated $31.5''$ from the primary, corresponding to a projected separation of $\sim$2400 AU, and is found at a position angle of 0.1°, effectively due north. This was not found to be a companion candidate in our EDR3 search because astrometric information for the primary is absent, presumably because it is a close binary. However, *Gaia* DR2 parallax measurements confirm the companion to be real, given parallaxes in DR2 differing by only 0.004 mas. Matching proper motions between both components provide further verification that the tertiary is part of the HD 161460 system.

4.5.3 Spectroscopic Binaries in our Variable Radial Velocity Sample

Of the seven K dwarfs targeted as RVV stars, four turned out to be spectroscopic binaries for which insufficient CHIRON data were available for solutions when this sample was created. The companions of DG Cap (HIP 102119) and HD 105065 (HIP 59000) are reported here

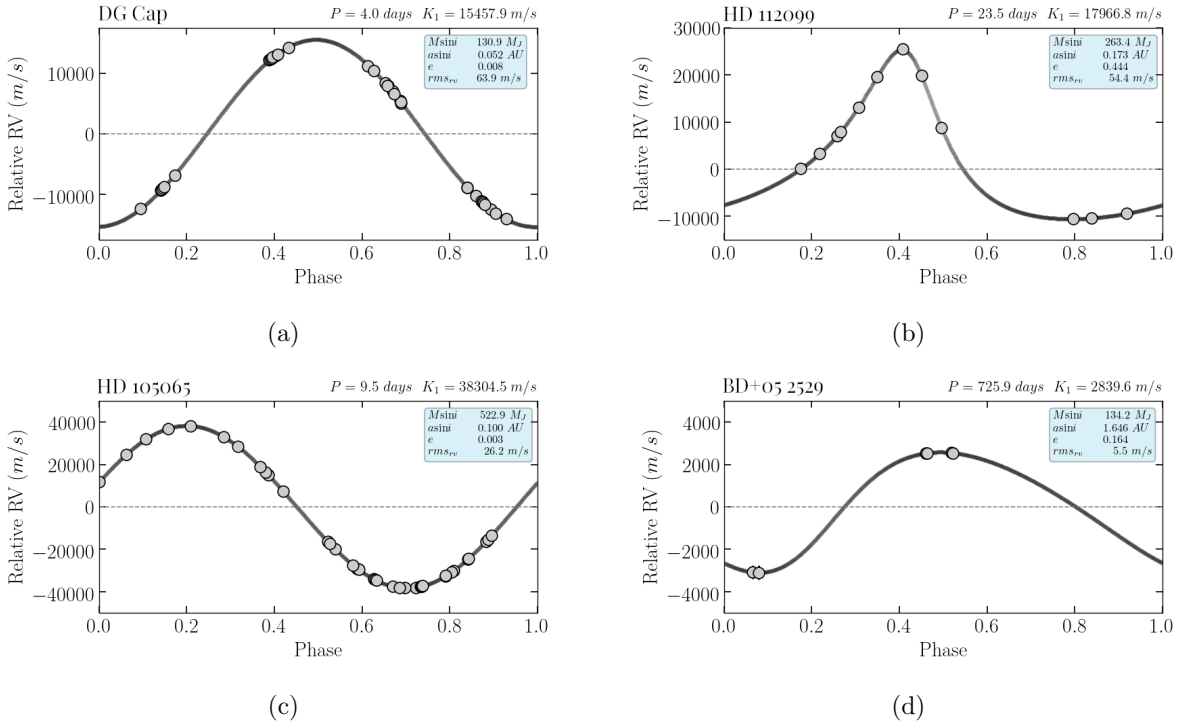

Figure 4.11 Phase-folded RV curves for (a) the newly discovered binary DG Cap, (b) the previously reported binary HD 112099, (c) the newly discovered binary HD 105065, and (d) the previously reported binary BD+05 2529.

for the first time, while those of HD 112099 (HIP 62942) and BD+05 2529 (HIP 57058) were previously reported by Griffin (2009) and Sperauskas et al. (2019), respectively. CHIRON data were reduced as described in Chapter 3 and phased to produce the RV curves shown in Figure 4.11 for DG Cap (HIP102119) with a period of 4.0 days and HD 105065 (HIP059000) with a period of 9.5 days. In §4.2.1 both (3) DG Cap, and (5) HD 105065, were flagged as being active based on the presence of Hα emission that is shown in Figure 4.2, but the activity may be induced by the close companion in each case.

Figure 4.11 also shows the CHIRON orbits of HD 112099 (HIP062942) and BD+05 2529 (HIP057058). For HD 112099, the 13 CHIRON measurements taken over 12 months yields

an orbital period of 23.5 days, matching the value given by Griffin (2009). For BD+05 2529, only 8 CHIRON measurements are available over 15 months, but that is sufficient to produce an orbital fit with a period of 726 days that is consistent with that derived by Sperauskas et al. (2019). While more data should be acquired to firm up both orbits, it is clear that the CHIRON data indicate changing RVs due to companions in both cases, and that neither system is necessarily young.

4.6 Benchmark Sample Systems that are Worthy of Note

Here we provide details for systems with notable attributes, listed in order of Right Ascension, with coordinate designations to start each entry. This list includes all of the RVV stars (numbered (1) through (7)) in Figure 4.7 and the lettered stars worthy of further comment in Figure 4.10(a).

0427+1415: (k) **HD 285828** is a known SB1 (Griffin 2012), which provides a ∼5 km/s offset in RV measurements between our CHIRON and *Gaia* epochs. This results in a slight offset of the point from the Hyades ovals in the panels of Figure 4.10. Nonetheless, the star is, indeed, a member of the Hyades.

0441+2054: (2) **V834 Tau** is a known rapid rotator, and was classified as a BY Draconis variable by Mishenina et al. (2012). BY Draconis variables are K or M type main sequence stars that exhibit variations in luminosity over short time periods primarily due to rotation

Table 4.3: K dwarf systems confirmed via *Gaia* EDR3 and WDS to have companions.

Target WDS Name (1)	Comp (2)	R.A. J2000.0 (3)	Decl. J2000.0 (4)	π mas (5)	σ_π mas (6)	ρ arcsec (7)	θ deg (8)	B_G mag (9)	K mag (10)	B_G−K mag (11)	Spectral Type (12)
o^2 Eri	A	04 15 16.3	−07 39 10	199.608	0.121	···	···	4.61	2.50	2.11	K0V
04153-0739 STF518	B	04 15 21.8	−07 39 29	199.691	0.051	83.34	var[a]	9.48	9.86	-0.38	DA3
04153-0739 STF518	C	04 15 21.5	−07 39 20	199.452	0.069	78.10	97.5	11.49	5.96	5.53	M5V
HD 285828[b]	A	04 27 25.3	+14 15 38	20.422	0.192	···	···	10.62J[c]	7.71J	2.91J	K2
···	B	···	···	···	···	SB1[d]	···	···	···	···	···
HD 285830	A	04 27 47.0	+14 25 04	20.353	0.016	···	···	9.68	7.35	2.33	K0
04278+1425 PAT9	B	···	···	···	···	0.91	15.0	···	···	···	···
AB Dor	A	05 28 44.9	−65 26 55	67.333	0.441	···	···	7.15	4.69	2.46	K0V
AB Dor	C	···	···	···	···	0.20	∼156	···	···	···	M8
05287-6527 CLO10	Ba	05 28 44.5	−65 26 46	66.992	0.081	8.92	347.1	13.08J	7.34J	5.74J	M5
05287-6527 CLO10	Bb	···	···	···	···	≤ 2.0	var	···	···	···	L5
UY Pic	A	05 36 56.9	−47 57 53	40.657	0.014	···	···	7.96	5.81	2.15	K0V
05369-4758 HDS751	B	05 36 55.1	−47 57 48	40.758	0.040	18.26	285.9	10.02	6.61	3.42	K6Ve
HD 50281	A	06 52 18.1	−05 10 25	114.355	0.042	···	···	6.80	4.11	2.69	K3V
06523-0510 WNO17	B	06 52 18.0	−05 11 24	114.291	0.022	58.83	180.6	10.33	5.72	4.60	M2V
DX Leo	A	09 32 43.8	+26 59 19	55.329	0.021	···	···	7.21	5.12	2.09	K0V
09327+2659 LDS3903	B	09 32 48.2	+26 59 44	55.292	0.071	65.01	67.3	16.06	9.47	6.58	M5V
20 Crt	A	11 34 29.5	−32 49 53	104.613	0.028	···	···	6.15	4.14	2.02	K0V
11345-3250 LDS6245	B	11 34 30.5	−32 50 02	104.657	0.027	15.30	128.3	14.92	···	···	DC8
BD+05 2529[e]	A	11 41 49.6	+05 08 26	31.762	0.381	···	···	9.80J	6.43J	3.37J	K4V
···	B	···	···	···	···	SB1	···	···	···	···	···
HD 105065	A	12 05 50.7	−18 52 31	43.365	0.092	···	···	10.21	6.62	3.59	K5V
12058-1853 WNO54	B	12 05 46.6	−18 49 32	43.695	0.030	187.77	342.2	16.49	10.32	6.18	M5V
HD 112099[f]	A	12 53 54.4	+06 45 46	36.594	0.061	···	···	8.44J	6.15J	2.29J	K1V
···	B	···	···	···	···	SB1	···	···	···	···	···
PX Vir	A	13 03 49.7	−05 09 43	46.100	0.810	···	···	···	5.72	···	K1V
13038-0510 EVT3	B	···	···	···	···	< 0.05	var	···	7.00	···	···
HD 139084	Aa	15 38 57.6	−57 42 27	25.829	0.201	···	···	8.08J	5.85J	2.23J	K0V
15390-5742 NLS2	Ab	···	···	···	···	∼0.1	var	···	···	···	MV
15390-5742 SKF1501	B	15 38 56.8	−57 42 19	25.440	0.017	10.32	323.3	14.95	9.19	5.77	M5Ve
HD 161460	A	17 48 33.7	−53 06 43	13.053	0.114	···	···	9.28J	6.78J	2.50J	K0IVJ
17486-5307 CVN29	B	···	···	···	···	SB2	···	···	···	···	···
···	C[g]	17 48 33.7	−53 06 12	13.049	0.019	31.5	0.1	14.21	9.27	4.95	···
18454-6452 SKF105	A	18 45 26.9	−64 52 17	34.736	0.158	···	···	4.83	4.30	0.53	A7V
CD-64 1208	Ba	18 45 36.9	−64 51 47	35.158	0.181	71.34	64.6	9.61	6.10	3.51	K5Ve
18454-6452 BIL4	Bb	···	···	···	···	0.18	∼95	···	···	···	K7
ϵ Indi	A	22 03 21.7	−56 47 10	274.843	0.096	···	···	4.91	2.24	2.67	K4V
22034-5647 SOZ1	Ba	22 04 10.5	−56 46 57	270.658	0.690	402.46	88.4	21.14J	11.21J	9.93J	T1V
22034-5647 VLK1	Bb	···	···	···	···	< 1.0	var	···	···	···	T6V

Notes for Columns: (1) object identifier (top) and WDS designation (bottom), (2) system component, (3) Right Ascension, (4) Declination, (5) trigonometric parallax, (6) error in trigonometric parallax, (7) angular separation from primary, (8) position angle relative to primary, where north is 0° and east is 90°, (9) *Gaia* EDR3 BP magnitude = B_G, (10) 2MASS K magnitude, (11) color, and (12) spectral type. Names are provided for targets included in the target sample and are not necessarily the system's primary.

[a] Varies in value
[b] Binary determination provided by Griffin (2012)
[c] Joint value indicated with J includes components below it
[d] SB1/SB2 indicates a single-lined/double-lined spectroscopic binary
[e] Binary determination provided by Sperauskas et al. (2019)
[f] Binary determination provided by Griffin (2009)
[g] New tertiary (see § 4.5.2)

(Mishenina et al. 2012). Mamajek & Hillenbrand (2008) reported an estimated age for V834 Tau of 49 ±37 Myr, using rotation–age and Calcium H and K emission–age correlations. This age estimate aligns with the trends shown in Figure 4.7, as all four plots presented there identify V834 Tau as young and active. Lehtinen et al. (2016) lists this dwarf as a member of Ursa Major moving group. However, using BANYAN Σ we find V834 Tau to be a field dwarf.

0528–6526: (j) **AB Dor** is the eponymous quadruple system central to the AB Doradus moving group. It is comprised of two wide binaries with primaries known as A and B separated by ∼9″, each with its own close component. As noted by Zuckerman et al. (2004), the AB Dor components have rapid rotation rates, with the A component rotating in 0.514 days and the B component in 0.38 days (Azulay et al. 2015). This elucidates both its highly broadened spectral lines displayed in Figure 4.1 and the difference between its γ velocity we and *Gaia* measure (Table 4.2). Our γ velocity for component A was used to compute the system's UVW, but that value catches the close pair at a velocity that does not represent the system's true velocity. Therefore, AB Dor falls outside the AB Dor region in Figure 4.10.

0932+2659: (1) **DX Leo** presented the greatest EW[Li I] value, 0.18 Å, of all the RVV K dwarfs examined. The star has $B_G - K = 2.09$, which meets our K dwarf inclusion criteria despite the G9V spectral type given in SIMBAD. DX Leo is classified as a BY Draconis variable in SIMBAD due to observed changes in luminosity caused by rapid rotation (Griffin 1994). Using the *Gaia* parallax and position data, along with Gagne et al. (2018)'s BANYAN

Σ code, we were able to show that DX Leo is a field star and not a member of any known moving association. Wang & Wei (2009) had already identified DX Leo as a young dwarf with a EW[Li I] value of 0.20 ± 0.005 Å and an age estimate of 30–100 Myr. We note that both results are similar to values measured for K dwarfs in the Pleiades, which have EW[Li I] of 0.1–0.2 Å and are ∼125 Myr old (Bouvier et al. 2018). Thus, our findings corroborate this age estimation and firmly characterize DX Leo as a young K dwarf within 20 pc.

1141+0508: (7) **BD+05 2529** is listed as a double-lined spectroscopic binary (SB2) by Halbwachs et al. (2018) using CORAVEL spectra. A year later, Sperauskas et al. (2019) used CORAVEL plus UVES echelle spectrograph data to identify BD+05 2529 as an SB1. In our study that was solely dependent on CHIRON spectra, we observed no evidence of double lines for this spectroscopic binary. However, in Figure 2.3 we clearly observe BD+05 2529 as the RVV star that is elevated above the main sequence, presumably because of the excess flux of the companion. There is an absence of the Li I, Hα, and Ca II signatures, as illustrated in Figure 4.2 and plot (b) & (c) of Figure 4.7. BANYAN Σ identified this as a field dwarf, and we concur.

1205–1852: (5) **HD 105065** (also (a)) was identified as active by Martinez-Arnaiz et al. (2010) with a $\log R'_{HK}$ of −4.12 and Gray et al. (2006) with a S-index of 3.15. Using the $\log R'_{HK}$ thresholds of activity set by Henry et al. (1996), HD 105065 is classified as very active with a value > -4.20. Hα is in absorption (Table 4.1), but the feature is weaker than

for Hyades cluster K dwarfs with estimated ages $\geq$ 700 Myr, implying youth. However, we have found that this is a close binary with orbital period of 9.5 days, and the companion may be inducing the activity. BANYAN Σ indicates that this as a field dwarf.

1253+0645: For (6) **HD 112099** (also (d)), our study reported EW[Hα] & EW[Li I] values below the thresholds set for high activity and youth. Plot (d) in Figure 4.7 illustrates this result with HD 112099 located firmly in the old locus of K dwarfs. Table 4.3 shows that Strassmeier et al. (2000) identified this target as a single-lined spectroscopic binary (SB1), however no orbital parameters were included with the first detection. Later, Griffin (2009), used observations from Strassmeier et al. (2000) to estimate a period of 23.5 days for the binary system. In contrast to our findings of inactivity based on the lack of Hα and Ca II emission in Figure 4.2, Gray et al. (2003), reported a $\log R'_{HK}$ of -4.71 and classified the star as active. However, using Henry et al. (1996)'s $\log R'_{HK}$ thresholds, HD 112099 would only be described as moderately active. BANYAN Σ indicates that this as a field dwarf, and we conclude that it is not particularly young.

1303–0509: (h) **PX Vir** is a close binary that has been previously identified as a member of the AB Doradus moving group (Schaefer et al. 2018; Zuckerman et al. 2004). However, we find from its spectral features that it shows signs of both inactivity and youth. The spectrum of PX Vir shown in Figure 4.2 contains Hα, Ca II (with no core emission), and Li I features, all in absorption. The former two indicate the system's lack of activity, which

would typically coincide with older stars. Yet, this is the only member of the field group to exhibit clear Li I absorption, a signature of youth. In addition, BANYAN Σ indicates that PX Vir is not a member of AB Dor, and is instead a field star. We propose that the PX Vir system be reclassified to the group of field stars.

1822+0142: (4) **BD+01 3657** is listed in SIMBAD as a rotationally variable star. Gray et al. (2006) tagged the dwarf as very active, with a –4.055 dex $\log R'_{HK}$ value, which is derived from the chromospherically sensitive Calcium H and K lines. We observe strong core emission in Hα, as shown in Figure 4.2 and derive EW[Hα] = -0.55, which agrees with the Gray et al. (2006) result. BANYAN Σ identified BD+01 3657 as a field dwarf, but it shows clear evidence of activity, implying youth.

1845–6451: (e) **CD−64 1208** is a close multiple. This triple exhibits some of the most rapid rotation observed in the β Pic moving group (Garcia-Alvarez et al. 2011), with a reported period 0.354 days by Messina et al. (2010). This explains the system's very broad and shallow spectral features (Figure 4.1) and disagreement between our γ velocity and that from *Gaia*.

2041–2219: (3) **DG Cap** (also (b)) is listed as having a very active chromosphere by Gray et al. (2006). Our chromospheric indicators, Hα and Ca II, confirm the star to be active, with significant core emission in both lines (Figure 4.2) — it exhibits the strongest

Hα emission of the seven RVV stars, with EW[Hα] = -0.85. This star turns out to be the fastest orbiting spectroscopic binary of the 7 RVV stars, with an orbital period of only 4.0 days. Presumably the companion is responsible for the inducing the activity, given the BANYAN Σ code showed no membership to any known moving associations.

2131+2320: ⓒ **LO Peg** is a variable star with an active chromosphere and an ultrafast rotational period of 0.423 days (Jeffries et al. 1994; Garcia-Alvarez et al. 2011). We show its Doppler-broadened spectrum in Figure 4.1, which presumably explains the difference between our γ velocity and that from *Gaia*.

In our analysis of the 7 RVV stars, we found that 5 exhibit indicators of activity and/or youth. Among these, 2 stars, specifically, manifest genuine signs of youth. The remaining 3 stars display activity indicators, two of which are possibly influenced by the presence of close companions, leading us to classify them as field stars. We also report the discovery of new companions to three of the stars. Close companions have been identified around DG Cap and HD 105065, exhibiting orbital periods of 4.0 and 9.5 days respectively. Additionally, a wide companion has been found orbiting HD 161460 at a substantial separation of 31.5″.

CHAPTER 5

Spectral and Kinematic Analysis of the Primary Sample of 615 K Dwarfs

5.1 Overview of Results

This work resulted in the collection of spectra for 615 K dwarfs within 33 pc of the Sun in an equatorial band of the sky spanning Declinations $+30°$ to $-30°$. These spectra have been analyzed to reach the goals of evaluating the stars as an ensemble to understand them as a population and to highlight intriguing individual stars. In this Chapter we describe the results, beginning with an overview of the spectral library created for the K dwarfs, including assessments of 50 individual stars worthy of note and the identification of two new double-lined spectroscopic binaries. This is followed by the results of spectral characterization efforts, including (a) identifying active and young stars in the Primary Sample via comparison to the Benchmark Sample described in Chapter 4, (b) deriving stellar properties for the stars, and (c) calculating the kinematic properties of the stars and evaluating what the results mean. For each of these efforts, spectra for most of the 615 stars can be used, although a small portion is dropped because either the stars are rapidly rotating and preclude analysis, or the individual spectra are too low S/N to yield reliable results.

5.2 Spectral Library of Primary Sample K dwarfs

In the framework of this investigation, we've developed a specialized spectral library[1], comprising (exactly) 600 CHIRON spectra of K dwarfs with a diverse range of $T_{\rm eff}$ and

[1] https://hodarijames.github.io/spectral$_l$*ibrary*/*page*1.*html*.*html*

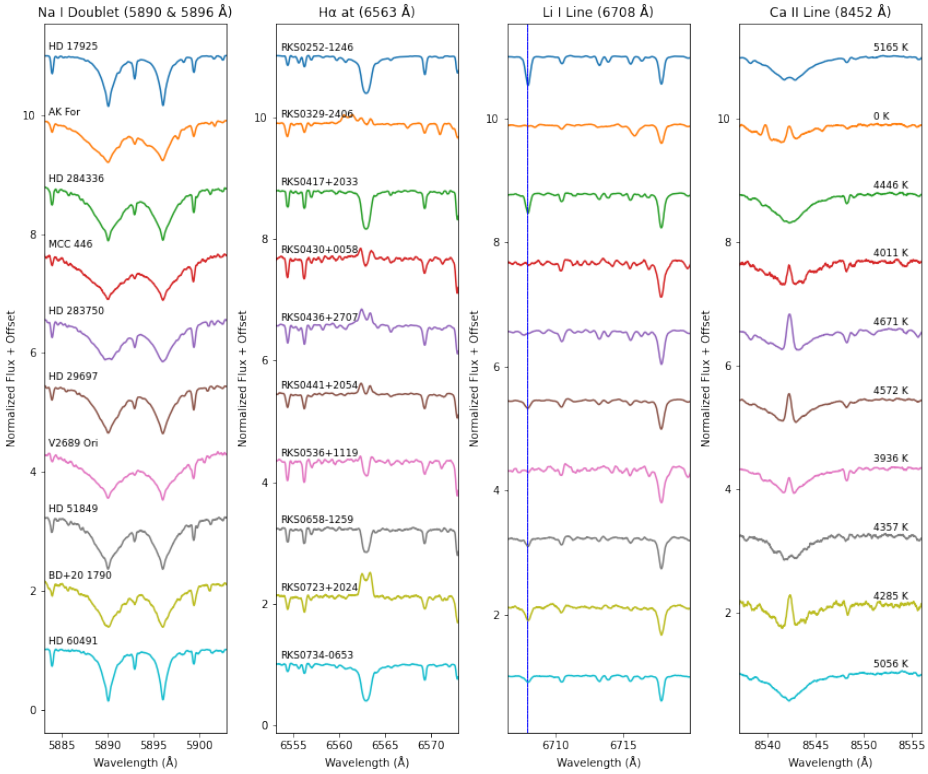

(a) Group A: RKS Names - RKS0252-1246 (young), RKS0329-2406 (active & SB2), RKS0417+2033 (young), RKS0430+0058 (active), RKS0436+2707 (active), RKS0441+2054 (young & active), RKS0536+1119 (active), RKS0658-1259 (young & active), RKS0723+2024 (young & active), RKS0734-0653 (young)

Figure 5.1 Spectral Plots for Noteworthy Systems from the Primary Sample (Group A)

[Fe/H]values. However, 15 stars have been excluded from further evaluation due to their inadequate signal-to-noise ratio (S/N). With S/N values less than 25, the quality of these spectra is insufficient for accurate and reliable interpretation. For more information regarding our S/N cutoff, please refer back to §3.4. This library primarily focuses on an intricate examination of four key spectral features that have been elaborated upon extensively in this thesis. These include the Na I doublet (at 5891.58 and 5897.56 Å), the Hα line (at 6562.8 Å), the Li I line (at 6707.8 Å), and the Ca II IRT line (at 8542 Å). Our spectral library, presented in a printed format in Appendix B, covers the broad spectrum of $T_{\rm eff}$ and

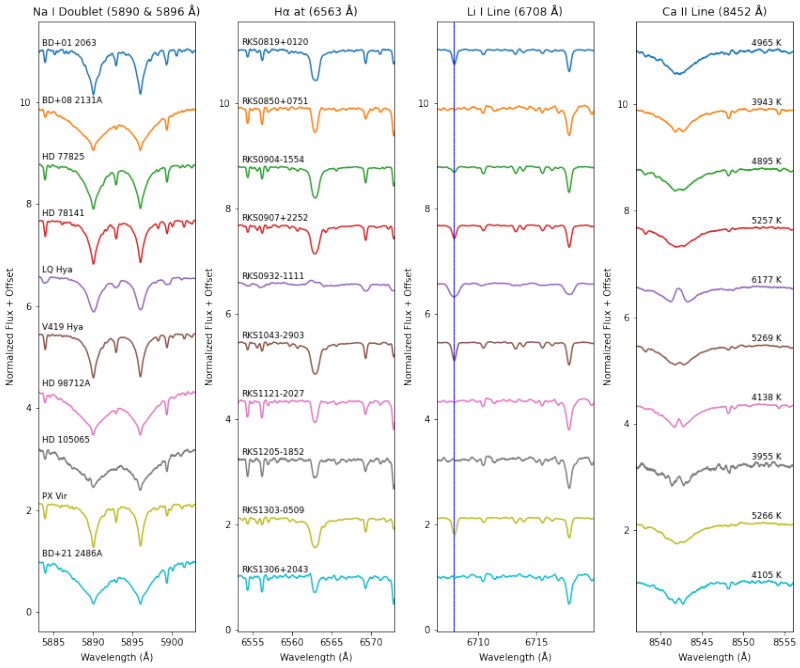

(a) Group B: RKS Names - RKS0819+0120 (young), RKS0850+0751 (active), RKS0904-1554 (young), RKS0907+2252 (young), RKS0932-1111 (young & active), RKS1043-2903 (young), RKS1121-2027 (active), RKS1205-1852 (active), RKS1303-0509 (young), RKS1306+2043 (active)

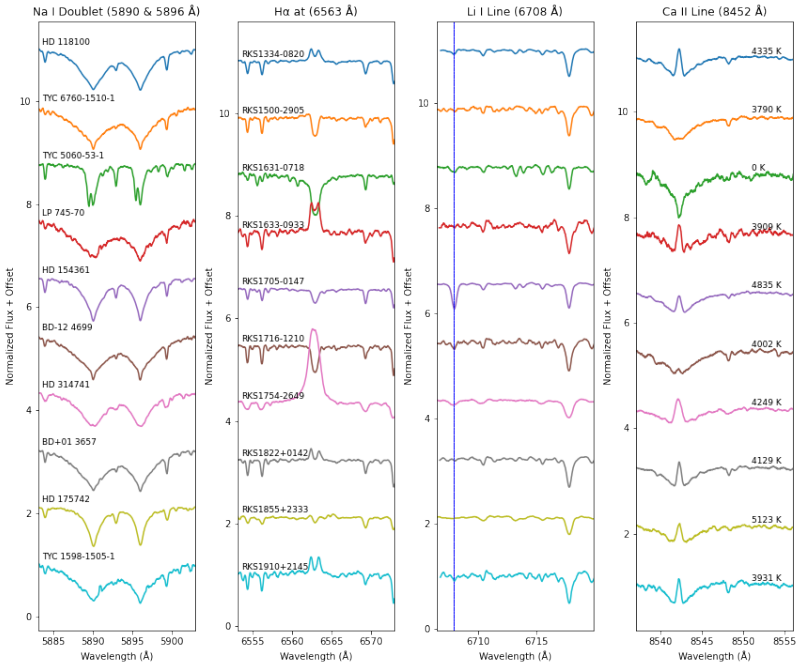

(b) Group C: RKS Names - RKS1334-0820 (active), RKS1500-2905 (active), RKS1631-0718 (young), RKS1633-0933 (active), RKS1705-0147 (young & active), RKS1716-1210 (young), RKS1754-2649 (young & active), RKS1822+0142 (active), RKS1855+2333 (active), RKS1910+2145 (active)

Figure 5.2 Spectral Plots for Noteworthy Systems from the Primary Sample (Group B & Group C)

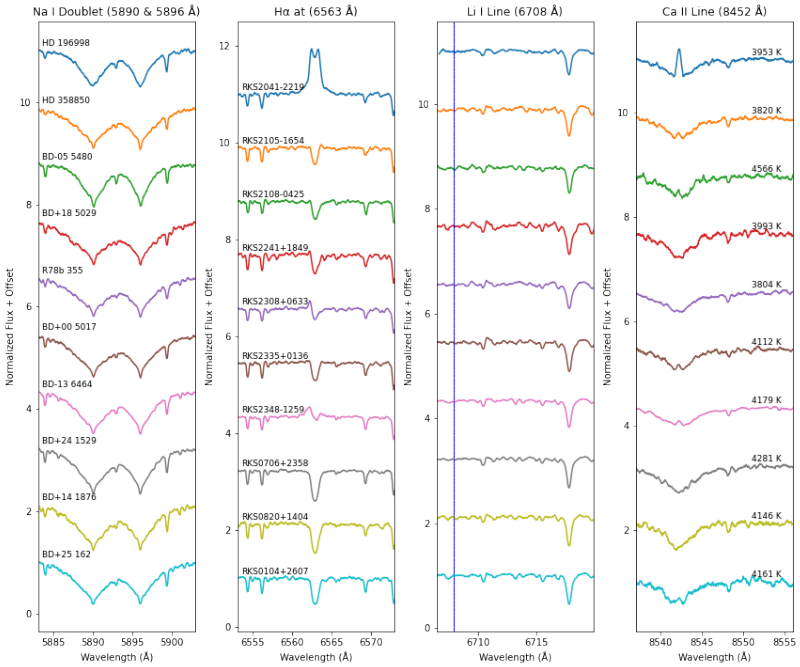

(a) Group D: RKS Names - RKS2041-2219 (active), RKS2105-1654 (active), RKS2108-0425 (active), RKS2241+1849 (active), RKS2308+0633 (active), RKS2335+0136 (active), RKS2348-1259 (active), RKS0706+2358 (young-AB Dor), RKS0820+1404 (young-AB Dor), RKS0104+2607 (young-Hyades)

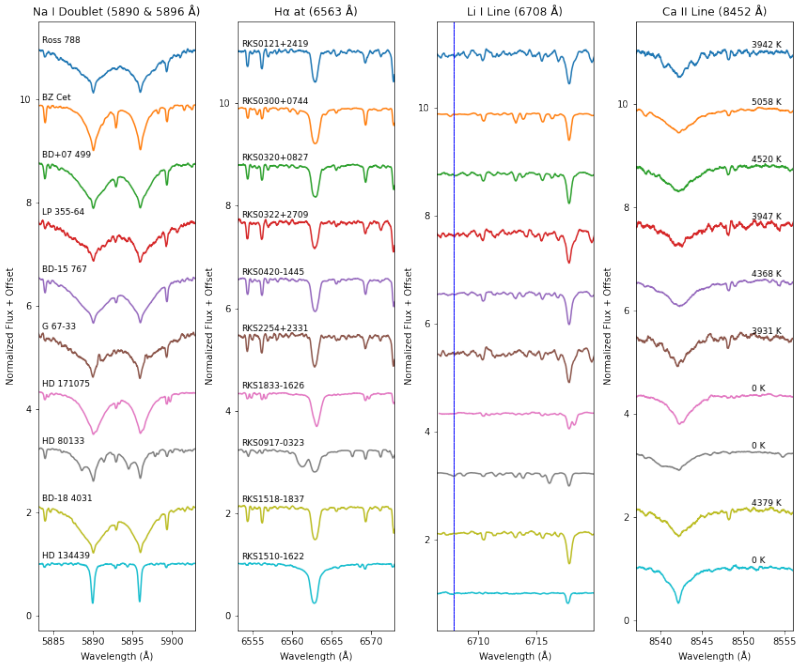

(b) Group E: RKS Names - RKS0121+2419 (young-Hyades), RKS0300+0744 (young-Hyades), RKS0320+0827 (young-Hyades), RKS0322+2709 (young-Hyades), RKS0420-1445 (young-Hyades), RKS2254+2331 (young-Hyades), RKS1833-1626 (new-SB2), RKS0917-0323 (new-SB2), RKS1518-1837 (possible white dwarf + K dwarf binary), RKS1510-1622 (halo star)

Figure 5.3 Spectral Plots for Noteworthy Systems from the Primary Sample (Group D & Group E)

[Fe/H]characterizing main sequence K stars. This extensive collection emphasizes the power of CHIRON's high-resolution spectra in recognizing subtle differences among K stars, and is paving the way for groundbreaking discoveries through the comparisons of stellar spectra.

Close examination of the spectra in the Spectral Library indicates that many of the stars are unusual compared to the majority of "normal" field K dwarfs. Figures 5.1, 5.2, and 5.3 exhibit spectra from 50 of these K dwarfs, based on their spectral properties and categorically arranged into five groups of 10 stars each — Groups A, B, C, D, E. Within each group, catalog names are given the in the first panel, RKS names in the second panel, a vertical blue line is shown at the location of the Li I line in the third panel, and the derived $T_{\rm eff}$ is given in the fourth panel. These figures offer a visual depiction of the variety of subgroups discernible within the spectra. The spectra are arranged in order of Right Ascension for the first 37 stars, all of which are active and/or young, as determined using the four features described below. These are followed by 13 stars, 2 of which are known AB Dor members and 7 of which are known Hyades members. The remaining four stars include two SB2s, one that is likely to have a white dwarf companion (RV plot given in §5.4.2), and one halo star. These stars are further elaborated upon in Section §5.8. There are myriad ways that the more than 600 stars might be compared to one another, so here we simply provide a few brief examples of how stars can be examined and related to one another.

Temperature Effects: Group A (Figure 5.1) includes stars that can be used to see the effects of temperature because there are perceptible differences in the Na I doublet line (shown in the far-left panel). Specifically, the lines are narrow for RKS0252-1246 with a

measured $T_{\rm eff}$ of 5165 K, but broaden discernibly in cooler K dwarfs such as RKS0417+2033 ($T_{\rm eff}$ = 4446 K) and RKS0430+0058 ($T_{\rm eff}$ = 4011 K). This transition is a clear indication of gravitational broadening, a phenomenon that was described in §3.5.

Activity Features: In Groups A, B, C, and D, we discern differences in chromospheric activity among stars, evident from the Hα (second panel) and Ca II (fourth panel from the right) lines. At least 10 stars show clear Hα emission features, and at least 20 show Ca II re-emission. For example, in Group C (see Figure 5.2), the Hα line exhibits emission in five of the ten stars presented, and there is strong core re-emission in the Ca II line for seven stars, with RKS1754-2649 showcasing the most pronounced re-emission feature. These emission features present a sharp contrast to the absorption lines characteristic of inactive stars, for which a full set of 10 are shown in Group E (see Figure 5.3). For instance, RKS0121+2419 and RKS0300+0744 exhibit the more commonly seen absorption lines for both Hα and Ca II. The emission at these lines, a trait typically associated with stars from young moving groups (as discussed in Section §4.2), is also discernible in Figure 4.1. This striking contrast in chromospheric activity, evident through our analysis of Hα and Ca II lines, highlights the power of spectroscopic methods in identifying and characterizing stellar populations.

Metallicity Differences: Group E also provides an opportunity to illustrate the differences evident in [Fe/H]among our K dwarfs by examining the presence or absence of Fe I lines, a notable characteristic of late-type stars. A prime example of this can be seen in Group E in Figure 5.3. The final star of this group, RKS1510-1622, is a known halo star with a [Fe/H]value of -1.44 dex, as reported in Soubiran et al. (2020)'s compilation of stel-

lar properties. Several Fe lines evident in other stars among the 50 shown are missing in RKS1510-1622, and in fact the Na I doublet is also much narrower. Upon closer inspection of RKS1510-1622's spectrum, particularly in the second panel (Hα panel) of Group E, we notice the absence of the two Fe I lines (at 6553.3 Å and 6556.8 Å), located to the left of the Hα line. Typically, these lines are prominent in the spectra of K dwarfs. In fact, the presence of these Fe I lines is distinctly apparent in the first six spectra of this group, including that of RKS0322+2709, which has a [Fe/H]value of + 0.13 dex, as determined in our study.

Spectroscopic Binaries: Our comprehensive Spectral Library also facilitates the visual detection of double-lined spectroscopic binaries (SB2s), as showcased in the spectra presented in Appendix B. Figures 5.1, 5.2, and 5.3 illustrate three among six SB2s that our library has helped identify. For instance, RKS0329-2406, represented in Group A of Figure 5.1, displays a distinctive spectrum characterized by both chromospheric activity and the presence of a binary system, as evidenced by the double-peaked Ca II core emission feature in the far-right panel. RKS1833-1626 and RKS0917-0323, found in Group E of Figure 5.3, are additional examples of SB2s. These systems are particularly noteworthy because they were first discovered during this study. The third panel of Group E (Li I panel) conspicuously presents a double-lined feature for the Ca I line at 6717 Å. Further discussions on these new discoveries can be found in Section §5.8.

To summarize, our spectral library facilitates a visual examination of K dwarfs, unearthing a variety of unique characteristics and differences between stars, from variations in chromospheric activity to the detection of binary systems. It offers an exhaustive view of

how distinct spectral features, such as the Na I doublet, Hα line, Li I line, Ca II IRT line, and Fe I lines evolve across a broad range of $T_{\rm eff}$ and [Fe/H]values that define main-sequence K dwarfs. With this visual groundwork in place, we now transition to subsequent sections for a more detailed analysis of the K dwarfs in our sample, including the determination of their EWs and other key stellar properties. Thus, our focus moving forward will be on extracting precise quantitative data from the stellar spectra, which will augment our understanding of these stellar objects.

5.2.1 Newly Discovered Spectroscopic Binaries

In the course of this study, two new double-lined spectroscopic binary systems (SB2s) were uncovered, HD 80133 and HD 171075. Their binary natures were evident in the CHIRON spectra, exhibiting distinct double-line features, as shown in in Group E of Figure 5.3. Specifically, the spectral window from 6705 to 6720 Å reveals a double-line Ca I feature at 6717 Å for these stars, indicative of their binary status. For these two systems, the 2.7″size of the fiber as projected on the sky is certainly much larger than the stars' separations, so the light from both stars in each system is sent to the spectrograph.

The discovery of these new SB2s poses challenges when employing the Empirical Spec-Match (ESM) method for estimating stellar properties. The overlying spectral lines from two stars in a binary system create abnormal spectra that complicate accurate property estimations of individual stars within the binary system. While disentangling the two spectra is possible, it is beyond the purposes of this thesis, given that only a few stars require this treatment among more than 600 targets. Despite this difficulty, it is a crucial finding that further

emphasizes the value of our spectral library and the role of high-resolution spectroscopy in identifying such systems.

5.3 Spectral Characterization of the Primary Sample K Dwarfs

5.3.1 Identifying Young and Active Stars using the Benchmark Sample

In §4.2 of Chapter 4, we introduced relationships using the Benchmark Sample of stars and evaluated 7 RVV stars. These relationships have been applied to our Primary Sample of K dwarfs. Out of these, 590 stars met our criteria, having at least one spectrum above the S/N cutoff of 25 and free from corruption, i.e., SB2 systems were removed.

Figure 5.4 presents the relationship between EW[Hα] and EW[Li I] for a sample of 590 stars. This plot shows the primary sample stars, represented by orange plus signs, and members of the benchmark sample included for comparison in the colors specified in the legend. We identify 37 stars falling outside the dotted rectangular region of older stars, indicating that they are either young or active based on their EW measurements. These K dwarfs have Li I EWs above the 0.05 Å threshold and/or Hα EWs below the 0.5 Å threshold. Among these, 16 stars show signs of youth, while 27 appear to be active. Only 6 stars exhibited both youth and activity signatures. The stars identified as having markers of youth or activity are listed below, numbered in order of RA and their RKSTAR ID number, with these numbers given in Figure 5.4. The remaining stars in our sample display relatively quiescent EW[Hα] and EW[Li I] values, indicating lower levels of chromospheric activity and lithium absorption, suggestive of more advanced ages, as well as having no close stellar

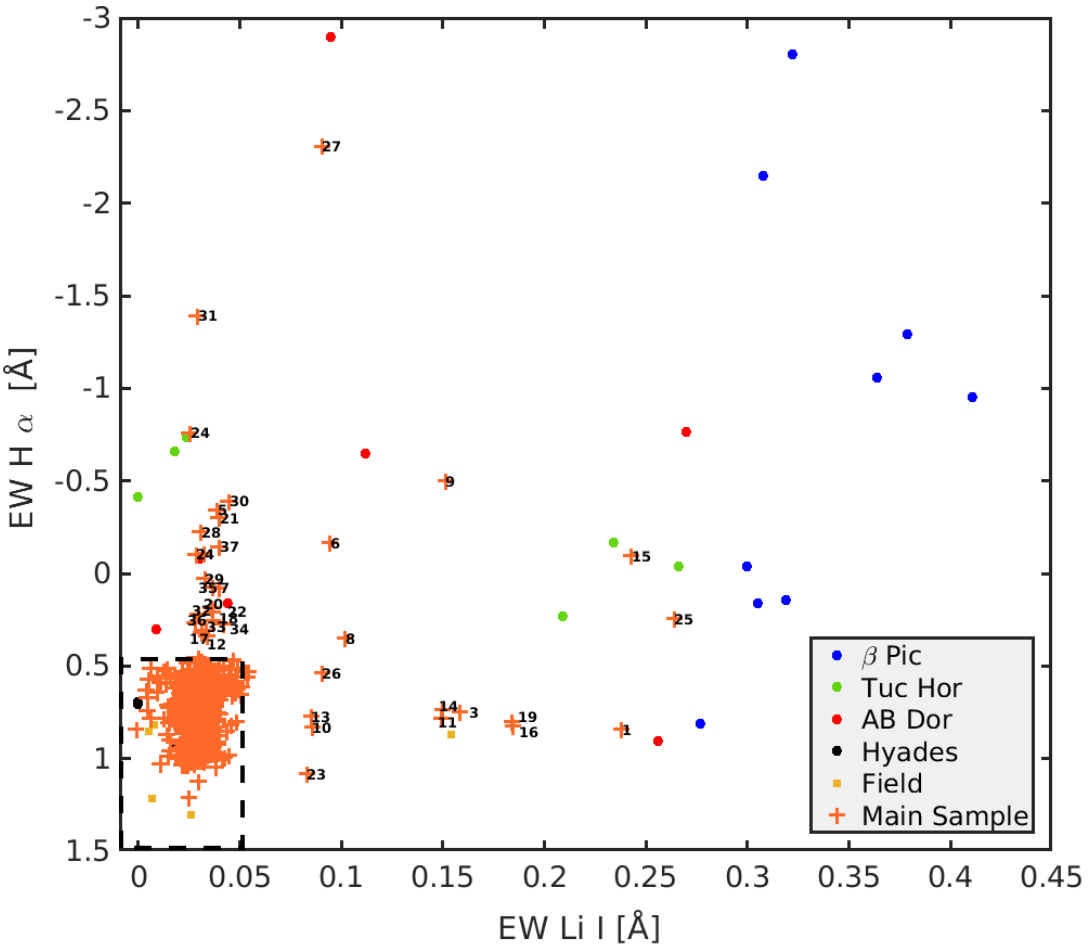

Figure 5.4 The plot presents EW[Hα] vs. EW[LiI] for 590 K dwarfs from our main sample, including a set of 35 benchmark stars with estimated ages. Highlighted in the plot are 37 stars recognized as young or active. Listed in order of RA or RKSTARS ID number, these stars are: (1) HD 17925, (2) AK For, (3) HD 284336, (4) MCC 446, (5) HD 283750, (6) HD 29697, (7) V2689 Ori, (8) HD 51849, (9) BD+20 1790, (10) HD 60491, (11) BD+01 2063, (12) BD+08 2131A, (13) HD 77825, (14) HD 78141, (15) LQ Hya, (16) V419 Hya, (17) HD 98712A, (18) HD 105065, (19) PX Vir, (20) BD+21 2486A, (21) HD 118100, (22) TYC 6760-1510-1, (23) TYC 5060-53-1, (24) LP 745-70, (25) HD 154361, (26) BD-12 4699, (27) HD 314741, (28) BD+01 3657, (29) HD 175742, (30) TYC 1598-1505-1, (31) HD 196998, (32) HD 358850, (33) BD-05 5480, (34) BD+18 5029, (35) R78b 355, (36) BD+00 5017, and (37) BD-13 6464.

companions that could induce activity.

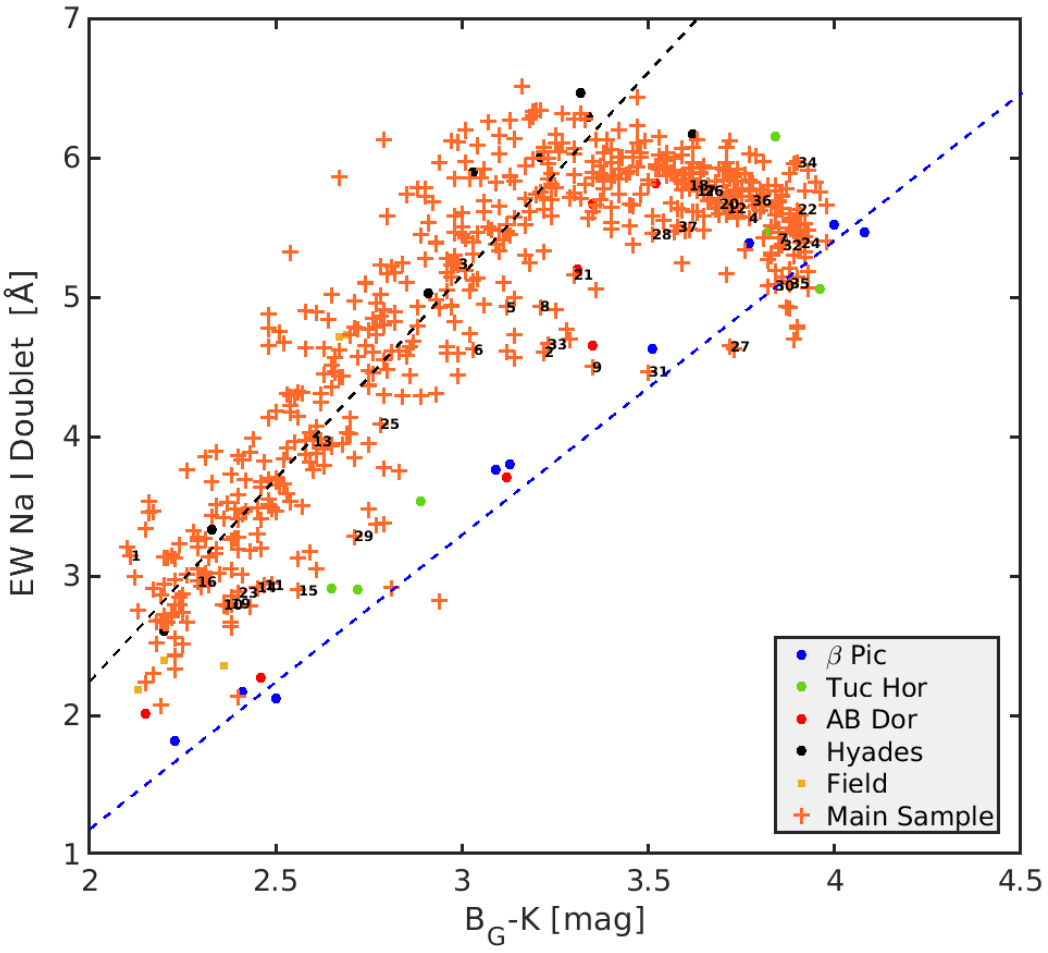

Figure 5.5 The plot displays EW[NaID] vs. $B_G - K$ color for 590 K dwarfs from our main sample, including a set of 35 benchmark stars with estimated ages. Stars are numbered as in Figure 5.4.

The 37 stars are also highlighted in Figure 5.5, which illustrates the relationship between EW[NaID] and $B_G - K$ color. This relationship can be used to evaluate ages, as was introduced for the benchmark sample in Figure 4.3. Recall that this relationship is particularly useful in the $B_G - K$ color range of 2.5–3.5, where the dispersion between younger and older

populations is noticeably larger. Within this color range, 15 of the stars initially pinpointed in Figure 5.4 are discernible as they fall significantly below the Hyades trend line in Figure 5.5. These stars present a diverse mix, encompassing those classified as young, those seen as active, and a group that exhibits both young and active characteristics. The position of these stars on the diagram underscores the utility of EW[NaID] as an additional discriminant for youth and activity among K dwarfs. The stars in this region that are not specifically tagged as young or active are likely to be binary systems that may display Na I features differently from single stars because the spectral lines are affected by combined light. This includes the data point that resides below the blue trend line at a $B_G - K = 2.95$, which implies that the binary nature of these stars can introduce additional complexity to their spectral characteristics. Therefore, overall the EW[NaID] vs. $B_G - K$ color relationship not only effectively distinguishes young or active stars but also hints at the presence of binary systems within our sample. This further underscores the multifaceted nature of our dataset and the richness of the information it can provide about K dwarf stars.

5.3.2 Revisiting the Ca II IRT Line

Figures 4.1 & 4.2 in Chapter 4 shed light on the contrasting profiles of the Ca II IRT line displayed by active and inactive stars. Specifically, active stars from young moving groups revealed core re-emission, while their inactive counterparts displayed typical absorption profiles. Yet, when the EW of the line was quantified, the anticipated correlation did not surface in the EW[CaII] vs. $B_G - K$ and EW[CaII] vs. Age plots, as depicted in Figure 4.4c and 4.4d, respectively.

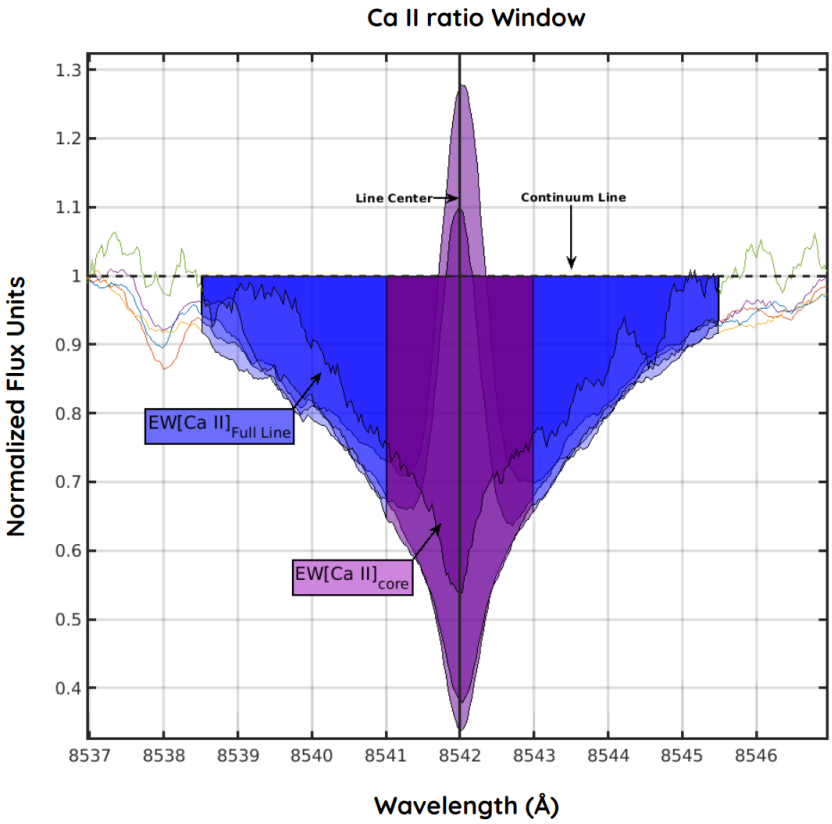

Figure 5.6 Illustration of the spectral window applied in the analysis of the Ca II IRT line. Spectra for five K dwarfs with different levels of absorption and re-emission are shown. The figure demonstrates the methodology used to measure the full line width spanning 7 Å (in blue) and the core line width confined to 2 Å (in purple). These two EW measurements are used to calculate the EW[Ca II]$_{ratio}$

In an effort to further harness the diagnostic potential of the Ca II IRT line, we reassessed this feature across the entire sample, employing a new approach: we developed a line ratio for the expansive Ca II absorption feature that considers both the overall feature and the core region where re-emission may be discernible. This methodology originated from the hypothesis that a quantitative indicator of core emission could serve as a more effective marker of stellar activity. To determine the width of the core for the Ca II line, we measured the average width of core emission features from the active stars in our benchmark sample.

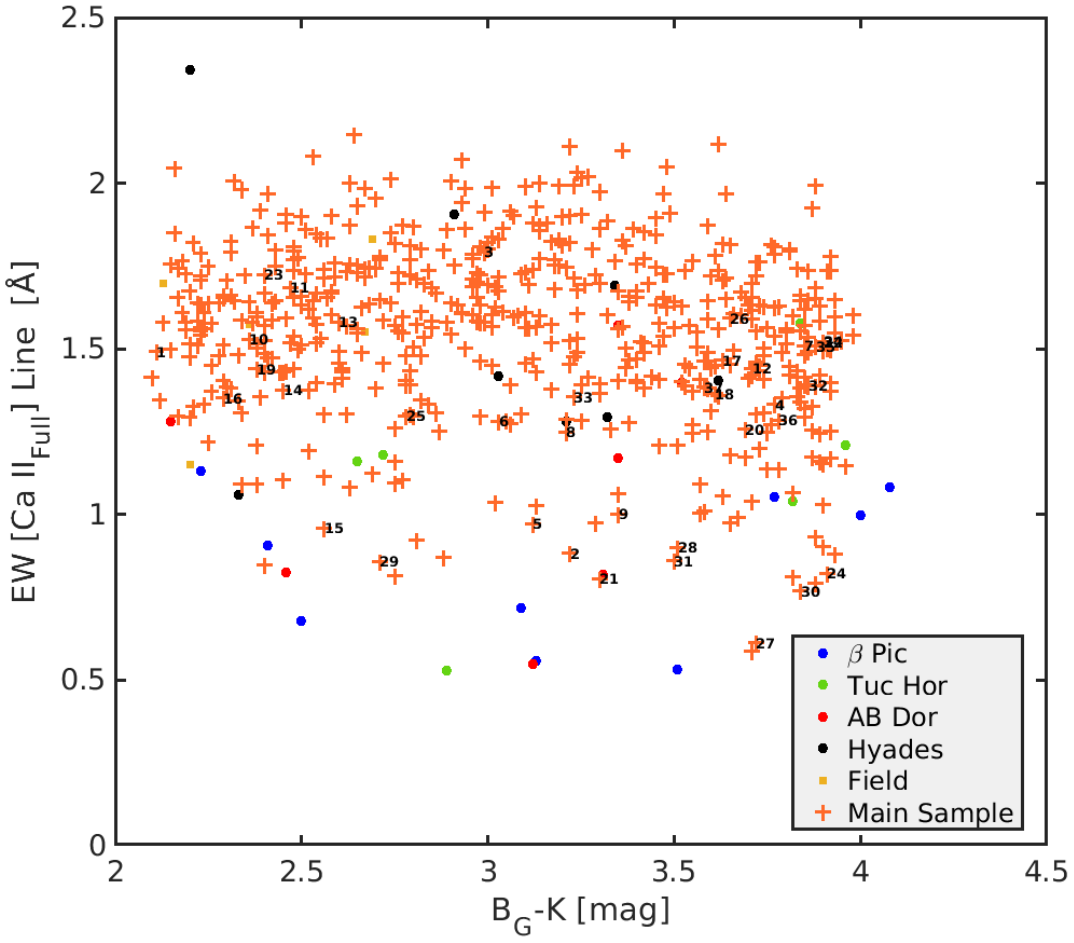

Figure 5.7 The plot illustrates EW[CaII IRT] Full against $B_G - K$ color for our sample of 590 K dwarfs, including a set of 35 benchmark stars with established ages. Stars are numbered as in Figure 5.4.

This ratio was then derived by measuring the full line's equivalent width (spreading across 7 Å) and the determined core line's equivalent width (restricted to 2 Å), with spectral window details provided in Table 3.3. The calculated ratio — the Ca II core EW divided by the Ca II full EW — is presented for the young or active population of our sample in Table A.3, and for the remainder of our primary sample in Appendix C.

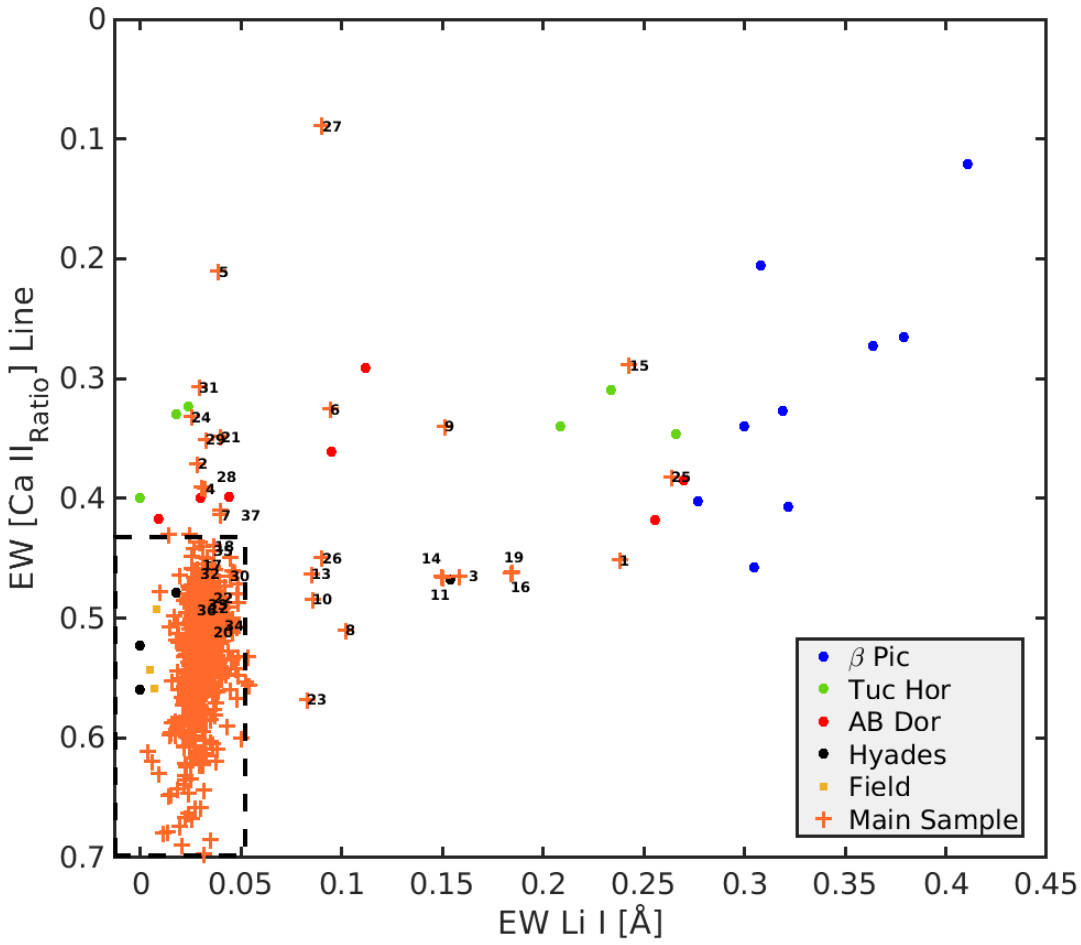

Figure 5.8 The plot contrasts EW[CaII IRT] Ratio with EW[LiI] for our sample of 590 K dwarfs, including a set of 35 benchmark stars with established ages. Stars are numbered as in Figure 5.4.

The ramifications of this refined approach are presented in Figure 5.7 & Figure 5.8. Figure 5.7 maps the full EW[CaII IRT] against the $B_G - K$ color, yielding no definitive trend, similar to the result observed in §4.2. A subset of the identified young or active stars does occupy lower values on the graph, but the separation is not clean. In contrast, Figure 5.8 compares the EW[CaII IRT] *ratio* with EW[LiI] and reveals a familiar pattern akin

to Figure 5.4. Here, most young or active stars found at smaller ratios than 0.43 distinguish themselves from the older or less active group found in the lower-left dotted rectangle. The EW[Ca II] ratio does appear to separate the older set of stars effectively, yet only 14 of the 27 original active stars identified via the EW[Hα] metric are recognized in this plot and no new active stars are identified.

Table 5.1: Spectroscopic Results and Derived Stellar Properties of 50 K Dwarfs Selected as Interesting from Our Primary Sample

RKSTAR ID	$T_{eff} \pm \sigma$ (K)	[Fe/H] $\pm\sigma$ (dex)	$\log g \pm \sigma$ (dex)	$v \sin i \pm \sigma$ (km s^{-1})	EW[Na I D] $\pm\sigma$ (Å)	EW[Hα] $\pm\sigma$ (Å)	EW[CaII] $\pm\sigma$ (Å)	EW[CaII]$_{ratio}\pm\sigma$ (Å)	EW[Li I] $\pm\sigma$ (Å)	Status
RKS0252−1246	5165 ± 54	0.11 ± 0.08	4.51 ± 0.11	<7 ± NM	3.15 ± 0.22	0.84 ± 0.10	1.49 ± 0.22	0.45 ± 0.09	0.24 ± 0.01	Y
RKS0329−2406	NM ± NM	NM ± NM	NM ± NM	NM ± NM	NM ± NM	NM ± NM	NM ± NM	NM ± NM	NM ± NM	A
RKS0417+2033	4446 ± 64	−0.06 ± 0.13	4.64 ± 0.10	<7 ± NM	5.24 ± 0.45	0.75 ± 0.06	1.79 ± 0.27	0.47 ± 0.09	0.16 ± 0.01	Y
RKS0430+0058	4011 ± 49	0.03 ± 0.09	4.68 ± 0.09	<7 ± NM	5.57 ± 0.59	−0.11 ± 0.01	1.33 ± 0.20	0.39 ± 0.08	0.03 ± 0.01	A
RKS0436+2707	4671 ± 126	0.15 ± 0.09	4.55 ± 0.13	<7 ± NM	4.93 ± 0.49	−0.34 ± 0.03	0.97 ± 0.15	0.21 ± 0.04	0.04 ± 0.01	A
RKS0441+2054	4572 ± 59	−0.22 ± 0.11	4.58 ± 0.11	7.99 ± 1.27	4.63 ± 0.38	−0.17 ± 0.01	1.28 ± 0.19	0.33 ± 0.06	0.09 ± 0.01	Y+A
RKS0536+1119	3936 ± 36	−0.09 ± 0.12	4.70 ± 0.10	<7 ± NM	5.42 ± 0.57	0.08 ± 0.01	1.51 ± 0.23	0.41 ± 0.08	0.04 ± 0.01	A
RKS0658−1259	4357 ± 95	−0.30 ± 0.09	4.66 ± 0.10	<7 ± NM	4.94 ± 0.40	0.35 ± 0.05	1.25 ± 0.19	0.51 ± 0.10	0.10 ± 0.01	Y+A
RKS0723+2024	4285 ± 329	−0.20 ± 0.25	4.65 ± 0.14	7.99 ± 1.56	4.50 ± 0.39	−0.50 ± 0.07	1.00 ± 0.15	0.34 ± 0.07	0.15 ± 0.01	Y+A
RKS0734−0653	5056 ± 42	−0.19 ± 0.11	4.57 ± 0.10	<7 ± NM	2.79 ± 0.17	0.83 ± 0.11	1.53 ± 0.23	0.48 ± 0.09	0.09 ± 0.01	Y
RKS0819+0120	4965 ± 50	−0.28 ± 0.09	4.56 ± 0.09	<7 ± NM	2.94 ± 0.15	0.78 ± 0.11	1.68 ± 0.25	0.46 ± 0.09	0.15 ± 0.01	Y
RKS0850+0751	3943 ± 57	−0.25 ± 0.14	4.70 ± 0.10	<7 ± NM	5.64 ± 0.58	0.34 ± 0.03	1.44 ± 0.22	0.49 ± 0.09	0.03 ± 0.01	A
RKS0904−1554	4895 ± 40	0.08 ± 0.07	4.50 ± 0.09	<7 ± NM	3.97 ± 0.30	0.77 ± 0.09	1.58 ± 0.24	0.46 ± 0.09	0.09 ± 0.01	Y
RKS0907+2252	5257 ± 43	0.13 ± 0.05	4.49 ± 0.11	<7 ± NM	2.92 ± 0.20	0.74 ± 0.08	1.38 ± 0.21	0.47 ± 0.09	0.15 ± 0.01	Y
RKS0932−1111	6177 ± 154	0.01 ± 0.13	4.31 ± 0.17	27.44 ± 3.9	2.90 ± 0.20	−0.09 ± 0.01	0.96 ± 0.14	0.29 ± 0.06	0.24 ± 0.02	Y+A
RKS1043−2903	5269 ± 33	0.14 ± 0.07	4.51 ± 0.10	<7 ± NM	2.96 ± 0.21	0.82 ± 0.08	1.35 ± 0.20	0.46 ± 0.09	0.18 ± 0.01	Y
RKS1121−2027	4138 ± 61	−0.13 ± 0.12	4.68 ± 0.10	<7 ± NM	5.77 ± 0.59	0.32 ± 0.04	1.47 ± 0.22	0.45 ± 0.09	0.03 ± 0.01	A
RKS1205−1852	3955 ± 39	−0.08 ± 0.13	4.70 ± 0.10	<7 ± NM	5.81 ± 0.66	0.26 ± 0.03	1.36 ± 0.20	0.44 ± 0.08	0.04 ± 0.01	A
RKS1303−0509	5266 ± 50	−0.05 ± 0.06	4.54 ± 0.11	<7 ± NM	2.80 ± 0.20	0.80 ± 0.07	1.44 ± 0.22	0.46 ± 0.09	0.18 ± 0.01	Y
RKS1306+2043	4105 ± 44	−0.19 ± 0.13	4.68 ± 0.10	<7 ± NM	5.68 ± 0.56	0.18 ± 0.02	1.26 ± 0.19	0.51 ± 0.10	0.04 ± 0.01	A

Continued on next page

Table 5.1 – continued from previous page

RKSTAR ID	$T_{eff} \pm \sigma$ (K)	[Fe/H] $\pm\sigma$ (dex)	$\log g \pm \sigma$ (dex)	$v \sin i \pm \sigma$ (km s^{-1})	EW[Na I D] $\pm\sigma$ (Å)	EW[Hα] $\pm\sigma$ (Å)	EW[CaII] $\pm\sigma$ (Å)	EW[CaII]$_{ratio}\pm\sigma$ (Å)	EW[Li I] $\pm\sigma$ (Å)	Status
RKS1334−0820	4335 ± 43	−0.10 ± 0.12	4.65 ± 0.09	8.14 ± 1.1	5.16 ± 0.47	−0.30 ± 0.04	0.81 ± 0.12	0.35 ± 0.07	0.04 ± 0.01	A
RKS1500−2905	3790 ± 52	−0.03 ± 0.05	4.71 ± 0.11	<7 ± NM	5.63 ± 0.61	0.21 ± 0.02	1.52 ± 0.23	0.48 ± 0.09	0.04 ± 0.01	A
RKS1631−0718	NM ± NM	NM ± NM	NM ± NM	NM ± NM	2.89 ± 0.22	1.08 ± 0.17	1.72 ± 0.26	0.57 ± 0.11	0.08 ± 0.01	Y
RKS1633−0933	3909 ± 59	0.20 ± 0.15	4.67 ± 0.10	<7 ± NM	5.39 ± 0.57	−0.76 ± 0.09	0.82 ± 0.12	0.33 ± 0.06	0.03 ± 0.01	A
RKS1705−0147	4835 ± 74	0.01 ± 0.11	4.50 ± 0.11	<7 ± NM	4.09 ± 0.32	0.24 ± 0.04	1.30 ± 0.19	0.38 ± 0.07	0.26 ± 0.01	Y+A
RKS1716−1210	4002 ± 39	−0.02 ± 0.08	4.68 ± 0.10	<7 ± NM	5.77 ± 0.62	0.54 ± 0.07	1.59 ± 0.24	0.45 ± 0.09	0.09 ± 0.01	Y
RKS1754−2649	4249 ± 152	−0.32 ± 0.19	4.68 ± 0.10	NM ± NM	4.65 ± 0.43	−2.31 ± 0.23	0.61 ± 0.09	0.09 ± 0.02	0.09 ± 0.01	Y+A
RKS1822+0142	4129 ± 41	−0.07 ± 0.10	4.67 ± 0.09	<7 ± NM	5.46 ± 0.55	−0.22 ± 0.03	0.90 ± 0.14	0.39 ± 0.08	0.03 ± 0.01	A
RKS1855+2333	5123 ± 95	0.01 ± 0.11	4.54 ± 0.11	14.82 ± 1.06	3.29 ± 0.25	0.03 ± 0.00	0.86 ± 0.13	0.35 ± 0.07	0.03 ± 0.01	A
RKS1910+2145	3931 ± 37	0.07 ± 0.09	4.67 ± 0.10	<7 ± NM	5.09 ± 0.54	−0.39 ± 0.05	0.77 ± 0.12	0.46 ± 0.09	0.04 ± 0.01	A
RKS2041−2219	3953 ± 62	−0.16 ± 0.17	4.69 ± 0.10	<7 ± NM	4.47 ± 0.37	−1.39 ± 0.17	0.86 ± 0.13	0.31 ± 0.06	0.03 ± 0.01	A
RKS2105−1654	3820 ± 49	−0.05 ± 0.06	4.70 ± 0.10	<7 ± NM	5.38 ± 0.56	0.22 ± 0.02	1.39 ± 0.21	0.46 ± 0.09	0.03 ± 0.01	A
RKS2108−0425	4566 ± 58	−0.40 ± 0.12	4.60 ± 0.12	<7 ± NM	4.67 ± 0.37	0.31 ± 0.04	1.35 ± 0.20	0.49 ± 0.09	0.03 ± 0.01	A
RKS2241+1849	3993 ± 36	0.03 ± 0.16	4.67 ± 0.10	<7 ± NM	5.97 ± 0.67	0.27 ± 0.04	1.52 ± 0.23	0.51 ± 0.10	0.04 ± 0.01	A
RKS2308+0633	3804 ± 35	0.10 ± 0.14	4.70 ± 0.09	<7 ± NM	5.10 ± 0.54	0.07 ± 0.01	1.51 ± 0.23	0.44 ± 0.09	0.04 ± 0.01	A
RKS2335+0136	4112 ± 31	0.05 ± 0.13	4.66 ± 0.09	<7 ± NM	5.69 ± 0.62	0.27 ± 0.03	1.28 ± 0.19	0.49 ± 0.09	0.03 ± 0.01	A
RKS2348−1259	4179 ± 59	−0.12 ± 0.09	4.68 ± 0.09	<7 ± NM	5.51 ± 0.54	−0.15 ± 0.02	1.38 ± 0.21	0.41 ± 0.08	0.04 ± 0.01	A
RKS0706+2358	4281 ± 52	−0.08 ± 0.12	4.66 ± 0.10	<7 ± NM	5.81 ± 0.57	0.72 ± 0.07	2.03 ± 0.31	0.44 ± 0.08	0.03 ± 0.01	Y−MG
RKS0820+1404	4146 ± 59	−0.09 ± 0.06	4.67 ± 0.09	<7 ± NM	5.92 ± 0.61	0.66 ± 0.10	1.52 ± 0.23	0.53 ± 0.10	0.04 ± 0.01	Y−MG
RKS0104+2607	4161 ± 59	−0.07 ± 0.11	4.67 ± 0.09	<7 ± NM	5.74 ± 0.60	0.60 ± 0.08	1.39 ± 0.21	0.49 ± 0.09	0.04 ± 0.01	Y−MG
RKS0121+2419	3942 ± 70	0.06 ± 0.14	4.68 ± 0.21	NM ± NM	5.77 ± 0.64	0.59 ± 0.06	1.38 ± 0.21	0.53 ± 0.10	0.05 ± 0.01	Y−MG

Continued on next page

Table 5.1 – continued from previous page

RKSTAR ID	$T_{eff} \pm \sigma$ (K)	[Fe/H] $\pm\sigma$ (dex)	$\log g \pm \sigma$ (dex)	$v \sin i \pm \sigma$ (km s^{-1})	EW[Na I D] $\pm\sigma$ (Å)	EW[Hα] $\pm\sigma$ (Å)	EW[CaII] $\pm\sigma$ (Å)	EW[CaII]$_{ratio}\pm\sigma$ (Å)	EW[Li I] $\pm\sigma$ (Å)	Status
RKS0300+0744	5058 ± 36	0.28 ± 0.05	4.49 ± 0.09	<7 ± NM	3.73 ± 0.27	0.91 ± 0.10	1.60 ± 0.24	0.47 ± 0.09	0.03 ± 0.01	Y−MG
RKS0320+0827	4520 ± 45	0.08 ± 0.07	4.60 ± 0.12	<7 ± NM	5.46 ± 0.50	0.75 ± 0.11	1.72 ± 0.26	0.47 ± 0.09	0.03 ± 0.01	Y−MG
RKS0322+2709	3947 ± 52	0.13 ± 0.12	4.68 ± 0.09	<7 ± NM	5.50 ± 0.61	0.52 ± 0.08	1.39 ± 0.21	0.50 ± 0.10	0.05 ± 0.01	Y−MG
RKS0420−1445	4368 ± 30	0.07 ± 0.09	4.64 ± 0.09	<7 ± NM	6.00 ± 0.62	0.72 ± 0.11	1.75 ± 0.26	0.47 ± 0.09	0.03 ± 0.01	Y−MG
RKS2254+2331	3931 ± 51	0.02 ± 0.13	4.67 ± 0.11	<7 ± NM	5.19 ± 0.56	0.57 ± 0.07	1.34 ± 0.20	0.59 ± 0.11	0.02 ± 0.01	Y−MG
RKS1833−1626	NM ± NM	NM ± NM	NM ± NM	NM ± NM	NM ± NM	NM ± NM	NM ± NM	NM ± NM	NM ± NM	New SB2
RKS0917−0323	NM ± NM	NM ± NM	NM ± NM	NM ± NM	NM ± NM	NM ± NM	NM ± NM	NM ± NM	NM ± NM	New SB2
RKS1518−1837	4379 ± 37	0.01 ± 0.05	4.64 ± 0.09	<7 ± NM	5.66 ± 0.52	0.73 ± 0.10	1.57 ± 0.24	0.51 ± 0.10	0.03 ± 0.01	BC
RKS1510−1622	NM ± NM	NM ± NM	NM ±	NM ± NM	1.15 ± 0.07	1.04 ± 0.10	1.48 ± 0.22	0.60 ± 0.11	0.02 ± 0.01	Halo

EW[NaID]: Equivalent width of the Na I doublet at 5889.95 Å & 5895.92 Å

EW[Hα]: Equivalent width of the Hα line at 6563 Å

EW[CaII]: Equivalent width of the Ca II infrared triplet line at 8542 Å

EW[CaII]$_{ratio}$: Equivalent width ratio (see §5.3.2) of Ca II infrared triplet line at 8542 Å

EW[Li I]: Equivalent width of the Li I line at 6707.8 Å

NM: Not Measured

In the Status column:

Y represents Youth,

A represents Active,

Y+A represents both Youth and Active,

Y-MG represents Young Moving Group,

New SB2 represents a new Spectroscopic Binary,

wd+BC represents White Dwarf Binary Candidate,

Halo represents Halo Star.

5.3.3 Stellar Properties of the Primary Sample

The ESM method described in §3.6 was leveraged to compute the stellar properties for our Primary Sample comprising 590 K dwarfs. The ESM tool is well-suited for this analysis given its ability to match the observed spectra to a library of well-studied stars, thus enabling the extraction of accurate stellar properties. Detailed outcomes of these measurements, inclusive of various properties like $T_{\rm eff}$, [Fe/H], $\log g$, and $v \sin i$ can be found in Appendix C.

In Figure 5.9, we display the relationship between metallicity ([Fe/H]) and effective temperature ($T_{\rm eff}$) across our sample. Orange plus symbols are the 590 stars in the Primary Sample and blue points are the stars in the ESM Library. The K dwarfs studied here have span a temperature range of 3600–5400 K and a metallicity range of -0.6 to $+0.4$ (with one exception at nearly $+0.6$ that is likely an errant point). A histogram positioned on the y-axis provides a count of stars possessing specific [Fe/H]values, sorted into bins of 0.1 dex. This distribution clearly illustrates that a considerable fraction of K dwarfs in our sample possess solar-like [Fe/H]values, specifically ranging from -0.2 to $+0.2$ dex. We find an average metallicity of -0.02 dex for the sample, corroborating the abundance of stars with solar-like metallicities.

A crucial limitation of this method is the noticeable gap in Yee et al. (2017)'s ESM Library of stars in portions of the regime that encompasses K dwarfs. There are few stars with $T_{\rm eff}$ between 4200–4700 K at any metallicity, and the range of unrepresented temperatures is even broader at metallicities outside the range of -0.4 to $+0.2$. Thus, the number of matches for our stars is subject to the limitations of the matching algorithm, resulting in what we expect

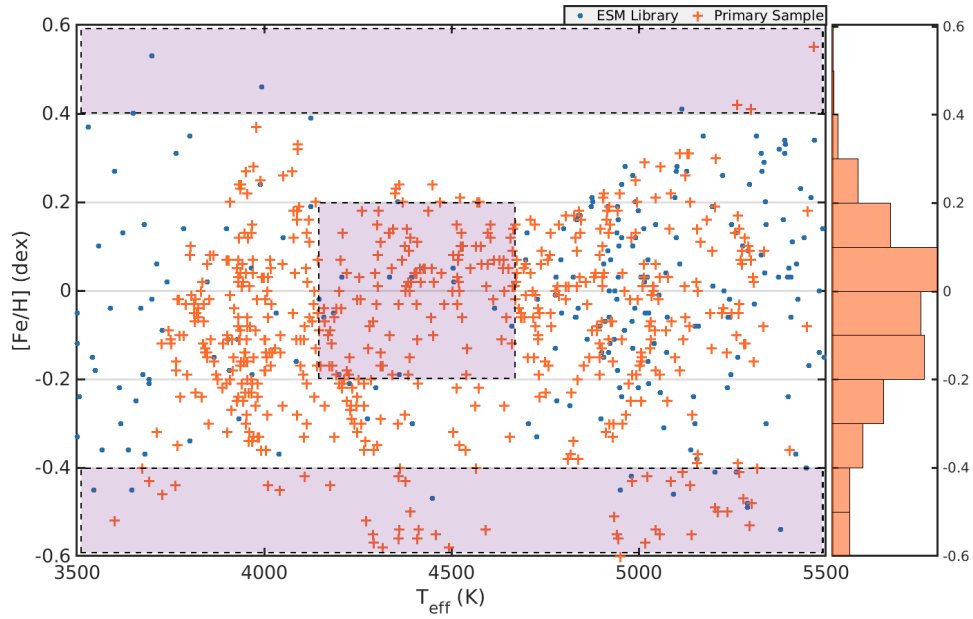

Figure 5.9 The scatter plot exhibits [Fe/H]and $T_{\rm eff}$ values determined via ESM for 590 K dwarfs within our primary sample, indicated by orange crosses. For comparison, this plot also includes 215 stars from the ESM library of Yee et al. (2017), marked by blue dots. Three regions of particular interest, denoted by the purple shaded boxes, highlight areas where ESM's library is sparse. Consequently, the reliability of estimated values in these regions may be diminished due to limited sample representation.

to be somewhat lower numbers of (especially) very high and very low metallicity stars, and perhaps fewer stars with $T_{\rm eff}$ near 4500 K. Increasing the number of K dwarfs in this $T_{\rm eff}$ range, particularly those with high metallicities, will be an essential task for future updates to the ESM Library, and can perhaps be future work based upon our own extensive set of K dwarf spectra.

With that *caveat* in mind, the low-metallicity end of our sample is in rather better shape than the high-metallicity regime. In particular, our sample encompasses 20 stars with [Fe/H]values less than -0.5 dex, comprising about 3% of the total. These low-metallicity K

dwarfs comprise an intriguing subset within our dataset, offering a complementary perspective to our younger and more active stars. Notably, none of the 37 stars identified as young or active in Section 5.3 show [Fe/H]values below -0.4 dex. This outcome underlines a clear distinction between the low-metallicity and active subsets in terms of age and metallicity, adding richness to our analysis.

A robust correlation between the projected rotational velocity ($v \sin i$) and stellar activity became apparent in our analysis of K dwarfs. This trend is discernible not only in the benchmark set represented in Table 4.1, but also in the primary sample detailed in Table 5.1. Our data reveals that each of the six K dwarfs within the primary sample exhibiting $v \sin i$ values exceeding 7 km s^{-1} also demonstrated evident chromospheric activity. This was determined by scrutinizing the Hα and Ca II line measurements captured in Figures 5.4 and 5.8 respectively. The stars thus identified comprise BD+20 1790, HD 29697, HD 118100, AK For, HD 175742, and LQ Hya.

However, an interesting anomaly arises when considering the broader sample of 26 K dwarfs identified as chromospherically active; not all of these displayed elevated $v \sin i$ values. This discrepancy may be attributed to the inclination angle at which we observe these stars. If the star's rotational axis is nearly aligned with our line of sight, the star could be rotating rapidly but we would not observe a large $v \sin i$ (i.e., the projected rotational velocity would be small). This concept is discussed extensively in the literature, such as in the work of Barnes (2003), and its potential impact on our results certainly warrants further study. Our research underscores the complexity of stellar activity and rotation, and emphasizes the

need for a holistic approach when attempting to understand the intricate dynamics of these processes.

5.4 Kinematics of the Primary Sample

Following our exploration of stellar properties, we now transition into examining the kinematics of K dwarfs in the Primary Sample. Given the established relationships between stellar kinematics, age, and metallicity, it becomes crucial to include this aspect in our holistic understanding of these stars. As we proceed, we will seek to interconnect the insights gained from kinematic analysis with the properties measured through ESM, further augmenting our understanding of K dwarfs in our vicinity.

The three-dimensional space motions, denoted as UVW, for each of the 590 K dwarfs from our primary sample offer insights that help to associate these individual stars with various identified moving groups and clusters present in the nearby Galaxy. On the flip side, these data can also be used to identify stars that do not conform to the typical Galactic motions. For our sample stars, essential astrometric data including the stellar positions, proper motions, and parallaxes from *Gaia* DR3, are detailed in Table A.2 in Appendix B, which also lists the B_G magnitudes and $B_G - K$ colors from *Gaia*. In addition, Table A.2 includes the systemic velocities (γ values) that were computed from our analysis of the CHIRON spectra, along with their counterparts measured by *Gaia*. Finally, the derived UVW space velocities are given, and these values pave the way for an in-depth kinematic analysis of our Primary Sample.

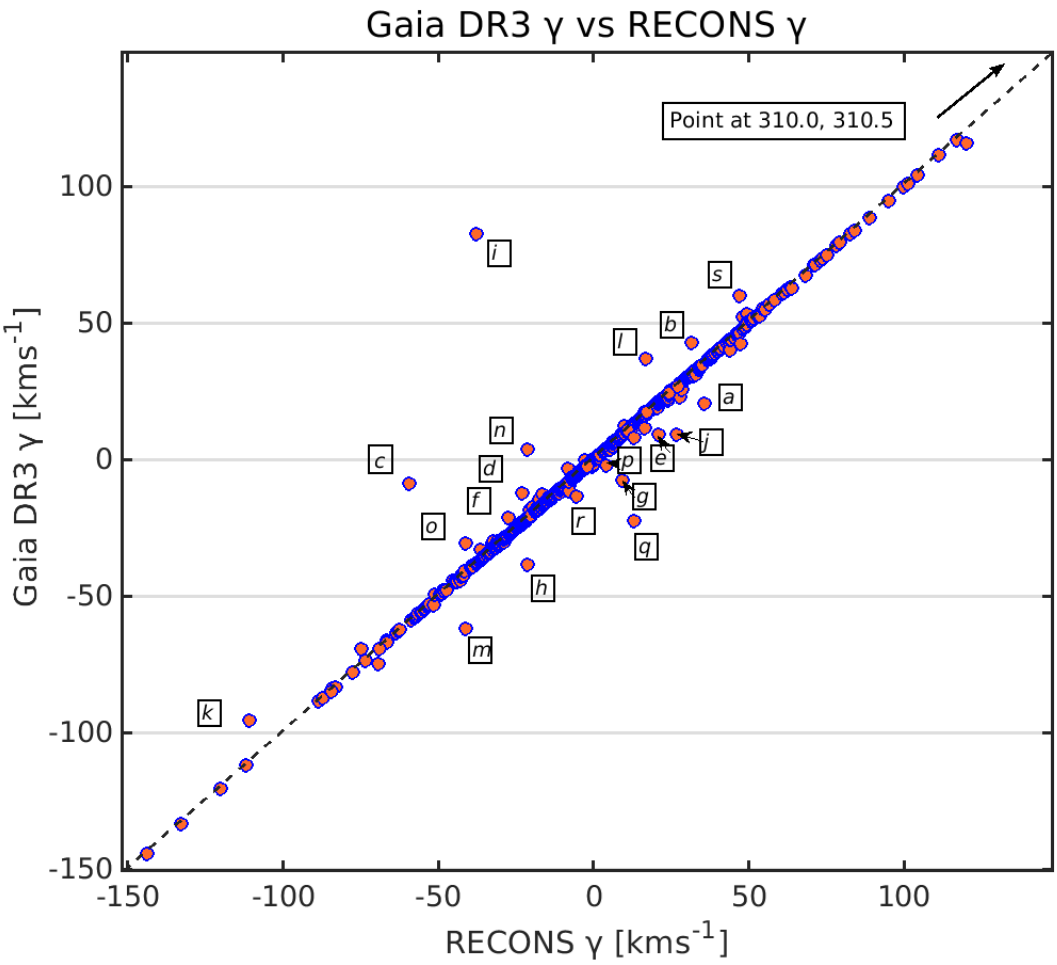

Figure 5.10 Plot showing a 1-to-1 correlation between CHIRON γ velocity and *Gaia* DR3 γ velocity, with the line indicating equal values. Outliers are labeled as follows: $\boxed{a}$ RKS0236-0309 (variable star), $\boxed{b}$ RKS0258+2646 (unknown), $\boxed{c}$ RKS0626+1845 (binary), $\boxed{d}$ RKS0907+2252 (young), $\boxed{e}$ RKS1108-2816 (unknown), $\boxed{f}$ RKS1253+0645 (binary, known SB1), $\boxed{g}$ RKS1303-0509 (young), $\boxed{h}$ RKS1504-1835 (binary, known SB1), $\boxed{i}$ RKS1518-1837 (possible binary with white dwarf component), $\boxed{j}$ RKS1528-0920 (binary, known SB2), $\boxed{k}$ RKS1555+1602 (variable star), $\boxed{l}$ RKS1605-2027 (binary, known SB2), $\boxed{m}$ RKS1833-1626 (new SB2), $\boxed{n}$ RKS1855+2333 (active), $\boxed{o}$ RKS2041-2219 (active), $\boxed{p}$ RKS2108-0425 (active), $\boxed{q}$ RKS2119-2621 (binary, known SB1), $\boxed{r}$ RKS2308+0633 (active), $\boxed{s}$ RKS2345+2933 (binary, known SB1).

5.4.1 CHIRON γ Velocities compared to Gaia DR3 Values

The kinematic attributes of the stars in our sample are illustrated in Figures 5.10 & 5.12. Figure 5.10 offers a comparison between the systemic (γ) velocities we measured using CHIRON data and those provided by *Gaia*. The stars deviating from the 1-to-1 dotted line are either multiples with orbits observed at different phases in their spectroscopic orbits, or stars displaying youth, activity, or rapid rotation for which radial velocities are difficult to measure (or may in fact change based on inherent changes in activity levels). These factors can, of course, work in combinations that result in offsets from the 1-to-1 line.

The main sample stars that show discrepancies between the measured CHIRON velocities and those provided by *Gaia* DR3 are marked in Figure 5.12 with boxed letters 'a' to 's', and ordered based on RKS ID or RA position. The identified stars with mismatched velocities are as follows, and explanations for the offsets are given, if known:
$\boxed{a}$ RKS0236-0309 (variable star), $\boxed{b}$ RKS0258+2646 (unknown), $\boxed{c}$ RKS0626+1845 (binary), $\boxed{d}$ RKS0907+2252 (young), $\boxed{e}$ RKS1108-2816 (unknown), $\boxed{f}$ RKS1253+0645 (binary, known SB1), $\boxed{g}$ RKS1303-0509 (young), $\boxed{h}$ RKS1504-1835 (binary, known SB1), $\boxed{i}$ RKS1518-1837 (possible binary with white dwarf component), $\boxed{j}$ RKS1528-0920 (binary, known SB2), $\boxed{k}$ RKS1555+1602 (variable star), $\boxed{l}$ RKS1605-2027 (binary, known SB2), $\boxed{m}$ RKS1833-1626 (new SB2), $\boxed{n}$ RKS1855+2333 (active), $\boxed{o}$ RKS2041-2219 (active), $\boxed{p}$ RKS2108-0425 (active), $\boxed{q}$ RKS2119-2621 (binary, known SB1), $\boxed{r}$ RKS2308+0633 (active), $\boxed{s}$ RKS2345+2933 (binary, known SB1).

Our compilation includes a diverse set of objects: 12 binaries, 5 active stars, 2 young

stars, 2 newly discovered SB2s, 2 variable stars, 1 possible binary containing a white dwarf, 1 eclipsing binary, and 3 stars with unknown reasons for their variations in radial velocities between *Gaia* and our measurements. In sum, this set of stars represents a wide spectrum of stellar characteristics, emphasizing the necessity for comprehensive follow-up studies to thoroughly comprehend their intrinsic properties and behavior. Three stars with yet to be classified variations serve as compelling cases. These stars may exhibit traits similar to the RVV stars explored in Chapter 4. To determine the presence of any unseen companions, these stars warrant additional observations and rigorous analyses.

One star that presents a fascinating case for further scrutiny is RKS1518-1837, also known as BD−18 4031. Despite the absence of any known companion, this star exhibits a significant variation from the radial velocity value given in *Gaia* DR3. Our curiosity piqued, we explored the research conducted by Leonardo Paredes in his doctoral thesis to gain deeper insights into the peculiar behavior of this star. The RECONS CHIRON team secured a set of 23 observations of this star, revealing some noteworthy dynamics. As depicted in the radial velocity plot in Figure 5.11, there is a companion with P_{orb} = 1636 days (about 4.5 years) in a highly elliptical orbit with an eccentricity e = 0.922. Fortunately, radial velocities were opportunistically secured just before and after periastron, so the orbit is reliable. Interestingly, Paredes' findings hint at the possibility that RKS1518-1837 could have a white dwarf companion, as is evidenced by the semi-amplitude of more than 11 km s^{-1}. However, the inclination of the orbit remains unknown, so a firm measurement of the secondary's mass remains elusive.[2] This case is just one example that underscores how

[2]Because the RKSTAR sample is defined to include only those systems with "forever" K dwarf primaries,

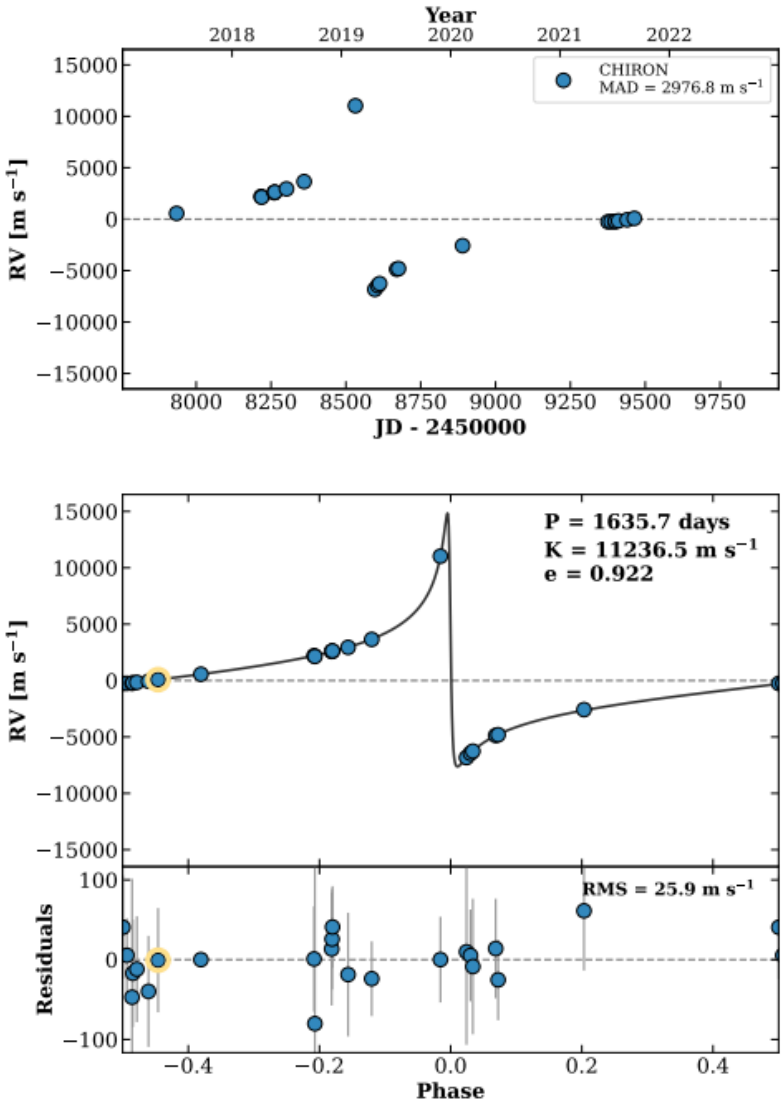

Figure 5.11 Graphical representations illustrating the radial velocity (RV) measurements of the star RKS1518-1837. The top plot presents observations from 2018 to 2021 taken with the CHIRON spectrograph on the CTIO/SMARTS 1.5m, showing obvious RV fluctuations. The lower panel is a phase-folded diagram that the star has a companion in a highly elliptical orbit with an eccentricity of e = 0.922. The data depicted are a part of the research by Paredes (2022).

detailed exploration of individual stars contributes to our understanding of their history and

and white dwarfs were the original primaries in their systems, stars are removed from the sample if the white dwarf nature of a companion is confirmed. Until the companion to RKS1518-1837 is confirmed to be a white dwarf, the star will remain in the RKSTAR sample.

dynamics, and only when each star is given its own careful characterization treatment can we truly understand the sample of nearby K dwarfs as a population.

5.4.2 Using Galactic Velocities to Identify Young K dwarfs

Figure 5.12 illustrates the UVW space motions for our Primary Sample of 590 K dwarf stars. The delicate dance of stellar motion depicted in these diagrams serves as a visual testament to the complex dynamics that govern these celestial bodies. The velocities shown in these plots were derived through a careful analysis of the values reported in Riedel et al. (2014) and Riedel et al. (2017), along with the use of the BANYAN Σ code as outlined in Gagne et al. (2018). This method, akin to the process described in §4.4 in Chapter 4, was instrumental in affirming the associations of any stars with known moving groups.

The AB Dor and Hyades groups, with their distinctive space motions of UVW = [−7 km/s, −27 km/s, −13 km/s] and [−41 km/s, −19 km/s, −1 km/s] respectively (Riedel et al. 2014), present particular points of interest for our study. Their positioning within this celestial map of motion underlines their individual characteristics within the grand scheme of stellar dynamics in the nearby Galaxy. These specific coordinates served as guiding landmarks in our kinematic analysis, enabling the successful identification of several stars within these groups in our primary sample. The AB Dor group includes four of our RKS stars shown with red x points in Figure 5.12, known as BD+24 1529, BD+20 1790, BD+14 1876, and LP 745-70. We find seven RKS stars shown with heavy black plus symbols to be members of the Hyades group, known as BD+25 162, Ross 788, BZ Cet, BD+07 499, LP 355-64, BD−15 767, and G 67-33, marked with black crosses. Table A.2 in Appendix B lists

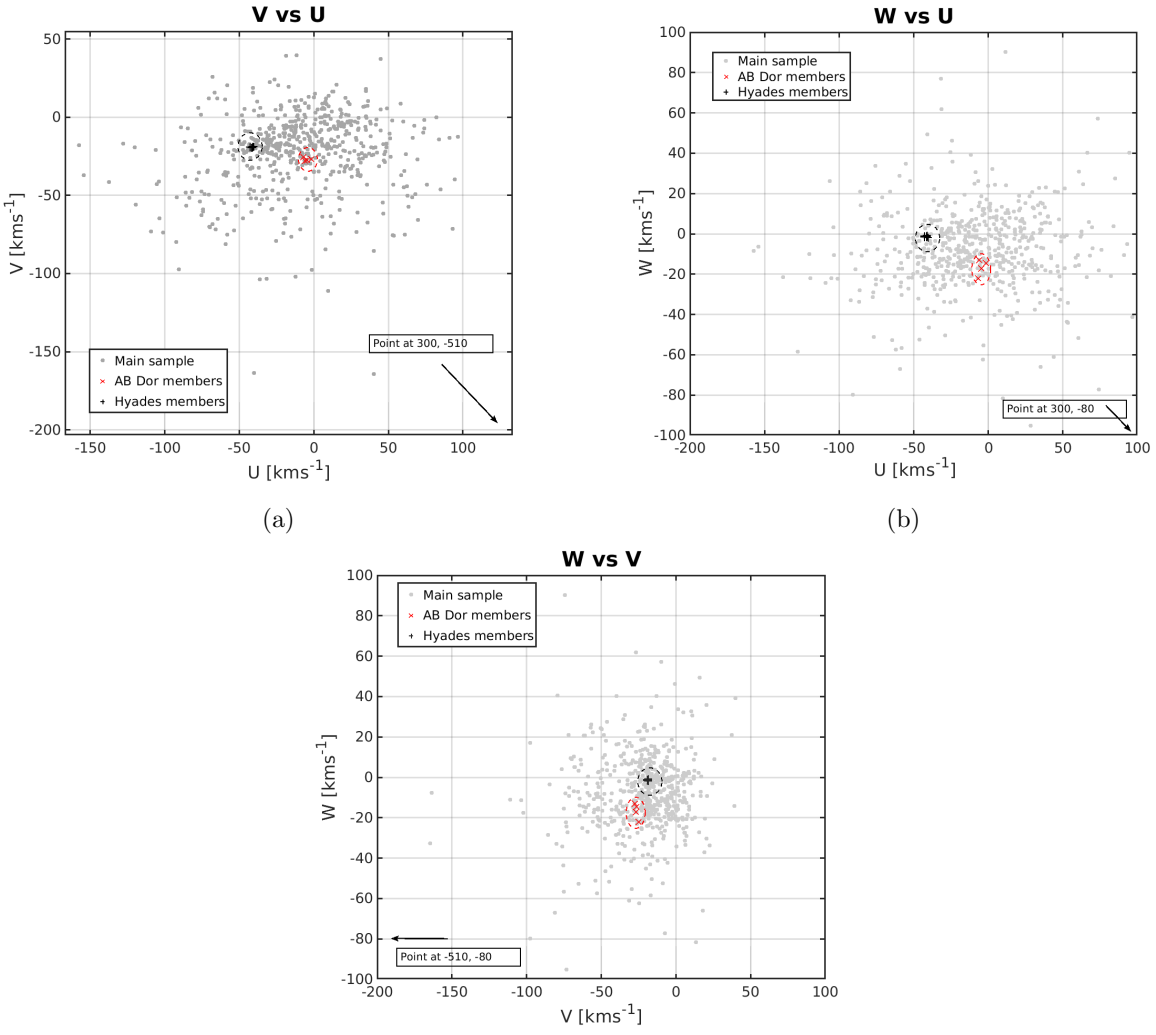

Figure 5.12 Diagrams illustrating the dynamics for members of the four moving groups and clusters utilized in the benchmark sample: (a) a graph depicting Galactic space motions with V plotted against U, (b) a plot illustrating W versus U Galactic space motions, and (c) a diagram showing W versus V Galactic space motions. Represented in these plots are 590 main sample stars, field stars indicated as grey circles, members of the Hyades cluster represented by black crosses, and AB Dor moving group members depicted as red X's. Specific Hyades stars include BD+25 162, Ross 788, BZ Cet, BD+07 499, LP 355-64, BD-15 767, and G 67-33. AB Dor group stars in the sample comprise BD+24 1529, BD+20 1790, BD+14 1876, and LP 745-70.

the UVW values for all of the stars analyzed in the Primary Sample and also membership to a group or the field. Intriguingly, of the 11 stars identified, nine (seven from the Hyades and two from the AB Dor group) were not initially detected via our spectroscopic analysis. This set of identifications effectively augments the count of young or active stars in our sample from 37 to 46, accounting for approximately 8% of the entire primary sample.

Our kinematic analysis, via the identification of complex dynamics, forms a basis for further investigation into Galactic populations. As we transition to examining the thin and thick disk populations using these same UVW motions, we expect to gain further understanding of the properties and distributions of these stellar bodies.

5.4.3 Galactic Populations within the Primary Sample

5.4.4 Identifying Galactic Populations via UVW Space Motions

In this section, we explore which populations our Primary Sample of 590 stars belong to within the context of the Milky Way Galaxy. This classification is based on the UVW space motions as reported in Table A.2 in Appendix B. To distinguish between the different populations, we use a Toomre diagram, a detailed description of which follows.

In Figure 5.13, we employ a Toomre diagram to differentiate the Galactic regions within our sample of 590 stars. Dotted curves drawn at velocities of 75 km/s and 180 km/s from Bensby et al. (2003) and Hinkel et al. (2014) provide provisional demarcations for the thin disk, thick disk, and halo populations. These population members are graphically represented as squares for the thin disk (475 stars = 80%), triangles for the thick disk (114 stars

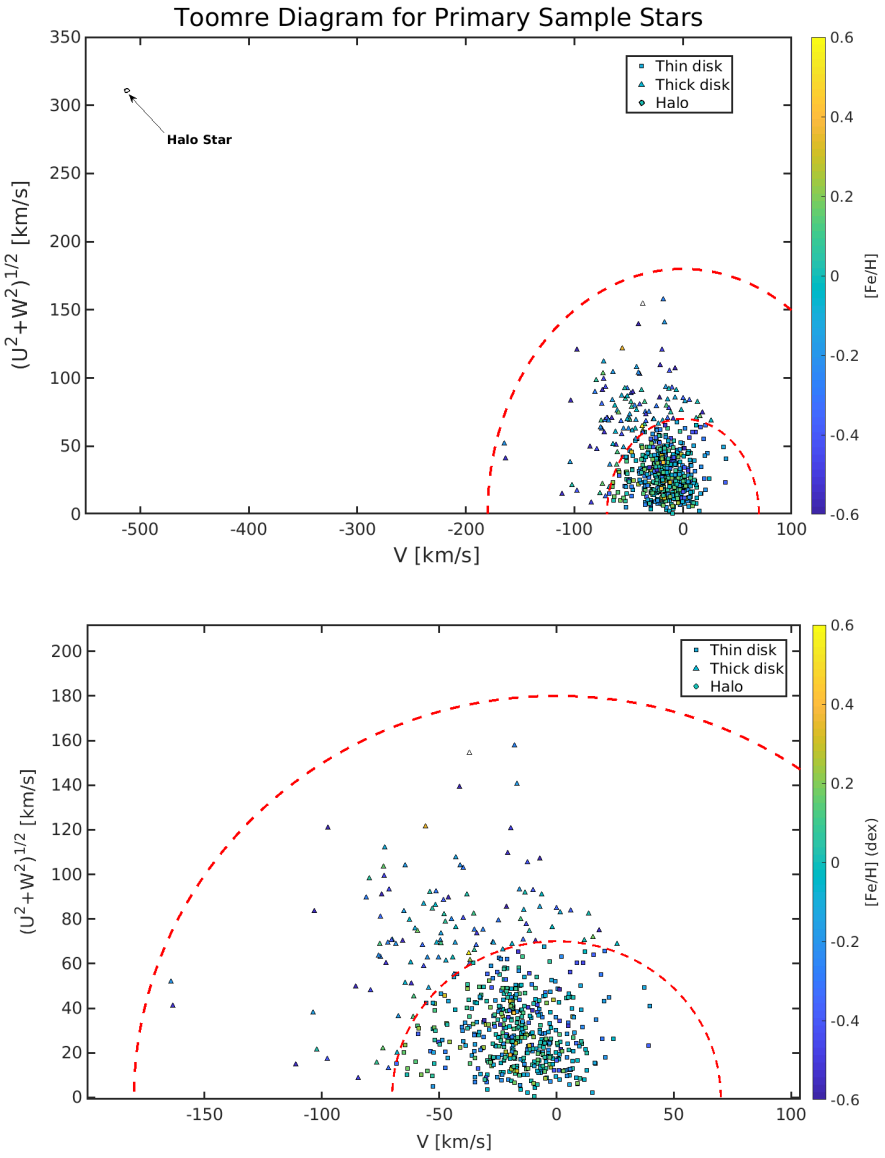

Figure 5.13 (a) The Toomre diagram of our 590-star sample helps distinguish Galactic regions. The dotted curves at 75 km/s and 180 km/s roughly delineate the thin disk, thick disk, and halo populations. The thin disk (squares), thick disk (triangles), and halo (circle) contain 473, 116, and 1 stars respectively. The overlaid color bar indicates metallicity ([Fe/H]) for each star. (b) A zoomed-in view of the Toomre diagram, focusing on the area with x values from -200 to +100 km/s and y values from 0 to 200 km/s, providing a more detailed look at the spatial distributions within the thin and thick disk populations.

= 20%), and a circle for the halo (1 star, effectively 0%). An overlaid color bar in the plot signifies the metallicity ([Fe/H]) corresponding to each star.

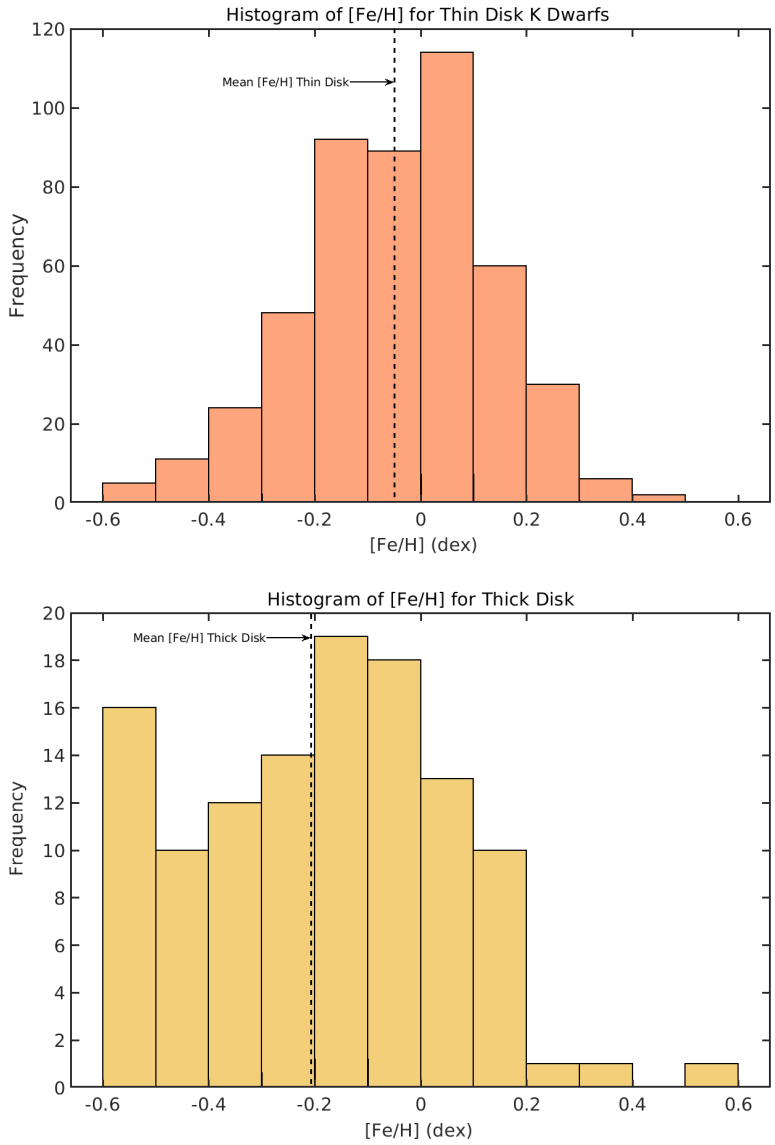

Figure 5.14 Histograms illustrating the [Fe/H] distribution of K dwarfs in two distinct populations within the Milky Way Galaxy. The top histogram represents the thin disk population, with a mean [Fe/H] value indicated by a vertical dashed line at -0.05 dex. The bottom histogram represents the thick disk population, with a mean [Fe/H] value indicated by a vertical dashed line at -0.21 dex.

In a bid for a more nuanced analysis, we juxtapose our results with those of Hinkel et al. (2014), who investigated a sample of over 2000 nearby stars. The proportions of thin and thick disk stars from our sample align well with her reported fractions — we identify 19% of nearby stars as members of the thick disk population, mirroring the 18% found by Hinkel et al. (2014), a comparable value also reported by Adibekyan et al. (2013). Similarly, Hinkel et al. (2014) observed negligible differences in the average [Fe/H]values between these two regions, a conclusion echoed in our findings.

As depicted in Figure 5.14, our study reveals that the mean [Fe/H]for the thin disk is -0.05 dex, while for the thick disk, it is -0.2 dex. This suggests that the thick disk population is approximately 30% more metal-poor than the thin disk. This contrast, albeit significant, is less marked than the disparities reported in earlier studies, which cited a difference of about -0.2 to -0.3 dex for nearby stars (Feltzing et al. 2003; Reddy et al. 2006). Furthermore, larger differences of about -0.5 dex have been reported in investigations covering a more extensive spatial extent of the Galaxy (Ivezić et al. 2008). Such observations imply a steeper metallicity gradient or that the thick disk's metallicity decreases progressively with increasing distance from the Galactic center.

One fact that stands out in our analysis is that of the 46 stars identified as young or active, only one K dwarf, HD 196998, falls in the thick disk population. This star is also known as DG Cap, and as described in §4.6, is an RV variable star with a close companion; we reported this star to be an SB1 in Hubbard-James et al. (2022). The rest of our young or active stars are members of the thin disk population.

Finally, we note the single outlier point on all four plots in Figure 5.12, located at the top left of Figure 5.13 (a). This outlier is HD 134439 (RKS ID = RKS1510-1622, a.k.a. LHS 53, GJ 579.2), a high proper motion star (3.68″/yr) at a distance of 29.4 pc. It is a known metal-poor subdwarf with [Fe/H]<-1.0 dex, and was probably accreted from a dwarf galaxy merger (Lim et al. 2021). The Galactic motions of this star place it firmly in the halo region of our Toomre diagram, making it the only halo star in our sample. As mentioned in §5.2, this star has a unique spectrum compared to all other K dwarfs in our sample and lies outside the boundaries of the ESM library, preventing the measurement of its $T_{\rm eff}$ and [Fe/H]using this tool.

5.5 42 Stars with Reported Exoplanets in our Primary Sample

According to the NASA Exoplanet Archive[3], as of May 14th, 2023, 42 of the 615 K dwarfs in the Primary Sample have been reported to have exoplanets, representing just 7% of the complete set of stars surveyed here. This is certainly an underestimate, as a systematic reconnaissance of even this set of the nearest K dwarfs has not been done. The RECONS group in fact embarked upon this spectroscopic survey with CHIRON precisely because the nearby K dwarfs have been neglected in planet searches — they are not as bright as G dwarfs at similar distances (nor are they as anthropocentrically favored), and do not reveal planets as low in mass or small in size as when M dwarfs are searched to the same precision with either radial velocity or transit methods, respectively.

Interestingly, for the current set of 42 known exoplanets, there appears to be no discernible

[3]https://exoplanetarchive.ipac.caltech.edu/

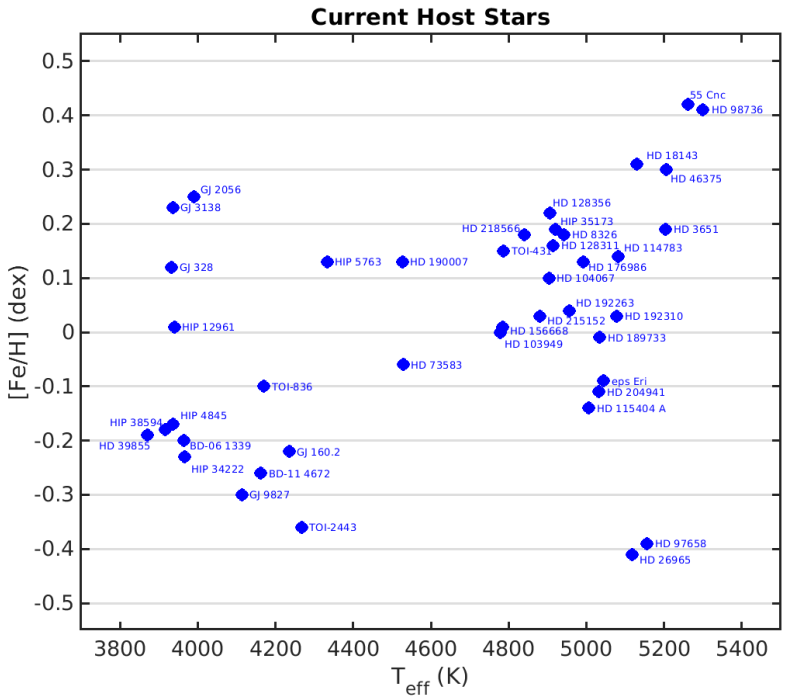

Figure 5.15 The 42 nearby K dwarfs reported to have exoplanets are shown on the [Fe/H]vs. $T_{\rm eff}$ plot in the same format as Figure 5.7. The stellar parameter values were determined via ESM. Note that planets have been reported orbiting K dwarfs throughout the range of metallicities measured. The K dwarfs highlighted here are: HD 3651 (RKS0039+2115), HIP 4845 (RKS0102-1025), HIP 5763 (RKS0113+1629), HD 8326 (RKS0122-2653), GJ 3138 (RKS0209-1620), TOI-2443 (RKS0240+0111), HIP 12961 (RKS0246-2305), HD 18143 (RKS0255+2652), eps Eri (RKS0332-0927), GJ 160.2 (RKS0406-2051), HD 26965 (RKS0415-0739), TOI-431 (RKS0533-2643), BD-06 1339 (RKS0553-0559), HD 39855 (RKS0554-1942), HD 46375 (RKS0633+0527), HIP 34222 (RKS0705+2728), GJ 2056 (RKS0712-2453), HIP 35173 (RKS0716-0339), HIP 38594 (RKS0754-2518), HD 73583 (RKS0838-1315), 55 Cnc (RKS0852+2819), GJ 328 (RKS0855+0132), HD 97658 (RKS1114+2542), HD 98736 (RKS1121+1811), HD 103949 (RKS1158-2355), HD 104067 (RKS1159-2021), HD 114783 (RKS1312-0215), HD 115404 A (RKS1316+1701), HD 128311 (RKS1436+0944), HD 128356 (RKS1437-2548), TOI-836 (RKS1500-2427), HD 156668 (RKS1717+2913), BD-11 4672 (RKS1833-1138), HD 176986 (RKS1903-1102), HD 189733 (RKS2000+2242), HD 190007 (RKS2002+0319), HD 192263 (RKS2013-0052), HD 192310 (RKS2015-2701), HD 204941 (RKS2132-2057), HD 215152 (RKS2243-0624), HD 218566 (RKS2309-0215), and GJ 9827 (RKS2327-0117). Names used are the identifiers used by the NASA Exoplanet Archive, with RKSTAR IDs in parentheses.

correlation between the host star's metallicity and the presence of an exoplanet. As depicted in Figure 5.15, these host stars span almost the full range of [Fe/H]values calculated using Empirical SpecMatch. Notably, the metal-rich host 55 Cancri (RKS0852+2819), with a [Fe/H]value of +0.42 dex, harbors five confirmed planetary companions, one of which, 55 Cancri f (Harriot), resides within the habitable zone (Butler et al. 1997; Fischer et al. 2008). However, with an $M_p \sin i = 45.8 \pm 12.7$ $M_\oplus$, it is unlikely to possess a solid surface conducive to life (Fischer et al. 2008). Conversely, GJ 9827 (RKS2327-0117), a K6V star with a [Fe/H]of -0.3 dex, hosts a multi-planetary system composed of three super-Earths in close orbit to the host star, each with short periods of less than 10 days (Niraula et al. 2017).

It is important to note that none of the 65 confirmed planets in our sample are currently deemed as promising candidates for habitability. However, hope is not lost. As we will introduce in the following section, there exists a set of stars within our sample that lack the youth and activity markers discussed herein and are also devoid of close binaries. These stars represent a new frontier for the continued search for potentially habitable exoplanets.

5.6 The Best 500 K Dwarfs for Exoplanet Searches — Calm Stars Without Close Companions

One of the primary outputs of this work is a set of stars deemed 'most suitable' for hosting life-bearing worlds. Through this research, we have identified 46 young and/or active stars that are presumably less suitable than astrophysically quiet, likely older stars. This work was conducted in parallel with a companion survey carried out on the same set of stars by Leonardo Paredes, who identified 48 stars in the sample with known companions within

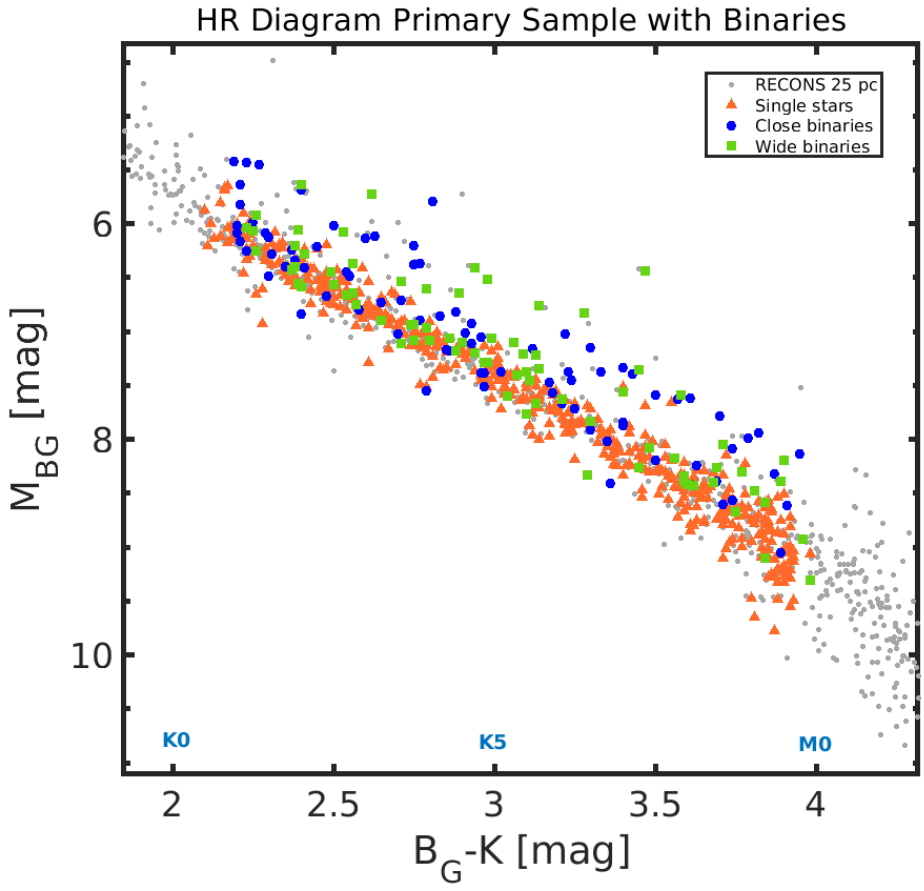

Figure 5.16 Updated HR diagram (original Figure 2.2) showcasing the RECONS sample of stars within 25 pc (grey dots), along with the 615 primary sample K dwarfs in the equatorial 33.3 pc sample. Single stars are marked as orange triangles, close binaries are represented by blue circles, and wide binaries are denoted by green squares. Notice the distinct sequence of multiple stars above the main sequence stars, as well as the presence of a modest collection of subdwarfs along the lower envelope of the main sequence. Magnitude data are sourced from *Gaia* DR3 ($BP = B_G$, updated from the original DR2 list) and 2MASS ($K_s = K$). Absolute B_G magnitudes were computed using *Gaia* DR3 parallax measurements, replacing the previous DR2 values. **Spectral type guidelines are provided along the x-axis for reference.**

a few astronomical units, along with another 31 with previously unknown companions at similar distances. Excluding these sets of young/active stars and those with close compan-

ions (including the two spectroscopic binaries discovered here), and accounting for overlaps between the samples, we are left with a list of 500 stars, presented in Table A.3. These stars can be considered the most suitable for hosting habitable planets. This is encouraging news—approximately 80% of K dwarfs in the solar neighborhood do not have (obviously) disqualifying attributes that would preclude them from having orbiting planets in at least relatively stable flux and dynamical environments.

This list of 500 stars may be further reduced by considering additional factors not covered by the RECONS work using CHIRON spectroscopy. For example, stellar companions at separations out to a few tens of AU may cause planets' orbital eccentricities to be enhanced, producing environments with large temperature fluctuations.

The updated HR diagram (Figure 5.16) provides valuable insights into this aspect. Close binaries, represented by blue circles, are defined as spectroscopic binary 1 (SB1) and spectroscopic binary 2 (SB2) systems with orbital periods less than a decade. They exhibit a distinct presence above the main sequence stars, indicative of their combined light contributing to their positions in the HR diagram. This underscores the importance of understanding stellar multiplicity when evaluating the suitability of stars for hosting habitable planets, as it is evident that close binaries may represent challenging environments for stable, habitable planets.

Furthermore, the prevalence of single and wide binary stars, marked as orange triangles and green squares respectively, emphasizes their potential as hosts for life-bearing worlds. The wide binaries are all resolved in Gaia, signifying the potential precision and accuracy

of the Gaia mission in identifying and characterizing such systems. This understanding of the different categories of stars and their implications for planetary habitability is a critical component of our ongoing studies into stellar and planetary dynamics.

K dwarfs with large and/or variable X-ray and ultraviolet fluxes may adversely affect atmospheres on any orbiting planets, although the effects of such high energy photons on planetary atmospheres are far from settled (Lammer et al. 2003; France et al. 2018). These are a few factors beyond the two addressed by this work (young/active stars) and the work by Paredes (companions), and are among those outlined in future work in Chapter 6.

5.7 Primary Sample Systems Worthy of Note

To readers: there will be a fairly large set of stars collected here for easy future reference. Each will have a brief description outlining why the star has been found to be interesting via this work. This list will include the 46 young/active stars found in the sample, the 1 halo star, 3 new binaries, a few exceptional stars reported to have planets, and a few other stars that simply must be described.

5.8 Primary Sample Systems Worthy of Note

RKS0252-1246: 1 **HD 17925** was initially identified as a young star due to its strong Li I feature (Cayrel de Strobel & Cayrel 1989). Despite its youth, our analysis did not classify it as chromospherically active. Examination of its Ca II line, as shown in Figure 5.1, revealed some core emission, yet the equivalent width relationships for Hα and the Ca II ratio did not indicate chromospheric activity. Moreover, using the BANYAN Σ tool, this star is not

linked to any specific moving group or cluster, suggesting it's a field star.

RKS0329-2406: [2] **AK For** is distinguished as an active and eclipsing binary system comprising two K-type stars, as described by Hełminiak et al. (2014). Our study, featuring its spectra in Figure 5.1, captures the spectral attributes of both these active stars. Uniquely, it stands as the sole double-lined spectroscopic binary in our sample that also presents Ca II core emission. Owing to its status as an SB2, we could not ascertain their specific stellar properties.

RKS0417+2033: [3] **HD 284336** is a previously unidentified young or active star that we have now classified as such. Our spectral examination, evident in Figure 5.1, reveals a noticeable presence of the Li I absorption line, typically indicative of stellar youth. Although not characterized by high rotational speed, as per our calculated $v \sin i$ values, HD 284336 is found within the thin disk population of the galaxy, a feature worth noting. This new discovery warrants further investigation.

RKS0430+0058: [4] **MCC 446** displays notable chromospheric activity according to our metrics used in this study. This late-type K dwarf, which currently has no detected companion, exhibits an Hα equivalent width of -0.11 Å, indicative of an emission line, and an EW[Ca II] ratio < 0.43—beyond the cutoff for activity as established in Figure 5.8. Despite its activity, MCC 446 has not been recognized as an active star within the solar neighbor-

hood in existing literature.

RKS0436+2707: 5 **HD 283750, also known as V833 Tau or BD +26 730**, is a renowned flare star in our solar neighborhood. Its activity and status as a single-lined spectroscopic binary (SB1) with a two-day period were first noted by Hartmann et al. (1981). HD 283750 is among the most active stars in our study, exhibiting an EW[Hα] of -0.34 Å and an EW[Ca II] ratio of 0.21. Interestingly, despite its elevated activity and binary status, its γ velocity—measured by RECONS—aligns with the Gaia DR3 value, as shown by its position on the 1-to-1 line in Figure 5.10.

RKS0441+2054: 6 **HD 29697 or V834 Tau** is a known active star and is also one of the seven RVV K dwarfs that were analyzed with our benchmark sample. It is described in more detail in § 4.6.

RKS0536+1119: 7 **V2689 Ori**, known as an active/variable star, was categorized as an RS CVn Variable by **?**, who also marked it as a young disk star that does not belong to any specific kinematic group. The BANYAN Σ analysis in our study concurs with this designation, reinforcing the status of V2689 Ori as an active field star. Figure 5.1 displays a faint yet distinct Ca II core emission.

RKS0658-1259: 8 **HD 51849**, identified as an active star with a stellar companion, was

classified as an SB1 with a separation of 0.5″by Tokovinin et al. (2019). Our research exhibits evidence of both activity and youthfulness in this proximate binary system. Figure 5.1 reveals a minor Li I absorption line, while Figure 5.4 indicates that HD 51849 doesn't align with the old locus for EW[Li I] and EW[H α].

RKS0723+2024: 9 **BD+20 1790** serves as a notable member of the AB Dor Moving Group. Recognized as a young star, it boasts an estimated age of 120 Myr. BD+20 1790 was flagged in our study as both youthful and active, as supported by spectroscopic and kinematic assessments. Notably, it displays a heightened rotational velocity with a $v \sin i$ measurement of 7.99 km/s. Its distinctive space motions further classify BD+20 1790 as a thin disk star.

RKS0734-0653: 10 **HD 60491**, categorized as a young star and potential member of the Ursa Majoris moving group by Montes et al. (2001), only meets one of the two kinematic criteria for association membership. Our analysis, as well as the BANYAN Σ tool, does not identify HD 60491 as part of any moving group. However, we do note the existence of a minor Li I absorption line in Figure 5.1, despite a lack of chromospheric activity at H α or Ca II.

RKS0819+0120: 11 **BD+01 2063**, acknowledged as a young star and a member of the Carina-near (estimated age ∼200 Myr) association (Ujjwal et al. 2020), is also placed in the Carina moving group by the BANYAN Σ tool. Although our analysis reveals a robust Li I

absorption line (as shown in Figure 5.2), there's no evidence of chromospheric activity.

RKS0850+0751: 12 **BD+08 2131A** is recognized as an active star with a close companion (separated by 1.5″) as per Mason et al. (2006). Based on its EW[H α] value, our study also classifies BD+08 2131A as an active star.

RKS0904-1554: 13 **HD 77825**, previously identified as a young star and a member of the Castor Moving Group (estimated age 200 Myr) by Montes et al. (2001), does not correlate with any moving group or association according to the BANYAN Σ tool. Our observations depict a faint but discernible Li I absorption line as seen in Figure 5.2. However, we found no additional spectroscopic signs of youth or activity.

RKS0907+2252: 14 **HD 78141**, identified as a young star by Stanford-Moore et al. (2020), is estimated to be between 50-400 Myr old, as evidenced by a strong Li I signature. Our study corroborates this, depicting a profound Li I absorption feature in Figure 5.2. Notably, HD 78141 deviates from the 1-to-1 line in Figure 5.10, likely due to its classification as an SB1 star with a period of 160 days (Griffin 2016).

RKS0932-1111: 15 **LQ Hya** is a well-known young and chromospherically active K dwarf, initially reported by Fekel et al. (1986), and classified as a BY Draconis variable. The spectrum of LQ Hya in Figure 5.2 reveals not only a Li I absorption line and Ca II core emission,

but also notably broader spectral lines compared to its K dwarf counterparts, attributable to rotational broadening. Our measurements give LQ Hya a $v \sin i$ value of 27.44 km/s.

RKS1043-2903: 16 **V419 Hya** is a recognized BY Draconis variable, with a debris disk reported by Plavchan et al. (2009) using data from the Spitzer Space Telescope. While our analysis categorizes V419 Hya as youthful due to a strong Li I absorption line, no signs of chromospheric activity were observed. Additionally Figure 5.2 shows a sall but clear core emision at the center of the Ca II line.

RKS1121-2027: 17 **HD 98712A**, part of a known binary system, displays chromospheric activity potentially linked to its close companion as reported by Paredes (2021). Our study identified this K dwarf as active based on both EW[H α] and EW[Ca II] ratio tests. The absence of the Li I feature adds credence that this activity is due to the presence of a close companion and not youth.

RKS1205-1852: 18 **HD 105065** is a known active star and is also one of the seven RVV K dwarfs that were analyzed with our benchmark sample. It is described in more detail in § 4.6.

RKS1303-0509: 19 **PX Vir** is also a member of our benchmark sample and was described in detail in § 4.6.

RKS1306+2043: 20 **BD+21 2486A** is the primary component of a multi-star system comprising at least three stellar bodies. This K5V star is orbited by an M4V and an L5 star, as reported by Gomes et al. (2013). In our investigation, BD+21 2486A exhibited signs of chromospheric activity. However, similar to HD 98712A, this activity is likely due to the influence of nearby companions, rather than indicating stellar youth.

RKS1822+0142: 28 **BD+01 3657** is a known active star and is also one of the seven RVV K dwarfs that were analyzed with our benchmark sample. It is described in more detail in § 4.6.

RKS2041-2219: 31 **HD 196998 or DG Cap** is a known active star and is also one of the seven RVV K dwarfs that were analyzed with our benchmark sample. As detailed in Section 5.4.2, **DG Cap** is uniquely positioned as the sole active star from our sample within the Milky Way Galaxy's thick disk population. It is described in more detail in § 4.6.

RKS0706+2358 **BD+24 1529**: Identified as a member of the AB Dor moving group from our kinematic analysis and the BANYAN Σ tool, this star has an estimated age of ∼120 Myr. Yet, it exhibits no spectroscopic signs of activity or youth, which isn't unusual for late K dwarfs (Soderblom 2010).

RKS0820+1404: **BD+14 1876**: Identified as a member of the AB Dor moving group from

our kinematic analysis and the BANYAN Σ tool, this star has an estimated age of ∼120 Myr. Yet, it exhibits no spectroscopic signs of activity or youth, which isn't unusual for late K dwarfs (Soderblom 2010)

RKS0104+2607: **BD+25 162** Identified as a member of the Hyades cluster from our kinematic analysis and the BANYAN Σ tool, this star has an estimated age of ∼700 Myr.

RKS0121+2419: **Ross 788** Identified as a member of the Hyades cluster from our kinematic analysis and the BANYAN Σ tool, this star has an estimated age of ∼700 Myr.

RKS0300+0744: **BZ Cet** Identified as a member of the Hyades cluster from our kinematic analysis and the BANYAN Σ tool, this star has an estimated age of ∼700 Myr.

RKS0320+0827: **BD+07 499** Identified as a member of the Hyades cluster from our kinematic analysis and the BANYAN Σ tool, this star has an estimated age of ∼700 Myr.

RKS0322+2709: **LP 355-64** Identified as a member of the Hyades cluster from our kinematic analysis and the BANYAN Σ tool, this star has an estimated age of ∼700 Myr.

RKS0420-1445: **BD-15 767** Identified as a member of the Hyades cluster from our kinematic analysis and the BANYAN Σ tool, this star has an estimated age of ∼700 Myr.

RKS2254+2331: **G 67-33** Identified as a member of the Hyades cluster from our kinematic analysis and the BANYAN Σ tool, this star has an estimated age of ∼700 Myr.

RKS0917-0323: **HD 80133**, is a newly identified double-lined spectroscopic binary system (SB2). The binary nature of HD 80133 became evident during our study, with distinct double-line features observed in the CHIRON spectra, particularly in the spectral window from 6705 to 6720 Å. The double-line Ca I feature at 6717 Åpresented in Figure 5.3 for this star indicates its binary status. Given the 2.7″size of the fiber as projected on the sky, it is certain that the light from both stars in this system is sent to the spectrograph, as their separation is much smaller than this size.

RKS1833-1626: **HD 171075** another newly uncovered SB2. The binary nature of HD 171075 is marked by distinct double-line features in the CHIRON spectra. A double-line Ca I feature at 6717 Å, in the spectral window from 6705 to 6720 Å, is a clear indication of its binary status. It is ensured that the light from both stars in the system is sent to the spectrograph, considering the 2.7″size of the fiber as projected on the sky and the significantly smaller star separation. Please refer to Group E of Figure 5.3 for more information.

RKS1518-1837: **BD-18 4031** is an intriguing case in our study. It showed significant radial velocity variation despite no known companion. Our CHIRON observations and Leonardo

Paredes' doctoral work Paredes 2021 hint at the presence of a white dwarf companion in a highly elliptical orbit with a period of about 4.5 years. Despite strong indications, including a semi-amplitude of more than 11 km s^{-1} shown in Figure 5.11, the orbit's inclination is undetermined, leaving the secondary's mass elusive. Further X-ray ad UV investigation of this potential K dwarf-white dwarf binary could provide valuable insights into stellar dynamics.

RKS1510-1622: **HD 134439** is uniquely characterized by its kinematic and spectroscopic properties. HD 134439 stands as the lone halo star in our sample. It is a high proper motion, metal-poor subdwarf that likely originated from a dwarf galaxy merger, exhibiting distinct kinematics that place it in the halo region of our Toomre diagram in Figure 5.13. Spectroscopically, as presented in Figure 5.3 its unique attributes include the absence of prominent Fe I lines typical of K dwarfs and a much narrower Na I doublet, earning it a unique spot outside the ESM library's boundaries. Its distinguishing features underscore the rich diversity in the stellar population.

RKS1819−0156: **HD 168442 or GJ 710**, currently categorized as a calm K dwarf in our study (see Table A.3), has a fascinating future in store. Projections indicate that in about 1.3 million years, this star will pass near the Sun at a distance of only 0.0636 parsecs (Bailer-Jones 2022). At such proximity, GJ 710 would shine as brightly as the most luminous planets in our sky. Additionally, its apparent motion across our sky would also be noticeable, peaking at about one arcminute per year (de la Fuente Marcos & de la Fuente Marcos 2018).

CHAPTER 6

Summary of Results and Future Plans

6.1 Key Science Results

Our study has brought forth several significant findings that have enriched our understanding of K dwarf stars in both our Benchmark and Primary Samples. Here, we highlight the key scientific outcomes of our investigation:

1. **Youth and Activity:** Leveraging both spectroscopic and kinematic techniques, we found that approximately 8% of K dwarfs in our sample are either young or active.

2. **Metal-Poor Population:** We have identified 21 K dwarfs in our sample with [Fe/H]values of -0.5 dex or less using the same techniques. This metal-poor population represents around 4% of the stars analyzed.

3. **Galactic Populations:** By employing Galactic UVW space velocities, we categorized our sample of 590 stars into three distinct populations: the thin disk (475 stars = 80%), the thick disk (114 stars = 20%), and the halo (1 star, effectively 0%).

4. **Spectral Library:** We have constructed a spectral library featuring high-resolution CHIRON spectra of 600 nearby K dwarfs. This initiative led to the discovery of two new SB2s, detailed in §5.2.1.

5. **Stellar Properties:** With a comprehensive methodology, we determined $T_{\rm eff}$, [Fe/H], $\log g$, and $v \sin i$ for over 95% of our 615 K dwarf sample. Employing Empirical Spec-Match, stellar properties for K dwarfs are found to be: temperatures from 3600–5500

K, metallicities from −0.6 to +0.55 dex, and rotational velocities measureable from 10–50 km/s.

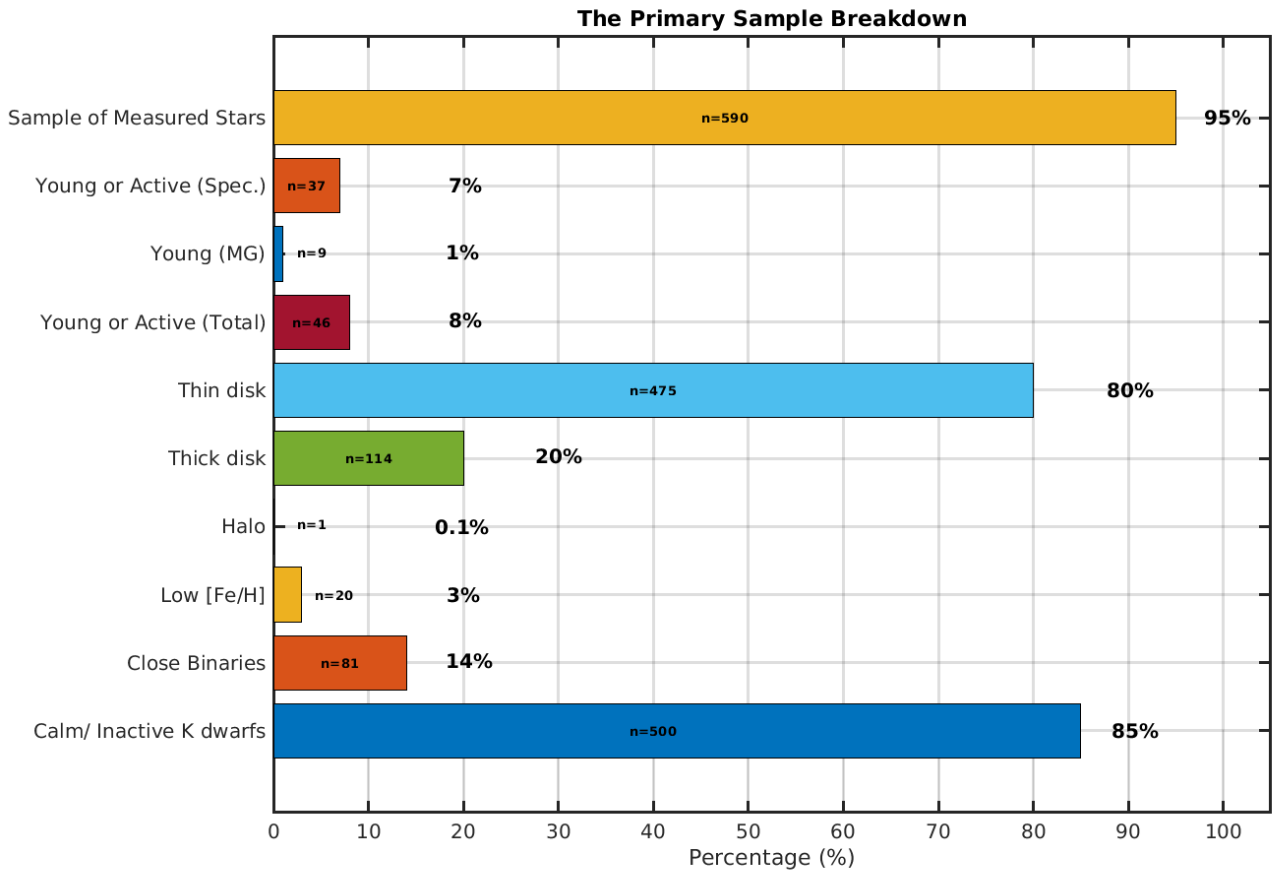

Figure 6.1 This bar plot illustrates the sizes of various sub-samples within our "analyzed" main study sample, which consists of 590 K dwarfs. The sub-samples include Young Active stars, Thin Disk stars, Thick Disk stars, Halo stars, stars with Low Metallicity, Close Binary stars, and Calm/Inactive stars.

6. **Benchmark Sample:** To aid the completion of this work a benchmark set of K dwarfs was constructed, composed of 35 K dwarfs from nearby moving associations and open clusters. These stars provide reliable age estimates, and the set includes 9 stars from the β Pic moving group (20 Myr), 6 from the Tucana-Horologium association (40 Myr), 7 from the AB Doradus moving group (120 Myr), 8 from the Hyades cluster (700 Myr), and 5 field K dwarfs with robust age estimates (1.5-5 Gyr). This sample is detailed in §2.4.

7. **Complementary Companion Survey:** Concurrent to our survey, a radial velocity search for close companions was conducted by Leonardo Paredes for an analogous set of about 700 K dwarfs. This endeavor identified 31 close binaries in our primary sample, augmented by 2 from our spectral library work and an additional 48 from the SB9 database and other literary sources, totaling 81 K dwarfs with close binaries.

8. **The Calm K Dwarfs:** Having identified 46 young or active K dwarfs and considering the 81 close-binary systems within our 615-star sample, we established a set of (exactly) 500 "Calm K dwarfs". This breakdown is illustrated visually in Figure 6.1. We propose these stars as optimal hosts for habitable planetary companions.

6.2 Contributions as CHIRON Data Tsar (2018–2022)

My tenure as the Data Manager for the CHIRON echelle spectrometer has afforded me the opportunity to contribute substantially to its effective use in research. CHIRON is the operating instrument at the CTIO/SMARTS 1.5m telescope. With over 300 operational nights per year, it generates an enormous volume of both calibration and scientific data for dozens of Principal Investigators in the U.S., Chile, and Europe.

As the Data Tsar, my responsibilities spanned from the organization and processing of this wealth of data to its distribution to the scientific community. This role required the development of comprehensive and efficient systems to manage large datasets, alongside the implementation of stringent quality control procedures to ensure the integrity and utility of the data.

From December 2017, the processed data have been a crucial component of numerous scientific endeavors. Datasets have facilitated the publication of over 70 peer-reviewed articles and been instrumental in the successful completion of seven Ph.D. dissertations. The data's broad application showcases the quality and scientific relevance of the processed datasets.

In addition, my contributions as the Data Tsar have led to my authorship in 12 peer-reviewed articles, further emphasizing the importance and impact of this role.[1] This role not only allowed me to contribute to a vital astronomical resource but offered me the opportunity to refine my data management and processing skills.

[1]For more information on my publications, visit `https://orcid.org/0000-0003-4568-2079`

6.3 Mentorship and Skill Development

Throughout my tenure as a graduate student at Georgia State University (GSU), I've seized numerous opportunities for both mentorship and to enhance my teaching abilities, which have significantly contributed to my professional development.

In my role as a co-lecturer for a synchronous variant of the introductory Astronomy course, ASTR 1000 (Introduction to the Universe), I facilitated the learning process for a diverse group of approximately 120 students. The course employed both online and in-person formats to broaden student accessibility. Over the semester, I delivered twelve lectures on a range of topics, from the Solar System to astrobiology and the potential for life beyond Earth, to stellar evolution. This experience allowed me to refine my pedagogical skills and gain proficiency in effectively communicating complex scientific concepts to a broad audience.

I also had the rewarding opportunity to mentor Astronomy Post-Baccalaureate student, D. Xavier Lesley, over a two-year period. During this mentorship, Mr. Lesley achieved notable academic milestones. He gained acceptance to the Physics Masters program at Southern Connecticut State University (SCSU) and earned the Best Graduate Astronomy Poster Presentation Award at the 2022 National Society of Black Physicists (NSBP) meeting. Impressively, he has recently been accepted into multiple Astronomy Ph.D. programs, including those at GSU and Ohio State University. Guiding a student through such pivotal career moments has enriched my capabilities as a mentor.

Additionally, I trained graduate students in stellar spectral analysis techniques, including RECONS students Sebastián Carrazco-Gaxiola and Tim Johns. The act of imparting com-

plex methodologies required effective communication skills, thereby enhancing my capacity to convey intricate scientific concepts. Concurrently, it reinforced my own comprehension of these techniques.

These experiences have furnished me with a robust set of skills in mentorship, pedagogy, and scientific communication, which will undoubtedly be invaluable in my future career endeavors.

6.4 Future Directions

Exoplanet Search: Subsequent observations will focus on the pursuit of terrestrial-sized exoplanets orbiting the "Calm K dwarfs" identified in our study. As a first step, a recent NEID proposal has been approved to conduct extreme precision radial velocity follow-up observations of 15 K dwarfs. These candidates were recognized as inactive through the integration of findings from this study and collaborative work by Leonardo Paredes.

Sample Expansion: The intention is to augment the quantity of stars evaluated with the spectroscopic and kinematic methodologies expounded here. As a reminder, the RKSTAR sample contains an additional ∼4,400 K dwarfs awaiting assessment. Thus far, we have procured CHIRON spectra for more than 1,000 additional K dwarfs within 50 pc not discussed in this study. This work will continue, bolstered by contributions from RECONS graduate students Sebastián Carrazco-Gaxiola and Tim Johns, in addition to the combined efforts of Leonardo Paredes and myself.

Chromospheric Activity Studies: To enhance our understanding of the high-energy emissions of K dwarfs, we plan to explore the correlation between the chromospheric activity indicators identified in this study, namely the Hα and Ca II IRT lines, and archival X-ray and UV data. A preliminary search revealed that over 300 RKSTAR members, each with a CHIRON spectrum, possess available ROSAT X-ray data and Galex FUV & NUV values. This line of research, similar to that conducted for M dwarfs and a select number of K dwarfs by Youngblood et al. (2017); Richey-Yowell et al. (2019); Melbourne et al. (2020); Richey-Yowell et al. (2022); Youngblood et al. (2022), holds great promise. Our comprehensive spectroscopic survey of all K dwarf primaries within 50 pc will yield a more refined list of the most "Calm K Dwarfs" in the Solar Neighborhood, and allow us to understand the context of our Earth and ourselves among the stars.

Appendices

Page left intentionally blank.

CHAPTER A

Tables

A Table of Astrometry and Photometry Data for Primary Sample

Table begins on next page.

Table A.1: Primary K dwarf Sample: Astrometry and Photometry Data

Star Identifiers		**Coordinates**		$\boldsymbol{\mu}$		$\boldsymbol{\pi}$		**Photometry**		
RKS ID	Simbad Name	R.A.	Decl.	$\mu_{R.A}$	μ_{Decl}	π	Dist.	$B_{Gaia\ DR3}$	B_G–K_S	M_{B_G}
...	...	(hh mm ss)	(±dd mm ss)	(mas yr^{-1})	(mas yr^{-1})	(mas)	(pc)	(mag)	(mag)	(mag)
RKS0000+1659	HD 224808	00 00 48.1	+16 59 17	−52.202	−307.385	33.259	30.07	9.02	2.68	6.63
RKS0001−1656	BD-17 6862	00 01 25.8	−16 56 54	293.902	−253.436	31.760	31.49	11.00	3.78	8.51
RKS0007−2349	HD 283	00 07 32.5	−23 49 07	320.873	91.243	30.493	32.79	8.91	2.23	6.33
RKS0012+2142	G 131-35	00 12 33.5	+21 42 48	190.416	−287.327	31.941	31.31	11.97	3.93	9.49
RKS0012+2705	BD+26 8	00 12 04.0	+27 05 56	283.168	−82.125	38.586	25.92	8.95	2.65	6.88
RKS0016−1435	BD-15 36	00 16 11.0	−14 35 27	0.787	−6.442	30.709	32.56	9.81	3.01	7.25
RKS0017+2057	G 131-51	00 17 59.1	+20 57 24	−252.047	−366.920	36.095	27.70	11.34	3.93	9.13
RKS0019−0303	LP 644-95	00 19 12.3	−03 03 13	−26.882	−217.813	32.057	31.19	11.16	3.70	8.69
RKS0019−0957	BD-10 47	00 19 05.5	−09 57 53	−36.325	−301.491	49.476	20.21	10.15	3.60	8.62
RKS0020+1738	StKM 1-25	00 20 57.1	+17 38 15	39.000	−82.391	33.447	29.90	11.47	3.93	9.09
RKS0021+2531	BD+24 32	00 21 16.0	+25 31 27	50.967	9.511	35.552	28.13	9.76	2.79	7.51
RKS0022−2701	HD 1815	00 22 23.5	−27 01 57	287.803	−423.699	45.954	21.76	8.53	2.40	6.84
RKS0024−2701	HD 2025	00 24 25.9	−27 01 36	665.755	83.964	55.824	17.91	8.15	2.59	6.88
RKS0036−0930	BD-10 109	00 36 00.0	−09 30 56	−175.500	−568.464	32.666	30.61	11.44	3.72	9.01
RKS0036+2610	BD+25 84	00 36 57.9	+26 10 54	76.163	41.996	43.614	22.93	9.28	3.10	7.48
RKS0039+2115	54 Psc	00 39 21.8	+21 15 01	−461.948	−369.624	90.025	11.11	6.10	2.10	5.87
RKS0042+2239	G 69-14	00 42 56.7	+22 39 34	400.809	22.307	31.842	31.41	11.80	3.98	9.31

Continued on next page

Table A.1 – *Continued from previous page*

RKS ID	Simbad Name	R.A.	Decl.	$\mu_{R.A}$	μ_{Decl}	π	Dist.	$B_{Gaia\ DR3}$	B_G–K_S	M_{B_G}
...	...	(hh mm ss)	(±dd mm ss)	(mas yr^{-1})	(mas yr^{-1})	(mas)	(pc)	(mag)	(mag)	(mag)
RKS0045+0147	HD 4256	00 45 04.8	+01 47 07	−49.971	−572.962	44.660	22.39	8.26	2.52	6.51
RKS0048+0516	HD 4628	00 48 22.9	+05 16 50	755.894	−1141.719	134.495	7.44	5.96	2.28	6.60
RKS0051−2254	HD 4967	00 51 34.0	−22 54 36	613.260	−276.452	65.090	15.36	9.19	3.45	8.26
RKS0051+1844	HD 4913	00 51 21.7	+18 44 21	53.397	−268.549	45.022	22.21	9.47	3.23	7.74
RKS0055−2940	HD 5425	00 55 49.2	−29 40 33	403.008	153.692	31.847	31.40	9.70	3.13	7.22
RKS0057+0551	BD+05 127	00 57 44.5	+05 51 20	−55.518	1.403	56.149	17.81	10.50	3.86	9.25
RKS0102−1025	BD-11 192	01 02 21.1	−10 25 25	26.088	−176.920	47.383	21.10	10.25	3.72	8.63
RKS0102+0503	HD 6101	01 02 24.5	+05 03 41	329.920	216.275	44.460	22.49	8.40	2.89	6.64
RKS0104−2536	HD 6378	01 04 24.1	−25 36 18	−34.460	−318.168	37.063	26.98	10.01	3.17	7.85
RKS0104+2607	BD+25 162	01 04 32.4	+26 07 12	315.458	13.620	33.565	29.79	10.26	3.30	7.89
RKS0105+1523	HD 6440A	01 05 29.9	+15 23 24	7.734	−199.039	36.698	27.25	9.36	2.88	7.18
RKS0107+2257	HD 6660	01 07 37.8	+22 57 17	103.168	−490.281	48.681	20.54	8.66	2.90	7.10
RKS0108+1714	BD+16 120	01 08 40.3	+17 14 33	−58.972	−584.111	34.945	28.62	10.79	3.51	8.51
RKS0112−2514	HD 7279	01 12 46.1	−25 14 08	128.337	19.842	44.191	22.63	9.79	3.37	8.02
RKS0113+1629	BD+15 176	01 13 58.8	+16 29 40	14.057	−56.980	31.237	32.01	10.10	3.19	7.57
RKS0116+2519	G 69-62	01 16 39.3	+25 19 53	429.196	−102.681	41.876	23.88	10.33	3.67	8.44
RKS0117−1530	HD 7808	01 17 34.0	−15 30 11	278.042	−475.234	30.817	32.45	9.98	2.81	7.42
RKS0118−0052	HD 7895	01 18 41.0	−00 52 03	432.564	−253.357	36.399	27.47	8.22	2.18	6.03
RKS0121+2419	Ross 788	01 21 29.3	+24 19 50	340.496	9.073	36.888	27.11	10.95	3.84	8.78
RKS0122−2653	HD 8326	01 22 07.6	−26 53 35	−58.320	−224.943	32.565	30.71	9.00	2.50	6.56

Continued on next page

Table A.1 – *Continued from previous page*

RKS ID	Simbad Name	R.A.	Decl.	$\mu_{R.A}$	μ_{Decl}	π	Dist.	$B_{Gaia\ DR3}$	B_G–K_S	M_{B_G}
...	...	(hh mm ss)	(±dd mm ss)	(mas yr^{-1})	(mas yr^{-1})	(mas)	(pc)	(mag)	(mag)	(mag)
RKS0123−1257	HD 8389	01 23 02.6	−12 57 57	461.900	−25.696	33.273	30.05	8.08	2.16	5.69
RKS0124+1829	HD 8553	01 24 53.9	+18 29 59	547.139	−190.327	31.837	31.41	8.72	2.32	6.23
RKS0125−0103	BD-01 184	01 25 09.4	−01 03 34	−193.863	−291.595	31.367	31.88	9.71	2.79	7.19
RKS0129+2143	EO Psc	01 29 04.8	+21 43 23	458.856	−183.920	42.946	23.29	7.97	2.60	6.13
RKS0135−2046	BD-21 262	01 35 45.6	−20 46 13	129.221	−25.598	38.134	26.22	10.33	3.38	8.24
RKS0139+1515	BD+14 251	01 39 56.1	+15 15 33	218.026	−58.777	41.108	24.33	9.34	3.02	7.41
RKS0142+2016	107 Psc	01 42 29.7	+20 16 06	−300.737	−673.539	130.823	7.64	5.46	2.17	6.04
RKS0146+1224	HD 10853	01 46 38.7	+12 24 42	31.282	−74.827	41.646	24.01	9.13	2.81	7.23
RKS0150+1817	Wolf 89	01 50 28.0	+18 17 46	240.056	−78.656	33.096	30.22	11.01	3.77	8.61
RKS0150+2927	HD 11130	01 50 07.8	+29 27 52	−35.343	−63.383	37.098	26.96	8.26	2.15	6.11
RKS0200+2636	StKM 1-223	02 00 20.1	+26 36 00	177.778	64.447	31.769	31.48	11.24	3.65	8.75
RKS0205−2804	CD-28 657	02 05 23.6	−28 04 11	334.431	421.454	38.355	26.07	11.14	3.98	9.06
RKS0209−1620	BD-17 400	02 09 10.9	−16 20 22	516.409	79.440	35.112	28.48	11.13	3.88	8.86
RKS0213−2111	BD-21 397	02 13 12.1	−21 11 47	375.454	55.718	42.123	23.74	10.09	3.59	8.21
RKS0214−0338	HD 13789	02 14 13.5	−03 38 06	−12.327	−219.261	43.977	22.74	8.79	2.78	7.01
RKS0215−1814	HD 14001A	02 15 46.1	−18 14 17	−33.203	−124.582	43.481	23.00	8.57	3.14	6.76
RKS0221−0652	HD 14635	02 21 44.4	−06 52 46	295.337	51.396	36.064	27.73	9.31	2.84	7.10
RKS0229−1958	HD 15468	02 29 01.7	−19 58 45	588.791	266.760	51.606	19.38	9.01	3.18	7.57
RKS0231−1516	HD 15767	02 31 42.4	−15 16 24	−73.371	−117.842	37.189	26.89	8.90	2.50	6.75
RKS0231−2001	BD-20 470	02 31 30.8	−20 01 41	192.285	26.473	30.283	33.02	10.44	3.27	7.85

Continued on next page

Table A.1 – *Continued from previous page*

RKS ID	Simbad Name	R.A.	Decl.	$\mu_{R.A}$	μ_{Decl}	π	Dist.	$B_{Gaia\ DR3}$	B_G–K_S	M_{B_G}
...	...	(hh mm ss)	(±dd mm ss)	(mas yr^{-1})	(mas yr^{-1})	(mas)	(pc)	(mag)	(mag)	(mag)
RKS0236−0309	FT Cet	02 36 41.7	−03 09 22	323.279	58.329	40.952	24.42	8.35	2.41	6.41
RKS0236−2331	HD 16270	02 36 00.7	−23 31 16	83.275	14.006	47.090	21.24	8.57	2.74	6.93
RKS0236−2710	HD 16280	02 36 00.7	−27 10 42	76.421	−167.867	30.274	33.03	9.71	2.79	7.12
RKS0236+0653	HD 16160	02 36 04.9	+06 53 12	1778.585	1477.306	138.340	7.23	6.05	2.57	6.75
RKS0240+0111	BD+00 444	02 40 42.8	+01 11 55	283.915	231.745	41.822	23.91	9.75	3.25	7.86
RKS0242+0322	BD+02 418	02 42 32.5	+03 22 26	−142.083	−147.996	40.770	24.53	10.39	3.56	8.44
RKS0243+1925	HD 16909	02 43 20.8	+19 25 45	455.659	2.846	53.558	18.67	8.47	2.93	7.11
RKS0246−2305	CD-23 1056	02 46 42.8	−23 05 11	294.717	140.966	42.693	23.42	10.49	3.75	8.64
RKS0246+1146	HD 17230	02 46 17.2	+11 46 30	263.883	−211.576	61.891	16.16	8.85	3.32	7.81
RKS0246+2538	HD 17190	02 46 15.2	+25 38 59	237.592	−149.140	39.612	25.24	8.11	2.24	6.10
RKS0247+2842	LP 298-33	02 47 55.8	+28 42 44	−164.751	11.869	34.859	28.69	11.36	3.88	9.07
RKS0248−1145	BD-12 525	02 48 06.5	−11 45 47	−65.330	−218.142	35.121	28.47	11.02	3.80	8.75
RKS0248+2704	HD 17382	02 48 09.1	+27 04 07	278.469	−119.187	43.570	22.95	7.82	2.20	6.02
RKS0250+1542	HD 17660	02 50 36.8	+15 42 35	342.378	−395.393	42.845	23.34	9.14	3.01	7.30
RKS0251−0816	BD-08 535	02 51 44.4	−08 16 09	29.919	−10.559	32.420	30.85	10.06	3.09	7.61
RKS0251+1038	BD+10 378	02 51 42.8	+10 38 42	−116.976	−136.349	34.550	28.94	10.22	3.24	7.91
RKS0252−1246	HD 17925	02 52 32.1	−12 46 10	397.353	−189.281	96.520	10.36	6.28	2.11	6.20
RKS0255+2652	HD 18143A	02 55 39.0	+26 52 23	264.596	−193.329	44.432	22.51	7.82	2.39	6.06
RKS0255+2807	G 36-45	02 55 41.2	+28 07 47	270.819	−146.473	30.197	33.12	11.30	3.78	8.70
RKS0257−2458	HD 18445	02 57 13.1	−24 58 30	12.814	−32.401	40.986	24.40	8.05	2.63	6.11

Continued on next page

Table A.1 – *Continued from previous page*

RKS ID	Simbad Name	R.A.	Decl.	$\mu_{R.A}$	μ_{Decl}	π	Dist.	$B_{Gaia\ DR3}$	B_G–K_S	M_{B_G}
...	...	(hh mm ss)	(±dd mm ss)	(mas yr^{-1})	(mas yr^{-1})	(mas)	(pc)	(mag)	(mag)	(mag)
RKS0258+2646	HD 18450	02 58 52.4	+26 46 26	−16.713	125.166	34.505	28.98	8.43	2.30	6.12
RKS0300+0744	BZ Cet	03 00 02.8	+07 44 59	328.026	21.181	42.078	23.77	8.22	2.38	6.34
RKS0303+2006	BD+19 451	03 03 49.0	+20 06 39	31.276	−64.930	46.760	21.39	8.86	2.90	7.21
RKS0306+0157	HD 19305	03 06 26.7	+01 57 54	389.253	−925.026	67.934	14.72	9.31	3.66	8.47
RKS0308−2410	CD-24 1458	03 08 25.6	−24 10 03	−13.731	−165.532	34.930	28.63	10.35	3.38	8.07
RKS0308−2445	AE For	03 08 06.6	−24 45 34	302.720	121.742	30.987	32.27	10.48	3.82	7.94
RKS0310+1203	BD+11 444	03 10 15.1	+12 03 01	248.714	−157.697	34.663	28.85	9.62	3.00	7.32
RKS0314−2626	HD 20280	03 14 44.6	−26 26 46	216.810	98.169	53.554	18.67	9.39	3.32	8.03
RKS0314+0858	HD 20165	03 14 47.2	+08 58 50	400.579	−404.425	43.265	23.11	8.04	2.29	6.22
RKS0320+0827	BD+07 499	03 20 29.1	+08 27 16	226.368	5.974	31.603	31.64	9.86	2.98	7.36
RKS0322+2709	LP 355-64	03 22 28.1	+27 09 21	220.912	−64.348	31.470	31.78	11.27	3.85	8.76
RKS0324−0521	HD 21197	03 24 59.7	−05 21 49	−230.883	−768.479	65.261	15.32	8.11	2.99	7.18
RKS0329−1140	BD-12 662	03 29 19.7	−11 40 42	54.471	−304.357	47.551	21.03	10.24	3.79	8.63
RKS0329−2406	AK For	03 29 22.8	−24 06 03	222.666	98.094	32.168	31.09	9.48	3.22	7.02
RKS0332−0927	eps Eri	03 32 55.8	−09 27 29	−974.758	20.876	310.577	3.22	4.00	2.22	6.46
RKS0341+0336	BD+03 515	03 41 10.5	+03 36 40	−44.557	−238.701	38.620	25.89	9.85	3.70	7.78
RKS0342−2427	CD-24 1826	03 42 44.6	−24 27 58	24.428	−374.003	38.386	26.05	9.42	2.98	7.34
RKS0343−1253	BD-13 718	03 43 06.1	−12 53 39	−236.402	30.031	35.254	28.37	11.11	3.61	8.85
RKS0343−1906	HD 23356	03 43 55.3	−19 06 39	310.097	157.185	71.751	13.94	7.32	2.48	6.60
RKS0343+1640	BD+16 502	03 43 52.5	+16 40 19	157.855	−316.199	58.036	17.23	10.17	3.92	8.99

Continued on next page

Table A.1 – *Continued from previous page*

RKS ID	Simbad Name	R.A.	Decl.	$\mu_{R.A}$	μ_{Decl}	π	Dist.	$B_{Gaia\ DR3}$	B_G–K_S	M_{B_G}
...	...	(hh mm ss)	(±dd mm ss)	(mas yr^{-1})	(mas yr^{-1})	(mas)	(pc)	(mag)	(mag)	(mag)
RKS0344+1155	BD+11 514	03 44 51.1	+11 55 12	314.056	127.537	45.626	21.92	9.34	3.14	7.64
RKS0345−2751	HD 23588A	03 45 24.1	−27 51 44	303.236	111.826	48.493	20.62	8.43	2.83	6.86
RKS0348+1512	BD+14 611	03 48 32.9	+15 12 07	98.993	−86.656	30.277	33.03	9.74	2.78	7.15
RKS0348+2519	HD 23742	03 48 26.3	+25 19 23	14.778	−99.028	30.952	32.31	8.75	2.25	6.20
RKS0349−1329	StKM 1-413	03 49 15.9	−13 29 29	−66.759	−108.320	30.401	32.89	11.13	3.66	8.54
RKS0349+0120	HD 24002	03 49 35.6	+01 20 53	264.734	−614.840	30.965	32.29	8.79	2.26	6.24
RKS0350−2349	CD-24 1905	03 50 19.5	−23 49 44	79.417	−235.115	30.736	32.54	10.07	3.16	7.51
RKS0354−0649	BD-07 699	03 54 35.4	−06 49 33	−5.526	527.349	63.814	15.67	9.26	3.63	8.28
RKS0357−0109	HD 24916	03 57 28.6	−01 09 34	−185.712	−142.905	65.426	15.28	8.30	2.96	7.38
RKS0404+2634	HG 8-5	04 04 15.2	+26 34 24	215.018	−112.141	33.425	29.92	11.46	3.83	9.08
RKS0406−2051	BD-21 784	04 06 34.8	−20 51 11	52.803	−778.887	38.645	25.88	9.92	3.22	7.86
RKS0407+1413	LP 474-123	04 07 43.9	+14 13 24	173.569	−156.671	32.129	31.12	11.03	3.85	8.56
RKS0408+1220	HD 26129	04 08 30.8	+12 20 16	154.412	−336.187	32.422	30.84	8.82	2.40	6.37
RKS0414+0301	HD 26794	04 14 30.2	+03 01 19	109.692	269.509	31.804	31.44	9.02	2.53	6.53
RKS0415−0739	omi02 Eri	04 15 16.3	−07 39 10	−2240.085	−3421.809	199.608	5.01	4.63	2.13	6.13
RKS0417+2033	HD 284336	04 17 26.9	+20 33 17	−40.677	−60.185	34.859	28.69	9.80	2.99	7.51
RKS0417+2240	HD 284310	04 17 06.8	+22 40 23	117.200	−43.134	31.117	32.14	10.01	3.17	7.47
RKS0419−0408	BD-04 797	04 19 05.7	−04 08 55	101.215	−11.348	34.197	29.24	10.76	3.62	8.43
RKS0420−1445	BD-15 767	04 20 10.5	−14 45 39	177.490	114.407	34.130	29.30	10.02	3.19	7.69
RKS0421−1945	CPD-20 550	04 21 31.6	−19 45 23	−202.984	−289.813	40.550	24.66	10.68	3.57	8.72

Continued on next page

Table A.1 – *Continued from previous page*

RKS ID	Simbad Name	R.A.	Decl.	$\mu_{R.A}$	μ_{Decl}	π	Dist.	$B_{Gaia\ DR3}$	B_G–K_S	M_{B_G}
...	...	(hh mm ss)	(±dd mm ss)	(mas yr^{-1})	(mas yr^{-1})	(mas)	(pc)	(mag)	(mag)	(mag)
RKS0427+2426	HD 283668	04 27 52.9	+24 26 41	395.967	53.392	33.987	29.42	9.63	2.61	7.29
RKS0429+2155	HD 28343	04 29 00.1	+21 55 21	−67.017	174.627	89.055	11.23	8.56	3.68	8.31
RKS0430+0058	MCC 446	04 30 16.7	+00 58 47	83.781	−67.425	37.534	26.64	10.77	3.77	8.64
RKS0436+2707	HD 283750	04 36 48.2	+27 07 55	232.170	−147.481	57.487	17.40	8.36	3.12	7.16
RKS0439+0952	HD 286955	04 39 42.6	+09 52 19	−14.957	−375.912	32.999	30.30	9.42	2.91	7.01
RKS0441+2054	HD 29697	04 41 18.8	+20 54 05	−234.261	−254.314	75.687	13.21	8.18	3.03	7.58
RKS0443+2741	HD 29883	04 43 35.4	+27 41 14	53.728	−265.039	45.779	21.84	8.22	2.46	6.52
RKS0445+0938	StKM 1-508	04 45 27.2	+09 38 27	150.579	−109.354	33.054	30.25	11.43	3.93	9.03
RKS0448−1056	HD 30523	04 48 01.1	−10 56 01	82.354	−108.922	37.775	26.47	9.72	3.12	7.61
RKS0449−1447	BD-15 869	04 49 32.7	−14 47 22	−205.593	−285.196	39.860	25.09	11.12	3.92	9.12
RKS0451+2837	HD 30754	04 51 33.3	+28 37 49	93.427	−62.934	30.622	32.66	9.76	2.88	7.19
RKS0453+2214	HD 30973	04 53 04.7	+22 14 06	146.828	−133.025	37.837	26.43	9.04	2.75	6.93
RKS0454+0722	HD 31208	04 54 16.6	+07 22 22	248.001	−201.860	33.764	29.62	8.43	2.25	6.07
RKS0455−2833	HD 31560	04 55 41.9	−28 33 50	187.891	−226.512	54.920	18.21	8.36	2.82	7.06
RKS0500−0545	HD 32147	05 00 48.9	−05 45 13	549.309	−1108.245	113.072	8.84	6.45	2.74	6.72
RKS0503−2315	CD-23 2363	05 03 21.8	−23 15 01	311.295	164.312	41.485	24.11	9.53	3.61	7.62
RKS0503+0322	StKM 1-542	05 03 32.1	+03 22 56	−17.118	−57.398	31.381	31.87	11.51	3.77	8.99
RKS0506−1102	HD 32965	05 06 30.0	−11 02 34	36.656	−55.104	32.688	30.59	9.83	3.00	7.40
RKS0506+1426	HD 32850	05 06 42.2	+14 26 46	279.258	−232.554	37.437	26.71	7.95	2.21	5.82
RKS0512+1943	HD 241596	05 12 53.4	+19 43 19	367.813	−673.761	32.452	30.81	10.06	2.99	7.62

Continued on next page

Table A.1 – *Continued from previous page*

RKS ID	Simbad Name	R.A.	Decl.	$\mu_{R.A}$	μ_{Decl}	π	Dist.	$B_{Gaia\ DR3}$	B_G–K_S	M_{B_G}
...	...	(hh mm ss)	(±dd mm ss)	(mas yr^{-1})	(mas yr^{-1})	(mas)	(pc)	(mag)	(mag)	(mag)
RKS0513−2158	BD-22 1050	05 13 59.1	−21 58 24	64.800	58.462	31.677	31.57	10.66	3.48	8.16
RKS0514+0039	HD 290054	05 14 48.1	+00 39 43	232.044	−444.715	34.656	28.86	10.23	3.24	7.93
RKS0514+1952	HD 241814	05 14 17.0	+19 52 58	245.075	−225.903	31.433	31.81	9.71	2.94	7.20
RKS0518−2123	HD 34751	05 18 47.1	−21 23 37	−137.035	−36.954	48.966	20.42	9.63	3.48	8.08
RKS0519−0304	HD 34673	05 19 12.6	−03 04 25	699.910	137.824	63.644	15.71	8.04	2.99	7.06
RKS0519−1550	HD 34865	05 19 59.5	−15 50 22	173.704	207.709	42.094	23.76	8.96	2.75	7.08
RKS0522+0236	HD 35112	05 22 37.4	+02 36 11	65.953	−182.170	50.517	19.80	8.01	2.71	6.53
RKS0523+1719	111 Tau B	05 23 38.3	+17 19 26	250.984	−5.707	68.766	14.54	8.17	2.94	7.36
RKS0528−0329	HD 36003	05 28 26.0	−03 29 58	−307.985	−797.411	77.350	12.93	7.88	3.00	7.32
RKS0533−2643	CD-26 2288	05 33 04.6	−26 43 28	16.886	150.779	30.652	32.62	9.36	2.64	6.79
RKS0534−2328	HD 37065	05 34 48.6	−23 28 08	318.502	−433.353	36.038	27.75	9.02	2.54	6.80
RKS0535+2805	HD 244957	05 35 00.8	+28 05 54	202.001	−269.940	30.497	32.79	10.30	3.30	7.72
RKS0536+1119	V2689 Ori	05 36 30.9	+11 19 40	−2.818	−56.350	87.530	11.42	9.12	3.85	8.83
RKS0542+0240	HD 38014	05 42 45.8	+02 40 44	253.898	−526.515	30.853	32.41	8.77	2.34	6.22
RKS0544−2225	AK Lep	05 44 26.5	−22 25 18	−304.905	−352.606	112.466	8.89	6.39	2.26	6.65
RKS0549−1734	HD 39071	05 49 22.5	−17 34 44	−22.088	101.175	34.984	28.58	8.74	2.42	6.46
RKS0552−2246	BD-22 1252	05 52 31.9	−22 46 36	260.359	318.698	30.663	32.61	10.81	3.45	8.24
RKS0553−0559	BD-06 1339	05 53 00.2	−05 59 41	−1.170	−346.762	49.249	20.30	9.95	3.65	8.41
RKS0554−1942	TYC 5939-2260-1	05 54 30.4	−19 42 05	96.224	−11.834	42.969	23.27	10.93	3.71	9.10
RKS0554+0208	HD 39715	05 54 28.5	+02 08 32	78.670	−645.334	38.928	25.69	9.07	2.72	7.02

Continued on next page

Table A.1 – *Continued from previous page*

RKS ID	Simbad Name	R.A.	Decl.	$\mu_{R.A}$	μ_{Decl}	π	Dist.	$B_{Gaia\ DR3}$	B_G–K_S	M_{B_G}
...	...	(hh mm ss)	(±dd mm ss)	(mas yr^{-1})	(mas yr^{-1})	(mas)	(pc)	(mag)	(mag)	(mag)
RKS0600+2101	HD 250268	06 00 53.9	+21 01 15	−33.434	−360.557	34.394	29.07	10.24	3.24	7.92
RKS0602+0848	PM J06027+0848	06 02 44.2	+08 48 30	71.263	21.360	32.837	30.45	11.24	3.76	8.82
RKS0608+2630	HD 252023	06 08 13.2	+26 30 08	−31.808	−42.078	37.610	26.59	9.51	2.97	7.39
RKS0609+0009	HD 291290	06 09 46.1	+00 09 32	151.556	−119.258	31.961	31.29	11.05	3.82	8.57
RKS0609+0540	HD 42182	06 09 35.9	+05 40 08	58.793	46.438	33.117	30.20	8.68	2.41	6.28
RKS0612+1023	TYC 734-1988-1	06 12 08.4	+10 23 39	−37.689	−32.886	32.268	30.99	9.98	3.10	7.52
RKS0614+0510	HD 43062	06 14 24.4	+05 10 05	56.997	−283.501	33.166	30.15	8.63	2.41	6.23
RKS0616+2512	HD 254229	06 16 39.5	+25 12 21	55.663	−403.005	32.600	30.67	9.60	2.85	7.17
RKS0617+1759	HD 254504	06 17 25.8	+17 59 21	113.620	−96.153	32.488	30.78	10.56	3.39	8.12
RKS0618−1352	BD-13 1434	06 18 22.1	−13 52 07	64.342	340.554	34.640	28.87	10.14	3.22	7.84
RKS0620+0215	HD 288595	06 20 13.2	+02 15 32	−123.806	−96.750	37.204	26.88	10.06	3.36	7.91
RKS0621−2212	HD 44573	06 21 33.1	−22 12 53	25.578	−239.215	34.813	28.72	8.70	2.42	6.41
RKS0626+1845	HD 45088	06 26 10.2	+18 45 24	−131.618	−150.565	68.414	14.62	7.02	2.75	6.20
RKS0629+2700	HD 257886	06 29 05.5	+27 00 31	−243.863	−418.372	34.824	28.72	8.81	2.45	6.52
RKS0630−1148	HD 45977	06 30 07.3	−11 48 32	−153.137	78.929	37.069	26.98	9.34	2.93	7.18
RKS0630+2104	TYC 1340-1480-1	06 30 24.9	+21 04 17	3.940	3.280	32.428	30.84	11.74	3.01	9.29
RKS0632−2701	CD-26 3096	06 32 08.8	−27 01 58	397.999	−245.483	33.263	30.06	11.66	3.87	9.27
RKS0633+0527	HD 46375	06 33 12.6	+05 27 46	111.624	−96.952	33.880	29.52	8.15	2.15	5.80
RKS0637+1945	HD 260564	06 37 05.2	+19 45 10	10.338	−34.272	31.642	31.60	10.39	3.23	7.89
RKS0641+2357	HD 47752	06 41 15.7	+23 57 27	205.776	−276.604	57.945	17.26	8.32	2.77	7.13

Continued on next page

Table A.1 – *Continued from previous page*

RKS ID	Simbad Name	R.A.	Decl.	$\mu_{R.A}$	μ_{Decl}	π	Dist.	$B_{Gaia\ DR3}$	B_G–K_S	M_{B_G}
...	...	(hh mm ss)	(±dd mm ss)	(mas yr^{-1})	(mas yr^{-1})	(mas)	(pc)	(mag)	(mag)	(mag)
RKS0647−1815	BPM 72121	06 47 15.7	−18 15 31	−104.162	67.317	32.249	31.01	10.79	3.59	8.33
RKS0652−0510	HD 50281	06 52 18.0	−05 10 25	−543.690	−3.515	114.355	8.74	6.82	2.71	7.11
RKS0652−2306	HD 50590	06 52 59.6	−23 06 27	218.942	76.576	32.852	30.44	9.22	2.63	6.80
RKS0658−1259	HD 51849	06 58 26.0	−12 59 30	87.759	−110.400	45.148	22.15	9.40	3.21	7.67
RKS0700−2847	WT 1539	07 00 09.4	−28 47 02	−219.158	−90.250	45.995	21.74	11.02	3.90	9.33
RKS0701−2556	HD 52698	07 01 13.7	−25 56 55	205.949	42.341	67.801	14.75	6.93	2.29	6.09
RKS0701+0655	HD 52456	07 01 35.5	+06 55 36	−30.703	27.847	35.450	28.21	8.38	2.23	6.13
RKS0702−0647	HD 52919	07 02 42.9	−06 47 57	−201.309	−313.607	52.319	19.11	8.60	2.85	7.19
RKS0705+2728	BD+27 1311	07 05 42.2	+27 28 14	−48.793	−96.691	43.800	22.83	10.41	3.63	8.62
RKS0706+2358	BD+24 1529	07 06 52.1	+23 58 08	−85.222	−205.040	31.318	31.93	10.37	3.24	7.85
RKS0707+0326	BD+03 1552	07 07 09.3	+03 26 50	12.724	−258.738	36.386	27.48	10.07	3.40	7.87
RKS0708−0958	HD 54359	07 08 09.3	−09 58 07	−200.743	27.576	35.267	28.36	9.09	2.58	6.83
RKS0708+2950	HD 53927	07 08 04.2	+29 50 04	−156.409	−294.060	43.505	22.99	8.55	2.49	6.74
RKS0710−1425	BD-14 1750	07 10 49.5	−14 25 58	−472.490	303.998	42.866	23.33	10.18	3.55	8.34
RKS0712−2453	CD-24 5005	07 12 04.8	−24 53 31	−114.392	−4.323	35.140	28.46	10.60	3.71	8.33
RKS0713+2500	HD 55458	07 13 53.1	+25 00 40	−405.406	−88.494	36.314	27.54	8.60	2.38	6.40
RKS0716−0339	BD-03 1821	07 16 10.6	−03 39 57	104.983	−50.553	30.072	33.25	9.25	2.58	6.64
RKS0723−2001	BD-19 1855	07 23 29.2	−20 01 24	45.201	−335.719	31.950	31.30	10.14	3.20	7.66
RKS0723+1257	HD 57901	07 23 47.0	+12 57 52	84.269	−424.947	41.616	24.03	8.42	2.53	6.52
RKS0723+2024	BD+20 1790	07 23 43.5	+20 24 58	−65.642	−230.692	36.086	27.71	10.23	3.35	8.02

Continued on next page

Table A.1 – *Continued from previous page*

RKS ID	Simbad Name	R.A.	Decl.	$\mu_{R.A}$	μ_{Decl}	π	Dist.	$B_{Gaia\ DR3}$	B_G–K_S	M_{B_G}
...	...	(hh mm ss)	(±dd mm ss)	(mas yr^{-1})	(mas yr^{-1})	(mas)	(pc)	(mag)	(mag)	(mag)
RKS0724−1753	BD-17 1959	07 24 34.2	−17 53 31	−48.216	−45.568	41.105	24.33	10.56	3.72	8.63
RKS0725−1041	LP 722-21	07 25 29.8	−10 41 59	−204.003	−197.594	30.228	33.08	11.81	3.89	9.21
RKS0726−1546	HD 58760	07 26 26.5	−15 46 13	45.620	−97.521	38.537	25.95	9.44	3.02	7.37
RKS0730−0340	G 112-24	07 30 17.5	−03 40 24	−154.577	44.804	40.832	24.49	10.66	3.92	8.72
RKS0731+1436	HD 59582	07 31 07.7	+14 36 50	75.902	−290.291	48.203	20.75	9.18	3.05	7.59
RKS0732+1719	G 88-36	07 32 02.8	+17 19 09	−218.530	−183.305	37.048	26.99	11.21	3.89	9.05
RKS0734−0653	HD 60491	07 34 26.1	−06 53 48	−80.259	−43.044	42.634	23.46	8.38	2.36	6.53
RKS0739−0335	HD 61606	07 39 59.3	−03 35 51	70.078	−278.117	71.032	14.08	7.40	2.52	6.66
RKS0741−2921	TYC 6552-2083-1	07 41 17.4	−29 21 32	−155.326	73.670	33.035	30.27	10.92	3.64	8.51
RKS0745+0208	BD+02 1766	07 45 01.1	+02 08 14	64.370	−203.410	37.520	26.65	10.42	3.65	8.29
RKS0752+2555	HD 63991	07 52 47.4	+25 55 35	39.769	−144.579	45.820	21.82	8.82	2.77	7.13
RKS0754−0124	HD 64606	07 54 34.1	−01 24 44	−251.957	−56.451	50.714	19.72	7.63	2.21	6.16
RKS0754−2518	CD-24 6144	07 54 10.8	−25 18 11	−300.856	201.042	56.236	17.78	9.98	3.81	8.73
RKS0754+1914	HD 64468	07 54 54.0	+19 14 10	95.082	−453.930	49.244	20.31	7.99	2.54	6.45
RKS0757−0048	HD 65277	07 57 57.7	−00 48 51	−157.142	7.580	56.641	17.66	8.31	2.80	7.08
RKS0758−1501	BD-14 2308	07 58 25.5	−15 01 13	14.886	−235.450	33.131	30.18	9.54	3.01	7.14
RKS0758−2537	HD 65486	07 58 04.3	−25 37 35	362.409	−245.786	54.157	18.46	8.66	2.83	7.33
RKS0759+2050	HD 65430	07 59 33.9	+20 50 38	176.032	−568.327	41.687	23.99	7.89	2.25	5.99
RKS0808+2106	BD+21 1764	08 08 13.1	+21 06 18	−296.698	−355.715	56.008	17.85	9.68	3.60	8.42
RKS0813−1355	BD-13 2439A	08 13 08.4	−13 55 01	−214.025	−483.213	46.956	21.30	9.77	3.95	8.13

Continued on next page

Table A.1 – *Continued from previous page*

RKS ID	Simbad Name	R.A.	Decl.	$\mu_{R.A}$	μ_{Decl}	π	Dist.	$B_{Gaia\ DR3}$	B_G–K_S	M_{B_G}
...	...	(hh mm ss)	(±dd mm ss)	(mas yr^{-1})	(mas yr^{-1})	(mas)	(pc)	(mag)	(mag)	(mag)
RKS0814+1301	HD 68834	08 14 35.9	+13 01 22	−420.800	97.364	51.975	19.24	9.03	3.14	7.61
RKS0815−2600	V430 Pup	08 15 40.0	−26 00 35	228.491	−191.450	34.929	28.63	10.35	3.47	8.07
RKS0817+1717	LSPM J0817+1717	08 17 08.0	+17 17 56	111.895	−110.611	35.260	28.36	9.71	2.98	7.45
RKS0819+0120	BD+01 2063	08 19 19.0	+01 20 19	−164.188	−53.295	44.676	22.38	8.58	2.47	6.83
RKS0820+1404	BD+14 1876	08 20 55.3	+14 04 16	−83.680	−261.769	43.979	22.74	10.00	3.42	8.22
RKS0823+2150	BD+22 1921	08 23 30.9	+21 50 57	298.440	−245.468	39.815	25.12	9.73	3.18	7.73
RKS0827+2855	BD+29 1754	08 27 11.4	+28 55 53	−234.426	230.256	32.245	31.01	9.85	2.96	7.39
RKS0832−2323	BD-22 2311	08 32 33.3	−23 23 06	−113.681	103.510	35.560	28.12	10.40	3.46	8.15
RKS0838−0415	G 114-7	08 38 19.2	−04 15 29	−39.555	−333.513	31.865	31.38	11.69	3.92	9.21
RKS0838−1315	HD 73583	08 38 45.2	−13 15 24	−63.831	38.482	31.657	31.59	9.91	2.96	7.41
RKS0839+0657	HD 73512	08 39 00.2	+06 57 19	−89.933	−294.119	37.971	26.34	8.12	2.50	6.02
RKS0839+1131	HD 73667	08 39 50.7	+11 31 21	−109.222	−500.395	54.251	18.43	7.82	2.38	6.49
RKS0840−0628	BD-05 2603	08 40 00.2	−06 28 33	118.812	−149.438	39.283	25.46	10.12	3.74	8.09
RKS0848+0628	BD+07 2031A	08 48 26.1	+06 28 06	222.052	−439.393	35.183	28.42	10.67	3.68	8.40
RKS0850+0751	BD+08 2131A	08 50 42.2	+07 51 52	−43.412	−26.991	56.007	17.85	9.31	3.71	8.05
RKS0852+2819	rho01 Cnc	08 52 35.8	+28 19 50	−485.681	−233.517	79.448	12.59	6.17	2.16	5.67
RKS0855+0132	BD+02 2098	08 55 07.6	+01 32 47	44.944	−1045.876	48.740	20.52	10.21	3.86	8.65
RKS0900+2127	HD 77065	09 00 47.4	+21 27 13	269.461	−342.965	30.318	32.98	8.99	2.35	6.40
RKS0901+1515	HD 77175A	09 01 17.4	+15 15 56	−125.926	−321.219	54.146	18.47	9.50	3.56	8.17
RKS0904−1554	HD 77825	09 04 20.6	−15 54 51	−107.742	−30.686	36.512	27.39	8.99	2.60	6.80

Continued on next page

Table A.1 – *Continued from previous page*

RKS ID	Simbad Name	R.A.	Decl.	$\mu_{R.A}$	μ_{Decl}	π	Dist.	$B_{Gaia\ DR3}$	B_G–K_S	M_{B_G}
...	...	(hh mm ss)	(±dd mm ss)	(mas yr^{-1})	(mas yr^{-1})	(mas)	(pc)	(mag)	(mag)	(mag)
RKS0905+2517	BD+25 2037	09 05 18.4	+25 17 52	−312.191	−285.040	34.755	28.77	10.76	3.46	8.47
RKS0907+2252	HD 78141	09 07 18.0	+22 52 21	−1.131	−62.641	39.533	25.30	8.23	2.45	6.21
RKS0909+0512	HD 78727	09 09 54.1	+05 12 12	−63.482	−23.814	38.279	26.12	8.61	2.54	6.53
RKS0914+0426	HD 79555	09 14 53.6	+04 26 34	−75.445	19.604	55.934	17.88	8.18	2.93	6.92
RKS0917−0323	HD 80133	09 17 55.3	−03 23 14	23.267	−63.897	30.980	32.28	7.99	2.27	5.45
RKS0918+2718	BD+27 1739	09 18 21.5	+27 18 41	−204.471	−164.758	47.718	20.96	9.77	3.53	8.16
RKS0919+0053	HD 80367	09 19 28.3	+00 53 49	−137.444	−125.758	34.942	28.62	8.36	2.32	6.08
RKS0920−0545	HD 80632	09 20 44.3	−05 45 14	−366.018	−116.556	41.415	24.15	9.33	3.06	7.42
RKS0929−0522	BD-04 2639	09 29 35.0	−05 22 21	−479.742	25.631	41.448	24.13	9.99	3.47	8.08
RKS0929+0539	HD 82106	09 29 54.8	+05 39 18	−502.655	108.537	78.195	12.79	7.44	2.65	6.91
RKS0932−1111	LQ Hya	09 32 25.5	−11 11 04	−248.040	34.277	54.736	18.27	8.01	2.56	6.70
RKS0932+2909	StKM 1-780	09 32 11.1	+29 09 25	24.976	−62.103	31.865	31.38	11.71	3.90	9.23
RKS0937+2231	BD+23 2124	09 37 58.3	+22 31 23	−78.691	−124.214	32.370	30.89	10.14	3.29	7.69
RKS0937+2241	BD+23 2121	09 37 11.3	+22 41 38	−151.288	−177.918	44.309	22.57	9.67	3.33	7.90
RKS0938+0240	Ross 888	09 38 23.9	+02 40 36	−335.022	−789.432	33.481	29.87	12.15	3.87	9.77
RKS0947+0134	G 53-4	09 47 16.6	+01 34 36	−49.929	283.062	33.495	29.86	11.18	3.62	8.80
RKS0952+0307	MCC 559	09 52 39.1	+03 07 48	−61.562	−32.972	37.280	26.82	10.81	3.73	8.67
RKS0952+0313	HD 85488	09 52 11.3	+03 13 18	−425.249	17.447	48.724	20.52	9.11	3.15	7.55
RKS0959−0911	BD-08 2813	09 59 11.3	−09 11 00	−56.468	−73.325	30.260	33.05	10.11	2.97	7.51
RKS1000+2433	DH Leo	10 00 01.7	+24 33 10	−236.138	−37.670	32.166	31.09	8.25	2.81	5.79

Continued on next page

Table A.1 – *Continued from previous page*

RKS ID	Simbad Name	R.A.	Decl.	$\mu_{R.A}$	μ_{Decl}	π	Dist.	$B_{Gaia\ DR3}$	B_G–K_S	M_{B_G}
...	...	(hh mm ss)	(±dd mm ss)	(mas yr^{-1})	(mas yr^{-1})	(mas)	(pc)	(mag)	(mag)	(mag)
RKS1001−1525	HD 86972	10 01 37.2	−15 25 29	−251.423	29.799	39.724	25.17	8.89	2.68	6.89
RKS1004−1143	HD 87424	10 04 37.6	−11 43 46	−191.589	−24.527	42.956	23.28	8.38	2.39	6.55
RKS1005+2629	HD 87445	10 05 26.5	+26 29 16	−187.376	−88.390	32.815	30.47	9.35	2.70	6.93
RKS1006+0257	BD+03 2316	10 06 56.8	+02 57 51	−67.570	−102.842	45.232	22.11	10.20	3.81	8.48
RKS1008+1159	HD 87884	10 08 12.7	+11 59 49	−254.399	8.127	41.275	24.23	8.37	2.49	6.45
RKS1011−2425	WT 1757	10 11 45.0	−24 25 33	175.564	−21.456	33.905	29.49	11.28	3.96	8.93
RKS1020−0128	HD 89668	10 20 43.4	−01 28 11	−664.872	−170.606	31.250	32.00	9.65	2.89	7.12
RKS1024−1024	BD-09 3063	10 24 14.9	−10 24 21	281.730	−249.188	34.450	29.03	10.22	3.30	7.91
RKS1026−0631	BD-05 3063	10 26 41.2	−06 31 34	0.476	−641.531	32.564	30.71	9.99	2.79	7.55
RKS1026+2638	HD 90442	10 26 59.5	+26 38 29	161.264	−85.840	33.637	29.73	8.46	2.20	6.09
RKS1028+0644	HD 90663	10 28 10.4	+06 44 06	26.402	327.844	38.324	26.09	8.76	2.50	6.68
RKS1030−2114	BD-20 3194	10 30 21.9	−21 14 12	−449.462	−47.151	34.578	28.92	9.86	3.04	7.55
RKS1032+0830	BD+09 2366	10 32 00.6	+08 30 38	83.625	−189.168	33.886	29.51	11.05	3.82	8.70
RKS1036−1350	V418 Hya	10 36 30.7	−13 50 35	−163.747	22.729	31.486	31.76	8.93	2.36	6.42
RKS1043−2903	V419 Hya	10 43 28.2	−29 03 51	−215.484	−49.892	46.493	21.51	7.95	2.29	6.29
RKS1046−2435	HD 93380	10 46 36.9	−24 35 07	−141.570	−110.039	46.970	21.29	9.61	3.17	7.97
RKS1053−1422	HD 94374	10 53 22.5	−14 22 28	−426.011	−314.120	30.943	32.32	9.49	2.70	6.94
RKS1054−0432	StKM 1-896	10 54 49.1	−04 32 30	−14.795	−25.276	35.406	28.24	10.81	3.73	8.56
RKS1056+0723	HD 94765	10 56 30.7	+07 23 18	−256.992	−77.410	57.802	17.30	7.60	2.40	6.41
RKS1057+2856	HD 94818	10 57 11.4	+28 56 16	353.581	−176.485	36.399	27.47	9.18	2.78	6.99

Continued on next page

Table A.1 – *Continued from previous page*

RKS ID	Simbad Name	R.A.	Decl.	$\mu_{R.A}$	μ_{Decl}	π	Dist.	$B_{Gaia\ DR3}$	B_G–K_S	M_{B_G}
...	...	(hh mm ss)	(±dd mm ss)	(mas yr^{-1})	(mas yr^{-1})	(mas)	(pc)	(mag)	(mag)	(mag)
RKS1059+2526	HD 95174A	10 59 38.3	+25 26 15	−176.719	−50.750	46.966	21.29	8.70	2.86	7.06
RKS1102−0919	AB Crt	11 02 50.1	−09 19 49	−193.329	−62.980	32.104	31.15	9.24	2.60	6.77
RKS1108−2816	CD-27 7881	11 08 06.3	−28 16 04	−513.129	−62.686	36.774	27.19	9.56	3.43	7.39
RKS1108+1546	HD 96692	11 08 31.7	+15 46 03	154.612	−375.862	35.504	28.17	9.96	3.14	7.71
RKS1111−1057	HD 97214	11 11 10.7	−10 57 03	−942.339	592.918	50.304	19.88	9.45	3.12	7.96
RKS1111−1459	HD 97233	11 11 33.1	−14 59 28	693.072	−599.182	51.875	19.28	9.27	3.40	7.84
RKS1113+0428	HD 97503	11 13 13.2	+04 28 56	−315.521	−33.135	54.506	18.35	8.95	3.10	7.63
RKS1114−2306	HD 97782A	11 14 48.1	−23 06 17	−296.253	−367.694	43.322	23.08	9.27	3.24	7.45
RKS1114+2542	HD 97658	11 14 33.1	+25 42 37	−107.475	48.770	46.376	21.56	7.97	2.24	6.30
RKS1115−1808	BD-17 3337	11 15 20.7	−18 08 37	144.005	−734.098	43.658	22.91	10.19	3.59	8.39
RKS1116−1441	BD-13 3333	11 16 22.1	−14 41 36	−174.273	−120.510	54.792	18.25	10.23	3.77	8.92
RKS1117−0158	BD-01 2505	11 17 13.6	−01 58 54	−568.300	−14.310	30.138	33.18	10.00	3.04	7.40
RKS1117−2748	CD-27 7978	11 17 07.5	−27 48 48	204.835	−76.123	56.686	17.64	10.01	3.81	8.78
RKS1121−2027	HD 98712A	11 21 26.6	−20 27 13	174.015	−79.428	72.864	13.72	8.93	3.63	8.24
RKS1121+1811	HD 98736	11 21 49.3	+18 11 24	−151.945	−92.386	30.947	32.31	8.20	2.17	5.65
RKS1125+2000	HD 99303	11 25 39.9	+20 00 07	−202.889	−91.698	31.718	31.53	8.55	2.20	6.06
RKS1126+1517	BD+16 2260	11 26 49.9	+15 17 38	140.892	−30.939	38.004	26.31	10.68	3.71	8.58
RKS1127+0358	BD+04 2470	11 27 38.5	+03 58 35	−97.463	14.092	34.812	28.73	10.90	3.91	8.61
RKS1128+0731	Wolf 397	11 28 27.7	+07 31 02	−272.264	−1220.417	35.332	28.30	10.42	3.36	8.16
RKS1134−1314	BD-12 3458	11 34 50.4	−13 14 31	−285.435	−68.710	33.061	30.25	10.58	3.25	8.18

Continued on next page

Table A.1 – *Continued from previous page*

RKS ID	Simbad Name	R.A.	Decl.	$\mu_{R.A}$	μ_{Decl}	π	Dist.	$B_{Gaia\ DR3}$	B_G–K_S	M_{B_G}
...	...	(hh mm ss)	(±dd mm ss)	(mas yr^{-1})	(mas yr^{-1})	(mas)	(pc)	(mag)	(mag)	(mag)
RKS1135+1658	BD+17 2376	11 35 59.1	+16 58 05	36.115	−36.192	31.326	31.92	9.81	2.97	7.29
RKS1139−2741	CD-26 8683	11 39 08.1	−27 41 46	358.571	−275.994	33.367	29.97	10.21	3.30	7.83
RKS1141+0508	BD+05 2529	11 41 49.5	+05 08 26	230.643	−469.130	31.762	31.48	9.82	3.40	7.33
RKS1147−1149	HD 102392A	11 47 03.8	−11 49 26	−204.675	−77.182	38.550	25.94	9.28	3.09	7.21
RKS1152+1845	HD 103072	11 52 08.3	+18 45 18	29.340	−302.855	37.315	26.80	8.62	2.35	6.48
RKS1154+2844	BD+29 2228	11 54 57.4	+28 44 15	191.379	−299.876	36.630	27.30	10.74	3.74	8.56
RKS1157−2608	HD 103836	11 57 16.2	−26 08 29	−351.016	145.344	38.915	25.70	9.17	2.76	7.12
RKS1157−2742	HD 103932	11 57 56.2	−27 42 25	−1080.901	−620.929	98.298	10.17	7.20	2.67	7.16
RKS1157+1959	GR Leo	11 57 28.9	+19 59 02	−387.041	53.876	36.024	27.76	8.28	2.19	6.06
RKS1158−2355	HD 103949	11 58 11.7	−23 55 25	−172.747	−54.305	37.736	26.50	8.94	2.63	6.82
RKS1159−2021	HD 104067	11 59 10.0	−20 21 13	141.706	−423.780	49.147	20.35	8.15	2.54	6.61
RKS1204−0013	BD+00 2888	12 04 47.8	−00 13 36	−156.816	−53.731	34.630	28.88	11.05	2.87	8.75
RKS1204+0911	HD 104828	12 04 17.4	+09 11 35	−253.985	39.231	30.631	32.65	10.09	3.03	7.52
RKS1205−1852	HD 105065	12 05 50.6	−18 52 30	−15.018	−317.780	43.365	23.06	10.23	3.61	8.42
RKS1206−2336	HD 105110	12 06 09.0	−23 36 08	62.696	−97.274	31.413	31.83	8.82	2.29	6.31
RKS1208−0028	Wolf 406	12 08 22.2	−00 28 57	−962.727	−93.993	34.329	29.13	11.49	3.90	9.17
RKS1209−2646	PM J12093-2646	12 09 23.4	−26 46 46	−70.695	−165.760	32.247	31.01	11.25	3.85	8.79
RKS1210−1126	LP 734-35	12 10 33.6	−11 26 59	−212.014	−75.400	32.269	30.99	11.39	3.74	8.93
RKS1220−1953	HD 107388	12 20 46.8	−19 53 45	−360.422	−61.197	34.016	29.40	9.24	2.65	6.90
RKS1222+2736	BD+28 2110	12 22 34.0	+27 36 16	−145.612	−29.342	33.685	29.69	11.11	3.89	8.75

Continued on next page

Table A.1 – *Continued from previous page*

RKS ID	Simbad Name	R.A.	Decl.	$\mu_{R.A}$	μ_{Decl}	π	Dist.	$B_{Gaia\ DR3}$	B_G–K_S	M_{B_G}
...	...	(hh mm ss)	(±dd mm ss)	(mas yr^{-1})	(mas yr^{-1})	(mas)	(pc)	(mag)	(mag)	(mag)
RKS1223+2754	Wolf 411	12 23 34.7	+27 54 47	−137.496	120.760	33.874	29.52	11.55	3.88	9.20
RKS1227+2701	HD 108421A	12 27 13.7	+27 01 28	94.194	−247.841	36.504	27.39	9.02	3.28	6.83
RKS1228−1654	HD 108564	12 28 19.1	−16 54 39	−558.284	45.113	36.677	27.27	9.67	2.77	7.49
RKS1228−1817	HD 108581	12 28 31.5	−18 17 50	171.727	−177.150	42.077	23.77	9.47	3.18	7.59
RKS1231+2013	HD 108984	12 31 18.2	+20 13 04	−22.018	−169.390	37.964	26.34	8.13	2.23	6.03
RKS1233−1438	HD 109333	12 33 59.7	−14 38 19	−504.453	−27.034	38.052	26.28	9.35	2.91	7.25
RKS1241+1522	HD 110315	12 41 06.4	+15 22 35	107.249	−370.333	70.879	14.11	8.15	3.07	7.40
RKS1241+1951	HD 110376	12 41 37.0	+19 51 05	22.364	−23.464	31.350	31.90	9.32	2.58	6.80
RKS1248−1543	HD 111312	12 48 32.2	−15 43 09	97.938	27.230	39.211	25.50	8.11	2.53	6.08
RKS1248−2448	HD 111261	12 48 10.7	−24 48 23	−315.440	169.488	53.333	18.75	9.13	3.10	7.76
RKS1250−0046	HD 111631	12 50 43.5	−00 46 05	−29.871	−397.002	93.855	10.65	8.72	3.84	8.58
RKS1253+0645	HD 112099	12 53 54.4	+06 45 46	−231.846	93.538	36.594	27.33	8.46	2.31	6.28
RKS1256−2455	CD-24 10619	12 56 30.0	−24 55 31	75.032	−218.445	32.240	31.02	10.28	3.27	7.82
RKS1257−1427	HD 112575	12 57 43.9	−14 27 48	−361.647	6.048	39.498	25.32	9.40	2.97	7.38
RKS1259−0950	HD 112758	12 59 01.5	−09 50 02	−824.458	195.008	49.826	20.07	7.76	2.23	6.25
RKS1300−0242	HD 112943	13 00 16.9	−02 42 17	−806.690	7.365	36.633	27.30	10.01	3.24	7.83
RKS1302−2647	HD 113194	13 02 20.6	−26 47 13	−157.133	−199.668	56.941	17.56	8.59	3.33	7.37
RKS1303−0509	PX Vir	13 03 49.7	−05 09 42	−189.811	−222.359	48.883	20.46	7.89	2.38	6.34
RKS1306+2043	BD+21 2486A	13 06 15.3	+20 43 45	−56.041	94.553	50.807	19.68	9.73	3.69	8.26
RKS1310+0932	BD+10 2518	13 10 16.9	+09 32 09	182.847	−153.041	36.082	27.71	9.54	2.85	7.33

Continued on next page

Table A.1 – *Continued from previous page*

RKS ID	Simbad Name	R.A.	Decl.	$\mu_{R.A}$	μ_{Decl}	π	Dist.	$B_{Gaia\ DR3}$	B_G–K_S	M_{B_G}
...	...	(hh mm ss)	(±dd mm ss)	(mas yr^{-1})	(mas yr^{-1})	(mas)	(pc)	(mag)	(mag)	(mag)
RKS1312−0215	HD 114783	13 12 43.7	−02 15 54	−138.362	10.284	47.553	21.03	7.80	2.33	6.19
RKS1316+1701	HD 115404	13 16 51.0	+17 01 01	636.285	−264.678	91.018	10.99	6.78	2.40	6.58
RKS1318−1446	BD-14 3687	13 18 05.8	−14 46 48	−332.778	−235.788	34.370	29.10	11.11	3.61	8.79
RKS1320+0407	HD 116012	13 20 43.7	+04 07 58	−506.786	201.404	33.008	30.30	8.83	2.44	6.42
RKS1323+0243	HD 116442	13 23 39.1	+02 43 23	12.467	199.291	60.282	16.59	7.27	2.17	6.17
RKS1327−2417	HD 116920	13 27 02.9	−24 17 25	−339.245	−67.008	33.480	29.87	8.95	2.50	6.57
RKS1331−0219	HD 117635	13 31 39.9	−02 19 02	−828.835	293.787	37.758	26.48	7.54	2.23	5.43
RKS1333+0835	HD 117936	13 33 32.4	+08 35 12	−506.365	93.771	55.124	18.14	8.20	2.71	6.91
RKS1334−0018	HD 118036A	13 34 16.2	−00 18 49	−197.844	20.178	37.198	26.88	7.87	2.62	5.72
RKS1334−0820	HD 118100	13 34 43.2	−08 20 31	−286.594	−91.681	48.823	20.48	9.42	3.30	7.86
RKS1334+0440	BD+05 2767	13 34 21.5	+04 40 02	153.856	−123.409	48.968	20.42	10.18	3.84	8.63
RKS1335−0023	BD+00 3077	13 35 24.7	−00 23 20	35.117	183.316	51.927	19.26	10.51	3.85	9.09
RKS1335+0650	HD 118206	13 35 06.3	+06 50 27	−94.864	−69.931	32.212	31.04	9.14	2.65	6.68
RKS1336+0746	BD+08 2735	13 36 56.6	+07 46 01	−775.548	−361.209	31.839	31.41	10.21	3.02	7.72
RKS1338−0614	BD-05 3740	13 38 58.6	−06 14 12	93.362	−182.358	41.338	24.19	10.97	3.91	9.05
RKS1340−0411	HD 118926	13 40 07.1	−04 11 09	−385.222	481.307	66.201	15.11	9.84	3.80	8.94
RKS1341−0007	HD 119217	13 41 55.6	−00 07 44	−162.206	−429.081	40.485	24.70	9.98	3.49	8.02
RKS1342−0141	HD 119291	13 42 26.0	−01 41 10	−289.030	−154.630	40.614	24.62	9.46	3.13	7.50
RKS1345−0437	BD-03 3527	13 45 05.3	−04 37 13	−163.825	−96.222	33.969	29.44	10.77	3.57	8.43
RKS1345+0850	HD 119802	13 45 14.7	+08 50 09	−66.359	−96.291	45.430	22.01	8.72	2.75	7.01

Continued on next page

Table A.1 – *Continued from previous page*

RKS ID	Simbad Name	R.A.	Decl.	$\mu_{R.A}$	μ_{Decl}	π	Dist.	$B_{Gaia\ DR3}$	B_G–K_S	M_{B_G}
...	...	(hh mm ss)	(±dd mm ss)	(mas yr^{-1})	(mas yr^{-1})	(mas)	(pc)	(mag)	(mag)	(mag)
RKS1345+1747	BD+18 2776	13 45 05.0	+17 47 07	450.974	−1833.253	77.441	12.91	10.02	3.80	9.47
RKS1347+0618	BD+07 2692	13 47 28.7	+06 18 56	−509.304	−110.996	31.842	31.41	10.24	3.23	7.75
RKS1349−2206	HD 120467	13 49 44.8	−22 06 39	−1749.861	−494.208	71.078	14.07	8.41	3.25	7.67
RKS1353+1256	BD+13 2721	13 53 27.5	+12 56 32	−171.758	−604.269	45.615	21.92	10.02	3.87	8.32
RKS1353+2748	HD 121131	13 53 05.2	+27 48 24	226.572	−375.790	33.899	29.50	8.58	2.23	6.23
RKS1359+2252	HD 122120	13 59 19.4	+22 52 11	−160.855	12.965	41.942	23.84	9.29	3.05	7.40
RKS1411−1236	HD 124106	14 11 46.1	−12 36 42	−254.019	−179.729	43.386	23.05	8.15	2.29	6.34
RKS1412+2348	GY Boo	14 12 41.5	+23 48 51	−26.858	−6.259	31.859	31.39	9.13	2.69	6.65
RKS1413−0657	BD-06 3950	14 13 31.1	−06 57 32	110.454	136.718	54.589	18.32	10.40	3.83	9.09
RKS1414−1521	HD 124498A	14 14 21.3	−15 21 22	−124.496	−168.123	34.497	28.99	10.50	3.90	8.19
RKS1418−0636	HD 125354	14 18 58.2	−06 36 12	2.712	−432.215	44.376	22.53	9.35	3.50	7.59
RKS1419−0509	HD 125455	14 19 34.8	−05 09 04	−632.951	−120.707	48.902	20.45	7.80	2.26	6.25
RKS1421+2937	BD+30 2512	14 21 57.2	+29 37 46	−631.662	−308.469	68.851	14.52	8.77	3.35	7.96
RKS1430−0838	HD 127339	14 30 47.7	−08 38 46	−1270.991	−238.517	63.363	15.78	9.63	3.86	8.64
RKS1432+1121	BD+11 2687	14 32 13.1	+11 21 11	57.222	171.892	33.059	30.25	9.91	3.40	7.51
RKS1433+0920	HD 127871	14 33 34.9	+09 20 03	158.362	−513.114	31.030	32.23	9.05	2.46	6.51
RKS1436+0944	HD 128311	14 36 00.5	+09 44 47	204.813	−250.457	61.279	16.32	7.70	2.56	6.64
RKS1437−2548	HD 128356	14 37 04.8	−25 48 09	−18.434	−139.584	38.381	26.05	8.51	2.51	6.43
RKS1442+1930	BD+20 3009	14 42 26.2	+19 30 12	−261.105	−178.351	42.318	23.63	10.26	3.60	8.39
RKS1444−2215	HD 129715	14 44 35.5	−22 15 11	−106.328	−338.884	33.008	30.30	9.54	2.97	7.13

Continued on next page

Table A.1 – *Continued from previous page*

RKS ID	Simbad Name	R.A.	Decl.	$\mu_{R.A}$	μ_{Decl}	π	Dist.	$B_{Gaia\ DR3}$	B_G–K_S	M_{B_G}
...	...	(hh mm ss)	(±dd mm ss)	(mas yr^{-1})	(mas yr^{-1})	(mas)	(pc)	(mag)	(mag)	(mag)
RKS1444+2211	BD+22 2742	14 44 11.9	+22 11 07	2.061	118.443	36.577	27.34	10.12	3.22	7.94
RKS1445+1350	HD 130004	14 45 24.1	+13 50 46	−231.639	−225.646	53.161	18.81	8.09	2.48	6.72
RKS1446+1629	BD+17 2785	14 46 23.2	+16 29 48	−108.619	−921.876	56.366	17.74	9.48	3.42	8.24
RKS1446+2730	HO Boo	14 46 03.0	+27 30 44	17.311	−40.992	37.759	26.48	8.19	2.21	6.08
RKS1447+0242	HD 130307	14 47 16.1	+02 42 11	−287.136	−78.612	51.764	19.32	8.00	2.38	6.57
RKS1450+0648	HD 130871	14 50 20.9	+06 48 53	−617.420	−66.234	32.198	31.06	9.31	2.59	6.85
RKS1451−2418	HD 130992	14 51 40.4	−24 18 14	−944.623	−431.624	59.639	16.77	8.05	2.67	6.93
RKS1453+2320	HD 131582	14 53 41.5	+23 20 42	−829.098	0.754	42.422	23.57	8.88	2.70	7.02
RKS1455−2707	HD 131719	14 55 55.0	−27 07 38	−103.875	−22.746	36.679	27.26	9.23	2.75	7.05
RKS1457−2124	HD 131977	14 57 28.0	−21 24 55	1031.472	−1723.619	169.884	5.89	5.98	2.93	7.13
RKS1500−1108	HD 132683	15 00 43.4	−11 08 06	−15.478	−481.098	56.068	17.84	9.72	3.73	8.46
RKS1500−2427	CD-23 12010	15 00 19.3	−24 27 14	−199.483	−27.997	36.353	27.51	10.15	3.35	7.95
RKS1500−2905	TYC 6760-1510-1	15 00 09.5	−29 05 27	−3.235	−0.553	31.434	31.81	11.53	3.90	9.02
RKS1501+1341	StKM 1-1198	15 01 06.5	+13 41 39	−143.444	7.435	30.708	32.56	11.24	3.71	8.68
RKS1501+1552	HD 132950	15 01 29.9	+15 52 07	102.907	−237.445	34.369	29.10	9.34	2.76	7.02
RKS1504−1835	HD 133412	15 04 53.9	−18 35 27	−126.232	−123.417	30.304	33.00	9.74	3.30	7.15
RKS1504+0538	BD+06 2986	15 04 53.5	+05 38 17	−607.626	−506.509	52.505	19.05	10.06	3.59	8.66
RKS1507+2456	BD+25 2874	15 07 23.5	+24 56 07	−845.741	494.217	52.542	19.03	10.29	3.82	8.89
RKS1509+2400	BD+24 2824	15 09 04.2	+24 00 57	−471.667	161.121	30.729	32.54	9.56	2.82	7.00
RKS1510−1622	HD 134439	15 10 13.0	−16 22 45	−998.064	−3542.267	34.018	29.40	9.26	2.28	6.92

Continued on next page

Table A.1 – *Continued from previous page*

RKS ID	Simbad Name	R.A.	Decl.	$\mu_{R.A}$	μ_{Decl}	π	Dist.	$B_{Gaia\ DR3}$	B_G–K_S	M_{B_G}
...	...	(hh mm ss)	(±dd mm ss)	(mas yr^{-1})	(mas yr^{-1})	(mas)	(pc)	(mag)	(mag)	(mag)
RKS1513−0347	BD-03 3746	15 13 59.6	−03 47 52	−739.759	151.196	38.872	25.73	10.05	3.14	8.00
RKS1515+0047	HD 135599	15 15 59.1	+00 47 46	178.098	−137.155	63.214	15.82	7.14	2.18	6.14
RKS1515+0735	BD+08 3000	15 15 45.4	+07 35 52	−28.365	−187.354	31.573	31.67	10.94	3.52	8.44
RKS1518−1837	BD-18 4031	15 18 39.5	−18 37 35	445.179	−357.981	36.562	27.35	10.59	3.36	8.41
RKS1519+0146	5 Ser B	15 19 19.2	+01 46 04	371.601	−507.580	39.771	25.14	10.34	3.59	8.34
RKS1519+1155	BD+12 2823	15 19 35.3	+11 55 19	−55.350	17.135	31.264	31.99	10.24	3.17	7.71
RKS1519+2912	BD+29 2654	15 19 21.1	+29 12 22	−141.017	395.497	35.666	28.04	10.47	3.37	8.23
RKS1520+1522	BD+15 2847	15 20 38.9	+15 22 48	−421.054	−162.399	32.589	30.69	9.03	2.79	6.60
RKS1522−0446	BD-04 3873	15 22 04.1	−04 46 38	−296.983	−12.500	52.210	19.15	9.70	3.52	8.29
RKS1522−1039	HD 136713	15 22 36.6	−10 39 40	−57.386	−203.772	45.280	22.08	8.20	2.48	6.48
RKS1522+0125	HD 136834	15 22 42.5	+01 25 07	−364.212	−364.113	38.501	25.97	8.52	2.48	6.45
RKS1525−2642	HD 137303	15 25 58.5	−26 42 20	−818.914	−9.972	45.098	22.17	9.04	2.88	7.31
RKS1527+0235	BD+03 3032	15 27 42.6	+02 35 51	−51.833	−18.405	35.355	28.28	10.45	3.55	8.19
RKS1527+1035	BD+11 2811	15 27 38.0	+10 35 39	−424.071	−262.344	36.548	27.36	10.07	3.42	7.88
RKS1528−0920	HD 137763	15 28 09.6	−09 20 52	73.584	−375.345	51.142	19.55	7.10	2.21	5.64
RKS1540−1802	HD 139763	15 40 34.5	−18 02 56	161.149	89.730	64.183	15.58	9.15	3.46	8.19
RKS1552+1052	BD+11 2874	15 52 08.2	+10 52 28	−265.282	−240.143	47.430	21.08	9.61	3.79	7.99
RKS1554−2600	HD 142288	15 54 38.4	−26 00 15	−230.613	101.047	42.135	23.73	9.43	3.19	7.55
RKS1555+1602	V383 Ser	15 55 19.0	+16 02 39	−222.347	−216.200	30.980	32.28	8.92	2.75	6.38
RKS1600−0147	BD-01 3125	16 00 16.4	−01 47 55	124.496	−135.307	32.659	30.62	10.50	3.35	8.07

Continued on next page

Table A.1 – *Continued from previous page*

RKS ID	Simbad Name	R.A.	Decl.	$\mu_{R.A}$	μ_{Decl}	π	Dist.	$B_{Gaia\ DR3}$	B_G–K_S	M_{B_G}
...	...	(hh mm ss)	(±dd mm ss)	(mas yr^{-1})	(mas yr^{-1})	(mas)	(pc)	(mag)	(mag)	(mag)
RKS1601−2625	PM J16016-2625	16 01 39.7	−26 25 15	137.855	−43.547	40.903	24.45	11.05	3.87	9.11
RKS1604−1126	HD 144088	16 04 26.7	−11 26 59	−56.334	−20.357	35.872	27.88	8.23	2.12	6.00
RKS1605−2027	HD 144253	16 05 40.4	−20 27 00	295.010	−351.096	55.881	17.90	7.63	2.77	6.37
RKS1607−0542	G 153-25	16 07 34.3	−05 42 25	150.204	−178.446	30.414	32.88	10.63	3.53	8.05
RKS1608−1308	HD 144840	16 08 24.4	−13 08 07	−61.587	−285.262	35.381	28.26	8.92	2.54	6.66
RKS1608+1713	BD+17 2966	16 08 05.3	+17 13 44	−58.384	37.008	31.243	32.01	9.37	2.62	6.84
RKS1613+1331	49 Ser A	16 13 18.4	+13 31 36	178.934	−419.941	41.129	24.31	7.57	2.40	5.64
RKS1615+0721	HD 146413A	16 15 57.0	+07 21 25	177.309	−476.105	37.057	26.99	9.51	3.45	7.35
RKS1620−0416	MCC 760	16 20 24.7	−04 16 02	−416.181	−20.667	34.076	29.35	10.92	3.84	8.58
RKS1621+1713	G 138-22	16 21 38.0	+17 13 33	−46.483	−271.741	30.917	32.34	10.85	3.48	8.30
RKS1624−1338	V2578 Oph	16 24 19.8	−13 38 29	−218.786	−206.551	46.869	21.34	8.61	2.61	6.96
RKS1625−2156	BD-21 4352	16 25 13.0	−21 56 14	−571.030	−337.799	53.739	18.61	10.62	3.90	9.27
RKS1626+1539	G 138-28	16 26 33.4	+15 39 53	9.327	265.259	36.492	27.40	10.78	3.58	8.59
RKS1627+0055	BD+01 3236	16 27 20.3	+00 55 29	−23.481	24.590	35.080	28.51	10.21	3.42	7.94
RKS1627+0718	HD 148467	16 27 56.9	+07 18 19	−248.797	−264.661	57.087	17.52	9.06	3.26	7.84
RKS1628+1824	HD 148653A	16 28 52.6	+18 24 50	−348.586	383.346	51.808	19.30	7.84	2.94	6.41
RKS1629+2346	BD+24 3014	16 29 14.3	+23 46 34	−63.012	−315.127	30.510	32.78	10.30	3.25	7.72
RKS1630−0359	BD-03 3952	16 30 43.0	−03 59 21	−154.528	−20.890	36.734	27.22	9.80	3.21	7.63
RKS1631−0718	TYC 5060-53-1	16 31 52.3	−07 18 18	−31.463	−51.070	44.494	22.47	11.23	2.40	9.47
RKS1632−1235	BD-12 4542	16 32 57.8	−12 35 30	−311.996	−223.853	31.538	31.71	10.83	3.58	8.32

Continued on next page

Table A.1 – *Continued from previous page*

RKS ID	Simbad Name	R.A.	Decl.	$\mu_{R.A}$	μ_{Decl}	π	Dist.	$B_{Gaia\ DR3}$	B_G–K_S	M_{B_G}
...	...	(hh mm ss)	(±dd mm ss)	(mas yr^{-1})	(mas yr^{-1})	(mas)	(pc)	(mag)	(mag)	(mag)
RKS1633−0933	LP 745-70	16 33 41.6	−09 33 11	−64.886	−177.913	32.166	31.09	11.46	3.91	9.00
RKS1647−0111	BD-00 3182	16 47 17.5	−01 11 20	−16.391	−244.176	32.988	30.31	10.96	3.54	8.55
RKS1649−2426	HD 151692	16 49 53.1	−24 26 48	−276.593	−109.082	30.134	33.19	9.81	2.92	7.20
RKS1650+1854	HD 151995	16 50 05.2	+18 54 01	−46.930	−71.976	36.474	27.42	9.09	2.72	6.90
RKS1654+1154	Ross 644	16 54 12.0	+11 54 52	−543.691	316.205	49.801	20.08	10.99	3.88	9.48
RKS1659−2616	CD-26 11751	16 59 33.2	−26 16 04	129.062	−286.615	35.983	27.79	10.61	3.69	8.39
RKS1701+2256	BD+23 3035	17 01 59.8	+22 56 09	−131.433	84.673	36.208	27.62	9.05	2.66	6.84
RKS1705−0147	HD 154361	17 05 08.5	−01 47 09	75.391	−43.474	32.185	31.07	9.58	2.78	7.12
RKS1705−0503	HD 154363	17 05 03.3	−05 03 59	−916.343	−1138.762	95.567	10.46	7.95	3.22	7.85
RKS1706−0610	HD 154518	17 06 08.2	−06 10 02	−92.239	−63.466	33.086	30.22	9.03	2.58	6.63
RKS1712+1821	HD 155712	17 12 37.6	+18 21 04	101.797	−116.867	48.046	20.81	8.18	2.51	6.59
RKS1714−0824	HD 155802A	17 14 08.0	−08 24 13	−99.844	71.943	33.660	29.71	8.73	2.56	6.37
RKS1715−2636	36 Oph A	17 15 20.7	−26 36 06	−498.600	−1149.158	168.003	5.95	5.31	3.47	6.44
RKS1716−1210	BD-12 4699	17 16 20.2	−12 10 41	143.442	−22.820	38.203	26.18	10.56	3.65	8.47
RKS1717+2913	HD 156668	17 17 40.4	+29 13 38	−72.481	216.849	41.110	24.32	8.66	2.66	6.73
RKS1722−1457	BD-14 4622	17 22 42.9	−14 57 37	−99.762	−222.434	32.688	30.59	11.14	3.71	8.71
RKS1725+0206	HD 157881	17 25 45.2	+02 06 41	−580.325	−1184.737	129.646	7.71	7.77	3.40	8.33
RKS1729−2350	HD 158233	17 29 06.5	−23 50 10	−288.666	−72.789	54.367	18.39	9.85	3.46	8.53
RKS1733+0914	RX J1733.1+0914	17 33 07.2	+09 14 37	31.156	−19.981	31.893	31.35	9.85	3.10	7.37
RKS1737−1314	HD 159911	17 37 46.4	−13 14 46	−17.393	−126.177	30.108	33.21	10.30	3.47	7.69

Continued on next page

Table A.1 – *Continued from previous page*

RKS ID	Simbad Name	R.A.	Decl.	$\mu_{R.A}$	μ_{Decl}	π	Dist.	$B_{Gaia\ DR3}$	B_G–K_S	M_{B_G}
...	...	(hh mm ss)	(±dd mm ss)	(mas yr^{-1})	(mas yr^{-1})	(mas)	(pc)	(mag)	(mag)	(mag)
RKS1737+2257	BD+23 3151A	17 37 48.7	+22 57 20	−151.591	−146.026	43.864	22.80	10.18	3.89	8.39
RKS1739+0333	HD 160346	17 39 16.9	+03 33 18	−194.607	−100.642	99.139	10.09	6.75	2.65	6.73
RKS1750−0603	HD 162283	17 50 34.0	−06 03 01	−27.710	−132.784	45.017	22.21	10.40	3.86	8.67
RKS1752−0733	HD 162598	17 52 16.6	−07 33 37	−229.391	352.900	32.625	30.65	10.17	3.20	7.74
RKS1753+2119	BD+21 3245	17 53 29.9	+21 19 31	−73.091	57.706	40.779	24.52	8.72	2.52	6.77
RKS1754−2649	HD 314741	17 54 54.1	−26 49 41	42.512	−104.292	31.797	31.45	10.63	3.72	8.14
RKS1755+0345	BD+03 3531a	17 55 24.7	+03 45 16	−79.622	24.274	39.740	25.16	10.37	3.55	8.37
RKS1755+1830	BD+18 3497	17 55 44.8	+18 30 01	−46.396	−47.430	44.431	22.51	9.43	3.13	7.67
RKS1757−2143	HD 163573	17 57 40.9	−21 43 10	39.986	−154.301	30.638	32.64	10.23	3.55	7.66
RKS1803+2545	Ross 820	18 03 47.7	+25 45 20	−46.836	−230.017	35.967	27.80	11.10	3.90	8.88
RKS1804+0149	HD 165045	18 04 01.8	+01 49 56	95.995	−28.119	32.691	30.59	8.33	2.22	5.90
RKS1809−0019	HD 166184	18 09 32.2	−00 19 37	79.076	−13.053	34.445	29.03	9.17	2.63	6.86
RKS1809−1202	BD-12 4935	18 09 33.2	−12 02 19	67.012	−206.816	36.670	27.27	10.73	3.74	8.55
RKS1815+1829	HD 348282	18 15 18.2	+18 29 59	50.137	59.561	34.260	29.19	10.29	3.47	7.96
RKS1816+1354	BD+13 3578	18 16 02.2	+13 54 48	98.790	−501.104	54.733	18.27	10.41	3.85	9.10
RKS1817+2640	HD 335828	18 17 49.8	+26 40 16	328.373	107.523	32.559	30.71	9.79	2.84	7.35
RKS1818−0642	HD 168159	18 18 40.6	−06 42 03	−67.145	−10.478	33.433	29.91	9.51	2.79	7.13
RKS1819−0156	HD 168442	18 19 50.8	−01 56 19	−0.414	−0.108	52.396	19.09	9.90	3.62	8.50
RKS1822+0142	BD+01 3657	18 22 17.2	+01 42 25	84.197	−19.688	37.864	26.41	10.37	3.51	8.26
RKS1829−0149	HD 170493	18 29 52.4	−01 49 05	172.063	−193.422	53.159	18.81	8.28	2.80	6.91

Continued on next page

Table A.1 – *Continued from previous page*

RKS ID	Simbad Name	R.A.	Decl.	$\mu_{R.A}$	μ_{Decl}	π	Dist.	$B_{Gaia\ DR3}$	B_G–K_S	M_{B_G}
...	...	(hh mm ss)	(±dd mm ss)	(mas yr^{-1})	(mas yr^{-1})	(mas)	(pc)	(mag)	(mag)	(mag)
RKS1829−2758	HD 170209	18 29 22.3	−27 58 19	−67.381	−448.343	36.727	27.23	9.62	3.13	7.44
RKS1829+0903	HD 170510	18 29 31.9	+09 03 43	188.790	72.824	36.263	27.58	8.88	2.55	6.68
RKS1831−1854	HD 170657	18 31 18.9	−18 54 31	−138.215	−195.466	75.848	13.18	7.04	2.34	6.44
RKS1833−1138	BD-11 4672	18 33 28.8	−11 38 09	−288.440	−235.615	36.753	27.21	10.25	3.38	8.08
RKS1833−1626	HD 171075	18 33 24.8	−16 26 39	−0.062	−40.448	31.686	31.56	9.32	2.88	6.82
RKS1833+2218	HD 171314	18 33 17.7	+22 18 51	−176.248	−472.619	42.725	23.41	9.14	2.98	7.29
RKS1847−0338	HD 173818	18 47 27.2	−03 38 23	−132.281	−274.867	70.134	14.26	9.05	3.47	8.28
RKS1848−1008	HD 173872	18 48 01.4	−10 08 46	111.073	−175.439	35.091	28.50	8.68	2.59	6.41
RKS1848+1044	HD 174080	18 48 29.2	+10 44 43	128.086	−436.538	59.235	16.88	8.20	2.81	7.06
RKS1848+1726	HD 229590	18 48 51.8	+17 26 20	−408.795	−422.823	59.778	16.73	9.42	3.50	8.30
RKS1850−2655	CD-27 13268	18 50 21.1	−26 55 25	−140.522	−23.186	56.660	17.65	9.94	3.76	8.71
RKS1854+0051	BD+00 4050	18 54 53.2	+00 51 46	−70.402	−126.769	40.120	24.93	10.85	3.88	8.87
RKS1854+1058	HD 230017A	18 54 53.6	+10 58 40	29.429	129.983	53.423	18.72	9.66	3.77	8.30
RKS1854+2844	PM J18547+2844	18 54 43.7	+28 44 55	−6.601	116.528	31.300	31.95	11.52	3.83	9.00
RKS1855+2333	HD 175742	18 55 53.2	+23 33 23	130.959	−283.563	46.883	21.33	8.35	2.71	6.71
RKS1858−0030	HD 176157	18 58 56.4	−00 30 14	−110.333	−117.935	31.864	31.38	8.60	2.22	6.12
RKS1858−1014	BD-10 4886	18 58 03.3	−10 14 37	102.458	−35.294	30.657	32.62	10.10	3.06	7.53
RKS1859+0759	BD+07 3922	18 59 38.6	+07 59 14	366.165	−181.279	35.331	28.30	11.07	3.92	8.81
RKS1859+1107	HD 230325	18 59 39.2	+11 07 04	10.513	64.025	32.922	30.37	9.44	2.80	7.03
RKS1901+0328	TYC 466-2991-1	19 01 51.0	+03 28 14	114.727	5.827	32.188	31.07	10.00	3.06	7.54

Continued on next page

Table A.1 – *Continued from previous page*

RKS ID	Simbad Name	R.A.	Decl.	$\mu_{R.A}$	μ_{Decl}	π	Dist.	$B_{Gaia\ DR3}$	B_G–K_S	M_{B_G}
...	...	(hh mm ss)	(±dd mm ss)	(mas yr^{-1})	(mas yr^{-1})	(mas)	(pc)	(mag)	(mag)	(mag)
RKS1903−1102	HD 176986	19 03 05.8	−11 02 38	−126.947	−235.938	35.858	27.89	8.65	2.43	6.42
RKS1907+0736	HD 178126	19 07 02.0	+07 36 57	−324.451	−759.860	40.945	24.42	9.45	2.98	7.51
RKS1908−1640	PM J19081-1640	19 08 10.7	−16 40 41	−89.429	−59.281	37.862	26.41	10.64	3.59	8.53
RKS1908+1627	HD 230742	19 08 02.6	+16 27 37	−144.978	−145.238	31.281	31.97	10.48	3.33	7.96
RKS1910+2145	TYC 1598-1505-1	19 10 32.1	+21 45 46	−12.226	−18.375	30.077	33.25	11.54	3.84	8.93
RKS1914+0209	BD+01 3942A	19 14 58.9	+02 09 54	353.721	388.672	37.240	26.85	10.47	3.29	8.33
RKS1915+1133	V1688 Aql	19 15 35.0	+11 33 16	183.498	−173.000	37.871	26.41	8.28	2.34	6.17
RKS1915+2453	HD 338030	19 15 18.8	+24 53 49	240.467	219.053	34.571	28.93	9.94	3.57	7.63
RKS1923−0635	HD 182085	19 23 16.4	−06 35 07	−171.915	−198.478	32.042	31.21	9.92	3.11	7.45
RKS1924−2203	CD-22 13916	19 24 34.2	−22 03 43	−230.901	−451.829	36.152	27.66	11.16	3.73	8.95
RKS1924+2525	PM J19244+2525	19 24 26.5	+25 25 50	−30.571	−75.070	31.436	31.81	11.18	3.75	8.67
RKS1928+1232	HD 231512A	19 28 15.3	+12 32 09	−52.786	−39.961	34.457	29.02	9.41	3.06	7.10
RKS1928+2854	PM J19284+2854	19 28 25.5	+28 54 10	−9.411	−40.796	38.595	25.91	11.09	3.85	9.02
RKS1929+0709	BD+06 4156	19 29 05.1	+07 09 35	246.236	240.500	37.828	26.44	10.90	3.71	8.79
RKS1930+2140	HD 344502	19 30 05.4	+21 40 34	−215.927	−200.287	34.456	29.02	10.18	3.11	7.87
RKS1932−1116	HD 183870	19 32 06.7	−11 16 29	234.587	18.156	56.566	17.68	7.75	2.42	6.51
RKS1932+0034	BD+00 4241	19 32 37.9	+00 34 39	218.117	25.030	45.142	22.15	10.67	3.86	8.94
RKS1934+0434	HD 184489	19 34 39.8	+04 34 57	524.409	311.083	69.257	14.44	9.57	3.65	8.77
RKS1936−1026	HD 184860A	19 36 45.6	−10 26 36	−290.800	−270.839	33.381	29.96	8.87	2.55	6.49
RKS1943+1005	HD 355784	19 43 25.3	+10 05 22	186.194	101.976	38.358	26.07	10.21	3.37	8.13

Continued on next page

Table A.1 – *Continued from previous page*

RKS ID	Simbad Name	R.A.	Decl.	$\mu_{R.A}$	μ_{Decl}	π	Dist.	$B_{Gaia\ DR3}$	B_G–K_S	M_{B_G}
...	...	(hh mm ss)	(±dd mm ss)	(mas yr^{-1})	(mas yr^{-1})	(mas)	(pc)	(mag)	(mag)	(mag)
RKS1952−2356	HD 187760	19 52 29.9	−23 56 57	19.739	−41.354	38.829	25.75	9.69	3.08	7.64
RKS1954−2356	HD 188088	19 54 17.7	−23 56 27	−124.167	−410.681	70.701	14.14	6.44	2.40	5.69
RKS1954+2013	PM J19546+2013	19 54 37.5	+20 13 06	−38.041	−62.894	36.385	27.48	11.06	3.83	8.86
RKS1957+1313	HD 356314	19 57 25.4	+13 13 24	−8.399	−42.734	38.172	26.20	10.39	3.53	8.30
RKS2000+2242	HD 189733	20 00 43.7	+22 42 39	−3.208	−250.323	50.567	19.78	7.91	2.37	6.43
RKS2002+0319	HD 190007	20 02 47.0	+03 19 34	−90.383	119.430	78.647	12.72	7.70	2.90	7.18
RKS2003+2005	HD 351151	20 03 00.9	+20 05 49	180.605	−12.572	33.297	30.03	10.84	3.57	8.45
RKS2003+2320	HD 190404	20 03 52.1	+23 20 26	−1003.993	−912.718	64.012	15.62	7.49	2.38	6.52
RKS2004+2547	HD 190470	20 04 10.0	+25 47 24	−75.404	−39.361	45.219	22.11	8.04	2.40	6.32
RKS2008+0640	BD+06 4450	20 08 24.3	+06 40 43	170.708	169.484	34.683	28.83	10.05	3.12	7.75
RKS2009−0307	BD-03 4797	20 09 41.0	−03 07 44	−196.994	−42.228	32.353	30.91	9.81	3.07	7.36
RKS2009−1417	HD 191285	20 09 36.4	−14 17 12	78.888	−91.878	31.793	31.45	10.00	3.03	7.51
RKS2009+1648	HD 191499A	20 09 34.3	+16 48 20	2.897	175.710	40.328	24.80	7.89	2.26	5.92
RKS2010−2029	HD 191391	20 10 19.5	−20 29 36	−427.582	−367.378	63.207	15.82	9.15	3.45	8.15
RKS2011+1611	HD 191785	20 11 06.0	+16 11 16	−415.062	398.487	48.926	20.44	7.55	2.20	6.00
RKS2012−1253	LP 754-50	20 12 09.4	−12 53 35	192.657	−194.040	35.433	28.22	11.54	3.92	9.29
RKS2013−0052	HD 192263	20 13 59.8	−00 52 00	−62.730	260.819	50.943	19.63	8.01	2.47	6.55
RKS2014−0716	BD-07 5223	20 14 28.1	−07 16 55	10.772	−271.100	46.139	21.67	10.42	3.69	8.74
RKS2015−2701	HD 192310	20 15 17.3	−27 01 58	1242.763	−181.175	113.487	8.81	5.95	2.45	6.23
RKS2016−0204	G 24-12	20 16 22.0	−02 04 08	289.952	−31.960	37.615	26.59	11.40	3.85	9.28

Continued on next page

Table A.1 – *Continued from previous page*

RKS ID	Simbad Name	R.A.	Decl.	$\mu_{R.A}$	μ_{Decl}	π	Dist.	$B_{Gaia\ DR3}$	B_G–K_S	M_{B_G}
...	...	(hh mm ss)	(±dd mm ss)	(mas yr^{-1})	(mas yr^{-1})	(mas)	(pc)	(mag)	(mag)	(mag)
RKS2030+2650	HD 340345	20 30 10.6	+26 50 34	−156.696	−132.110	49.029	20.40	9.94	3.59	8.39
RKS2035+0607	HD 196124	20 35 12.7	+06 07 37	389.050	−227.706	33.105	30.21	9.14	2.61	6.74
RKS2038+2346	HD 347103	20 38 26.2	+23 46 41	57.141	−55.187	30.108	33.21	8.96	2.33	6.35
RKS2039+1004	HD 196794	20 39 22.0	+10 04 32	318.015	21.314	33.442	29.90	8.75	2.34	6.37
RKS2041−0529	BD-06 5559	20 41 40.6	−05 29 34	77.431	65.218	32.629	30.65	10.77	3.54	8.34
RKS2041−2219	HD 196998	20 41 42.2	−22 19 20	656.071	−538.708	41.326	24.20	10.11	3.50	8.19
RKS2042−2116	HD 197092	20 42 05.8	−21 16 37	−43.396	−47.034	50.528	19.79	9.49	2.31	8.01
RKS2042+2050	HD 197396	20 42 49.3	+20 50 40	−80.975	−353.247	40.418	24.74	8.49	2.48	6.52
RKS2044−2121	BD-21 5811	20 44 00.6	−21 21 20	57.414	−276.408	38.427	26.02	10.10	3.35	8.02
RKS2047+1051	BD+10 4379	20 47 16.8	+10 51 36	89.598	−591.623	31.500	31.75	9.96	2.96	7.45
RKS2050+2923	HD 198550	20 50 10.5	+29 23 02	−3.077	−36.291	49.594	20.16	8.57	2.96	7.05
RKS2053−0245	BD-03 5059	20 53 56.9	−02 45 57	−610.881	−369.029	30.951	32.31	11.30	3.63	8.75
RKS2055+1310	BD+12 4499	20 55 06.8	+13 10 36	557.515	369.828	42.368	23.60	9.04	2.86	7.18
RKS2059−1042	HD 199704	20 59 14.4	−10 42 49	47.133	−21.561	30.898	32.36	8.74	2.48	6.19
RKS2059+0333	Wolf 901	20 59 08.5	+03 33 09	324.815	−725.883	30.573	32.71	12.22	3.81	9.65
RKS2105−1654	HD 358850	21 05 43.4	−16 54 49	−14.502	−58.404	45.729	21.87	10.55	3.86	8.85
RKS2105+0704	HD 200779	21 05 19.7	+07 04 09	78.562	−563.909	66.463	15.05	8.53	3.22	7.64
RKS2107−1355	HD 200968A	21 07 10.3	−13 55 22	382.969	−50.693	57.524	17.38	7.40	2.38	6.20
RKS2108−0425	BD-05 5480	21 08 45.4	−04 25 36	−80.356	−29.119	34.851	28.69	9.66	3.23	7.37
RKS2116+0923	HD 202575	21 16 32.4	+09 23 37	145.631	−118.603	61.838	16.17	8.15	2.76	7.11

Continued on next page

Table A.1 – *Continued from previous page*

RKS ID	Simbad Name	R.A.	Decl.	$\mu_{R.A}$	μ_{Decl}	π	Dist.	$B_{Gaia\ DR3}$	B_G–K_S	M_{B_G}
...	...	(hh mm ss)	(±dd mm ss)	(mas yr^{-1})	(mas yr^{-1})	(mas)	(pc)	(mag)	(mag)	(mag)
RKS2118+0009	HD 202751	21 18 02.9	+00 09 41	467.408	−188.341	49.480	20.21	8.41	2.67	6.88
RKS2119−2621	HD 202940	21 19 45.6	−26 21 10	−589.253	−351.160	54.029	18.51	6.76	2.19	5.42
RKS2120−1951	HD 203040	21 20 13.8	−19 51 08	−173.094	−721.088	63.386	15.78	9.34	3.62	8.35
RKS2122+1052	BD+10 4534	21 22 26.6	+10 52 25	−56.796	32.881	47.139	21.21	10.16	3.72	8.53
RKS2125+2712	HD 204079	21 25 29.0	+27 12 38	−180.426	−155.050	39.704	25.19	8.50	2.30	6.49
RKS2126+0344	MCC 70	21 26 42.4	+03 44 13	−39.991	−53.594	36.065	27.73	10.72	3.72	8.51
RKS2130−1230	HD 204587	21 30 02.7	−12 30 36	1019.796	−259.597	56.427	17.72	9.32	3.44	8.08
RKS2131+2320	BD+22 4409	21 31 01.7	+23 20 07	134.654	−144.889	41.291	24.22	9.52	3.14	7.60
RKS2132−2057	HD 204941	21 32 23.5	−20 57 26	−278.868	−124.315	34.883	28.67	8.67	2.31	6.38
RKS2141+1115	HD 206315	21 41 01.3	+11 15 46	−75.119	−109.887	31.429	31.82	9.41	2.77	6.90
RKS2149−1140	BD-12 6102	21 49 45.9	−11 40 57	−301.923	−309.560	32.601	30.67	11.10	3.75	8.67
RKS2149+0543	HD 207491	21 49 12.2	+05 43 22	541.955	−27.034	44.308	22.57	8.90	2.74	7.13
RKS2152+0154	HD 207874	21 52 06.5	+01 54 23	−75.157	−188.519	32.559	30.71	8.42	2.24	5.98
RKS2153−1249	LP 758-74	21 53 07.5	−12 49 40	−145.789	−135.860	41.525	24.08	11.24	3.88	9.33
RKS2153+2055	HD 208038	21 53 05.3	+20 55 49	−5.257	−100.693	43.032	23.24	8.41	2.46	6.58
RKS2153+2850	StKM 1-1953	21 53 07.2	+28 50 15	−60.215	−60.393	37.020	27.01	11.71	3.92	9.55
RKS2155−2942	HD 208272	21 55 41.9	−29 42 22	57.238	−180.083	30.631	32.65	8.68	2.19	6.11
RKS2210+2247	BD+22 4567	22 10 31.4	+22 47 49	−570.445	−50.947	30.098	33.22	9.43	2.62	6.82
RKS2214+2751	G 188-49	22 14 31.4	+27 51 18	−211.582	532.399	50.819	19.68	10.57	3.84	9.10
RKS2224+2233	BD+21 4747A	22 24 45.5	+22 33 04	−183.490	−76.657	47.923	20.87	9.16	3.40	7.56

Continued on next page

Table A.1 – *Continued from previous page*

RKS ID	Simbad Name	R.A.	Decl.	$\mu_{R.A}$	μ_{Decl}	π	Dist.	$B_{Gaia\ DR3}$	B_G–K_S	M_{B_G}
...	...	(hh mm ss)	(±dd mm ss)	(mas yr^{-1})	(mas yr^{-1})	(mas)	(pc)	(mag)	(mag)	(mag)
RKS2226−1911	HD 212658	22 26 13.5	−19 11 18	235.022	−24.894	39.162	25.53	9.49	3.01	7.45
RKS2239+0406	HD 214683	22 39 50.7	+04 06 58	178.160	108.808	44.298	22.57	8.71	2.57	6.94
RKS2240−2940	HD 214749	22 40 43.3	−29 40 28	380.494	−16.944	75.325	13.28	8.07	3.03	7.45
RKS2241+1849	BD+18 5029	22 41 35.0	+18 49 27	253.146	89.570	32.355	30.91	10.96	3.90	8.51
RKS2243−0624	HD 215152	22 43 21.3	−06 24 02	−154.095	−289.915	46.332	21.58	8.34	2.56	6.67
RKS2247+1823	BD+17 4808	22 47 13.6	+18 23 04	251.849	88.602	37.466	26.69	9.25	2.82	7.12
RKS2248+2443	MCC 209	22 48 35.5	+24 43 26	176.900	9.335	33.265	30.06	11.18	3.74	8.79
RKS2251+1358	HD 216259	22 51 26.3	+13 58 11	406.237	202.500	44.310	22.57	8.51	2.43	6.74
RKS2252+2324	BD+22 4725	22 52 02.5	+23 24 47	131.463	−153.777	35.778	27.95	10.03	3.21	7.80
RKS2254+2331	G 67-33	22 54 30.8	+23 31 06	257.604	73.767	30.045	33.28	11.35	3.84	8.74
RKS2258−1338	HD 217065	22 58 06.2	−13 38 33	37.471	−327.776	35.828	27.91	10.36	3.34	8.13
RKS2259−1122	BD-12 6393	22 59 53.6	−11 22 54	220.305	−69.587	38.467	26.00	10.82	3.72	8.75
RKS2300−2231	HD 217357	23 00 16.1	−22 31 27	−902.073	58.045	121.472	8.23	8.12	3.64	8.54
RKS2301−0350	HD 217580	23 01 51.5	−03 50 55	402.754	−213.667	61.834	16.17	7.71	2.48	6.67
RKS2307−2309	HD 218294	23 07 07.0	−23 09 34	156.276	−255.086	45.236	22.11	9.84	3.42	8.12
RKS2308+0633	R78b 355	23 08 52.4	+06 33 39	103.611	8.284	30.217	33.09	11.13	3.88	8.53
RKS2309−0215	HD 218566	23 09 10.7	−02 15 38	631.540	−97.397	34.696	28.82	8.83	2.61	6.53
RKS2309+1425	AG+14 2584	23 09 54.9	+14 25 35	−120.438	−96.616	39.756	25.15	10.48	3.64	8.48
RKS2310−2955	HD 218760	23 10 48.8	−29 55 03	450.855	−26.061	36.331	27.52	8.88	2.56	6.68
RKS2316+0541	BD+04 4988	23 16 51.8	+05 41 45	22.924	−27.149	38.041	26.29	10.76	3.73	8.66

Continued on next page

Table A.1 – *Continued from previous page*

RKS ID	Simbad Name	R.A.	Decl.	$\mu_{R.A}$	μ_{Decl}	π	Dist.	$B_{Gaia\ DR3}$	B_G–K_S	M_{B_G}
...	...	(hh mm ss)	(±dd mm ss)	(mas yr^{-1})	(mas yr^{-1})	(mas)	(pc)	(mag)	(mag)	(mag)
RKS2317−2323	CD-24 17578	23 17 00.2	−23 23 46	306.993	−243.221	43.027	23.24	11.11	3.86	9.28
RKS2323−1045	HD 220339	23 23 04.8	−10 45 51	452.192	260.311	52.164	19.17	8.02	2.43	6.61
RKS2326+0853	G 29-33	23 26 12.3	+08 53 37	518.989	213.396	44.357	22.54	10.81	3.89	9.05
RKS2327−0117	BD-02 5958	23 27 04.8	−01 17 10	375.977	215.870	33.725	29.65	10.60	3.41	8.24
RKS2328+1604	BD+15 4829	23 28 26.1	+16 04 00	49.093	−96.953	32.307	30.95	10.05	3.04	7.60
RKS2332−1650	HD 221503	23 32 49.3	−16 50 44	341.147	−219.108	68.736	14.55	8.85	3.38	8.04
RKS2335+0136	BD+00 5017	23 35 00.2	+01 36 19	340.029	28.456	47.964	20.85	9.82	3.78	8.22
RKS2340+2021	HD 222474A	23 40 51.4	+20 21 57	221.765	53.256	39.406	25.38	8.53	2.98	6.51
RKS2342−0234	BD-03 5691	23 42 10.6	−02 34 36	−236.112	−345.177	40.297	24.82	10.57	3.71	8.60
RKS2345+2933	HD 222935	23 45 09.9	+29 33 42	947.116	−3.907	33.609	29.75	8.61	2.37	6.24
RKS2348−1259	BD-13 6464	23 48 25.6	−12 59 14	235.082	15.172	35.002	28.57	9.87	3.58	7.59
RKS2349+0310	HD 223374	23 49 01.1	+03 10 52	67.704	−0.423	39.893	25.07	8.63	2.46	6.63
RKS2350−2924	HD 223515	23 50 14.9	−29 24 06	186.978	18.881	38.757	25.80	8.10	2.23	6.04
RKS2353+2901	BD+28 4660	23 53 08.5	+29 01 05	−78.549	19.390	50.228	19.91	9.98	3.59	8.48
RKS2355+2211	HD 224129	23 55 26.5	+22 11 35	202.046	−147.050	39.256	25.47	8.99	2.79	6.96
RKS2358+0949	HD 224476	23 58 19.8	+09 49 50	69.094	−1.768	33.441	29.90	8.56	2.31	6.18
RKS2359−2602	HD 224607	23 59 13.6	−26 02 55	−229.465	12.377	43.873	22.79	8.93	2.82	7.14
RKS2359+0639	HD 224660A	23 59 47.7	+06 39 50	−58.704	−166.828	43.435	23.02	9.15	3.14	7.34

B Table of Kinematic Properties for Primary Sample

Table A.2: Primary K dwarf Sample: Kinematic Properties

RKS ID	$\gamma_{Gaia_{DR3}}$	γ_{REC}	$\sigma_{\gamma_{REC}}$	U	V	W	Group	Disk
...	(km s^{-1})	(km s^{-1})	(km s^{-1})	(km s^{-1})	(km s^{-1})	(km s^{-1})	...	...
RKS0000+1659	−17.92	−17.65	0.04	29.50	−33.84	−16.46	Field	Thin disk
RKS0001−1656	0.47	0.58	0.04	−20.08	−51.95	−15.93	Field	Thin disk
RKS0007−2349	−43.17	−43.08	0.04	−55.34	−16.44	34.82	Field	Thin disk
RKS0012+2142	−5.02	−5.01	0.05	−5.64	−39.08	−32.91	Field	Thin disk
RKS0012+2705	12.50	12.57	0.04	−30.26	−11.37	−20.62	Field	Thin disk
RKS0016−1435	−13.51	−13.62	0.04	0.26	−4.41	12.92	Field	Thin disk
RKS0017+2057	−49.24	−49.51	0.05	62.59	−44.15	1.22	Field	Thick disk
RKS0019−0303	−20.92	−20.97	0.05	21.36	−31.58	6.30	Field	Thin disk
RKS0019−0957	−10.72	−11.02	0.04	17.88	−25.36	2.30	Field	Thin disk
RKS0020+1738	−2.49	−2.14	0.05	0.72	−10.82	−7.35	Field	Thin disk
RKS0021+2531	−22.21	−22.20	0.04	0.99	−18.89	13.52	Field	Thin disk
RKS0022−2701	−2.53	−0.54	0.04	−4.09	−52.60	−3.02	Field	Thin disk
RKS0024−2701	3.05	3.23	0.04	−52.03	−21.61	−9.09	Field	Thin disk
RKS0036−0930	29.72	29.80	0.05	60.50	−44.71	−51.80	Field	Thick disk
RKS0036+2610	−15.46	−15.32	0.04	−2.71	−12.84	12.32	Field	Thin disk
RKS0039+2115	−33.07	−32.95	0.03	40.07	−19.47	8.44	Field	Thin disk
RKS0042+2239	3.98	4.23	0.05	−53.43	−27.01	−2.16	Field	Thin disk
RKS0045+0147	9.38	9.45	0.03	31.21	−37.85	−37.54	Field	Thin disk
RKS0048+0516	−10.37	−10.22	0.04	−1.07	−47.50	−13.26	Field	Thin disk

Continued on next page

Table A.2 – *Continued from previous page*

RKS ID	$\gamma_{Gaia_{DR3}}$	γ_{REC}	$\sigma_{\gamma_{REC}}$	U	V	W	Group	Disk
...	(km s^{-1})	(km s^{-1})	(km s^{-1})	(km s^{-1})	(km s^{-1})	(km s^{-1})	...	...
RKS0051−2254	14.52	14.62	0.04	−27.15	−40.24	−16.03	Field	Thin disk
RKS0051+1844	6.51	6.63	0.04	3.40	−15.59	−24.91	Field	Thin disk
RKS0055−2940	7.43	7.69	0.03	−62.58	−14.34	−7.68	Field	Thin disk
RKS0057+0551	−15.97	−16.08	0.05	8.97	−4.42	13.43	Field	Thin disk
RKS0102−1025	8.84	9.03	0.04	5.42	−13.67	−13.62	Field	Thin disk
RKS0102+0503	...	20.35	0.04	−46.30	5.25	−3.42	Field	Thin disk
RKS0104−2536	5.70	5.58	0.04	26.26	−31.14	−6.90	Field	Thin disk
RKS0104+2607	8.39	8.36	0.04	−41.29	−18.78	−1.19	Hyades	Thin disk
RKS0105+1523	−5.98	−5.79	0.04	11.54	−19.80	−13.05	Field	Thin disk
RKS0107+2257	6.59	6.63	0.03	4.20	−28.13	−40.19	Field	Thin disk
RKS0108+1714	−56.38	−56.88	0.05	60.89	−75.07	−15.37	Field	Thick disk
RKS0112−2514	−4.67	−4.73	0.04	−12.00	−6.11	5.93	Field	Thin disk
RKS0113+1629	26.07	26.19	0.04	−10.39	7.15	−24.62	Field	Thin disk
RKS0116+2519	−23.10	−23.39	0.04	−23.81	−48.81	9.70	Field	Thin disk
RKS0117−1530	−7.04	−7.08	0.03	7.72	−84.56	−3.62	Field	Thick disk
RKS0118−0052	16.81	17.15	0.04	−34.96	−52.55	−23.93	Field	Thin disk
RKS0121+2419	10.74	10.93	0.04	−41.06	−18.69	−0.74	Hyades	Thin disk
RKS0122−2653	21.02	21.05	0.03	24.10	−22.70	−22.16	Field	Thin disk
RKS0123−1257	34.60	34.69	0.04	−58.88	−37.34	−26.20	Field	Thick disk
RKS0124+1829	6.99	7.05	0.04	−58.55	−62.06	−14.49	Field	Thick disk
RKS0125−0103	−5.35	−5.28	0.04	46.78	−17.26	−18.50	Field	Thin disk

Continued on next page

Table A.2 – *Continued from previous page*

RKS ID	$\gamma_{Gaia_{DR3}}$	γ_{REC}	$\sigma_{\gamma_{REC}}$	U	V	W	Group	Disk
...	(km s^{-1})	(km s^{-1})	(km s^{-1})	(km s^{-1})	(km s^{-1})	(km s^{-1})	...	...
RKS0129+2143	21.35	20.79	0.04	−44.73	−30.93	−21.28	Field	Thin disk
RKS0135−2046	18.97	18.82	0.05	−14.46	−12.49	−16.04	Field	Thin disk
RKS0139+1515	−21.54	−21.44	0.04	−5.52	−29.40	15.59	Field	Thin disk
RKS0142+2016	−33.70	−33.63	0.04	34.90	−24.95	2.15	Field	Thin disk
RKS0146+1224	21.59	21.68	0.04	−11.07	0.63	−20.80	Field	Thin disk
RKS0150+1817	22.38	22.19	0.04	−35.09	−18.52	−15.08	Field	Thin disk
RKS0150+2927	−39.60	−39.53	0.04	29.97	−24.06	13.10	Field	Thin disk
RKS0200+2636	−17.91	−18.47	0.05	−9.37	−20.80	24.84	Field	Thin disk
RKS0205−2804	3.30	3.45	0.05	−64.92	12.04	8.63	Field	Thin disk
RKS0209−1620	13.07	13.01	0.04	−60.59	−36.88	10.66	Field	Thick disk
RKS0213−2111	2.92	3.05	0.04	−34.55	−22.77	11.04	Field	Thin disk
RKS0214−0338	−8.80	−8.67	0.04	17.44	−18.04	−2.47	Field	Thin disk
RKS0215−1814	...	3.10	0.04	9.92	−8.24	−6.39	Field	Thin disk
RKS0221−0652	26.12	26.27	0.04	−42.93	−18.64	−7.21	Field	Thin disk
RKS0229−1958	27.46	27.66	0.04	−62.05	−20.92	−1.78	Field	Thin disk
RKS0231−1516	−28.44	−28.39	0.04	27.71	−2.76	18.55	Field	Thin disk
RKS0231−2001	22.24	22.20	0.04	−30.85	−19.87	−8.33	Field	Thin disk
RKS0236−0309	20.53	35.58	0.04	−47.69	−17.35	−11.69	Field	Thin disk
RKS0236−2331	16.25	16.49	0.04	−12.13	−7.82	−11.66	Field	Thin disk
RKS0236−2710	11.64	11.73	0.04	7.13	−29.49	−7.16	Field	Thin disk
RKS0236+0653	25.21	24.39	0.03	−75.74	1.59	33.67	Field	Thick disk

Continued on next page

Table A.2 – *Continued from previous page*

RKS ID	$\gamma_{Gaia_{DR3}}$	γ_{REC}	$\sigma_{\gamma_{REC}}$	U	V	W	Group	Disk
...	(km s^{-1})	(km s^{-1})	(km s^{-1})	(km s^{-1})	(km s^{-1})	(km s^{-1})	...	...
RKS0240+0111	72.93	72.91	0.04	−77.58	6.11	−31.39	Field	Thick disk
RKS0242+0322	−6.80	−6.98	0.05	22.51	−2.75	−10.18	Field	Thin disk
RKS0243+1925	32.98	33.69	0.04	−50.16	−15.43	−2.85	Field	Thin disk
RKS0246−2305	32.49	32.43	0.04	−43.33	−17.73	−13.24	Field	Thin disk
RKS0246+1146	10.82	11.00	0.04	−14.61	−22.48	−8.55	Field	Thin disk
RKS0246+2538	14.06	14.13	0.04	−25.42	−24.71	−8.37	Field	Thin disk
RKS0247+2842	1.61	1.53	0.04	12.33	16.46	−9.16	Field	Thin disk
RKS0248−1145	30.44	30.31	0.04	7.52	−18.68	−38.19	Field	Thin disk
RKS0248+2704	10.13	11.19	0.05	−25.34	−23.76	−2.12	Field	Thin disk
RKS0250+1542	−29.19	−28.93	0.04	11.36	−63.38	6.34	Field	Thin disk
RKS0251−0816	18.17	18.14	0.04	−11.89	−4.95	−13.59	Field	Thin disk
RKS0251+1038	0.20	0.27	0.05	16.17	−2.85	−18.39	Field	Thin disk
RKS0252−1246	17.80	18.12	0.06	−15.33	−21.81	−9.21	Field	Thin disk
RKS0255+2652	31.92	32.09	0.04	−39.29	−19.83	−17.75	Field	Thin disk
RKS0255+2807	50.52	50.74	0.04	−62.77	−22.84	−21.19	Field	Thick disk
RKS0257−2458	...	49.20	0.09	−17.11	−17.19	−43.00	Field	Thin disk
RKS0258+2646	42.58	31.48	0.04	−26.26	24.36	−3.00	Field	Thin disk
RKS0300+0744	28.62	28.83	0.04	−42.96	−18.88	−0.93	Hyades	Thin disk
RKS0303+2006	44.89	44.98	0.04	−35.93	5.89	−27.40	Field	Thin disk
RKS0306+0157	−31.35	−31.18	0.04	35.98	−67.51	4.95	Field	Thick disk
RKS0308−2410	16.43	16.42	0.04	10.29	−19.03	−17.60	Field	Thin disk

Continued on next page

Table A.2 – *Continued from previous page*

RKS ID	$\gamma_{Gaia_{DR3}}$	γ_{REC}	$\sigma_{\gamma_{REC}}$	U	V	W	Group	Disk
...	(km s^{-1})	(km s^{-1})	(km s^{-1})	(km s^{-1})	(km s^{-1})	(km s^{-1})	...	...
RKS0308−2445	74.40	NM	NM	NM	NM	NM	...	...
RKS0310+1203	38.91	38.89	0.04	−41.38	−32.09	−19.80	Field	Thin disk
RKS0314−2626	15.14	15.32	0.04	−22.91	−12.18	−2.25	Field	Thin disk
RKS0314+0858	−16.73	−16.65	0.04	5.54	−63.74	8.60	Field	Thin disk
RKS0320+0827	30.81	30.94	0.05	−41.71	−19.25	−0.81	Hyades	Thin disk
RKS0322+2709	30.13	29.95	0.05	−41.53	−19.27	−1.43	Hyades	Thin disk
RKS0324−0521	−13.36	−13.10	0.04	47.81	−28.78	−21.32	Field	Thin disk
RKS0329−1140	13.49	13.52	0.04	7.89	−28.20	−16.60	Field	Thin disk
RKS0329−2406	...	43.73	0.25	...	...	...	Field	...
RKS0332−0927	...	16.29	0.04	−3.54	7.11	−20.59	Field	Thin disk
RKS0341+0336	0.40	1.65	0.12	13.96	−18.45	−18.86	Field	Thin disk
RKS0342−2427	15.99	16.06	0.04	25.60	−37.96	−17.43	Field	Thin disk
RKS0343−1253	−53.21	−52.97	0.05	44.76	37.27	20.99	Field	Thin disk
RKS0343−1906	25.17	25.30	0.04	−30.42	−14.86	−4.57	Field	Thin disk
RKS0343+1640	34.10	34.41	0.05	−28.99	−23.32	−25.17	Field	Thin disk
RKS0344+1155	83.68	83.88	0.04	−89.03	−6.38	−17.59	Field	Thick disk
RKS0345−2751	32.36	32.57	0.04	−35.98	−26.92	−6.26	Field	Thin disk
RKS0348+1512	−43.22	−43.01	0.04	34.13	−24.37	22.70	Field	Thin disk
RKS0348+2519	−69.17	−69.00	0.04	62.60	−27.89	17.32	...	...
RKS0349−1329	−5.26	−5.32	0.05	18.75	−3.53	−7.62	Field	Thin disk
RKS0349+0120	−12.70	NM	NM	NM	NM	NM	...	...

Continued on next page

Table A.2 – *Continued from previous page*

RKS ID	$\gamma_{Gaia_{DR3}}$	γ_{REC}	$\sigma_{\gamma_{REC}}$	U	V	W	Group	Disk
...	(km s^{-1})	(km s^{-1})	(km s^{-1})	(km s^{-1})	(km s^{-1})	(km s^{-1})	...	...
RKS0350−2349	−0.33	−0.31	0.04	22.27	−31.06	2.04	Field	Thin disk
RKS0354−0649	62.14	62.23	0.04	−66.53	15.64	−27.13	Field	Thick disk
RKS0357−0109	3.41	3.51	0.04	7.82	0.55	−15.46	Field	Thin disk
RKS0404+2634	62.23	62.47	0.05	−67.88	−18.96	−10.87	Field	Thick disk
RKS0406−2051	25.17	25.18	0.04	53.49	−75.93	−34.32	Field	Thick disk
RKS0407+1413	−18.23	−18.07	0.04	13.13	−34.69	11.88	Field	Thin disk
RKS0408+1220	4.96	5.11	0.04	2.22	−52.12	−15.17	Field	Thin disk
RKS0414+0301	56.80	56.56	0.03	−70.26	11.99	0.32	Field	Thick disk
RKS0415−0739	−42.47	−42.30	0.04	96.75	−12.37	−41.36	Field	Thick disk
RKS0417+2033	14.24	14.29	0.04	−10.09	−1.49	−14.07	Field	Thin disk
RKS0417+2240	27.96	28.00	0.03	−31.18	−13.15	−1.17	Field	Thin disk
RKS0419−0408	36.87	36.91	0.04	−32.33	−19.14	−12.25	Field	Thin disk
RKS0420−1445	36.62	36.49	0.04	−42.85	−18.80	−1.36	Hyades	Thin disk
RKS0421−1945	21.57	21.33	0.05	19.32	−15.86	−39.25	Field	Thin disk
RKS0427+2426	67.57	68.14	0.04	−81.66	−21.34	25.01	Field	Thick disk
RKS0429+2155	−35.74	−35.48	0.04	33.34	6.76	14.17	Field	Thin disk
RKS0430+0058	28.35	28.32	0.06	−22.68	−18.96	−10.61	Field	Thin disk
RKS0436+2707	40.18	43.68	0.09	−46.50	−15.75	−3.58	Field	Thin disk
RKS0439+0952	−24.94	NM	NM	NM	NM	NM	...	...
RKS0441+2054	0.55	1.19	0.16	4.83	−3.49	−20.85	Field	Thin disk
RKS0443+2741	17.64	17.87	0.04	−17.66	−22.75	−16.56	Field	Thin disk

Continued on next page

Table A.2 – *Continued from previous page*

RKS ID	$\gamma_{Gaia_{DR3}}$	γ_{REC}	$\sigma_{\gamma_{REC}}$	U	V	W	Group	Disk
...	(km s^{-1})	(km s^{-1})	(km s^{-1})	(km s^{-1})	(km s^{-1})	(km s^{-1})	...	...
RKS0445+0938	94.67	94.79	0.05	−86.31	−38.20	−28.10	Field	Thick disk
RKS0448−1056	27.16	27.32	0.05	−13.79	−26.73	−11.65	Field	Thin disk
RKS0449−1447	27.86	28.00	0.05	8.87	−20.09	−45.28	Field	Thin disk
RKS0451+2837	6.48	6.41	0.04	−9.07	−15.70	4.08	Field	Thin disk
RKS0453+2214	26.24	26.31	0.04	−27.15	−23.85	−1.73	Field	Thin disk
RKS0454+0722	46.46	46.78	0.04	−38.77	−51.75	−4.84	Field	Thin disk
RKS0455−2833	5.97	6.20	0.04	10.01	−23.60	5.13	Field	Thin disk
RKS0500−0545	21.36	21.61	0.03	5.04	−54.89	−10.87	Field	Thin disk
RKS0503−2315	115.94	119.90	0.04	−92.31	−79.88	−33.05	Field	Thick disk
RKS0503+0322	−3.79	−3.80	0.05	7.53	−4.09	−4.78	Field	Thin disk
RKS0506−1102	30.17	30.42	0.05	−18.61	−22.33	−13.13	Field	Thin disk
RKS0506+1426	24.76	NM	NM	NM	NM	NM	...	...
RKS0512+1943	−0.50	−0.41	0.04	9.76	−111.16	−11.02	Field	Thick disk
RKS0513−2158	52.67	53.51	0.04	−41.26	−32.29	−16.99	Field	Thin disk
RKS0514+0039	13.41	13.18	0.04	13.59	−68.18	−6.95	Field	Thin disk
RKS0514+1952	43.92	44.04	0.04	−42.11	−51.82	2.80	Field	Thin disk
RKS0518−2123	26.89	27.12	0.04	−13.06	−10.74	−25.27	Field	Thin disk
RKS0519−0304	88.48	88.79	0.04	−85.46	−56.61	14.10	Field	Thick disk
RKS0519−1550	−14.15	−14.05	0.05	−8.45	11.16	30.52	Field	Thin disk
RKS0522+0236	36.98	37.60	0.04	−26.49	−28.70	−14.80	Field	Thin disk
RKS0523+1719	38.03	38.30	0.04	−38.74	−14.67	7.11	Field	Thin disk

Continued on next page

Table A.2 – *Continued from previous page*

RKS ID	$\gamma_{Gaia_{DR3}}$	γ_{REC}	$\sigma_{\gamma_{REC}}$	U	V	W	Group	Disk
...	(km s^{-1})	(km s^{-1})	(km s^{-1})	(km s^{-1})	(km s^{-1})	(km s^{-1})	...	...
RKS0528−0329	−55.70	−55.49	0.04	74.14	−1.76	−18.00	Field	Thick disk
RKS0533−2643	48.66	48.72	0.04	−46.79	−22.95	−14.42	Field	Thin disk
RKS0534−2328	−28.47	−28.53	0.04	60.79	−34.23	30.83	Field	Thick disk
RKS0535+2805	30.44	30.55	0.04	−31.16	−51.99	2.48	Field	Thin disk
RKS0536+1119	21.36	21.66	0.05	−19.70	−7.53	−5.79	Field	Thin disk
RKS0542+0240	52.89	53.00	0.03	−12.17	−102.09	−17.45	Field	Thick disk
RKS0544−2225	−9.80	−9.57	0.04	17.64	5.15	−11.83	Field	Thin disk
RKS0549−1734	4.18	4.32	0.04	−12.96	6.85	0.83	Field	Thin disk
RKS0552−2246	78.18	78.09	0.04	−85.96	−48.13	20.97	Field	Thick disk
RKS0553−0559	22.97	23.04	0.04	0.23	−34.88	−20.69	Field	Thin disk
RKS0554−1942	44.02	43.90	0.05	−27.64	−35.03	−7.10	Field	Thin disk
RKS0554+0208	−33.90	−33.81	0.04	65.91	−51.09	−21.37	Field	Thick disk
RKS0600+2101	−2.13	−2.09	0.04	8.68	−40.03	−28.59	Field	Thin disk
RKS0602+0848	−39.13	−39.25	0.05	36.37	10.45	14.97	Field	Thin disk
RKS0608+2630	25.57	28.47	0.04	−28.44	−5.01	−4.52	Field	Thin disk
RKS0609+0009	36.95	36.88	0.04	−21.56	−41.00	5.71	Field	Thin disk
RKS0609+0540	60.77	60.75	0.03	−57.38	−22.39	3.46	Field	Thin disk
RKS0612+1023	40.65	40.69	0.04	−37.36	−14.70	−9.89	Field	Thin disk
RKS0614+0510	71.23	71.24	0.04	−47.46	−64.58	−19.00	Field	Thick disk
RKS0616+2512	42.19	47.26	0.04	−41.85	−60.77	−16.99	Field	Thick disk
RKS0617+1759	4.08	3.90	0.04	0.91	−20.54	8.00	Field	Thin disk

Continued on next page

Table A.2 – *Continued from previous page*

RKS ID	$\gamma_{Gaia_{DR3}}$	γ_{REC}	$\sigma_{\gamma_{REC}}$	U	V	W	Group	Disk
...	(km s^{-1})	(km s^{-1})	(km s^{-1})	(km s^{-1})	(km s^{-1})	(km s^{-1})	...	...
RKS0618−1352	101.05	101.15	0.04	−103.80	−41.16	3.33	Field	Thick disk
RKS0620+0215	31.49	31.71	0.04	−24.55	−16.78	−22.84	Field	Thin disk
RKS0621−2212	−31.45	−31.22	0.04	44.98	4.89	−0.53	Field	Thin disk
RKS0626+1845	...	−59.51	0.09	58.29	8.74	−16.11	Field	Thin disk
RKS0629+2700	−47.73	−47.67	0.03	43.82	−31.30	−60.97	Field	Thick disk
RKS0630−1148	43.24	43.33	0.04	−41.99	−13.29	−20.57	Field	Thin disk
RKS0630+2104	...	45.00	0.05	−43.85	−9.00	4.68	Field	Thin disk
RKS0632−2701	73.46	73.47	0.05	−1.23	−97.69	17.16	Field	Thick disk
RKS0633+0527	−1.09	−1.03	0.04	9.17	−16.93	7.64	Field	Thin disk
RKS0637+1945	82.49	82.72	0.04	−78.79	−24.65	7.49	Field	Thick disk
RKS0641+2357	−44.59	−44.27	0.04	48.81	−19.27	−1.42	Field	Thin disk
RKS0647−1815	99.62	99.65	0.04	−75.46	−62.73	−25.16	Field	Thick disk
RKS0652−0510	−7.34	−7.07	0.04	0.02	12.79	−19.86	Field	Thin disk
RKS0652−2306	61.20	61.27	0.04	−36.11	−55.50	22.15	Field	Thin disk
RKS0658−1259	−4.65	−5.03	0.05	13.68	−6.80	3.36	Field	Thin disk
RKS0700−2847	47.92	47.91	0.05	−22.32	−36.07	−33.05	Field	Thin disk
RKS0701−2556	12.44	9.81	0.04	−3.50	−12.05	12.44	Field	Thin disk
RKS0701+0655	−12.09	−11.89	0.04	7.88	10.02	−3.10	Field	Thin disk
RKS0702−0647	−30.60	−30.48	0.04	34.41	6.99	−28.91	Field	Thin disk
RKS0705+2728	−22.90	−22.60	0.05	20.48	−4.26	−14.52	Field	Thin disk
RKS0706+2358	6.99	6.99	0.04	−7.17	−25.40	−21.95	AB Dor	Thin disk

Continued on next page

Table A.2 – *Continued from previous page*

RKS ID	$\gamma_{Gaia_{DR3}}$	γ_{REC}	$\sigma_{\gamma_{REC}}$	U	V	W	Group	Disk
...	(km s^{-1})	(km s^{-1})	(km s^{-1})	(km s^{-1})	(km s^{-1})	(km s^{-1})	...	...
RKS0707+0326	−17.45	−19.70	0.04	31.83	−16.56	−15.49	Field	Thin disk
RKS0708−0958	26.41	26.58	0.03	−29.83	−6.77	−22.64	Field	Thin disk
RKS0708+2950	19.63	19.68	0.04	−23.58	−26.43	−21.21	Field	Thin disk
RKS0710−1425	71.21	71.04	0.04	−86.73	−15.69	−33.76	Field	Thick disk
RKS0712−2453	41.60	41.69	0.04	−26.80	−30.01	−18.91	Field	Thin disk
RKS0713+2500	−54.43	−54.54	0.04	34.95	18.07	−66.04	Field	Thick disk
RKS0716−0339	10.96	11.12	0.03	1.22	−17.96	11.71	Field	Thin disk
RKS0723−2001	12.61	12.53	0.03	31.36	−37.07	−18.04	Field	Thin disk
RKS0723+1257	37.79	37.88	0.03	−15.83	−60.08	−3.20	Field	Thin disk
RKS0723+2024	7.56	7.88	0.18	−5.02	−27.18	−17.05	AB Dor	Thin disk
RKS0724−1753	−8.79	−8.48	0.05	6.82	5.63	−7.23	Field	Thin disk
RKS0725−1041	27.89	27.62	0.05	−11.57	−29.75	−41.56	Field	Thin disk
RKS0726−1546	−1.08	−1.07	0.04	10.93	−7.51	−0.78	Field	Thin disk
RKS0730−0340	45.78	45.79	0.04	−44.17	−20.83	−7.80	Field	Thin disk
RKS0731+1436	65.77	NM	NM	NM	NM	NM	...	...
RKS0732+1719	22.72	27.67	0.05	−30.24	−22.84	−25.71	Field	Thin disk
RKS0734−0653	−9.96	−9.67	0.06	6.09	5.93	−11.13	Field	Thin disk
RKS0739−0335	−18.40	−18.19	0.04	25.22	−2.38	−7.47	Field	Thin disk
RKS0741−2921	31.51	31.63	0.04	−31.48	−19.08	−15.95	Field	Thin disk
RKS0745+0208	−34.77	−34.66	0.04	42.16	−1.36	−12.20	Field	Thin disk
RKS0752+2555	−43.51	−43.38	0.04	41.74	−4.83	−18.90	Field	Thin disk

Continued on next page

Table A.2 – *Continued from previous page*

RKS ID	$\gamma_{Gaia_{DR3}}$	γ_{REC}	$\sigma_{\gamma_{REC}}$	U	V	W	Group	Disk
...	(km s^{-1})	(km s^{-1})	(km s^{-1})	(km s^{-1})	(km s^{-1})	(km s^{-1})	...	...
RKS0754−0124	108.60	NM	NM	NM	NM	NM	...	...
RKS0754−2518	63.08	63.35	0.04	−53.93	−43.60	−11.57	Field	Thick disk
RKS0754+1914	−18.56	−18.63	0.03	29.57	−35.41	−14.55	Field	Thin disk
RKS0757−0048	−4.62	−4.44	0.03	−3.37	6.09	−12.03	Field	Thin disk
RKS0758−1501	52.12	47.88	0.03	−4.70	−57.69	−9.06	Field	Thin disk
RKS0758−2537	−8.19	−8.00	0.04	34.99	−8.17	15.57	Field	Thin disk
RKS0759+2050	−28.16	−28.37	0.04	46.34	−54.57	−16.03	Field	Thick disk
RKS0808+2106	79.32	79.17	0.04	−73.24	−49.24	3.87	Field	Thick disk
RKS0813−1355	8.00	NM	NM	NM	NM	NM	Field	...
RKS0814+1301	21.10	21.39	0.04	−39.97	4.25	−19.84	Field	Thin disk
RKS0815−2600	12.78	12.70	0.04	30.51	−26.63	12.57	Field	Thin disk
RKS0817+1717	−22.70	−22.47	0.04	29.95	−6.97	−2.59	Field	Thin disk
RKS0819+0120	...	27.59	0.06	−26.05	−19.04	−7.43	Field	Thin disk
RKS0820+1404	7.22	7.17	0.05	−1.97	−26.77	−14.43	AB Dor	Thin disk
RKS0823+2150	−27.30	−26.93	0.04	47.28	−23.53	7.25	Field	Thin disk
RKS0827+2855	54.85	55.06	0.04	−67.97	25.73	9.11	Field	Thick disk
RKS0832−2323	25.02	25.15	0.04	−28.78	−14.98	−0.12	Field	Thin disk
RKS0838−0415	52.96	52.95	0.05	−9.03	−71.63	−9.37	Field	Thick disk
RKS0838−1315	20.46	20.64	0.05	−19.80	−12.52	1.41	Field	Thin disk
RKS0839+0657	...	...	...	...	...	...	Field	...
RKS0839+1131	−12.02	−12.04	0.04	18.08	−30.90	−29.43	Field	Thin disk

Continued on next page

Table A.2 – *Continued from previous page*

RKS ID	$\gamma_{Gaia_{DR3}}$	γ_{REC}	$\sigma_{\gamma_{REC}}$	U	V	W	Group	Disk
...	(km s^{-1})	(km s^{-1})	(km s^{-1})	(km s^{-1})	(km s^{-1})	(km s^{-1})	...	...
RKS0840−0628	−12.32	−11.28	0.11	25.10	−5.04	−1.61	Field	Thin disk
RKS0848+0628	...	−23.26	0.04	58.52	−37.07	−11.94	Field	Thick disk
RKS0850+0751	...	−12.73	0.06	7.06	5.38	−10.11	Field	Thin disk
RKS0852+2819	27.19	27.27	0.04	−37.16	−18.14	−8.22	Field	Thin disk
RKS0855+0132	−4.27	−4.10	0.04	52.87	−75.35	−43.70	Field	Thick disk
RKS0900+2127	6.39	NM	NM	NM	NM	NM	...	...
RKS0901+1515	−12.34	−12.19	0.04	9.91	−19.43	−24.19	Field	Thin disk
RKS0904−1554	4.57	4.59	0.05	−8.75	−5.70	−11.11	Field	Thin disk
RKS0905+2517	−24.96	−24.80	0.05	−3.10	−29.48	−55.33	Field	Thin disk
RKS0907+2252	−12.41	−23.16	0.08	17.88	0.35	−16.52	Field	Thin disk
RKS0909+0512	−8.95	−8.71	0.03	1.07	2.85	−11.71	Field	Thin disk
RKS0914+0426	12.19	13.32	0.04	−12.77	−6.79	3.47	Field	Thin disk
RKS0917−0323	...	23.03	0.09	...	...	...	Field	...
RKS0918+2718	6.62	6.72	0.04	−15.76	−17.89	−12.54	Field	Thin disk
RKS0919+0053	51.06	51.03	0.04	−31.97	−46.63	6.81	Field	Thin disk
RKS0920−0545	37.00	36.96	0.04	−39.69	−37.28	−18.27	Field	Thin disk
RKS0929−0522	27.63	27.72	0.04	−53.60	−21.03	−21.72	Field	Thin disk
RKS0929+0539	29.75	29.86	0.04	−40.92	−13.76	−0.07	Field	Thin disk
RKS0932−1111	6.99	7.50	1.37	−20.23	−5.44	−9.37	Field	Thin disk
RKS0932+2909	−29.78	−29.73	0.06	23.95	−2.42	−20.08	Field	Thin disk
RKS0937+2231	...	−4.02	0.04	−1.19	−16.72	−14.11	Field	Thin disk

Continued on next page

Table A.2 – *Continued from previous page*

RKS ID	$\gamma_{Gaia_{DR3}}$	γ_{REC}	$\sigma_{\gamma_{REC}}$	U	V	W	Group	Disk
...	(km s^{-1})	(km s^{-1})	(km s^{-1})	(km s^{-1})	(km s^{-1})	(km s^{-1})	...	...
RKS0937+2241	−36.38	−36.27	0.04	15.42	−7.49	−40.57	Field	Thin disk
RKS0938+0240	116.98	116.99	0.06	−40.21	−163.57	−7.58	Field	Thick disk
RKS0947+0134	31.11	31.05	0.05	−38.10	10.16	32.62	Field	Thin disk
RKS0952+0307	13.36	13.43	0.04	−10.01	−12.42	2.15	Field	Thin disk
RKS0952+0313	21.36	NM	NM	NM	NM	NM	...	...
RKS0959−0911	30.89	32.78	0.04	−10.87	−33.44	6.92	Field	Thin disk
RKS1000+2433	−0.72	NM	NM	NM	NM	NM	...	...
RKS1001−1525	19.06	19.33	0.05	−30.28	−18.28	−5.95	Field	Thin disk
RKS1004−1143	−12.34	−12.10	0.05	−12.02	4.69	−20.84	Field	Thin disk
RKS1005+2629	0.37	0.33	0.04	−18.22	−16.46	−17.11	Field	Thin disk
RKS1006+0257	−15.92	−15.46	0.04	5.40	−0.14	−19.39	Field	Thin disk
RKS1008+1159	6.59	6.83	0.05	−26.77	−7.16	−11.56	Field	Thin disk
RKS1011−2425	10.41	10.31	0.05	20.25	−6.26	16.39	Field	Thin disk
RKS1020−0128	23.07	23.12	0.03	−76.59	−53.83	−51.12	Field	Thick disk
RKS1024−1024	−3.49	−3.58	0.04	50.77	−10.58	−1.34	Field	Thin disk
RKS1026−0631	30.64	32.24	0.05	40.39	−85.52	−28.56	Field	Thick disk
RKS1026+2638	−13.72	−14.44	0.04	29.30	−3.35	−1.34	Field	Thin disk
RKS1028+0644	24.78	25.00	0.03	−24.03	20.37	35.89	Field	Thin disk
RKS1030−2114	31.55	31.56	0.04	−50.24	−43.73	−19.95	Field	Thin disk
RKS1032+0830	...	−39.24	0.05	34.83	0.57	−34.12	Field	Thin disk
RKS1036−1350	18.90	19.06	0.04	−25.03	−18.81	1.55	Field	Thin disk

Continued on next page

Table A.2 – *Continued from previous page*

RKS ID	$\gamma_{Gaia_{DR3}}$	γ_{REC}	$\sigma_{\gamma_{REC}}$	U	V	W	Group	Disk
...	(km s^{-1})	(km s^{-1})	(km s^{-1})	(km s^{-1})	(km s^{-1})	(km s^{-1})	...	...
RKS1043−2903	22.57	22.89	0.07	−15.10	−28.04	−4.22	Field	Thin disk
RKS1046−2435	−11.93	−11.97	0.04	−6.16	1.81	−20.73	Field	Thin disk
RKS1053−1422	74.79	74.89	0.04	−36.07	−103.70	−11.41	Field	Thick disk
RKS1054−0432	17.06	16.94	0.05	−2.61	−14.05	9.90	Field	Thin disk
RKS1056+0723	5.32	5.44	0.04	−16.47	−14.06	−6.72	Field	Thin disk
RKS1057+2856	−30.54	−32.93	0.04	60.09	−2.82	−10.67	Field	Thin disk
RKS1059+2526	−2.99	−2.81	0.04	−12.42	−9.52	−10.37	Field	Thin disk
RKS1102−0919	−6.33	−6.48	0.05	−19.33	−10.24	−21.56	Field	Thin disk
RKS1108−2816	...	20.69	0.04	−50.98	−42.34	−21.84	Field	Thin disk
RKS1108+1546	104.19	104.13	0.04	11.45	−74.38	90.14	Field	Thick disk
RKS1111−1057	37.40	37.08	0.04	−106.14	−20.75	26.23	Field	Thick disk
RKS1111−1459	−14.13	−13.82	0.04	82.24	0.00	−20.89	Field	Thick disk
RKS1113+0428	16.40	16.51	0.04	−25.07	−19.97	2.64	Field	Thin disk
RKS1114−2306	32.26	32.11	0.04	−5.72	−55.92	−23.27	...	...
RKS1114+2542	−1.82	−1.59	0.04	−10.94	1.18	−5.20	Field	Thin disk
RKS1115−1808	8.07	7.96	0.04	53.40	−43.25	−44.03	Field	Thick disk
RKS1116−1441	16.11	16.33	0.04	−7.67	−23.29	−1.19	Field	Thin disk
RKS1117−0158	4.56	4.65	0.04	−76.96	−35.27	−29.16	Field	Thick disk
RKS1117−2748	−20.70	−20.39	0.04	15.28	20.75	−9.27	Field	Thin disk
RKS1121−2027	−0.15	−2.79	0.05	12.13	3.62	−1.54	Field	Thin disk
RKS1121+1811	−3.42	−3.32	0.04	−13.37	−19.83	−13.46	Field	Thin disk

Continued on next page

Table A.2 – *Continued from previous page*

RKS ID	$\gamma_{Gaia_{DR3}}$	γ_{REC}	$\sigma_{\gamma_{REC}}$	U	V	W	Group	Disk
...	(km s^{-1})	(km s^{-1})	(km s^{-1})	(km s^{-1})	(km s^{-1})	(km s^{-1})	...	...
RKS1125+2000	4.22	4.47	0.04	−21.62	−24.51	−7.68	Field	Thin disk
RKS1126+1517	−4.34	−4.32	0.04	17.91	4.59	0.81	Field	Thin disk
RKS1127+0358	−2.89	−2.30	0.04	−12.26	−2.27	−5.44	Field	Thin disk
RKS1128+0731	39.51	39.56	0.04	40.19	−164.40	−32.70	Field	Thick disk
RKS1134−1314	82.68	82.41	0.04	−25.21	−79.24	40.62	Field	Thick disk
RKS1135+1658	0.03	−0.02	0.04	7.26	−2.63	0.51	Field	Thin disk
RKS1139−2741	38.15	38.07	0.04	69.54	−27.12	3.27	Field	Thick disk
RKS1141+0508	18.95	18.96	0.04	62.68	−50.18	−0.49	Field	Thick disk
RKS1147−1149	18.64	18.81	0.03	−15.58	−28.83	1.88	Field	Thin disk
RKS1152+1845	1.74	1.73	0.04	20.97	−32.34	−3.45	Field	Thin disk
RKS1154+2844	−14.71	−17.55	0.04	42.32	−22.62	−11.17	Field	Thin disk
RKS1157−2608	−10.61	−10.59	0.04	−47.40	−2.56	−1.01	Field	Thin disk
RKS1157−2742	48.29	48.51	0.04	−20.45	−74.07	−7.97	Field	Thick disk
RKS1157+1959	4.91	5.06	0.05	−48.47	−17.27	−4.73	Field	Thin disk
RKS1158−2355	−10.30	−10.21	0.03	−18.53	−5.11	−15.88	Field	Thin disk
RKS1159−2021	14.89	15.04	0.04	33.01	−26.42	−17.21	Field	Thin disk
RKS1204−0013	...	−18.50	0.07	−16.55	−6.23	−23.33	Field	Thin disk
RKS1204+0911	−6.64	−7.16	0.04	−37.20	−10.32	−11.94	Field	Thin disk
RKS1205−1852	−3.16	−8.27	0.05	11.71	−14.11	−30.69	Field	Thin disk
RKS1206−2336	40.29	40.43	0.04	25.03	−32.83	15.34	Field	Thin disk
RKS1208−0028	3.99	4.24	0.05	−109.12	−73.19	−24.43	Field	Thick disk

Continued on next page

Table A.2 – *Continued from previous page*

RKS ID	$\gamma_{Gaia_{DR3}}$	γ_{REC}	$\sigma_{\gamma_{REC}}$	U	V	W	Group	Disk
...	(km s^{-1})	(km s^{-1})	(km s^{-1})	(km s^{-1})	(km s^{-1})	(km s^{-1})	...	...
RKS1209−2646	10.35	10.45	0.05	3.61	−23.81	−15.20	Field	Thin disk
RKS1210−1126	21.75	23.73	0.05	−17.56	−36.14	6.43	Field	Thin disk
RKS1220−1953	−11.82	−11.64	0.04	−43.33	−21.28	−20.02	Field	Thin disk
RKS1222+2736	−22.24	−22.27	0.04	−13.44	−12.52	−24.40	Field	Thin disk
RKS1223+2754	−31.27	−31.40	0.05	−21.87	6.58	−33.47	Field	Thin disk
RKS1227+2701	...	−4.67	0.04	27.08	−21.46	−3.63	Field	Thin disk
RKS1228−1654	111.33	111.20	0.05	−31.58	−103.32	77.04	Field	Thick disk
RKS1228−1817	−5.01	−4.89	0.04	23.28	1.46	−15.88	Field	Thin disk
RKS1231+2013	−9.04	−8.23	0.04	8.55	−18.17	−10.93	Field	Thin disk
RKS1233−1438	5.93	6.12	0.04	−50.52	−37.97	−1.94	Field	Thin disk
RKS1241+1522	24.23	24.22	0.03	20.82	−21.44	18.93	Field	Thin disk
RKS1241+1951	−9.74	−8.03	0.04	4.46	−0.17	−8.29	Field	Thin disk
RKS1248−1543	...	−0.12	0.06	8.61	8.47	2.29	Field	Thin disk
RKS1248−2448	−13.27	−13.13	0.04	−34.23	1.43	3.41	Field	Thin disk
RKS1250−0046	4.39	4.63	0.04	9.53	−17.52	−5.29	Field	Thin disk
RKS1253+0645	−21.41	−27.63	0.04	−36.79	0.98	−21.40	Field	Thin disk
RKS1256−2455	17.12	16.97	0.04	27.24	−21.70	−15.11	Field	Thin disk
RKS1257−1427	−6.46	−6.65	0.04	−38.96	−19.98	−3.43	Field	Thin disk
RKS1259−0950	4.98	5.87	0.04	−71.05	−33.97	18.16	Field	Thick disk
RKS1300−0242	−16.06	−16.04	0.04	−91.86	−51.20	−9.85	Field	Thick disk
RKS1302−2647	−17.56	−41.98	0.04	−25.72	11.74	−37.56	...	...

Continued on next page

Table A.2 – *Continued from previous page*

RKS ID	$\gamma_{Gaia_{DR3}}$	γ_{REC}	$\sigma_{\gamma_{REC}}$	U	V	W	Group	Disk
...	(km s^{-1})	(km s^{-1})	(km s^{-1})	(km s^{-1})	(km s^{-1})	(km s^{-1})	...	...
RKS1303−0509	−7.55	9.15	0.07	−2.29	−29.56	−2.91	Field	Thin disk
RKS1306+2043	−2.80	−2.69	0.05	−9.53	4.44	−1.38	Field	Thin disk
RKS1310+0932	18.70	18.88	0.04	34.62	−6.10	10.10	Field	Thin disk
RKS1312−0215	−12.07	−12.02	0.03	−15.82	−2.88	−8.78	Field	Thin disk
RKS1316+1701	7.62	7.79	0.04	35.91	7.49	1.92	Field	Thin disk
RKS1318−1446	11.99	11.98	0.05	−19.12	−53.64	−8.08	Field	Thin disk
RKS1320+0407	−21.38	−21.24	0.03	−79.72	−15.17	0.17	Field	Thick disk
RKS1323+0243	28.30	28.47	0.04	2.61	4.90	32.04	Field	Thin disk
RKS1327−2417	−13.49	−13.62	0.04	−42.63	−26.12	−9.12	Field	Thin disk
RKS1331−0219	−53.51	−51.83	0.05	−119.98	−19.38	−10.14	Field	Thick disk
RKS1333+0835	−6.35	−6.08	0.04	−40.25	−19.04	3.99	Field	Thin disk
RKS1334−0018	...	−6.11	0.04	−23.33	−11.64	0.03	Field	Thin disk
RKS1334−0820	−22.80	−22.20	0.17	−28.27	−14.66	−18.23	Field	Thin disk
RKS1334+0440	14.40	14.59	0.04	22.98	−3.25	6.21	Field	Thin disk
RKS1335−0023	4.87	5.05	0.04	−3.51	13.01	11.59	Field	Thin disk
RKS1335+0650	7.99	8.08	0.03	−2.65	−17.90	6.22	Field	Thin disk
RKS1336+0746	−88.51	−88.60	0.04	−90.69	−97.43	−79.74	Field	Thick disk
RKS1338−0614	8.18	8.30	0.04	21.22	−11.23	−6.65	Field	Thin disk
RKS1340−0411	27.68	27.75	0.04	−24.18	−0.56	46.19	Field	Thin disk
RKS1341−0007	46.28	46.22	0.04	29.44	−61.01	20.78	Field	Thick disk
RKS1342−0141	−42.89	−42.81	0.04	−36.15	−22.30	−38.63	Field	Thin disk

Continued on next page

Table A.2 – *Continued from previous page*

RKS ID	$\gamma_{Gaia_{DR3}}$	γ_{REC}	$\sigma_{\gamma_{REC}}$	U	V	W	Group	Disk
...	(km s^{-1})	(km s^{-1})	(km s^{-1})	(km s^{-1})	(km s^{-1})	(km s^{-1})	...	...
RKS1345−0437	5.03	5.00	0.04	−8.98	−25.38	1.81	Field	Thin disk
RKS1345+0850	−13.38	−13.22	0.04	−4.49	−10.38	−13.99	Field	Thin disk
RKS1345+1747	20.75	20.40	0.05	93.04	−71.34	−5.09	Field	Thick disk
RKS1347+0618	−30.46	−30.44	0.04	−60.25	−54.97	−17.24	Field	Thick disk
RKS1349−2206	−37.95	−37.81	0.04	−101.03	−73.74	−22.15	Field	Thick disk
RKS1353+1256	−12.59	−16.49	0.04	17.22	−59.20	−27.06	Field	Thin disk
RKS1353+2748	49.28	49.30	0.04	66.39	−13.01	40.24	Field	Thick disk
RKS1359+2252	−57.48	−57.42	0.04	−28.92	−16.06	−50.36	Field	Thin disk
RKS1411−1236	3.14	3.32	0.04	−10.44	−32.49	−1.46	Field	Thin disk
RKS1412+2348	−12.10	−11.85	0.04	−5.56	−5.00	−10.07	Field	Thin disk
RKS1413−0657	−1.63	−1.80	0.05	0.72	15.19	2.19	Field	Thin disk
RKS1414−1521	1.65	NM	NM	NM	NM	NM	...	...
RKS1418−0636	...	16.33	0.05	29.22	−37.14	−12.86	Field	Thin disk
RKS1419−0509	−9.97	−9.80	0.04	−42.70	−46.15	6.66	Field	Thin disk
RKS1421+2937	−37.19	−37.05	0.04	−23.72	−52.57	−19.70	Field	Thin disk
RKS1430−0838	−22.49	−22.38	0.04	−69.94	−69.91	9.01	Field	Thick disk
RKS1432+1121	−44.17	−42.98	0.04	−29.57	22.50	−33.79	Field	Thin disk
RKS1433+0920	30.52	30.59	0.04	75.88	−42.98	−7.84	Field	Thick disk
RKS1436+0944	−9.72	−9.59	0.05	16.58	−4.43	−20.59	Field	Thin disk
RKS1437−2548	39.76	39.93	0.03	31.39	−28.95	8.57	Field	Thin disk
RKS1442+1930	−27.95	−27.91	0.04	−16.71	−38.63	−16.18	Field	Thin disk

Continued on next page

Table A.2 – *Continued from previous page*

RKS ID	$\gamma_{Gaia_{DR3}}$	γ_{REC}	$\sigma_{\gamma_{REC}}$	U	V	W	Group	Disk
...	(km s^{-1})	(km s^{-1})	(km s^{-1})	(km s^{-1})	(km s^{-1})	(km s^{-1})	...	...
RKS1444−2215	8.64	9.03	0.03	7.75	−45.48	−23.55	Field	Thin disk
RKS1444+2211	−30.19	−30.34	0.04	−22.01	4.96	−25.44	Field	Thin disk
RKS1445+1350	−9.82	−9.67	0.04	−5.05	−29.61	−4.77	Field	Thin disk
RKS1446+1629	42.88	42.76	0.04	63.59	−57.17	24.72	Field	Thick disk
RKS1446+2730	−20.66	−20.49	0.04	−1.66	−7.86	−19.66	Field	Thin disk
RKS1447+0242	12.55	12.89	0.04	−4.73	−23.24	18.62	Field	Thin disk
RKS1450+0648	−32.29	−32.15	0.04	−67.98	−68.32	10.18	Field	Thick disk
RKS1451−2418	−57.23	−57.17	0.03	−83.52	−51.60	−21.07	Field	Thick disk
RKS1453+2320	−32.92	−36.53	0.04	−69.81	−70.37	9.63	Field	Thick disk
RKS1455−2707	16.25	16.44	0.04	5.55	−17.08	11.69	Field	Thin disk
RKS1457−2124	26.75	NM	NM	NM	NM	NM	Field	Thin disk
RKS1500−1108	14.71	14.76	0.04	24.30	−33.03	−13.89	Field	Thin disk
RKS1500−2427	−26.56	−26.38	0.04	−35.48	−10.73	−3.41	Field	Thin disk
RKS1500−2905	18.03	18.10	0.06	14.37	−7.49	8.07	Field	Thin disk
RKS1501+1341	−22.96	−22.85	0.05	−25.48	−17.20	−8.27	Field	Thin disk
RKS1501+1552	−1.55	−1.55	0.04	28.53	−14.65	−15.75	Field	Thin disk
RKS1504−1835	...	−21.38	0.04	−23.26	−21.15	−15.21	Field	Thin disk
RKS1504+0538	−83.91	−84.15	0.04	−57.95	−74.99	−56.58	Field	Thick disk
RKS1507+2456	−69.17	−74.90	0.18	−105.32	−42.94	−21.99	Field	Thick disk
RKS1509+2400	−55.90	−55.77	0.04	−81.64	−47.85	−8.24	Field	Thick disk
RKS1510−1622	310.27	310.05	0.07	302.96	−512.37	−69.55	Kapteyn	Halo

Continued on next page

Table A.2 – *Continued from previous page*

RKS ID	$\gamma_{Gaia_{DR3}}$	γ_{REC}	$\sigma_{\gamma_{REC}}$	U	V	W	Group	Disk
...	(km s^{-1})	(km s^{-1})	(km s^{-1})	(km s^{-1})	(km s^{-1})	(km s^{-1})	...	...
RKS1513−0347	−111.95	−112.23	0.05	−137.49	−41.32	−21.55	Field	Thick disk
RKS1515+0047	−3.36	−3.16	0.05	10.00	1.13	−13.89	Field	Thin disk
RKS1515+0735	39.55	39.75	0.04	38.64	−19.26	22.93	Field	Thin disk
RKS1518−1837	82.52	−38.05	0.04	9.93	13.60	−81.55	Field	Thick disk
RKS1519+0146	55.29	54.37	0.08	...	...	...	Field	...
RKS1519+1155	12.45	12.31	0.04	1.27	−1.53	14.99	Field	Thin disk
RKS1519+2912	−25.57	−25.63	0.05	−59.67	11.46	−8.89	Field	Thin disk
RKS1520+1522	...	−67.57	0.04	−53.56	−72.57	−27.21	Field	Thick disk
RKS1522−0446	−19.09	−19.01	0.04	−27.55	−18.13	1.46	Field	Thin disk
RKS1522−1039	−6.15	−5.99	0.03	−0.45	−19.12	−12.70	Field	Thin disk
RKS1522+0125	−26.46	−26.39	0.03	−18.87	−64.53	−14.03	Field	Thin disk
RKS1525−2642	−133.45	−133.17	0.04	−157.33	−17.95	−8.34	Field	Thick disk
RKS1527+0235	−42.54	−42.57	0.04	−31.92	−9.82	−27.41	Field	Thin disk
RKS1527+1035	−21.88	−21.74	0.03	−20.05	−65.14	3.32	Field	Thin disk
RKS1528−0920	9.01	26.60	0.04	...	...	...	Field	Thin disk
RKS1540−1802	4.47	4.80	0.04	8.03	11.99	−0.58	Field	Thin disk
RKS1552+1052	−1.15	−0.73	0.04	3.38	−34.63	8.32	Field	Thin disk
RKS1554−2600	5.20	5.32	0.04	−6.82	−9.86	26.21	Field	Thin disk
RKS1555+1602	...	−110.98	0.04	−59.21	−81.06	−67.04	Field	Thick disk
RKS1600−0147	24.09	24.10	0.04	35.29	−0.22	−6.91	Field	Thin disk
RKS1601−2625	−20.88	−20.52	0.05	−12.32	10.87	−20.78	Field	Thin disk

Continued on next page

Table A.2 – *Continued from previous page*

RKS ID	$\gamma_{Gaia_{DR3}}$	γ_{REC}	$\sigma_{\gamma_{REC}}$	U	V	W	Group	Disk
...	(km s^{-1})	(km s^{-1})	(km s^{-1})	(km s^{-1})	(km s^{-1})	(km s^{-1})	...	...
RKS1604−1126	−32.28	−32.09	0.04	−29.90	−6.85	−12.31	Field	Thin disk
RKS1605−2027	...	16.60	0.04	...	...	...	Field	...
RKS1607−0542	21.82	22.01	0.04	38.19	−4.14	−18.19	Field	Thin disk
RKS1608−1308	−37.83	−37.65	0.03	−25.28	−34.08	−33.86	Field	Thin disk
RKS1608+1713	−21.55	−21.59	0.04	−20.47	−10.07	−7.48	Field	Thin disk
RKS1613+1331	18.16	18.30	0.04	51.21	−13.62	−17.17	Field	Thin disk
RKS1615+0721	3.80	5.15	0.04	46.92	−27.77	−35.75	Field	Thin disk
RKS1620−0416	−120.48	−120.38	0.04	−119.41	−55.75	−22.02	Field	Thick disk
RKS1621+1713	18.34	18.33	0.05	38.78	−24.26	5.52	Field	Thin disk
RKS1624−1338	7.14	7.30	0.04	5.71	−29.99	6.89	Field	Thin disk
RKS1625−2156	...	−63.04	0.05	−70.38	−49.38	−2.75	Field	Thick disk
RKS1626+1539	−52.98	−52.96	0.05	−58.44	2.06	−23.97	Field	Thin disk
RKS1627+0055	−14.58	−14.64	0.04	−14.53	−2.84	−4.00	Field	Thin disk
RKS1627+0718	−36.42	−36.18	0.04	−20.55	−39.86	−14.39	Field	Thin disk
RKS1628+1824	...	−31.44	0.04	−54.29	−11.54	12.50	Field	Thin disk
RKS1629+2346	−29.78	−32.44	0.04	16.98	−51.57	−24.45	Field	Thin disk
RKS1630−0359	−17.25	−17.19	0.03	−19.25	−17.48	4.94	Field	Thin disk
RKS1631−0718	...	NM	NM	NM	NM	NM	...	...
RKS1632−1235	−77.90	−77.64	0.04	−74.20	−60.25	−14.93	Field	Thick disk
RKS1633−0933	−14.79	−13.90	0.07	−6.22	−27.74	−12.81	AB Dor	Thin disk
RKS1647−0111	19.12	19.02	0.05	32.14	−23.02	−5.99	Field	Thin disk

Continued on next page

Table A.2 – *Continued from previous page*

RKS ID	$\gamma_{Gaia_{DR3}}$	γ_{REC}	$\sigma_{\gamma_{REC}}$	U	V	W	Group	Disk
...	(km s^{-1})	(km s^{-1})	(km s^{-1})	(km s^{-1})	(km s^{-1})	(km s^{-1})	...	...
RKS1649−2426	−29.76	−29.87	0.03	−36.72	−38.21	16.48	Field	Thin disk
RKS1650+1854	−5.69	−5.60	0.03	1.96	−12.28	−1.19	Field	Thin disk
RKS1654+1154	−66.35	−66.69	0.05	−78.64	−39.82	16.18	Field	Thick disk
RKS1659−2616	14.93	15.06	0.04	19.83	−21.15	−33.18	Field	Thin disk
RKS1701+2256	−25.06	−24.92	0.04	−26.52	−18.15	2.67	Field	Thin disk
RKS1705−0147	−14.01	−13.48	0.13	−7.18	−2.27	−17.01	Field	Thin disk
RKS1705−0503	34.12	34.12	0.04	46.65	−61.77	20.69	Field	Thick disk
RKS1706−0610	−16.27	−16.22	0.03	−13.20	−18.60	0.46	Field	Thin disk
RKS1712+1821	19.68	19.81	0.03	22.97	9.75	−1.92	Field	Thin disk
RKS1714−0824	−33.79	−33.36	0.05	−36.22	−7.57	6.64	Field	Thin disk
RKS1715−2636	0.26	0.41	0.04	0.22	−34.65	−7.00	Field	Thin disk
RKS1716−1210	5.34	5.50	0.05	8.03	8.84	−14.57	Field	Thin disk
RKS1717+2913	−44.68	−44.51	0.03	−45.28	−22.37	−11.21	Field	Thin disk
RKS1722−1457	−84.84	−84.65	0.04	−75.22	−47.39	−22.60	Field	Thick disk
RKS1725+0206	−23.87	−23.58	0.04	0.61	−52.80	−9.69	Field	Thin disk
RKS1729−2350	−32.27	−32.28	0.04	−33.10	−20.44	14.23	Field	Thin disk
RKS1733+0914	−24.27	−23.78	0.04	−16.61	−11.36	−13.82	Field	Thin disk
RKS1737−1314	−17.11	−56.61	0.00	−49.17	−29.78	−17.36	Field	Thin disk
RKS1737+2257	2.80	3.03	0.04	13.79	−15.20	10.26	Field	Thin disk
RKS1739+0333	22.08	22.67	0.03	21.48	1.64	12.64	Field	Thin disk
RKS1750−0603	−26.03	−26.08	0.04	−18.52	−21.45	−8.98	Field	Thin disk

Continued on next page

Table A.2 – *Continued from previous page*

RKS ID	$\gamma_{Gaia_{DR3}}$	γ_{REC}	$\sigma_{\gamma_{REC}}$	U	V	W	Group	Disk
...	(km s^{-1})	(km s^{-1})	(km s^{-1})	(km s^{-1})	(km s^{-1})	(km s^{-1})	...	...
RKS1752−0733	−24.41	−24.58	0.04	−40.72	15.89	49.33	Field	Thin disk
RKS1753+2119	−13.29	−13.13	0.05	−13.29	−9.52	4.73	Field	Thin disk
RKS1754−2649	−32.04	−31.28	0.46	−30.89	−11.78	−12.95	Field	Thin disk
RKS1755+0345	−8.67	−8.46	0.04	−8.32	−6.79	7.41	Field	Thin disk
RKS1755+1830	−29.80	−29.68	0.04	−16.14	−24.67	−7.89	Field	Thin disk
RKS1757−2143	...	−2.61	0.04	0.14	−17.71	−17.36	Field	Thin disk
RKS1803+2545	5.51	5.67	0.05	28.39	−13.28	−2.59	Field	Thin disk
RKS1804+0149	−11.54	−7.91	0.06	−5.66	0.01	−15.52	Field	Thin disk
RKS1809−0019	−39.41	−39.06	0.04	−34.23	−14.17	−16.56	Field	Thin disk
RKS1809−1202	−1.31	−1.18	0.04	5.89	−18.36	−20.48	Field	Thin disk
RKS1815+1829	1.77	1.59	0.04	−5.77	8.90	−2.46	Field	Thin disk
RKS1816+1354	6.31	6.40	0.05	33.09	−18.40	−23.75	Field	Thin disk
RKS1817+2640	−49.24	−49.44	0.04	−46.26	−8.90	−52.49	Field	Thick disk
RKS1818−0642	−28.54	−28.51	0.04	−24.37	−16.74	5.62	Field	Thin disk
RKS1819−0156	−14.42	−14.39	0.04	−12.67	−6.65	−1.51	Field	Thin disk
RKS1822+0142	−17.25	−16.89	0.09	−14.56	−5.74	−12.56	Field	Thin disk
RKS1829−0149	−54.90	−54.75	0.03	−42.55	−32.88	−25.29	Field	Thin disk
RKS1829−2758	−31.20	−30.99	0.04	−27.70	−58.58	−13.64	Field	Thin disk
RKS1829+0903	−42.36	−42.15	0.04	−42.49	−9.01	−24.27	Field	Thin disk
RKS1831−1854	−43.38	−43.15	0.04	−38.09	−24.64	5.27	Field	Thin disk
RKS1833−1138	−87.20	−87.44	0.04	−65.96	−71.83	21.08	Field	Thick disk

Continued on next page

Table A.2 – *Continued from previous page*

RKS ID	$\gamma_{Gaia_{DR3}}$	γ_{REC}	$\sigma_{\gamma_{REC}}$	U	V	W	Group	Disk
...	(km s^{-1})	(km s^{-1})	(km s^{-1})	(km s^{-1})	(km s^{-1})	(km s^{-1})	...	...
RKS1833−1626	−30.67	−41.50	0.06	...	...	...	Field	...
RKS1833+2218	38.33	38.38	0.04	67.41	−5.30	5.77	Field	Thin disk
RKS1847−0338	15.38	15.54	0.04	23.62	−10.40	−0.73	Field	Thin disk
RKS1848−1008	53.31	49.18	0.04	49.24	5.76	−27.35	Field	Thin disk
RKS1848+1044	−7.30	−7.10	0.04	14.43	−22.88	−25.38	Field	Thin disk
RKS1848+1726	−22.09	−22.06	0.04	17.14	−47.37	11.14	Field	Thin disk
RKS1850−2655	22.06	22.00	0.04	24.28	−3.11	5.21	Field	Thin disk
RKS1854+0051	24.49	24.70	0.05	30.06	−0.33	0.41	Field	Thin disk
RKS1854+1058	−26.56	−26.20	0.04	−27.07	−9.63	0.94	Field	Thin disk
RKS1854+2844	−34.22	−34.30	0.05	−31.47	−22.31	0.92	Field	Thin disk
RKS1855+2333	3.69	−21.60	0.40	6.44	−25.75	−27.56	Field	Thin disk
RKS1858−0030	29.92	29.95	0.04	37.88	−2.73	5.61	Field	Thin disk
RKS1858−1014	−44.75	−44.87	0.04	−43.11	−17.26	−11.74	Field	Thin disk
RKS1859+0759	−83.57	−83.39	0.04	−62.12	−52.93	−57.44	Field	Thick disk
RKS1859+1107	−28.59	−28.44	0.04	−26.78	−13.32	1.22	Field	Thin disk
RKS1901+0328	−35.19	−35.17	0.04	−33.29	−14.61	−14.18	Field	Thin disk
RKS1903−1102	37.42	37.62	0.03	48.72	−16.80	−3.73	Field	Thin disk
RKS1907+0736	9.10	8.90	0.04	69.85	−65.57	−7.11	Field	Thick disk
RKS1908−1640	−35.91	−35.98	0.04	−28.07	−22.29	13.78	Field	Thin disk
RKS1908+1627	−63.57	−63.59	0.04	−19.15	−67.95	5.19	Field	Thick disk
RKS1910+2145	−31.84	−31.80	0.06	−15.60	−27.79	−2.79	Field	Thin disk

Continued on next page

Table A.2 – *Continued from previous page*

RKS ID	$\gamma_{Gaia_{DR3}}$	γ_{REC}	$\sigma_{\gamma_{REC}}$	U	V	W	Group	Disk
...	(km s^{-1})	(km s^{-1})	(km s^{-1})	(km s^{-1})	(km s^{-1})	(km s^{-1})	...	...
RKS1914+0209	−144.20	−143.97	0.05	...	...	...	Field	...
RKS1915+1133	−58.17	−57.99	0.04	−34.24	−47.58	−30.39	Field	Thin disk
RKS1915+2453	−74.99	−69.67	0.14	−71.36	−34.90	−23.12	Field	Thick disk
RKS1923−0635	...	24.62	0.04	41.49	−19.15	5.23	Field	Thin disk
RKS1924−2203	52.39	52.58	0.05	68.25	−49.16	−10.77	Field	Thick disk
RKS1924+2525	−11.26	−10.88	0.05	4.95	−15.46	−2.10	Field	Thin disk
RKS1928+1232	−18.47	−18.44	0.04	−5.98	−19.16	4.50	Field	Thin disk
RKS1928+2854	−14.74	−14.70	0.05	−2.24	−15.17	−2.73	Field	Thin disk
RKS1929+0709	14.94	14.92	0.04	−18.45	39.25	−14.22	Field	Thin disk
RKS1930+2140	11.53	11.34	0.04	38.09	−12.06	13.20	Field	Thin disk
RKS1932−1116	−49.03	−48.87	0.04	−50.32	−14.93	−4.70	Field	Thin disk
RKS1932+0034	−48.17	−48.06	0.05	−47.63	−21.01	−11.43	Field	Thin disk
RKS1934+0434	−58.93	−58.70	0.04	−69.24	−14.29	−13.79	Field	Thick disk
RKS1936−1026	62.78	63.83	0.03	83.95	−14.05	3.76	Field	Thick disk
RKS1943+1005	−12.12	−12.39	0.04	−25.83	4.54	−12.40	Field	Thin disk
RKS1952−2356	−22.56	−22.49	0.04	−20.12	−10.21	5.29	Field	Thin disk
RKS1954−2356	...	NM	NM	NM	NM	NM	...	...
RKS1954+2013	...	−48.60	0.05	−17.50	−46.22	3.44	Field	Thin disk
RKS1957+1313	5.91	5.90	0.04	7.45	1.31	−2.61	Field	Thin disk
RKS2000+2242	−2.53	−2.15	0.05	16.17	−12.37	−11.87	Field	Thin disk
RKS2002+0319	−30.49	−30.31	0.03	−22.12	−16.49	15.45	Field	Thin disk

Continued on next page

Table A.2 – *Continued from previous page*

RKS ID	$\gamma_{Gaia_{DR3}}$	γ_{REC}	$\sigma_{\gamma_{REC}}$	U	V	W	Group	Disk
...	(km s^{-1})	(km s^{-1})	(km s^{-1})	(km s^{-1})	(km s^{-1})	(km s^{-1})	...	...
RKS2003+2005	...	−62.56	0.05	−43.49	−49.16	−16.45	Field	Thin disk
RKS2003+2320	−2.50	−2.54	0.04	85.05	−46.05	27.37	Field	Thick disk
RKS2004+2547	−7.39	−7.19	0.04	3.87	−9.62	4.86	Field	Thin disk
RKS2008+0640	−34.14	−34.02	0.04	−47.06	−4.85	−0.22	Field	Thin disk
RKS2009−0307	−7.99	−7.90	0.03	11.82	−14.71	24.04	Field	Thin disk
RKS2009−1417	−18.12	−18.03	0.04	−16.54	−17.84	−7.68	Field	Thin disk
RKS2009+1648	−30.98	−30.78	0.04	−30.53	−14.50	15.22	Field	Thin disk
RKS2010−2029	21.45	21.27	0.04	39.92	−23.92	8.61	Field	Thin disk
RKS2011+1611	−49.37	−49.26	0.04	−31.35	−26.84	61.90	Field	Thick disk
RKS2012−1253	27.46	27.57	0.05	16.57	−5.53	−42.35	Field	Thin disk
RKS2013−0052	−10.95	−10.83	0.04	−16.04	10.55	19.28	Field	Thin disk
RKS2014−0716	7.03	7.16	0.05	15.71	−18.83	−15.06	Field	Thin disk
RKS2015−2701	−54.41	−54.34	0.03	−72.33	−11.55	−18.45	Field	Thick disk
RKS2016−0204	−16.53	−16.52	0.05	−29.43	−7.47	−26.51	Field	Thin disk
RKS2030+2650	...	16.34	0.05	24.08	8.47	2.86	Field	Thin disk
RKS2035+0607	−42.41	−42.36	0.03	−39.97	−47.03	−46.39	Field	Thick disk
RKS2038+2346	−22.17	−21.99	0.04	−7.86	−22.62	−8.16	Field	Thin disk
RKS2039+1004	−53.51	−53.43	0.04	−57.81	−35.47	−17.20	Field	Thin disk
RKS2041−0529	−12.48	−12.63	0.04	−19.33	1.25	0.78	Field	Thin disk
RKS2041−2219	−61.72	−41.36	0.10	−64.56	−65.05	−52.85	Field	Thick disk
RKS2042−2116	...	19.89	0.05	18.60	2.35	−8.95	Field	Thin disk

Continued on next page

Table A.2 – *Continued from previous page*

RKS ID	$\gamma_{Gaia_{DR3}}$	γ_{REC}	$\sigma_{\gamma_{REC}}$	U	V	W	Group	Disk
...	(km s^{-1})	(km s^{-1})	(km s^{-1})	(km s^{-1})	(km s^{-1})	(km s^{-1})	...	...
RKS2042+2050	−36.74	−36.66	0.04	18.62	−52.34	−8.02	Field	Thin disk
RKS2044−2121	...	−73.70	0.04	−52.48	−56.59	26.23	Field	Thick disk
RKS2047+1051	58.57	58.35	0.04	74.09	−7.17	−77.28	Field	Thick disk
RKS2050+2923	−8.69	−8.71	0.04	0.15	−9.36	−0.51	Field	Thin disk
RKS2053−0245	14.34	14.55	0.05	94.66	−39.77	40.24	Field	Thick disk
RKS2055+1310	−40.88	−41.66	0.03	−84.70	−7.09	−10.72	Field	Thick disk
RKS2059−1042	−30.22	−28.96	0.03	−22.65	−17.43	9.20	Field	Thin disk
RKS2059+0333	5.72	5.70	0.06	28.59	−73.36	−95.07	Field	Thick disk
RKS2105−1654	...	−20.88	0.05	−11.35	−14.26	11.94	Field	Thin disk
RKS2105+0704	−66.81	−66.64	0.04	−14.94	−76.49	3.93	Field	Thick disk
RKS2107−1355	−33.16	−32.87	0.04	−41.51	−18.55	−5.20	Field	Thin disk
RKS2108−0425	−2.02	3.78	0.05	11.38	−0.97	4.36	Field	Thin disk
RKS2116+0923	−18.35	−18.08	0.04	−10.67	−19.92	−4.83	Field	Thin disk
RKS2118+0009	−27.48	−27.42	0.03	−36.95	−32.51	−25.70	Field	Thin disk
RKS2119−2621	−22.40	12.90	0.05	51.42	−25.15	22.64	Field	Thin disk
RKS2120−1951	17.80	17.87	0.04	35.82	−43.11	−15.91	Field	Thin disk
RKS2122+1052	8.53	8.40	0.04	5.62	8.85	2.07	Field	Thin disk
RKS2125+2712	−29.96	−31.05	0.04	20.65	−34.77	11.63	Field	Thin disk
RKS2126+0344	−4.95	−4.91	0.04	5.12	−8.21	2.77	Field	Thin disk
RKS2130−1230	−84.69	−84.66	0.04	−103.45	−64.59	−10.43	Field	Thick disk
RKS2131+2320	−22.84	NM	NM	NM	NM	NM	...	...

Continued on next page

Table A.2 – *Continued from previous page*

RKS ID	$\gamma_{Gaia_{DR3}}$	γ_{REC}	$\sigma_{\gamma_{REC}}$	U	V	W	Group	Disk
...	(km s^{-1})	(km s^{-1})	(km s^{-1})	(km s^{-1})	(km s^{-1})	(km s^{-1})	...	...
RKS2132−2057	32.48	32.50	0.03	52.66	−2.13	−0.72	Field	Thin disk
RKS2141+1115	−49.49	−51.35	0.04	−0.13	−49.77	23.74	Field	Thin disk
RKS2149−1140	20.93	21.11	0.04	61.91	−23.75	−1.44	Field	Thin disk
RKS2149+0543	−11.03	−10.94	0.04	−46.93	−16.15	−32.05	Field	Thin disk
RKS2152+0154	−26.61	−26.68	0.04	11.42	−36.75	10.21	Field	Thin disk
RKS2153−1249	6.38	6.13	0.05	21.87	−8.68	1.27	Field	Thin disk
RKS2153+2055	13.43	13.69	0.05	10.00	6.94	−12.75	Field	Thin disk
RKS2153+2850	19.77	19.56	0.05	13.27	16.55	−7.20	Field	Thin disk
RKS2155−2942	−12.22	−12.00	0.04	−7.83	−30.58	1.73	Field	Thin disk
RKS2210+2247	−24.46	−24.30	0.04	73.29	−9.89	57.09	Field	Thick disk
RKS2214+2751	20.06	20.04	0.05	−11.71	39.82	39.18	Field	Thin disk
RKS2224+2233	−7.09	−7.07	0.04	18.51	−5.78	7.80	Field	Thin disk
RKS2226−1911	−21.10	−20.82	0.04	−31.49	−16.05	1.65	Field	Thin disk
RKS2239+0406	23.71	24.05	0.04	−16.72	19.50	−20.44	Field	Thin disk
RKS2240−2940	−0.31	−0.02	0.05	−19.81	−7.03	−11.51	Field	Thin disk
RKS2241+1849	−15.48	−14.90	0.04	−39.31	−14.98	−0.48	Field	Thin disk
RKS2243−0624	−13.88	−13.78	0.03	22.82	−27.22	7.53	Field	Thin disk
RKS2247+1823	−24.07	−23.81	0.04	−34.26	−22.10	6.72	Field	Thin disk
RKS2248+2443	16.02	16.26	0.04	−22.19	7.75	−18.68	Field	Thin disk
RKS2251+1358	1.28	1.30	0.04	−48.11	1.40	−6.55	Field	Thin disk
RKS2252+2324	−8.28	−7.92	0.04	−4.09	−20.71	−18.32	Field	Thin disk

Continued on next page

Table A.2 – *Continued from previous page*

RKS ID	$\gamma_{Gaia_{DR3}}$	γ_{REC}	$\sigma_{\gamma_{REC}}$	U	V	W	Group	Disk
...	(km s^{-1})	(km s^{-1})	(km s^{-1})	(km s^{-1})	(km s^{-1})	(km s^{-1})	...	...
RKS2254+2331	−14.21	−14.11	0.05	−40.53	−18.46	−1.71	Hyades	Thin disk
RKS2258−1338	9.70	9.90	0.04	17.17	−35.06	−21.90	Field	Thin disk
RKS2259−1122	−36.16	−35.96	0.05	−29.06	−31.06	17.17	Field	Thin disk
RKS2300−2231	15.85	16.03	0.04	34.86	16.90	0.42	Field	Thin disk
RKS2301−0350	−44.17	−45.49	0.03	−27.82	−46.82	18.03	Field	Thin disk
RKS2307−2309	15.23	15.26	0.04	1.18	−26.03	−23.16	Field	Thin disk
RKS2308+0633	−13.35	−5.74	0.06	−15.17	−8.20	−1.28	Field	Thin disk
RKS2309−0215	−37.99	−37.81	0.03	−74.16	−59.10	−7.77	Field	Thick disk
RKS2309+1425	−2.16	−2.39	0.04	18.18	−3.76	−0.32	Field	Thin disk
RKS2310−2955	−13.14	−12.91	0.04	−54.28	−24.21	−10.29	Field	Thin disk
RKS2316+0541	−9.05	−9.21	0.04	−1.38	−9.20	4.23	Field	Thin disk
RKS2317−2323	51.66	51.45	0.05	−3.60	−24.51	−62.41	Field	Thin disk
RKS2323−1045	33.83	33.98	0.04	−40.71	18.97	−37.23	Field	Thin disk
RKS2326+0853	−44.71	−44.66	0.05	−59.46	−35.11	28.70	Field	Thick disk
RKS2327−0117	32.01	31.82	0.04	−58.13	20.56	−30.40	Field	Thin disk
RKS2328+1604	−53.66	−53.72	0.04	4.39	−50.25	24.40	Field	Thin disk
RKS2332−1650	−1.14	−0.77	0.05	−13.92	−22.43	−9.25	Field	Thin disk
RKS2335+0136	−10.44	−10.46	0.05	−31.02	−16.85	0.21	Field	Thin disk
RKS2340+2021	−18.04	−17.54	0.04	−23.63	−20.69	8.60	Field	Thin disk
RKS2342−0234	22.60	23.75	0.05	44.74	−8.30	−30.24	Field	Thin disk
RKS2345+2933	59.83	46.82	0.04	−127.78	−16.74	−58.56	Field	Thick disk

Continued on next page

Table A.2 – *Continued from previous page*

RKS ID	$\gamma_{Gaia_{DR3}}$	γ_{REC}	$\sigma_{\gamma_{REC}}$	U	V	W	Group	Disk
...	(km s^{-1})	(km s^{-1})	(km s^{-1})	(km s^{-1})	(km s^{-1})	(km s^{-1})	...	...
RKS2348−1259	−9.04	−7.92	0.05	−29.61	−14.27	0.24	Field	Thin disk
RKS2349+0310	−18.74	−18.69	0.04	−6.27	−13.80	13.57	Field	Thin disk
RKS2350−2924	10.91	11.02	0.04	−18.56	−6.72	−16.13	Field	Thin disk
RKS2353+2901	1.78	1.83	0.05	5.26	5.41	2.18	Field	Thin disk
RKS2355+2211	−11.66	−11.45	0.04	−11.14	−28.08	−11.36	Field	Thin disk
RKS2358+0949	−0.31	−0.22	0.04	−8.41	−4.62	−1.98	Field	Thin disk
RKS2359−2602	1.67	1.69	0.04	21.33	12.37	3.36	Field	Thin disk
RKS2359+0639	6.30	6.44	0.04	13.52	−5.89	−14.01	Field	Thin disk

C Table of Stellar Properties for Primary Sample

Table Key:

EW[NaID]: Equivalent width of the Na I doublet at 5889.95 Å & 5895.92 Å

EW[Hα]: Equivalent width of the Hα line at 6563 Å

EW[CaII]: Equivalent width of the Ca II infrared triplet line at 8542 Å

EW[CaII]$_{ratio}$: Equivalent width ratio (see §5.3.2) of Ca II infrared triplet line at 8542 Å

EW[Li I]: Equivalent width of the Li I line at 6707.8 Å

NM: Not Measured

In the Status column:

Y represents Youth,

A represents Active,

Y+A represents both Youth and Active,

Y-MG represents Young Moving Group,

New SB2 represents a new Spectroscopic Binary,

wd+BC represents White Dwarf Binary Candidate,

Halo represents Halo Star.

SB1 represents known single-lined Spectroscopic Binary.

SB2 represents known double-lined Spectroscopic Binary.

C-KD represents Calm K dwarfs identified by this work.

Table A.3: Spectroscopic Results and Derived Stellar Properties of 50 K Dwarfs Selected as Interesting from Our Primary Sample

RKSTAR ID	$T_{eff} \pm \sigma$ (K)	[Fe/H] $\pm\sigma$ (dex)	$\log g \pm \sigma$ (dex)	$v \sin i \pm \sigma$ (km s^{-1})	EW[Na I D] $\pm\sigma$ (Å)	EW[Hα] $\pm\sigma$ (Å)	EW[CaII] $\pm\sigma$ (Å)	EW[CaII]$_{ratio}\pm\sigma$ (Å)	EW[Li I] $\pm\sigma$ (Å)	Status
RKS0000+1659	4896 ± 46	-0.12 ± 0.10	4.52 ± 0.10	<7 ± NM	3.95 ± 0.27	0.92 ± 0.09	1.75 ± 0.26	0.53 ± 0.10	0.03 ± 0.01	C-KD
RKS0001-1656	4017 ± 380	0.05 ± 0.22	4.67 ± 0.17	<7 ± NM	4.35 ± 0.50	0.58 ± 0.08	1.14 ± 0.17	0.47 ± 0.09	0.02 ± 0.01	C-KD
RKS0007-2349	5212 ± 44	-0.50 ± 0.09	4.54 ± 0.09	<7 ± NM	2.42 ± 0.16	1.02 ± 0.12	1.63 ± 0.25	0.54 ± 0.10	0.02 ± 0.01	C-KD
RKS0012+2705	4805 ± 35	-0.02 ± 0.05	4.50 ± 0.09	<7 ± NM	4.51 ± 0.35	0.90 ± 0.09	1.56 ± 0.23	0.54 ± 0.10	0.03 ± 0.01	C-KD
RKS0012+2142	3764 ± 49	-0.18 ± 0.06	4.75 ± 0.10	<7 ± NM	5.91 ± 0.64	0.54 ± 0.07	1.55 ± 0.23	0.56 ± 0.11	0.03 ± 0.01	C-KD
RKS0016-1435	4580 ± 31	0.06 ± 0.06	4.57 ± 0.10	<7 ± NM	5.19 ± 0.44	0.82 ± 0.12	1.57 ± 0.23	0.53 ± 0.10	0.03 ± 0.01	C-KD
RKS0017+2057	3806 ± 65	-0.01 ± 0.16	4.70 ± 0.11	<7 ± NM	5.07 ± 0.50	0.54 ± 0.07	0.88 ± 0.13	0.71 ± 0.14	0.02 ± 0.00	C-KD
RKS0019-0957	3918 ± 91	-0.15 ± 0.15	4.69 ± 0.10	<7 ± NM	5.48 ± 0.52	0.65 ± 0.07	1.31 ± 0.20	0.57 ± 0.11	0.02 ± 0.01	C-KD
RKS0019-0303	3949 ± 40	-0.23 ± 0.11	4.71 ± 0.09	<7 ± NM	5.84 ± 0.65	0.62 ± 0.08	1.41 ± 0.21	0.54 ± 0.10	0.03 ± 0.01	C-KD
RKS0020+1738	3832 ± 44	0.00 ± 0.12	4.69 ± 0.11	<7 ± NM	5.48 ± 0.60	0.51 ± 0.05	1.65 ± 0.25	0.49 ± 0.09	0.05 ± 0.02	C-KD
RKS0021+2531	4628 ± 42	0.07 ± 0.07	4.56 ± 0.11	<7 ± NM	6.13 ± 0.68	0.83 ± 0.09	1.77 ± 0.27	0.50 ± 0.10	0.03 ± 0.01	C-KD
RKS0022-2701	5003 ± 46	-0.17 ± 0.06	4.56 ± 0.09	<7 ± NM	3.19 ± 0.21	0.91 ± 0.13	1.43 ± 0.21	0.54 ± 0.10	0.03 ± 0.01	CB
RKS0024-2701	4825 ± 52	-0.34 ± 0.08	4.53 ± 0.10	<7 ± NM	3.82 ± 0.25	0.91 ± 0.08	1.72 ± 0.26	0.52 ± 0.10	0.02 ± 0.01	C-KD
RKS0036-0930	3833 ± 124	-0.24 ± 0.33	4.74 ± 0.15	<7 ± NM	5.62 ± 0.55	0.58 ± 0.09	1.30 ± 0.20	0.59 ± 0.11	0.03 ± 0.01	C-KD
RKS0036+2610	4381 ± 39	0.14 ± 0.07	4.63 ± 0.09	<7 ± NM	6.16 ± 0.66	0.78 ± 0.08	1.56 ± 0.23	0.55 ± 0.10	0.03 ± 0.01	C-KD
RKS0039+2115	5204 ± 60	0.19 ± 0.07	4.44 ± 0.12	<7 ± NM	3.21 ± 0.23	1.01 ± 0.11	1.41 ± 0.21	0.62 ± 0.12	0.03 ± 0.01	C-KD
RKS0042+2239	3817 ± 41	-0.23 ± 0.06	4.78 ± 0.11	<7 ± NM	5.66 ± 0.61	0.52 ± 0.08	1.60 ± 0.24	0.52 ± 0.10	0.03 ± 0.01	C-KD
RKS0045+0147	4905 ± 50	0.21 ± 0.07	4.51 ± 0.10	<7 ± NM	4.68 ± 0.39	0.87 ± 0.13	1.38 ± 0.21	0.54 ± 0.10	0.04 ± 0.01	C-KD
RKS0048+0516	4956 ± 45	-0.30 ± 0.08	4.57 ± 0.10	<7 ± NM	3.32 ± 0.22	0.98 ± 0.11	1.64 ± 0.25	0.56 ± 0.11	0.02 ± 0.01	C-KD
RKS0051+1844	4278 ± 65	-0.13 ± 0.12	4.66 ± 0.09	<7 ± NM	6.00 ± 0.60	0.76 ± 0.11	1.48 ± 0.22	0.54 ± 0.10	0.03 ± 0.01	C-KD

Continued on next page

Table A.3 – continued from previous page

RKSTAR ID	$T_{eff} \pm \sigma$ (K)	[Fe/H] $\pm\sigma$ (dex)	$\log g \pm \sigma$ (dex)	$v \sin i \pm \sigma$ (km s^{-1})	EW[Na I D] $\pm\sigma$ (Å)	EW[Hα] $\pm\sigma$ (Å)	EW[CaII] $\pm\sigma$ (Å)	EW[CaII]$_{ratio}\pm\sigma$ (Å)	EW[Li I] $\pm\sigma$ (Å)	Status
RKS0051-2254	4134 ± 43	-0.24 ± 0.08	4.69 ± 0.10	<7 ± NM	5.90 ± 0.59	0.68 ± 0.08	1.63 ± 0.25	0.51 ± 0.10	0.03 ± 0.01	C-KD
RKS0055-2940	4409 ± 43	0.11 ± 0.09	4.63 ± 0.09	<7 ± NM	5.87 ± 0.57	0.82 ± 0.10	1.93 ± 0.29	0.49 ± 0.10	0.04 ± 0.01	C-KD
RKS0057+0551	3785 ± 61	-0.10 ± 0.14	4.72 ± 0.11	<7 ± NM	5.72 ± 0.61	0.51 ± 0.08	1.49 ± 0.22	0.52 ± 0.10	0.04 ± 0.01	C-KD
RKS0102-1025	3937 ± 34	-0.17 ± 0.06	4.71 ± 0.09	<7 ± NM	5.85 ± 0.63	0.64 ± 0.10	1.45 ± 0.22	0.53 ± 0.10	0.03 ± 0.01	C-KD
RKS0102+0503	4766 ± 58	-0.08 ± 0.08	4.50 ± 0.10	<7 ± NM	4.29 ± 0.32	0.84 ± 0.10	1.58 ± 0.24	0.52 ± 0.10	0.03 ± 0.01	C-KD
RKS0104-2536	4266 ± 48	-0.26 ± 0.11	4.66 ± 0.10	<7 ± NM	5.71 ± 0.52	0.73 ± 0.09	1.57 ± 0.24	0.53 ± 0.10	0.03 ± 0.01	C-KD
RKS0104+2607	4161 ± 59	-0.07 ± 0.11	4.67 ± 0.09	<7 ± NM	5.74 ± 0.60	0.60 ± 0.08	1.39 ± 0.21	0.49 ± 0.09	0.04 ± 0.01	Y-MG
RKS0105+1523	4670 ± 32	-0.02 ± 0.06	4.56 ± 0.10	<7 ± NM	4.79 ± 0.38	0.84 ± 0.12	1.80 ± 0.27	0.51 ± 0.10	0.03 ± 0.01	C-KD
RKS0107+2257	4569 ± 42	0.20 ± 0.06	4.54 ± 0.09	<7 ± NM	5.78 ± 0.56	0.83 ± 0.09	1.54 ± 0.23	0.54 ± 0.10	0.04 ± 0.01	C-KD
RKS0108+1714	3928 ± 57	-0.25 ± 0.07	4.70 ± 0.09	<7 ± NM	5.58 ± 0.52	0.69 ± 0.11	1.21 ± 0.18	0.71 ± 0.14	0.02 ± 0.01	C-KD
RKS0112-2514	4177 ± 50	-0.09 ± 0.15	4.67 ± 0.09	<7 ± NM	5.94 ± 0.62	0.66 ± 0.10	1.44 ± 0.22	0.53 ± 0.10	0.03 ± 0.01	C-KD
RKS0113+1629	4333 ± 47	0.13 ± 0.05	4.64 ± 0.09	<7 ± NM	6.30 ± 0.68	0.79 ± 0.07	1.99 ± 0.30	0.49 ± 0.09	0.03 ± 0.01	C-KD
RKS0116+2519	3946 ± 42	-0.16 ± 0.10	4.70 ± 0.09	<7 ± NM	5.71 ± 0.63	0.68 ± 0.10	0.99 ± 0.15	0.66 ± 0.13	0.03 ± 0.01	C-KD
RKS0117-1530	5302 ± 41	-0.48 ± 0.07	4.17 ± 0.11	<7 ± NM	2.92 ± 0.19	0.61 ± 0.07	0.92 ± 0.14	0.46 ± 0.09	0.02 ± 0.01	C-KD
RKS0118-0052	5333 ± 47	-0.08 ± 0.09	4.55 ± 0.11	<7 ± NM	2.52 ± 0.16	1.01 ± 0.08	1.77 ± 0.26	0.51 ± 0.10	0.03 ± 0.01	C-KD
RKS0121+2419	3942 ± 70	0.06 ± 0.14	4.68 ± 0.21	NM ± NM	5.77 ± 0.64	0.59 ± 0.06	1.38 ± 0.21	0.53 ± 0.10	0.05 ± 0.01	Y-MG
RKS0122-2653	4943 ± 34	0.18 ± 0.07	4.51 ± 0.10	<7 ± NM	4.18 ± 0.30	0.93 ± 0.10	1.63 ± 0.24	0.54 ± 0.10	0.03 ± 0.01	C-KD
RKS0123-1257	5467 ± 45	0.55 ± 0.06	4.51 ± 0.10	<7 ± NM	3.46 ± 0.22	0.98 ± 0.09	2.05 ± 0.31	0.50 ± 0.10	0.04 ± 0.01	C-KD
RKS0124+1829	5125 ± 43	-0.06 ± 0.06	4.54 ± 0.12	<7 ± NM	2.94 ± 0.18	0.96 ± 0.12	1.64 ± 0.25	0.52 ± 0.10	0.03 ± 0.01	C-KD
RKS0125-0103	4633 ± 66	-0.11 ± 0.13	4.58 ± 0.09	<7 ± NM	4.80 ± 0.37	0.86 ± 0.12	1.81 ± 0.27	0.51 ± 0.10	0.03 ± 0.01	C-KD
RKS0129+2143	4962 ± 57	0.00 ± 0.07	4.51 ± 0.12	<7 ± NM	4.00 ± 0.33	0.83 ± 0.12	1.49 ± 0.22	0.52 ± 0.10	0.03 ± 0.01	SB2

Continued on next page

Table A.3 – continued from previous page

RKSTAR ID	$T_{eff} \pm \sigma$ (K)	[Fe/H] $\pm\sigma$ (dex)	$\log g \pm \sigma$ (dex)	$v \sin i \pm \sigma$ (km s^{-1})	EW[Na I D] $\pm\sigma$ (Å)	EW[Hα] $\pm\sigma$ (Å)	EW[CaII] $\pm\sigma$ (Å)	EW[CaII]$_{ratio}\pm\sigma$ (Å)	EW[Li I] $\pm\sigma$ (Å)	Status
RKS0135-2046	4087 ± 47	-0.28 ± 0.08	4.70 ± 0.10	<7 ± NM	5.77 ± 0.57	0.66 ± 0.08	1.64 ± 0.25	0.51 ± 0.10	0.03 ± 0.01	C-KD
RKS0139+1515	4426 ± 38	0.05 ± 0.05	4.64 ± 0.09	<7 ± NM	5.86 ± 0.56	0.79 ± 0.12	1.69 ± 0.25	0.54 ± 0.10	0.02 ± 0.01	C-KD
RKS0142+2016	5307 ± 56	0.02 ± 0.06	4.54 ± 0.11	<7 ± NM	2.91 ± 0.19	1.02 ± 0.08	1.30 ± 0.19	0.64 ± 0.12	0.02 ± 0.01	C-KD
RKS0146+1224	4680 ± 63	-0.04 ± 0.06	4.54 ± 0.10	<7 ± NM	4.61 ± 0.36	0.77 ± 0.10	1.57 ± 0.24	0.49 ± 0.09	0.03 ± 0.01	C-KD
RKS0150+2927	5297 ± 47	-0.53 ± 0.13	4.51 ± 0.11	<7 ± NM	2.24 ± 0.15	1.04 ± 0.11	1.50 ± 0.23	0.56 ± 0.11	0.02 ± 0.01	C-KD
RKS0150+1817	3943 ± 55	0.02 ± 0.09	4.68 ± 0.11	<7 ± NM	5.84 ± 0.65	0.64 ± 0.08	1.81 ± 0.27	0.48 ± 0.09	0.03 ± 0.01	C-KD
RKS0200+2636	3913 ± 55	-0.27 ± 0.10	4.71 ± 0.09	<7 ± NM	5.59 ± 0.55	0.59 ± 0.07	0.98 ± 0.15	0.68 ± 0.13	0.01 ± 0.01	C-KD
RKS0205-2804	3768 ± 47	-0.02 ± 0.21	4.74 ± 0.12	<7 ± NM	5.40 ± 0.60	0.60 ± 0.06	1.54 ± 0.23	0.55 ± 0.11	0.05 ± 0.01	C-KD
RKS0209-1620	3936 ± 52	0.23 ± 0.07	4.67 ± 0.09	<7 ± NM	5.57 ± 0.59	0.65 ± 0.08	1.68 ± 0.25	0.52 ± 0.10	0.03 ± 0.01	C-KD
RKS0213-2111	4050 ± 34	0.26 ± 0.07	4.66 ± 0.09	<7 ± NM	5.77 ± 0.68	0.62 ± 0.08	1.59 ± 0.24	0.49 ± 0.09	0.02 ± 0.01	C-KD
RKS0214-0338	4698 ± 44	0.06 ± 0.10	4.55 ± 0.13	<7 ± NM	4.86 ± 0.40	0.83 ± 0.09	1.39 ± 0.21	0.53 ± 0.10	0.03 ± 0.01	C-KD
RKS0215-1814	4687 ± 31	-0.06 ± 0.06	4.55 ± 0.10	<7 ± NM	4.73 ± 0.39	0.79 ± 0.10	1.60 ± 0.24	0.50 ± 0.10	0.03 ± 0.01	C-KD
RKS0221-0652	4639 ± 63	0.07 ± 0.06	4.56 ± 0.11	<7 ± NM	5.25 ± 0.46	0.80 ± 0.11	1.74 ± 0.26	0.47 ± 0.09	0.04 ± 0.01	C-KD
RKS0229-1958	4376 ± 40	-0.28 ± 0.09	4.66 ± 0.10	<7 ± NM	5.25 ± 0.44	0.73 ± 0.07	1.68 ± 0.25	0.50 ± 0.10	0.03 ± 0.01	CB
RKS0231-2001	4257 ± 30	-0.02 ± 0.07	4.66 ± 0.09	<7 ± NM	6.31 ± 0.68	0.75 ± 0.11	2.02 ± 0.30	0.47 ± 0.09	0.04 ± 0.01	C-KD
RKS0231-1516	4920 ± 66	-0.11 ± 0.09	4.54 ± 0.10	<7 ± NM	3.71 ± 0.26	0.88 ± 0.10	1.66 ± 0.25	0.50 ± 0.10	0.03 ± 0.01	C-KD
RKS0236-2331	4722 ± 66	0.15 ± 0.07	4.51 ± 0.09	<7 ± NM	5.10 ± 0.44	0.79 ± 0.11	1.64 ± 0.25	0.46 ± 0.09	0.03 ± 0.01	C-KD
RKS0236-2710	4611 ± 42	-0.02 ± 0.07	4.61 ± 0.09	<7 ± NM	4.91 ± 0.39	0.85 ± 0.11	1.72 ± 0.26	0.54 ± 0.10	0.03 ± 0.01	C-KD
RKS0236+0653	4732 ± 54	-0.11 ± 0.07	4.52 ± 0.10	<7 ± NM	4.31 ± 0.31	0.91 ± 0.10	1.83 ± 0.28	0.53 ± 0.10	0.03 ± 0.01	C-KD
RKS0236-0309	5046 ± 35	0.21 ± 0.08	4.51 ± 0.09	<7 ± NM	3.83 ± 0.30	0.90 ± 0.14	1.47 ± 0.22	0.48 ± 0.09	0.04 ± 0.01	SB1
RKS0240+0111	4267 ± 64	-0.36 ± 0.08	4.68 ± 0.09	<7 ± NM	5.78 ± 0.55	0.77 ± 0.11	1.91 ± 0.29	0.50 ± 0.10	0.02 ± 0.01	C-KD

Continued on next page

Table A.3 – continued from previous page

RKSTAR ID	$T_{eff} \pm \sigma$ (K)	[Fe/H] $\pm\sigma$ (dex)	$\log g \pm \sigma$ (dex)	$v \sin i \pm \sigma$ (km s^{-1})	EW[Na I D] $\pm\sigma$ (Å)	EW[Hα] $\pm\sigma$ (Å)	EW[CaII] $\pm\sigma$ (Å)	EW[CaII]$_{ratio}\pm\sigma$ (Å)	EW[Li I] $\pm\sigma$ (Å)	Status
RKS0242+0322	4010 ± 67	-0.06 ± 0.05	4.69 ± 0.11	<7 ± NM	5.68 ± 0.58	0.47 ± 0.07	1.55 ± 0.23	0.46 ± 0.09	0.05 ± 0.01	C-KD
RKS0243+1925	4637 ± 40	0.05 ± 0.06	4.57 ± 0.11	<7 ± NM	4.98 ± 0.42	0.76 ± 0.07	1.61 ± 0.24	0.49 ± 0.09	0.03 ± 0.01	SB1
RKS0246+2538	5268 ± 40	-0.03 ± 0.06	4.55 ± 0.09	<7 ± NM	2.85 ± 0.20	1.00 ± 0.11	1.61 ± 0.24	0.55 ± 0.11	0.02 ± 0.01	C-KD
RKS0246+1146	4253 ± 59	0.03 ± 0.08	4.66 ± 0.09	<7 ± NM	6.32 ± 0.69	0.76 ± 0.08	1.89 ± 0.28	0.51 ± 0.10	0.03 ± 0.01	C-KD
RKS0246-2305	3940 ± 35	0.01 ± 0.15	4.68 ± 0.11	<7 ± NM	5.65 ± 0.65	0.58 ± 0.09	1.56 ± 0.23	0.50 ± 0.10	0.04 ± 0.01	C-KD
RKS0247+2842	3843 ± 67	-0.13 ± 0.13	4.70 ± 0.09	<7 ± NM	5.89 ± 0.64	0.57 ± 0.07	1.65 ± 0.25	0.54 ± 0.10	0.03 ± 0.01	C-KD
RKS0248-1145	3927 ± 34	0.05 ± 0.14	4.67 ± 0.10	<7 ± NM	5.71 ± 0.62	0.61 ± 0.06	1.56 ± 0.23	0.53 ± 0.10	0.03 ± 0.01	C-KD
RKS0248+2704	5335 ± 36	0.09 ± 0.05	4.53 ± 0.09	<7 ± NM	2.66 ± 0.18	0.98 ± 0.09	1.52 ± 0.23	0.50 ± 0.10	0.03 ± 0.01	SB1
RKS0250+1542	4438 ± 83	0.18 ± 0.11	4.60 ± 0.13	<7 ± NM	6.20 ± 0.68	0.76 ± 0.12	1.45 ± 0.22	0.56 ± 0.11	0.03 ± 0.01	C-KD
RKS0251+1038	4226 ± 60	-0.19 ± 0.11	4.67 ± 0.09	<7 ± NM	5.58 ± 0.54	0.62 ± 0.06	1.68 ± 0.25	0.49 ± 0.09	0.02 ± 0.01	C-KD
RKS0251-0816	4416 ± 46	0.05 ± 0.05	4.64 ± 0.09	<7 ± NM	5.38 ± 0.49	0.69 ± 0.08	1.30 ± 0.20	0.55 ± 0.11	0.04 ± 0.01	C-KD
RKS0252-1246	5165 ± 54	0.11 ± 0.08	4.51 ± 0.11	<7 ± NM	3.15 ± 0.22	0.84 ± 0.10	1.49 ± 0.22	0.45 ± 0.09	0.24 ± 0.01	Y
RKS0255+2652	5130 ± 36	0.31 ± 0.07	4.46 ± 0.10	<7 ± NM	3.48 ± 0.21	0.96 ± 0.10	1.92 ± 0.29	0.51 ± 0.10	0.03 ± 0.01	C-KD
RKS0255+2807	3937 ± 33	-0.09 ± 0.14	4.69 ± 0.10	<7 ± NM	5.83 ± 0.65	0.52 ± 0.08	1.63 ± 0.24	0.51 ± 0.10	0.03 ± 0.01	C-KD
RKS0257-2458	4868 ± 52	-0.15 ± 0.14	4.50 ± 0.11	<7 ± NM	3.91 ± 0.27	0.89 ± 0.07	1.87 ± 0.28	0.48 ± 0.09	0.03 ± 0.01	SB1
RKS0258+2646	5191 ± 30	-0.05 ± 0.05	4.53 ± 0.10	<7 ± NM	2.93 ± 0.17	0.97 ± 0.10	1.39 ± 0.21	0.62 ± 0.12	0.04 ± 0.01	CB
RKS0300+0744	5058 ± 36	0.28 ± 0.05	4.49 ± 0.09	<7 ± NM	3.73 ± 0.27	0.91 ± 0.10	1.60 ± 0.24	0.47 ± 0.09	0.03 ± 0.01	Y-MG
RKS0303+2006	4551 ± 37	0.05 ± 0.06	4.59 ± 0.10	<7 ± NM	5.27 ± 0.44	0.85 ± 0.09	2.01 ± 0.30	0.49 ± 0.09	0.03 ± 0.01	C-KD
RKS0306+0157	4000 ± 37	-0.18 ± 0.11	4.68 ± 0.10	<7 ± NM	5.80 ± 0.62	0.66 ± 0.06	1.50 ± 0.22	0.55 ± 0.11	0.03 ± 0.01	C-KD
RKS0308-2445	NM ±	NM ±	NM ± NM	NM ± NM	NM ± NM	NM ± NM	NM ± NM	NM ± NM	NM ± NM	SB2
RKS0308-2410	4181 ± 69	-0.17 ± 0.10	4.67 ± 0.09	<7 ± NM	6.03 ± 0.61	0.71 ± 0.10	1.66 ± 0.25	0.53 ± 0.10	0.02 ± 0.01	C-KD

Continued on next page

Table A.3 – continued from previous page

RKSTAR ID	$T_{eff} \pm \sigma$ (K)	[Fe/H] $\pm\sigma$ (dex)	$\log g \pm \sigma$ (dex)	$v \sin i \pm \sigma$ (km s^{-1})	EW[Na I D] $\pm\sigma$ (Å)	EW[Hα] $\pm\sigma$ (Å)	EW[CaII] $\pm\sigma$ (Å)	EW[CaII]$_{ratio}\pm\sigma$ (Å)	EW[Li I] $\pm\sigma$ (Å)	Status
RKS0310+1203	4531 ± 40	0.10 ± 0.05	4.57 ± 0.09	<7 ± NM	5.60 ± 0.52	0.78 ± 0.11	1.82 ± 0.27	0.47 ± 0.09	0.03 ± 0.01	C-KD
RKS0314-2626	4232 ± 57	-0.26 ± 0.09	4.67 ± 0.09	<7 ± NM	5.70 ± 0.54	0.67 ± 0.11	1.60 ± 0.24	0.50 ± 0.10	0.03 ± 0.01	C-KD
RKS0314+0858	5157 ± 47	0.00 ± 0.07	4.52 ± 0.13	<7 ± NM	3.25 ± 0.23	0.99 ± 0.13	1.40 ± 0.21	0.60 ± 0.11	0.02 ± 0.01	C-KD
RKS0320+0827	4520 ± 45	0.08 ± 0.07	4.60 ± 0.12	<7 ± NM	5.46 ± 0.50	0.75 ± 0.11	1.72 ± 0.26	0.47 ± 0.09	0.03 ± 0.01	Y-MG
RKS0322+2709	3947 ± 52	0.13 ± 0.12	4.68 ± 0.09	<7 ± NM	5.50 ± 0.61	0.52 ± 0.08	1.39 ± 0.21	0.50 ± 0.10	0.05 ± 0.01	Y-MG
RKS0324-0521	4469 ± 56	0.20 ± 0.09	4.59 ± 0.11	<7 ± NM	6.11 ± 0.64	0.83 ± 0.07	1.58 ± 0.24	0.54 ± 0.10	0.03 ± 0.01	C-KD
RKS0329-1140	3966 ± 55	0.13 ± 0.12	4.67 ± 0.11	<7 ± NM	5.66 ± 0.64	0.63 ± 0.08	1.35 ± 0.20	0.56 ± 0.11	0.04 ± 0.01	C-KD
RKS0329-2406	NM ±	NM ±	NM ± NM	NM ± NM	NM ± NM	NM ± NM	NM ± NM	NM ± NM	NM ± NM	A+CB
RKS0332-0927	5044 ± 51	-0.09 ± 0.07	4.55 ± 0.10	<7 ± NM	3.15 ± 0.21	0.93 ± 0.11	1.58 ± 0.24	0.51 ± 0.10	0.03 ± 0.01	C-KD
RKS0341+0336	3971 ± 59	-0.15 ± 0.07	4.70 ± 0.10	5.27 ± 1.28	5.92 ± 0.65	0.63 ± 0.05	1.63 ± 0.24	0.52 ± 0.10	0.04 ± 0.01	SB2
RKS0342-2427	4448 ± 33	0.05 ± 0.05	4.63 ± 0.09	<7 ± NM	5.86 ± 0.56	0.82 ± 0.12	1.81 ± 0.27	0.53 ± 0.10	0.03 ± 0.01	C-KD
RKS0343-1253	3890 ± 127	-0.12 ± 0.27	4.69 ± 0.10	<7 ± NM	5.49 ± 0.53	0.59 ± 0.09	0.26 ± 0.04	1.93 ± 0.37	0.01 ± 0.00	C-KD
RKS0343+1640	3899 ± 38	0.07 ± 0.14	4.66 ± 0.11	<7 ± NM	5.40 ± 0.57	0.60 ± 0.09	1.74 ± 0.26	0.48 ± 0.09	0.03 ± 0.01	C-KD
RKS0343-1906	4925 ± 57	-0.07 ± 0.08	4.51 ± 0.11	<7 ± NM	3.70 ± 0.25	0.94 ± 0.09	1.74 ± 0.26	0.52 ± 0.10	0.03 ± 0.01	C-KD
RKS0344+1155	4358 ± 33	-0.03 ± 0.06	4.65 ± 0.09	<7 ± NM	5.84 ± 0.54	0.79 ± 0.10	1.77 ± 0.27	0.53 ± 0.10	0.03 ± 0.01	C-KD
RKS0345-2751	4821 ± 38	-0.23 ± 0.06	4.50 ± 0.10	<7 ± NM	3.76 ± 0.24	0.81 ± 0.13	1.70 ± 0.25	0.48 ± 0.09	0.03 ± 0.01	C-KD
RKS0348+2519	5158 ± 110	-0.37 ± 0.14	4.55 ± 0.21	NM ± NM	2.52 ± 0.15	1.03 ± 0.11	1.22 ± 0.18	0.68 ± 0.13	0.01 ± 0.00	C-KD
RKS0348+1512	4641 ± 43	0.00 ± 0.05	4.58 ± 0.10	<7 ± NM	5.02 ± 0.41	0.86 ± 0.12	1.48 ± 0.22	0.58 ± 0.11	0.03 ± 0.01	C-KD
RKS0349-1329	3962 ± 35	-0.08 ± 0.09	4.70 ± 0.10	<7 ± NM	5.69 ± 0.61	0.61 ± 0.06	1.61 ± 0.24	0.49 ± 0.09	0.04 ± 0.01	C-KD
RKS0349+0120	NM ±	NM ±	NM ± NM	NM ± NM	NM ± NM	NM ± NM	NM ± NM	NM ± NM	NM ± NM	NM
RKS0350-2349	4351 ± 35	0.23 ± 0.07	4.63 ± 0.09	<7 ± NM	6.51 ± 0.74	0.78 ± 0.10	1.88 ± 0.28	0.50 ± 0.10	0.02 ± 0.01	C-KD

Continued on next page

Table A.3 – continued from previous page

RKSTAR ID	$T_{eff} \pm \sigma$ (K)	[Fe/H] $\pm\sigma$ (dex)	$\log g \pm \sigma$ (dex)	$v \sin i \pm \sigma$ (km s^{-1})	EW[Na I D] $\pm\sigma$ (Å)	EW[Hα] $\pm\sigma$ (Å)	EW[CaII] $\pm\sigma$ (Å)	EW[CaII]$_{ratio}\pm\sigma$ (Å)	EW[Li I] $\pm\sigma$ (Å)	Status
RKS0354-0649	4087 ± 35	0.18 ± 0.08	4.65 ± 0.09	<7 ± NM	6.13 ± 0.70	0.70 ± 0.11	1.82 ± 0.27	0.51 ± 0.10	0.04 ± 0.01	C-KD
RKS0357-0109	4503 ± 50	0.00 ± 0.07	4.62 ± 0.11	<7 ± NM	5.17 ± 0.44	0.77 ± 0.12	1.71 ± 0.26	0.48 ± 0.09	0.03 ± 0.01	C-KD
RKS0404+2634	3823 ± 48	-0.06 ± 0.05	4.70 ± 0.10	<7 ± NM	5.51 ± 0.57	0.57 ± 0.07	1.74 ± 0.26	0.49 ± 0.09	0.04 ± 0.01	C-KD
RKS0406-2051	4235 ± 37	-0.22 ± 0.07	4.68 ± 0.09	<7 ± NM	6.04 ± 0.60	0.76 ± 0.11	2.11 ± 0.32	0.47 ± 0.09	0.02 ± 0.01	C-KD
RKS0407+1413	3967 ± 42	0.15 ± 0.09	4.66 ± 0.10	<7 ± NM	5.63 ± 0.64	0.65 ± 0.08	1.62 ± 0.24	0.53 ± 0.10	0.03 ± 0.01	C-KD
RKS0408+1220	5011 ± 68	0.01 ± 0.09	4.50 ± 0.09	<7 ± NM	3.58 ± 0.24	0.96 ± 0.15	1.67 ± 0.25	0.55 ± 0.11	0.03 ± 0.01	C-KD
RKS0414+0301	4813 ± 55	0.01 ± 0.08	4.51 ± 0.10	<7 ± NM	3.92 ± 0.25	0.92 ± 0.10	2.08 ± 0.31	0.49 ± 0.09	0.04 ± 0.01	C-KD
RKS0415-0739	5117 ± 51	-0.41 ± 0.08	4.49 ± 0.19	<7 ± NM	2.75 ± 0.19	1.00 ± 0.08	1.58 ± 0.24	0.56 ± 0.11	0.02 ± 0.01	C-KD
RKS0417+2240	4344 ± 61	0.14 ± 0.07	4.64 ± 0.09	<7 ± NM	5.94 ± 0.64	0.79 ± 0.10	1.83 ± 0.27	0.48 ± 0.09	0.04 ± 0.01	C-KD
RKS0417+2033	4446 ± 64	-0.06 ± 0.13	4.64 ± 0.10	<7 ± NM	5.24 ± 0.45	0.75 ± 0.06	1.79 ± 0.27	0.47 ± 0.09	0.16 ± 0.01	Y
RKS0419-0408	4082 ± 62	0.04 ± 0.20	4.67 ± 0.11	<7 ± NM	6.08 ± 0.67	0.55 ± 0.09	2.12 ± 0.32	0.43 ± 0.08	0.02 ± 0.01	C-KD
RKS0420-1445	4368 ± 30	0.07 ± 0.09	4.64 ± 0.09	<7 ± NM	6.00 ± 0.62	0.72 ± 0.11	1.75 ± 0.26	0.47 ± 0.09	0.03 ± 0.01	Y-MG
RKS0421-1945	3971 ± 30	-0.33 ± 0.07	4.70 ± 0.09	<7 ± NM	5.91 ± 0.61	0.62 ± 0.08	1.09 ± 0.16	0.68 ± 0.13	0.03 ± 0.01	C-KD
RKS0427+2426	4952 ± 30	-0.60 ± 0.05	4.54 ± 0.09	<7 ± NM	3.05 ± 0.17	0.90 ± 0.14	1.44 ± 0.22	0.59 ± 0.11	0.02 ± 0.01	C-KD
RKS0429+2155	4089 ± 44	0.32 ± 0.13	4.65 ± 0.10	<7 ± NM	5.83 ± 0.66	0.67 ± 0.08	1.60 ± 0.24	0.51 ± 0.10	0.04 ± 0.01	C-KD
RKS0430+0058	4011 ± 49	0.03 ± 0.09	4.68 ± 0.09	<7 ± NM	5.57 ± 0.59	-0.11 ± 0.01	1.33 ± 0.20	0.39 ± 0.08	0.03 ± 0.01	A
RKS0436+2707	4671 ± 126	0.15 ± 0.09	4.55 ± 0.13	<7 ± NM	4.93 ± 0.49	-0.34 ± 0.03	0.97 ± 0.15	0.21 ± 0.04	0.04 ± 0.01	A+SB1
RKS0439+0952	NM ±	NM ±	NM ± NM	NM ± NM	NM ± NM	NM ± NM	NM ± NM	NM ± NM	NM ± NM	SB1
RKS0441+2054	4572 ± 59	-0.22 ± 0.11	4.58 ± 0.11	7.99 ± 1.27	4.63 ± 0.38	-0.17 ± 0.01	1.28 ± 0.19	0.33 ± 0.06	0.09 ± 0.01	Y+A
RKS0443+2741	4983 ± 35	-0.19 ± 0.07	4.57 ± 0.10	<7 ± NM	3.20 ± 0.18	0.96 ± 0.13	1.88 ± 0.28	0.52 ± 0.10	0.03 ± 0.01	C-KD
RKS0445+0938	3835 ± 58	0.02 ± 0.12	4.69 ± 0.11	<7 ± NM	5.18 ± 0.53	0.58 ± 0.07	1.60 ± 0.24	0.49 ± 0.10	0.03 ± 0.01	C-KD

Continued on next page

Table A.3 – continued from previous page

RKSTAR ID	$T_{eff} \pm \sigma$ (K)	[Fe/H] $\pm\sigma$ (dex)	$\log g \pm \sigma$ (dex)	$v \sin i \pm \sigma$ (km s^{-1})	EW[Na I D] $\pm\sigma$ (Å)	EW[Hα] $\pm\sigma$ (Å)	EW[CaII] $\pm\sigma$ (Å)	EW[CaII]$_{ratio}\pm\sigma$ (Å)	EW[Li I] $\pm\sigma$ (Å)	Status
RKS0448-1056	4392 ± 55	0.02 ± 0.08	4.64 ± 0.10	<7 ± NM	5.47 ± 0.49	0.72 ± 0.09	1.88 ± 0.28	0.45 ± 0.09	0.03 ± 0.01	C-KD
RKS0449-1447	3817 ± 31	-0.02 ± 0.11	4.71 ± 0.10	<7 ± NM	5.43 ± 0.58	0.53 ± 0.06	1.25 ± 0.19	0.55 ± 0.11	0.05 ± 0.01	C-KD
RKS0451+2837	4597 ± 40	0.13 ± 0.06	4.54 ± 0.10	<7 ± NM	5.79 ± 0.56	0.83 ± 0.12	1.80 ± 0.27	0.49 ± 0.09	0.04 ± 0.01	C-KD
RKS0453+2214	4758 ± 36	0.07 ± 0.05	4.55 ± 0.09	<7 ± NM	4.37 ± 0.32	0.85 ± 0.10	1.57 ± 0.24	0.51 ± 0.10	0.04 ± 0.01	C-KD
RKS0454+0722	5284 ± 32	0.12 ± 0.07	4.53 ± 0.10	<7 ± NM	2.87 ± 0.18	0.96 ± 0.09	1.75 ± 0.26	0.47 ± 0.09	0.03 ± 0.01	C-KD
RKS0455-2833	4613 ± 43	0.07 ± 0.07	4.58 ± 0.11	<7 ± NM	5.17 ± 0.45	0.86 ± 0.10	1.80 ± 0.27	0.49 ± 0.10	0.03 ± 0.01	C-KD
RKS0500-0545	4712 ± 69	0.16 ± 0.10	4.53 ± 0.12	<7 ± NM	5.10 ± 0.42	0.88 ± 0.10	2.01 ± 0.30	0.51 ± 0.10	0.04 ± 0.01	C-KD
RKS0503-2315	4143 ± 64	0.07 ± 0.07	4.67 ± 0.09	<7 ± NM	5.93 ± 0.59	0.71 ± 0.09	1.78 ± 0.27	0.51 ± 0.10	0.01 ± 0.01	CB
RKS0503+0322	3812 ± 47	-0.03 ± 0.09	4.69 ± 0.10	<7 ± NM	5.77 ± 0.62	0.52 ± 0.07	1.54 ± 0.23	0.51 ± 0.10	0.05 ± 0.01	C-KD
RKS0506-1102	4504 ± 35	0.08 ± 0.06	4.60 ± 0.10	<7 ± NM	5.45 ± 0.50	0.74 ± 0.07	1.80 ± 0.27	0.46 ± 0.09	0.03 ± 0.01	C-KD
RKS0506+1426	NM ±	NM ±	NM ± NM	NM ± NM	NM ± NM	NM ± NM	NM ± NM	NM ± NM	NM ± NM	SB1
RKS0512+1943	4413 ± 81	-0.54 ± 0.14	4.64 ± 0.11	<7 ± NM	4.60 ± 0.33	0.81 ± 0.08	1.80 ± 0.27	0.52 ± 0.10	0.02 ± 0.01	C-KD
RKS0513-2158	4120 ± 56	-0.06 ± 0.09	4.67 ± 0.09	<7 ± NM	6.00 ± 0.64	0.71 ± 0.08	1.73 ± 0.26	0.48 ± 0.09	0.04 ± 0.01	C-KD
RKS0514+1952	4523 ± 35	0.21 ± 0.05	4.56 ± 0.09	<7 ± NM	5.97 ± 0.61	0.84 ± 0.13	1.98 ± 0.30	0.48 ± 0.09	0.03 ± 0.01	C-KD
RKS0514+0039	4271 ± 55	-0.34 ± 0.13	4.67 ± 0.09	<7 ± NM	5.70 ± 0.53	0.74 ± 0.08	1.49 ± 0.22	0.59 ± 0.11	0.02 ± 0.01	C-KD
RKS0518-2123	4159 ± 52	-0.04 ± 0.14	4.67 ± 0.09	<7 ± NM	6.03 ± 0.64	0.70 ± 0.11	1.63 ± 0.24	0.51 ± 0.10	0.04 ± 0.01	C-KD
RKS0519-0304	4725 ± 62	-0.08 ± 0.09	4.53 ± 0.11	<7 ± NM	4.44 ± 0.30	0.86 ± 0.09	1.91 ± 0.29	0.50 ± 0.10	0.03 ± 0.01	C-KD
RKS0519-1550	4752 ± 37	-0.23 ± 0.14	4.51 ± 0.09	<7 ± NM	4.47 ± 0.35	0.77 ± 0.08	1.26 ± 0.19	0.55 ± 0.11	0.02 ± 0.01	C-KD
RKS0522+0236	4895 ± 68	-0.15 ± 0.11	4.52 ± 0.11	<7 ± NM	3.85 ± 0.28	0.89 ± 0.10	1.77 ± 0.27	0.51 ± 0.10	0.03 ± 0.01	C-KD
RKS0523+1719	4521 ± 44	0.00 ± 0.08	4.62 ± 0.10	<7 ± NM	4.93 ± 0.37	0.74 ± 0.12	1.86 ± 0.28	0.45 ± 0.09	0.03 ± 0.01	C-KD
RKS0528-0329	4406 ± 49	-0.03 ± 0.17	4.64 ± 0.10	<7 ± NM	5.50 ± 0.49	0.83 ± 0.08	1.70 ± 0.25	0.55 ± 0.11	0.02 ± 0.01	C-KD

Continued on next page

Table A.3 – continued from previous page

RKSTAR ID	$T_{eff} \pm \sigma$ (K)	[Fe/H] $\pm\sigma$ (dex)	$\log g \pm \sigma$ (dex)	$v \sin i \pm \sigma$ (km s^{-1})	EW[Na I D] $\pm\sigma$ (Å)	EW[Hα] $\pm\sigma$ (Å)	EW[CaII] $\pm\sigma$ (Å)	EW[CaII]$_{ratio}\pm\sigma$ (Å)	EW[Li I] $\pm\sigma$ (Å)	Status
RKS0533-2643	4787 ± 34	0.15 ± 0.06	4.51 ± 0.10	<7 ± NM	4.84 ± 0.38	0.88 ± 0.09	2.15 ± 0.32	0.45 ± 0.09	0.03 ± 0.01	C-KD
RKS0534-2328	4912 ± 32	-0.32 ± 0.05	4.57 ± 0.10	<7 ± NM	3.53 ± 0.23	0.93 ± 0.10	1.40 ± 0.21	0.60 ± 0.12	0.02 ± 0.01	C-KD
RKS0535+2805	4261 ± 65	0.18 ± 0.09	4.65 ± 0.09	<7 ± NM	6.28 ± 0.70	0.75 ± 0.09	1.98 ± 0.30	0.51 ± 0.10	0.04 ± 0.01	C-KD
RKS0536+1119	3936 ± 36	-0.09 ± 0.12	4.70 ± 0.10	<7 ± NM	5.42 ± 0.57	0.08 ± 0.01	1.51 ± 0.23	0.41 ± 0.08	0.04 ± 0.01	A
RKS0542+0240	5056 ± 32	0.03 ± 0.07	4.48 ± 0.10	<7 ± NM	3.20 ± 0.20	0.96 ± 0.13	1.98 ± 0.30	0.50 ± 0.10	0.03 ± 0.01	C-KD
RKS0544-2225	4903 ± 57	0.03 ± 0.08	4.52 ± 0.10	<7 ± NM	3.76 ± 0.27	0.89 ± 0.10	1.58 ± 0.24	0.50 ± 0.10	0.03 ± 0.01	C-KD
RKS0549-1734	5013 ± 38	0.03 ± 0.11	4.52 ± 0.10	<7 ± NM	3.69 ± 0.26	0.92 ± 0.10	1.64 ± 0.25	0.51 ± 0.10	0.03 ± 0.01	C-KD
RKS0552-2246	3992 ± 40	-0.36 ± 0.07	4.70 ± 0.09	<7 ± NM	5.51 ± 0.50	0.70 ± 0.09	1.84 ± 0.28	0.50 ± 0.10	0.02 ± 0.01	C-KD
RKS0553-0559	3965 ± 56	-0.20 ± 0.12	4.69 ± 0.11	<7 ± NM	5.94 ± 0.63	0.70 ± 0.09	1.81 ± 0.27	0.51 ± 0.10	0.03 ± 0.01	C-KD
RKS0554+0208	4718 ± 60	-0.06 ± 0.06	4.53 ± 0.13	<7 ± NM	4.58 ± 0.35	0.87 ± 0.11	1.59 ± 0.24	0.55 ± 0.10	0.03 ± 0.01	C-KD
RKS0554-1942	3871 ± 55	-0.19 ± 0.15	4.70 ± 0.09	<7 ± NM	5.76 ± 0.59	0.61 ± 0.09	1.42 ± 0.21	0.59 ± 0.11	0.03 ± 0.01	C-KD
RKS0600+2101	4213 ± 31	-0.20 ± 0.05	4.68 ± 0.09	<7 ± NM	5.79 ± 0.56	0.69 ± 0.10	1.61 ± 0.24	0.53 ± 0.10	0.03 ± 0.01	C-KD
RKS0602+0848	3915 ± 76	-0.11 ± 0.11	4.69 ± 0.11	<7 ± NM	5.34 ± 0.55	0.62 ± 0.08	1.27 ± 0.19	0.59 ± 0.11	0.02 ± 0.01	C-KD
RKS0608+2630	4540 ± 32	-0.19 ± 0.05	4.60 ± 0.10	<7 ± NM	4.93 ± 0.39	0.77 ± 0.08	1.58 ± 0.24	0.52 ± 0.10	0.03 ± 0.01	C-KD
RKS0609+0540	5046 ± 39	0.06 ± 0.05	4.47 ± 0.10	<7 ± NM	3.45 ± 0.21	0.97 ± 0.08	1.97 ± 0.30	0.50 ± 0.10	0.03 ± 0.01	C-KD
RKS0609+0009	3932 ± 49	0.24 ± 0.08	4.67 ± 0.13	<7 ± NM	5.08 ± 0.58	0.62 ± 0.07	1.60 ± 0.24	0.47 ± 0.09	0.03 ± 0.01	C-KD
RKS0612+1023	4407 ± 38	0.04 ± 0.05	4.64 ± 0.09	<7 ± NM	6.03 ± 0.61	0.80 ± 0.12	1.99 ± 0.30	0.47 ± 0.09	0.04 ± 0.01	C-KD
RKS0614+0510	5088 ± 34	-0.07 ± 0.08	4.51 ± 0.11	<7 ± NM	3.01 ± 0.17	0.96 ± 0.10	1.84 ± 0.28	0.51 ± 0.10	0.03 ± 0.01	C-KD
RKS0616+2512	4605 ± 56	0.12 ± 0.08	4.55 ± 0.12	<7 ± NM	5.74 ± 0.57	0.82 ± 0.10	1.58 ± 0.24	0.49 ± 0.09	0.03 ± 0.01	CB
RKS0617+1759	4114 ± 32	-0.21 ± 0.13	4.68 ± 0.11	<7 ± NM	6.13 ± 0.66	0.75 ± 0.11	1.86 ± 0.28	0.51 ± 0.10	0.03 ± 0.01	C-KD
RKS0618-1352	4267 ± 86	-0.21 ± 0.12	4.67 ± 0.10	<7 ± NM	5.63 ± 0.50	0.76 ± 0.09	1.90 ± 0.29	0.49 ± 0.09	0.03 ± 0.00	C-KD

Continued on next page

Table A.3 – continued from previous page

RKSTAR ID	$T_{eff} \pm \sigma$ (K)	[Fe/H] $\pm\sigma$ (dex)	$\log g \pm \sigma$ (dex)	$v \sin i \pm \sigma$ (km s^{-1})	EW[Na I D] $\pm\sigma$ (Å)	EW[Hα] $\pm\sigma$ (Å)	EW[CaII] $\pm\sigma$ (Å)	EW[CaII]$_{ratio}\pm\sigma$ (Å)	EW[Li I] $\pm\sigma$ (Å)	Status
RKS0620+0215	4220 ± 41	0.04 ± 0.10	4.66 ± 0.09	<7 ± NM	6.13 ± 0.64	0.73 ± 0.11	2.10 ± 0.31	0.47 ± 0.09	0.03 ± 0.01	C-KD
RKS0621-2212	5039 ± 34	0.00 ± 0.07	4.54 ± 0.10	<7 ± NM	3.47 ± 0.24	0.95 ± 0.10	1.47 ± 0.22	0.55 ± 0.10	0.03 ± 0.01	C-KD
RKS0626+1845	5269 ± 132	-0.41 ± 0.17	4.41 ± 0.26	<7 ± NM	3.48 ± 0.36	0.55 ± 0.06	0.82 ± 0.12	0.48 ± 0.09	0.01 ± 0.00	SB2
RKS0629+2700	4979 ± 33	-0.25 ± 0.06	4.57 ± 0.10	<7 ± NM	3.30 ± 0.22	0.96 ± 0.14	1.10 ± 0.17	0.71 ± 0.14	0.02 ± 0.00	C-KD
RKS0630-1148	4565 ± 30	0.10 ± 0.08	4.56 ± 0.11	<7 ± NM	5.39 ± 0.48	0.83 ± 0.12	2.07 ± 0.31	0.44 ± 0.08	0.03 ± 0.01	C-KD
RKS0630+2104	4929 ± 69	-0.07 ± 0.15	2.88 ± 0.15	<7 ± NM	3.03 ± 0.17	1.12 ± 0.13	1.84 ± 0.28	0.62 ± 0.12	0.03 ± 0.00	C-KD
RKS0632-2701	3674 ± 47	-0.40 ± 0.05	4.82 ± 0.09	<7 ± NM	4.94 ± 0.44	0.56 ± 0.09	1.33 ± 0.20	0.58 ± 0.11	0.04 ± 0.01	C-KD
RKS0633+0527	5206 ± 33	0.30 ± 0.05	4.42 ± 0.09	<7 ± NM	3.34 ± 0.24	1.01 ± 0.08	1.76 ± 0.26	0.54 ± 0.10	0.04 ± 0.01	C-KD
RKS0637+1945	4260 ± 61	-0.30 ± 0.06	4.68 ± 0.09	<7 ± NM	5.84 ± 0.54	0.75 ± 0.09	1.99 ± 0.30	0.50 ± 0.10	0.03 ± 0.01	C-KD
RKS0641+2357	4695 ± 65	-0.06 ± 0.06	4.54 ± 0.11	<7 ± NM	4.73 ± 0.37	0.84 ± 0.09	1.55 ± 0.23	0.55 ± 0.11	0.02 ± 0.01	C-KD
RKS0647-1815	3981 ± 37	-0.02 ± 0.13	4.69 ± 0.10	<7 ± NM	5.63 ± 0.58	0.67 ± 0.10	1.65 ± 0.25	0.50 ± 0.10	0.04 ± 0.01	C-KD
RKS0652-0510	4675 ± 48	0.04 ± 0.06	4.56 ± 0.11	<7 ± NM	4.78 ± 0.37	0.84 ± 0.10	1.78 ± 0.27	0.49 ± 0.09	0.03 ± 0.01	C-KD
RKS0652-2306	4760 ± 33	-0.17 ± 0.07	4.51 ± 0.10	<7 ± NM	3.79 ± 0.22	0.91 ± 0.12	2.00 ± 0.30	0.49 ± 0.09	0.03 ± 0.01	C-KD
RKS0658-1259	4357 ± 95	-0.30 ± 0.09	4.66 ± 0.10	<7 ± NM	4.94 ± 0.40	0.35 ± 0.05	1.25 ± 0.19	0.51 ± 0.10	0.10 ± 0.01	Y+A
RKS0700-2847	3751 ± 55	-0.12 ± 0.17	4.75 ± 0.12	<7 ± NM	4.80 ± 0.42	0.50 ± 0.06	1.49 ± 0.22	0.51 ± 0.10	0.03 ± 0.01	C-KD
RKS0701-2556	5137 ± 66	0.20 ± 0.08	4.48 ± 0.10	<7 ± NM	3.28 ± 0.24	0.96 ± 0.09	1.66 ± 0.25	0.49 ± 0.09	0.04 ± 0.01	CB
RKS0701+0655	5272 ± 45	0.07 ± 0.08	4.54 ± 0.11	<7 ± NM	2.97 ± 0.19	1.01 ± 0.10	1.54 ± 0.23	0.56 ± 0.11	0.03 ± 0.01	C-KD
RKS0702-0647	4593 ± 52	0.01 ± 0.08	4.59 ± 0.11	<7 ± NM	5.11 ± 0.42	0.85 ± 0.10	1.68 ± 0.25	0.53 ± 0.10	0.03 ± 0.01	C-KD
RKS0705+2728	3966 ± 64	-0.23 ± 0.19	4.70 ± 0.10	<7 ± NM	5.81 ± 0.62	0.59 ± 0.09	1.06 ± 0.16	0.65 ± 0.12	0.02 ± 0.01	C-KD
RKS0706+2358	4281 ± 52	-0.08 ± 0.12	4.66 ± 0.10	<7 ± NM	5.81 ± 0.57	0.72 ± 0.07	2.03 ± 0.31	0.44 ± 0.08	0.03 ± 0.01	Y-MG
RKS0707+0326	4203 ± 39	0.07 ± 0.05	4.66 ± 0.09	<7 ± NM	6.06 ± 0.65	0.74 ± 0.11	1.40 ± 0.21	0.58 ± 0.11	0.02 ± 0.01	SB1

Continued on next page

Table A.3 – continued from previous page

RKSTAR ID	$T_{eff} \pm \sigma$ (K)	[Fe/H] $\pm\sigma$ (dex)	$\log g \pm \sigma$ (dex)	$v \sin i \pm \sigma$ (km s^{-1})	EW[Na I D] $\pm\sigma$ (Å)	EW[Hα] $\pm\sigma$ (Å)	EW[CaII] $\pm\sigma$ (Å)	EW[CaII]$_{ratio}\pm\sigma$ (Å)	EW[Li I] $\pm\sigma$ (Å)	Status
RKS0708+2950	4931 ± 34	-0.33 ± 0.05	4.57 ± 0.10	<7 ± NM	3.49 ± 0.23	0.95 ± 0.14	1.77 ± 0.27	0.52 ± 0.10	0.02 ± 0.01	C-KD
RKS0708-0958	4854 ± 47	-0.17 ± 0.08	4.51 ± 0.11	<7 ± NM	3.87 ± 0.26	0.88 ± 0.10	1.67 ± 0.25	0.52 ± 0.10	0.03 ± 0.01	C-KD
RKS0710-1425	4003 ± 49	-0.18 ± 0.10	4.69 ± 0.10	<7 ± NM	5.98 ± 0.63	0.66 ± 0.08	1.77 ± 0.27	0.50 ± 0.10	0.05 ± 0.01	C-KD
RKS0712-2453	3990 ± 47	0.25 ± 0.16	4.67 ± 0.11	<7 ± NM	5.72 ± 0.63	0.70 ± 0.07	1.70 ± 0.25	0.54 ± 0.10	0.02 ± 0.01	C-KD
RKS0713+2500	5046 ± 40	-0.54 ± 0.05	4.54 ± 0.09	<7 ± NM	2.67 ± 0.16	0.98 ± 0.11	1.21 ± 0.18	0.67 ± 0.13	0.02 ± 0.01	C-KD
RKS0716-0339	4921 ± 40	0.19 ± 0.08	4.51 ± 0.10	<7 ± NM	4.63 ± 0.37	0.91 ± 0.14	1.90 ± 0.29	0.50 ± 0.10	0.03 ± 0.01	C-KD
RKS0723-2001	4310 ± 35	0.11 ± 0.06	4.65 ± 0.09	<7 ± NM	6.34 ± 0.68	0.78 ± 0.10	1.90 ± 0.28	0.51 ± 0.10	0.02 ± 0.01	C-KD
RKS0723+2024	4285 ± 329	-0.20 ± 0.25	4.65 ± 0.14	7.99 ± 1.56	4.50 ± 0.39	-0.50 ± 0.07	1.00 ± 0.15	0.34 ± 0.07	0.15 ± 0.01	Y+A
RKS0723+1257	4898 ± 53	0.14 ± 0.11	4.51 ± 0.10	<7 ± NM	4.31 ± 0.31	0.92 ± 0.14	1.64 ± 0.25	0.56 ± 0.11	0.04 ± 0.01	C-KD
RKS0724-1753	3954 ± 33	-0.06 ± 0.06	4.70 ± 0.09	<7 ± NM	5.88 ± 0.65	0.49 ± 0.05	1.76 ± 0.26	0.46 ± 0.09	0.04 ± 0.01	C-KD
RKS0725-1041	4418 ± 126	0.02 ± 0.06	4.62 ± 0.11	<7 ± NM	4.70 ± 0.51	0.47 ± 0.06	1.25 ± 0.19	0.50 ± 0.10	0.05 ± 0.01	C-KD
RKS0726-1546	4541 ± 32	-0.13 ± 0.14	4.60 ± 0.11	<7 ± NM	5.05 ± 0.42	0.76 ± 0.07	1.63 ± 0.24	0.51 ± 0.10	0.02 ± 0.01	CB
RKS0730-0340	3951 ± 38	0.04 ± 0.06	4.69 ± 0.09	<7 ± NM	5.29 ± 0.55	0.57 ± 0.06	1.78 ± 0.27	0.46 ± 0.09	0.03 ± 0.01	C-KD
RKS0731+1436	NM ±	NM ±	NM ± NM	NM ± NM	NM ± NM	NM ± NM	NM ± NM	NM ± NM	NM ± NM	NM
RKS0732+1719	3909 ± 36	-0.01 ± 0.10	4.67 ± 0.11	<7 ± NM	5.50 ± 0.57	0.50 ± 0.07	1.58 ± 0.24	0.51 ± 0.10	0.04 ± 0.01	CB
RKS0734-0653	5056 ± 42	-0.19 ± 0.11	4.57 ± 0.10	<7 ± NM	2.79 ± 0.17	0.83 ± 0.11	1.53 ± 0.23	0.48 ± 0.09	0.09 ± 0.01	Y
RKS0739-0335	4907 ± 42	0.04 ± 0.07	4.53 ± 0.10	<7 ± NM	3.84 ± 0.28	0.88 ± 0.08	1.62 ± 0.24	0.50 ± 0.10	0.03 ± 0.01	C-KD
RKS0741-2921	4003 ± 36	-0.11 ± 0.12	4.68 ± 0.10	<7 ± NM	5.93 ± 0.65	0.62 ± 0.08	1.97 ± 0.30	0.47 ± 0.09	0.05 ± 0.01	C-KD
RKS0745+0208	4075 ± 32	0.27 ± 0.09	4.66 ± 0.10	<7 ± NM	5.93 ± 0.68	0.67 ± 0.09	1.45 ± 0.22	0.54 ± 0.10	0.03 ± 0.01	C-KD
RKS0752+2555	4646 ± 48	-0.06 ± 0.06	4.59 ± 0.10	<7 ± NM	4.79 ± 0.37	0.82 ± 0.10	1.60 ± 0.24	0.54 ± 0.10	0.03 ± 0.01	C-KD
RKS0754-2518	3916 ± 40	-0.18 ± 0.14	4.69 ± 0.10	<7 ± NM	5.43 ± 0.55	0.57 ± 0.07	1.80 ± 0.27	0.49 ± 0.09	0.04 ± 0.01	C-KD

Continued on next page

Table A.3 – continued from previous page

RKSTAR ID	$T_{eff} \pm \sigma$ (K)	[Fe/H] $\pm\sigma$ (dex)	$\log g \pm \sigma$ (dex)	$v \sin i \pm \sigma$ (km s^{-1})	EW[Na I D] $\pm\sigma$ (Å)	EW[Hα] $\pm\sigma$ (Å)	EW[CaII] $\pm\sigma$ (Å)	EW[CaII]$_{ratio}\pm\sigma$ (Å)	EW[Li I] $\pm\sigma$ (Å)	Status
RKS0754-0124	NM ±	NM ±	NM ± NM	NM ± NM	NM ± NM	NM ± NM	NM ± NM	NM ± NM	NM ± NM	SB1
RKS0754+1914	4916 ± 66	0.18 ± 0.10	4.51 ± 0.11	<7 ± NM	4.18 ± 0.31	0.91 ± 0.10	1.85 ± 0.28	0.53 ± 0.10	0.04 ± 0.01	SB1
RKS0757-0048	4703 ± 59	-0.15 ± 0.13	4.55 ± 0.11	<7 ± NM	4.48 ± 0.32	0.88 ± 0.09	1.87 ± 0.28	0.52 ± 0.10	0.03 ± 0.01	C-KD
RKS0758-2537	4656 ± 84	-0.33 ± 0.14	4.56 ± 0.13	<7 ± NM	4.62 ± 0.35	0.78 ± 0.11	1.54 ± 0.23	0.52 ± 0.10	0.03 ± 0.01	C-KD
RKS0758-1501	4574 ± 53	0.20 ± 0.06	4.54 ± 0.10	<7 ± NM	5.97 ± 0.59	0.83 ± 0.12	1.99 ± 0.30	0.50 ± 0.10	0.04 ± 0.01	C-KD
RKS0759+2050	5285 ± 40	-0.12 ± 0.06	4.53 ± 0.10	<7 ± NM	2.74 ± 0.18	1.00 ± 0.09	1.64 ± 0.25	0.55 ± 0.10	0.03 ± 0.01	SB1
RKS0808+2106	4043 ± 58	-0.14 ± 0.10	4.69 ± 0.10	<7 ± NM	5.89 ± 0.62	0.63 ± 0.07	1.72 ± 0.26	0.48 ± 0.09	0.03 ± 0.01	C-KD
RKS0813-1355	3823 ± 70	-0.04 ± 0.14	4.69 ± 0.21	NM ± NM	5.82 ± 0.62	0.56 ± 0.06	1.52 ± 0.23	0.53 ± 0.10	0.03 ± 0.01	CB
RKS0814+1301	4384 ± 54	0.02 ± 0.09	4.64 ± 0.10	<7 ± NM	5.57 ± 0.51	0.79 ± 0.10	1.87 ± 0.28	0.48 ± 0.09	0.03 ± 0.01	C-KD
RKS0815-2600	4120 ± 41	0.11 ± 0.11	4.67 ± 0.10	<7 ± NM	6.44 ± 0.77	0.73 ± 0.08	1.97 ± 0.30	0.48 ± 0.09	0.02 ± 0.01	C-KD
RKS0817+1717	4481 ± 57	-0.03 ± 0.09	4.64 ± 0.10	<7 ± NM	5.30 ± 0.46	0.73 ± 0.08	1.63 ± 0.25	0.47 ± 0.09	0.03 ± 0.01	C-KD
RKS0819+0120	4965 ± 50	-0.28 ± 0.09	4.56 ± 0.09	<7 ± NM	2.94 ± 0.15	0.78 ± 0.11	1.68 ± 0.25	0.46 ± 0.09	0.15 ± 0.01	Y
RKS0820+1404	4146 ± 59	-0.09 ± 0.06	4.67 ± 0.09	<7 ± NM	5.92 ± 0.61	0.66 ± 0.10	1.52 ± 0.23	0.53 ± 0.10	0.04 ± 0.01	Y-MG
RKS0823+2150	4343 ± 64	-0.19 ± 0.07	4.66 ± 0.09	<7 ± NM	5.62 ± 0.52	0.72 ± 0.08	1.77 ± 0.27	0.48 ± 0.09	0.03 ± 0.01	C-KD
RKS0827+2855	4515 ± 52	-0.03 ± 0.11	4.61 ± 0.12	<7 ± NM	5.28 ± 0.43	0.81 ± 0.10	1.69 ± 0.25	0.49 ± 0.09	0.03 ± 0.01	C-KD
RKS0832-2323	4132 ± 62	-0.03 ± 0.10	4.67 ± 0.09	<7 ± NM	6.00 ± 0.64	0.61 ± 0.08	1.51 ± 0.23	0.50 ± 0.10	0.04 ± 0.01	C-KD
RKS0838-0415	3714 ± 46	-0.32 ± 0.11	4.78 ± 0.10	<7 ± NM	5.33 ± 0.53	0.58 ± 0.08	1.50 ± 0.22	0.56 ± 0.11	0.04 ± 0.01	C-KD
RKS0838-1315	4529 ± 60	-0.06 ± 0.12	4.62 ± 0.10	<7 ± NM	5.05 ± 0.42	0.73 ± 0.10	1.60 ± 0.24	0.49 ± 0.09	0.03 ± 0.01	C-KD
RKS0839+0657	NM ± NM	NM ± NM	NM ± NM	NM ± NM	NM ± NM	NM ± NM	NM ± NM	NM ± NM	NM ± NM	SB2
RKS0839+1131	5056 ± 59	-0.55 ± 0.07	4.54 ± 0.09	<7 ± NM	2.86 ± 0.17	0.98 ± 0.11	1.50 ± 0.23	0.58 ± 0.11	0.02 ± 0.01	C-KD
RKS0840-0628	3931 ± 35	-0.08 ± 0.09	4.70 ± 0.09	<7 ± NM	5.57 ± 0.57	0.59 ± 0.06	1.31 ± 0.20	0.56 ± 0.11	0.03 ± 0.01	CB

Continued on next page

Table A.3 – continued from previous page

RKSTAR ID	$T_{eff} \pm \sigma$ (K)	[Fe/H] $\pm\sigma$ (dex)	$\log g \pm \sigma$ (dex)	$v \sin i \pm \sigma$ (km s^{-1})	EW[Na I D] $\pm\sigma$ (Å)	EW[Hα] $\pm\sigma$ (Å)	EW[CaII] $\pm\sigma$ (Å)	EW[CaII]$_{ratio}\pm\sigma$ (Å)	EW[Li I] $\pm\sigma$ (Å)	Status
RKS0848+0628	3987 ± 35	-0.33 ± 0.06	4.71 ± 0.10	<7 ± NM	5.64 ± 0.55	0.63 ± 0.09	1.67 ± 0.25	0.51 ± 0.10	0.02 ± 0.01	C-KD
RKS0850+0751	3943 ± 57	-0.25 ± 0.14	4.70 ± 0.10	<7 ± NM	5.64 ± 0.58	0.34 ± 0.03	1.44 ± 0.22	0.49 ± 0.09	0.03 ± 0.01	A
RKS0852+2819	5262 ± 59	0.42 ± 0.08	4.40 ± 0.16	<7 ± NM	3.54 ± 0.27	1.02 ± 0.12	1.85 ± 0.28	0.52 ± 0.10	0.03 ± 0.01	C-KD
RKS0855+0132	3933 ± 41	0.12 ± 0.13	4.67 ± 0.11	<7 ± NM	5.73 ± 0.64	0.66 ± 0.09	1.74 ± 0.26	0.52 ± 0.10	0.04 ± 0.01	C-KD
RKS0900+2127	NM ±	NM ±	NM ± NM	NM ± NM	NM ± NM	NM ± NM	NM ± NM	NM ± NM	NM ± NM	SB1
RKS0901+1515	4229 ± 63	-0.27 ± 0.08	4.67 ± 0.09	<7 ± NM	5.90 ± 0.60	0.70 ± 0.11	1.50 ± 0.23	0.55 ± 0.11	0.02 ± 0.01	C-KD
RKS0904-1554	4895 ± 40	0.08 ± 0.07	4.50 ± 0.09	<7 ± NM	3.97 ± 0.30	0.77 ± 0.09	1.58 ± 0.24	0.46 ± 0.09	0.09 ± 0.01	Y
RKS0905+2517	3968 ± 45	-0.34 ± 0.09	4.70 ± 0.09	<7 ± NM	5.38 ± 0.48	0.69 ± 0.10	1.21 ± 0.18	0.66 ± 0.13	0.03 ± 0.01	C-KD
RKS0907+2252	5257 ± 43	0.13 ± 0.05	4.49 ± 0.11	<7 ± NM	2.92 ± 0.20	0.74 ± 0.08	1.38 ± 0.21	0.47 ± 0.09	0.15 ± 0.01	Y+SB1
RKS0909+0512	4827 ± 108	0.17 ± 0.12	4.52 ± 0.12	<7 ± NM	5.32 ± 0.47	0.90 ± 0.10	1.52 ± 0.23	0.58 ± 0.11	0.04 ± 0.01	C-KD
RKS0914+0426	4787 ± 49	-0.01 ± 0.08	4.52 ± 0.12	<7 ± NM	4.31 ± 0.32	0.75 ± 0.07	1.61 ± 0.24	0.48 ± 0.09	0.03 ± 0.01	CB
RKS0917-0323	NM ± NM	NM ± NM	NM ± NM	NM ± NM	NM ± NM	NM ± NM	NM ± NM	NM ± NM	NM ± NM	New SB2
RKS0918+2718	4079 ± 53	0.18 ± 0.12	4.66 ± 0.10	<7 ± NM	6.16 ± 0.72	0.65 ± 0.09	1.74 ± 0.26	0.47 ± 0.09	0.03 ± 0.01	C-KD
RKS0919+0053	5154 ± 34	0.02 ± 0.07	4.50 ± 0.09	<7 ± NM	3.14 ± 0.20	0.97 ± 0.09	2.01 ± 0.30	0.50 ± 0.10	0.03 ± 0.01	C-KD
RKS0920-0545	4429 ± 41	0.05 ± 0.05	4.64 ± 0.09	<7 ± NM	5.92 ± 0.58	0.82 ± 0.09	1.91 ± 0.29	0.51 ± 0.10	0.03 ± 0.01	C-KD
RKS0929-0522	4133 ± 32	0.00 ± 0.09	4.67 ± 0.09	<7 ± NM	6.23 ± 0.70	0.67 ± 0.09	1.66 ± 0.25	0.53 ± 0.10	0.03 ± 0.01	C-KD
RKS0929+0539	4842 ± 55	0.03 ± 0.11	4.51 ± 0.11	<7 ± NM	3.95 ± 0.25	0.85 ± 0.11	1.73 ± 0.26	0.48 ± 0.09	0.03 ± 0.01	C-KD
RKS0932+2909	3773 ± 64	-0.02 ± 0.06	4.71 ± 0.11	<7 ± NM	5.14 ± 0.53	0.51 ± 0.07	0.90 ± 0.14	0.64 ± 0.12	0.03 ± 0.01	C-KD
RKS0932-1111	6177 ± 154	0.01 ± 0.13	4.31 ± 0.17	27.44 ± 3.9	2.90 ± 0.20	-0.09 ± 0.01	0.96 ± 0.14	0.29 ± 0.06	0.24 ± 0.02	Y+A
RKS0937+2241	4200 ± 41	0.00 ± 0.05	4.66 ± 0.09	<7 ± NM	6.28 ± 0.70	0.76 ± 0.10	1.26 ± 0.19	0.64 ± 0.12	0.02 ± 0.01	C-KD
RKS0937+2231	4303 ± 41	0.01 ± 0.06	4.65 ± 0.09	<7 ± NM	5.71 ± 0.55	0.72 ± 0.10	1.72 ± 0.26	0.47 ± 0.09	0.03 ± 0.01	C-KD

Continued on next page

Table A.3 – continued from previous page

RKSTAR ID	$T_{eff} \pm \sigma$ (K)	[Fe/H] $\pm\sigma$ (dex)	$\log g \pm \sigma$ (dex)	$v \sin i \pm \sigma$ (km s^{-1})	EW[Na I D] $\pm\sigma$ (Å)	EW[Hα] $\pm\sigma$ (Å)	EW[CaII] $\pm\sigma$ (Å)	EW[CaII]$_{ratio}\pm\sigma$ (Å)	EW[Li I] $\pm\sigma$ (Å)	Status
RKS0938+0240	3601 ± 52	-0.52 ± 0.09	4.85 ± 0.12	<7 ± NM	4.93 ± 0.40	0.47 ± 0.07	1.93 ± 0.29	0.50 ± 0.10	0.03 ± 0.02	C-KD
RKS0947+0134	3837 ± 74	-0.12 ± 0.14	4.70 ± 0.10	<7 ± NM	5.61 ± 0.58	0.56 ± 0.08	1.56 ± 0.23	0.49 ± 0.09	0.03 ± 0.01	C-KD
RKS0952+0313	NM ±	NM ±	NM ± NM	NM ± NM	NM ± NM	NM ± NM	NM ± NM	NM ± NM	NM ± NM	NM
RKS0952+0307	3950 ± 35	-0.14 ± 0.06	4.71 ± 0.09	<7 ± NM	5.73 ± 0.62	0.61 ± 0.08	1.43 ± 0.22	0.53 ± 0.10	0.04 ± 0.01	C-KD
RKS0959-0911	4537 ± 32	-0.36 ± 0.11	4.61 ± 0.10	<7 ± NM	4.94 ± 0.39	0.75 ± 0.09	1.65 ± 0.25	0.50 ± 0.10	0.03 ± 0.01	CB
RKS1000+2433	NM ±	NM ±	NM ± NM	NM ± NM	NM ± NM	NM ± NM	NM ± NM	NM ± NM	NM ± NM	SB2
RKS1001-1525	4845 ± 52	0.13 ± 0.07	4.50 ± 0.10	<7 ± NM	4.43 ± 0.34	0.79 ± 0.07	1.63 ± 0.25	0.48 ± 0.09	0.03 ± 0.01	C-KD
RKS1004-1143	5030 ± 51	-0.13 ± 0.08	4.57 ± 0.10	<7 ± NM	3.28 ± 0.24	0.86 ± 0.10	1.36 ± 0.20	0.52 ± 0.10	0.03 ± 0.01	C-KD
RKS1005+2629	4741 ± 60	0.09 ± 0.13	4.54 ± 0.14	<7 ± NM	4.73 ± 0.38	0.83 ± 0.09	1.74 ± 0.26	0.50 ± 0.10	0.03 ± 0.01	C-KD
RKS1006+0257	4019 ± 44	-0.03 ± 0.12	4.67 ± 0.10	<7 ± NM	5.98 ± 0.68	0.63 ± 0.07	1.45 ± 0.22	0.54 ± 0.10	0.03 ± 0.01	C-KD
RKS1008+1159	5097 ± 45	-0.15 ± 0.09	4.56 ± 0.11	<7 ± NM	2.95 ± 0.20	0.85 ± 0.09	1.50 ± 0.22	0.49 ± 0.09	0.04 ± 0.01	C-KD
RKS1011-2425	3854 ± 47	-0.02 ± 0.10	4.68 ± 0.10	<7 ± NM	5.75 ± 0.62	0.58 ± 0.09	1.15 ± 0.17	0.61 ± 0.12	0.03 ± 0.01	C-KD
RKS1020-0128	4520 ± 33	0.02 ± 0.07	4.62 ± 0.10	<7 ± NM	5.45 ± 0.48	0.84 ± 0.12	1.86 ± 0.28	0.53 ± 0.10	0.03 ± 0.01	C-KD
RKS1024-1024	4246 ± 44	-0.26 ± 0.10	4.68 ± 0.09	<7 ± NM	6.03 ± 0.59	0.74 ± 0.12	1.70 ± 0.25	0.55 ± 0.11	0.03 ± 0.01	C-KD
RKS1026-0631	4946 ± 33	-0.56 ± 0.06	4.55 ± 0.09	<7 ± NM	3.38 ± 0.18	0.86 ± 0.09	1.72 ± 0.26	0.53 ± 0.10	0.02 ± 0.01	CB
RKS1026+2638	5261 ± 36	-0.10 ± 0.07	4.57 ± 0.09	<7 ± NM	2.72 ± 0.19	1.00 ± 0.08	1.48 ± 0.22	0.55 ± 0.11	0.03 ± 0.01	SB1
RKS1028+0644	4930 ± 60	-0.16 ± 0.13	4.54 ± 0.09	<7 ± NM	3.69 ± 0.24	0.94 ± 0.09	1.90 ± 0.29	0.51 ± 0.10	0.03 ± 0.01	C-KD
RKS1030-2114	4409 ± 59	-0.11 ± 0.08	4.65 ± 0.10	<7 ± NM	5.46 ± 0.48	0.76 ± 0.09	1.61 ± 0.24	0.51 ± 0.10	0.03 ± 0.01	C-KD
RKS1032+0830	3888 ± 110	-0.22 ± 0.18	4.70 ± 0.09	<7 ± NM	5.80 ± 0.60	0.57 ± 0.08	1.07 ± 0.16	0.64 ± 0.12	0.02 ± 0.01	C-KD
RKS1036-1350	5039 ± 33	0.01 ± 0.06	4.54 ± 0.09	<7 ± NM	3.42 ± 0.25	0.94 ± 0.10	1.64 ± 0.25	0.50 ± 0.10	0.03 ± 0.01	C-KD
RKS1043-2903	5269 ± 33	0.14 ± 0.07	4.51 ± 0.10	<7 ± NM	2.96 ± 0.21	0.82 ± 0.08	1.35 ± 0.20	0.46 ± 0.09	0.18 ± 0.01	Y

Continued on next page

Table A.3 – continued from previous page

RKSTAR ID	$T_{eff} \pm \sigma$ (K)	[Fe/H] $\pm\sigma$ (dex)	$\log g \pm \sigma$ (dex)	$v \sin i \pm \sigma$ (km s^{-1})	EW[Na I D] $\pm\sigma$ (Å)	EW[Hα] $\pm\sigma$ (Å)	EW[CaII] $\pm\sigma$ (Å)	EW[CaII]$_{ratio}\pm\sigma$ (Å)	EW[Li I] $\pm\sigma$ (Å)	Status
RKS1046-2435	4408 ± 61	-0.56 ± 0.10	4.67 ± 0.09	<7 ± NM	5.30 ± 0.46	0.71 ± 0.08	1.38 ± 0.21	0.57 ± 0.11	0.02 ± 0.01	C-KD
RKS1053-1422	4750 ± 50	-0.16 ± 0.13	4.52 ± 0.11	<7 ± NM	4.14 ± 0.27	0.90 ± 0.11	1.95 ± 0.29	0.51 ± 0.10	0.03 ± 0.01	C-KD
RKS1054-0432	3977 ± 40	-0.09 ± 0.07	4.69 ± 0.11	<7 ± NM	5.86 ± 0.66	0.56 ± 0.06	1.20 ± 0.18	0.57 ± 0.11	0.05 ± 0.01	C-KD
RKS1056+0723	5014 ± 67	0.06 ± 0.10	4.53 ± 0.11	<7 ± NM	3.41 ± 0.24	0.91 ± 0.08	1.57 ± 0.24	0.48 ± 0.09	0.03 ± 0.01	C-KD
RKS1057+2856	4674 ± 50	0.07 ± 0.06	4.55 ± 0.11	<7 ± NM	5.23 ± 0.45	0.84 ± 0.10	1.41 ± 0.21	0.57 ± 0.11	0.03 ± 0.01	C-KD
RKS1059+2526	4724 ± 38	-0.01 ± 0.06	4.56 ± 0.09	<7 ± NM	4.44 ± 0.34	0.78 ± 0.10	1.67 ± 0.25	0.48 ± 0.09	0.03 ± 0.01	C-KD
RKS1102-0919	4902 ± 38	-0.07 ± 0.06	4.52 ± 0.10	<7 ± NM	3.76 ± 0.26	0.80 ± 0.08	1.46 ± 0.22	0.50 ± 0.10	0.03 ± 0.01	C-KD
RKS1108-2816	4221 ± 59	-0.18 ± 0.12	4.67 ± 0.09	<7 ± NM	6.00 ± 0.61	0.73 ± 0.08	1.70 ± 0.25	0.53 ± 0.10	0.03 ± 0.01	CB
RKS1108+1546	4290 ± 51	-0.55 ± 0.08	4.68 ± 0.09	<7 ± NM	5.00 ± 0.36	0.77 ± 0.08	1.86 ± 0.28	0.52 ± 0.10	0.02 ± 0.01	C-KD
RKS1111-1057	4360 ± 160	-0.54 ± 0.08	4.67 ± 0.11	<7 ± NM	4.61 ± 0.32	0.76 ± 0.11	1.74 ± 0.26	0.53 ± 0.10	0.02 ± 0.01	C-KD
RKS1111-1459	4302 ± 65	-0.35 ± 0.14	4.67 ± 0.10	<7 ± NM	5.54 ± 0.50	0.74 ± 0.11	1.66 ± 0.25	0.53 ± 0.10	0.02 ± 0.01	CB
RKS1113+0428	4389 ± 44	0.00 ± 0.09	4.64 ± 0.09	<7 ± NM	5.65 ± 0.53	0.72 ± 0.07	1.73 ± 0.26	0.48 ± 0.09	0.03 ± 0.01	C-KD
RKS1114+2542	5156 ± 45	-0.39 ± 0.07	4.56 ± 0.09	<7 ± NM	2.80 ± 0.19	1.01 ± 0.11	1.56 ± 0.23	0.56 ± 0.11	0.03 ± 0.01	C-KD
RKS1114-2306	NM ±	NM ±	NM ± NM	NM ± NM	NM ± NM	NM ± NM	NM ± NM	NM ± NM	NM ± NM	NM
RKS1115-1808	4013 ± 48	-0.14 ± 0.17	4.68 ± 0.09	<7 ± NM	6.06 ± 0.67	0.67 ± 0.09	1.49 ± 0.22	0.55 ± 0.10	0.02 ± 0.01	C-KD
RKS1116-1441	3899 ± 67	-0.21 ± 0.15	4.70 ± 0.10	<7 ± NM	5.78 ± 0.61	0.58 ± 0.09	1.63 ± 0.24	0.52 ± 0.10	0.04 ± 0.01	C-KD
RKS1117-2748	3908 ± 42	-0.20 ± 0.11	4.70 ± 0.09	<7 ± NM	5.66 ± 0.61	0.54 ± 0.07	1.42 ± 0.21	0.53 ± 0.10	0.03 ± 0.01	C-KD
RKS1117-0158	4376 ± 50	0.10 ± 0.06	4.64 ± 0.09	<7 ± NM	6.09 ± 0.60	0.82 ± 0.08	1.86 ± 0.28	0.53 ± 0.10	0.02 ± 0.01	C-KD
RKS1121-2027	4138 ± 61	-0.13 ± 0.12	4.68 ± 0.10	<7 ± NM	5.77 ± 0.59	0.32 ± 0.04	1.47 ± 0.22	0.45 ± 0.09	0.03 ± 0.01	A+CB
RKS1121+1811	5299 ± 98	0.41 ± 0.09	4.44 ± 0.12	<7 ± NM	3.46 ± 0.26	0.99 ± 0.08	1.74 ± 0.26	0.55 ± 0.11	0.04 ± 0.01	C-KD
RKS1125+2000	5292 ± 62	0.10 ± 0.08	4.54 ± 0.11	<7 ± NM	3.14 ± 0.22	0.98 ± 0.10	1.67 ± 0.25	0.50 ± 0.10	0.03 ± 0.01	C-KD

Continued on next page

Table A.3 – continued from previous page

RKSTAR ID	$T_{eff} \pm \sigma$ (K)	[Fe/H] $\pm\sigma$ (dex)	$\log g \pm \sigma$ (dex)	$v \sin i \pm \sigma$ (km s^{-1})	EW[Na I D] $\pm\sigma$ (Å)	EW[Hα] $\pm\sigma$ (Å)	EW[CaII] $\pm\sigma$ (Å)	EW[CaII]$_{ratio}\pm\sigma$ (Å)	EW[Li I] $\pm\sigma$ (Å)	Status
RKS1126+1517	3968 ± 45	-0.21 ± 0.06	4.71 ± 0.09	<7 ± NM	5.91 ± 0.63	0.64 ± 0.09	1.62 ± 0.24	0.53 ± 0.10	0.04 ± 0.01	C-KD
RKS1127+0358	3971 ± 41	0.28 ± 0.08	4.67 ± 0.10	<7 ± NM	5.59 ± 0.63	0.58 ± 0.06	1.74 ± 0.26	0.49 ± 0.09	0.04 ± 0.01	CB
RKS1128+0731	3876 ± 34	-0.20 ± 0.06	4.70 ± 0.09	<7 ± NM	5.06 ± 0.42	0.70 ± 0.10	1.83 ± 0.27	0.51 ± 0.10	0.02 ± 0.01	C-KD
RKS1134-1314	4011 ± 69	-0.44 ± 0.12	4.71 ± 0.09	<7 ± NM	4.91 ± 0.36	0.71 ± 0.09	2.02 ± 0.30	0.50 ± 0.10	0.02 ± 0.01	C-KD
RKS1135+1658	4513 ± 38	-0.22 ± 0.07	4.62 ± 0.10	<7 ± NM	5.15 ± 0.43	0.84 ± 0.10	1.70 ± 0.26	0.53 ± 0.10	0.03 ± 0.01	C-KD
RKS1139-2741	4249 ± 53	-0.24 ± 0.06	4.67 ± 0.10	<7 ± NM	6.06 ± 0.60	0.79 ± 0.09	1.86 ± 0.28	0.52 ± 0.10	0.03 ± 0.01	C-KD
RKS1141+0508	4207 ± 50	-0.21 ± 0.10	4.67 ± 0.09	<7 ± NM	5.85 ± 0.57	0.71 ± 0.08	1.76 ± 0.26	0.51 ± 0.10	0.03 ± 0.01	SB1
RKS1147-1149	4524 ± 53	0.10 ± 0.06	4.58 ± 0.11	<7 ± NM	5.82 ± 0.55	0.82 ± 0.08	1.73 ± 0.26	0.54 ± 0.10	0.03 ± 0.01	C-KD
RKS1152+1845	5007 ± 35	-0.25 ± 0.07	4.57 ± 0.09	<7 ± NM	3.02 ± 0.19	0.97 ± 0.10	1.72 ± 0.26	0.52 ± 0.10	0.03 ± 0.01	C-KD
RKS1154+2844	3935 ± 33	-0.11 ± 0.06	4.70 ± 0.09	<7 ± NM	5.92 ± 0.67	0.59 ± 0.06	1.50 ± 0.23	0.53 ± 0.10	0.03 ± 0.01	CB
RKS1157-2608	4720 ± 50	-0.15 ± 0.13	4.53 ± 0.12	<7 ± NM	4.60 ± 0.35	0.88 ± 0.09	1.70 ± 0.25	0.53 ± 0.10	0.03 ± 0.01	C-KD
RKS1157+1959	5296 ± 47	0.09 ± 0.07	4.53 ± 0.10	<7 ± NM	2.68 ± 0.19	0.95 ± 0.11	1.56 ± 0.23	0.48 ± 0.09	0.03 ± 0.01	C-KD
RKS1157-2742	4513 ± 41	0.15 ± 0.10	4.58 ± 0.11	<7 ± NM	5.86 ± 0.57	0.85 ± 0.09	1.99 ± 0.30	0.50 ± 0.10	0.03 ± 0.01	C-KD
RKS1158-2355	4784 ± 53	0.01 ± 0.08	4.54 ± 0.11	<7 ± NM	4.64 ± 0.36	0.89 ± 0.09	1.75 ± 0.26	0.53 ± 0.10	0.03 ± 0.01	C-KD
RKS1159-2021	4904 ± 47	0.10 ± 0.06	4.50 ± 0.11	<7 ± NM	4.22 ± 0.31	0.92 ± 0.08	1.67 ± 0.25	0.52 ± 0.10	0.03 ± 0.01	C-KD
RKS1204+0911	4459 ± 50	-0.55 ± 0.09	4.65 ± 0.12	<7 ± NM	5.12 ± 0.42	0.81 ± 0.11	1.67 ± 0.25	0.57 ± 0.11	0.02 ± 0.01	C-KD
RKS1204-0013	4735 ± 41	-0.24 ± 0.09	4.52 ± 0.09	<7 ± NM	4.69 ± 0.39	0.78 ± 0.11	1.25 ± 0.19	0.55 ± 0.11	0.02 ± 0.01	C-KD
RKS1205-1852	3955 ± 39	-0.08 ± 0.13	4.70 ± 0.10	<7 ± NM	5.81 ± 0.66	0.26 ± 0.03	1.36 ± 0.20	0.44 ± 0.08	0.04 ± 0.01	A+CB
RKS1206-2336	5136 ± 49	-0.08 ± 0.07	4.55 ± 0.09	<7 ± NM	3.20 ± 0.22	0.98 ± 0.11	1.66 ± 0.25	0.53 ± 0.10	0.03 ± 0.01	C-KD
RKS1208-0028	3774 ± 64	-0.10 ± 0.14	4.74 ± 0.13	<7 ± NM	5.44 ± 0.57	0.59 ± 0.09	1.52 ± 0.23	0.53 ± 0.10	0.04 ± 0.01	C-KD
RKS1209-2646	3920 ± 46	-0.04 ± 0.12	4.68 ± 0.10	<7 ± NM	5.69 ± 0.63	0.60 ± 0.07	1.32 ± 0.20	0.57 ± 0.11	0.03 ± 0.01	C-KD

Continued on next page

Table A.3 – continued from previous page

RKSTAR ID	$T_{eff} \pm \sigma$ (K)	[Fe/H] $\pm\sigma$ (dex)	$\log g \pm \sigma$ (dex)	$v \sin i \pm \sigma$ (km s^{-1})	EW[Na I D] $\pm\sigma$ (Å)	EW[Hα] $\pm\sigma$ (Å)	EW[CaII] $\pm\sigma$ (Å)	EW[CaII]$_{ratio}\pm\sigma$ (Å)	EW[Li I] $\pm\sigma$ (Å)	Status
RKS1210-1126	3843 ± 51	-0.14 ± 0.16	4.70 ± 0.09	<7 ± NM	5.72 ± 0.60	0.56 ± 0.07	1.48 ± 0.22	0.51 ± 0.10	0.04 ± 0.01	C-KD
RKS1220-1953	4835 ± 31	0.09 ± 0.07	4.51 ± 0.10	<7 ± NM	4.35 ± 0.33	0.85 ± 0.07	1.55 ± 0.23	0.51 ± 0.10	0.03 ± 0.01	C-KD
RKS1222+2736	3954 ± 38	0.22 ± 0.10	4.67 ± 0.11	<7 ± NM	5.30 ± 0.57	0.61 ± 0.08	1.16 ± 0.17	0.70 ± 0.13	0.05 ± 0.01	C-KD
RKS1223+2754	3744 ± 48	-0.09 ± 0.05	4.72 ± 0.09	<7 ± NM	5.21 ± 0.52	0.57 ± 0.09	1.39 ± 0.21	0.59 ± 0.11	0.03 ± 0.01	C-KD
RKS1227+2701	4698 ± 62	-0.01 ± 0.11	4.57 ± 0.11	<7 ± NM	4.77 ± 0.39	0.88 ± 0.09	1.80 ± 0.27	0.52 ± 0.10	0.03 ± 0.01	C-KD
RKS1228-1654	4942 ± 36	-0.55 ± 0.07	4.55 ± 0.09	<7 ± NM	3.37 ± 0.16	0.86 ± 0.11	1.87 ± 0.28	0.52 ± 0.10	0.02 ± 0.01	C-KD
RKS1228-1817	4334 ± 52	0.13 ± 0.06	4.64 ± 0.09	<7 ± NM	6.28 ± 0.68	0.78 ± 0.08	1.75 ± 0.26	0.53 ± 0.10	0.03 ± 0.01	C-KD
RKS1231+2013	5275 ± 53	0.06 ± 0.07	4.53 ± 0.11	<7 ± NM	3.13 ± 0.22	1.00 ± 0.11	1.71 ± 0.26	0.51 ± 0.10	0.03 ± 0.01	C-KD
RKS1233-1438	4518 ± 60	0.07 ± 0.06	4.60 ± 0.13	<7 ± NM	5.53 ± 0.51	0.82 ± 0.09	1.75 ± 0.26	0.50 ± 0.10	0.03 ± 0.01	C-KD
RKS1241+1522	4358 ± 70	-0.42 ± 0.14	4.67 ± 0.21	NM ± NM	5.50 ± 0.48	0.83 ± 0.09	1.90 ± 0.29	0.51 ± 0.10	0.03 ± 0.01	C-KD
RKS1241+1951	4889 ± 31	-0.09 ± 0.06	4.51 ± 0.10	<7 ± NM	3.97 ± 0.27	0.93 ± 0.12	1.67 ± 0.25	0.54 ± 0.10	0.03 ± 0.01	SB1
RKS1248-2448	4362 ± 55	-0.40 ± 0.08	4.66 ± 0.10	<7 ± NM	5.48 ± 0.48	0.76 ± 0.08	1.61 ± 0.24	0.52 ± 0.10	0.03 ± 0.01	C-KD
RKS1248-1543	5028 ± 46	-0.08 ± 0.06	4.56 ± 0.10	<7 ± NM	3.59 ± 0.28	0.89 ± 0.09	1.59 ± 0.24	0.50 ± 0.10	0.03 ± 0.01	C-KD
RKS1250-0046	3969 ± 56	0.07 ± 0.12	4.67 ± 0.10	<7 ± NM	5.59 ± 0.63	0.62 ± 0.10	1.66 ± 0.25	0.50 ± 0.10	0.03 ± 0.01	C-KD
RKS1253+0645	5222 ± 31	-0.05 ± 0.05	4.58 ± 0.10	<7 ± NM	3.00 ± 0.21	0.97 ± 0.10	1.38 ± 0.21	0.56 ± 0.11	0.03 ± 0.01	SB1
RKS1256-2455	4248 ± 36	-0.02 ± 0.05	4.66 ± 0.09	<7 ± NM	6.10 ± 0.65	0.70 ± 0.09	1.41 ± 0.21	0.54 ± 0.10	0.03 ± 0.01	C-KD
RKS1257-1427	4504 ± 31	-0.32 ± 0.06	4.62 ± 0.10	<7 ± NM	5.23 ± 0.43	0.83 ± 0.07	1.73 ± 0.26	0.53 ± 0.10	0.03 ± 0.01	SB1
RKS1259-0950	5237 ± 39	-0.50 ± 0.06	4.40 ± 0.20	<7 ± NM	2.44 ± 0.15	1.01 ± 0.14	1.57 ± 0.23	0.55 ± 0.11	0.02 ± 0.01	SB1
RKS1300-0242	4241 ± 35	-0.30 ± 0.07	4.68 ± 0.09	<7 ± NM	5.88 ± 0.57	0.76 ± 0.09	1.53 ± 0.23	0.58 ± 0.11	0.02 ± 0.01	C-KD
RKS1302-2647	NM ±	NM ±	NM ± NM	NM ± NM	NM ± NM	NM ± NM	NM ± NM	NM ± NM	NM ± NM	CB
RKS1303-0509	5266 ± 50	-0.05 ± 0.06	4.54 ± 0.11	<7 ± NM	2.80 ± 0.20	0.80 ± 0.07	1.44 ± 0.22	0.46 ± 0.09	0.18 ± 0.01	Y+SB1

Continued on next page

Table A.3 – continued from previous page

RKSTAR ID	$T_{eff} \pm \sigma$ (K)	[Fe/H] $\pm\sigma$ (dex)	$\log g \pm \sigma$ (dex)	$v \sin i \pm \sigma$ (km s^{-1})	EW[Na I D] $\pm\sigma$ (Å)	EW[Hα] $\pm\sigma$ (Å)	EW[CaII] $\pm\sigma$ (Å)	EW[CaII]$_{ratio}\pm\sigma$ (Å)	EW[Li I] $\pm\sigma$ (Å)	Status
RKS1306+2043	4105 ± 44	-0.19 ± 0.13	4.68 ± 0.10	<7 ± NM	5.68 ± 0.56	0.18 ± 0.02	1.26 ± 0.19	0.51 ± 0.10	0.04 ± 0.01	A
RKS1310+0932	4642 ± 63	-0.26 ± 0.13	4.57 ± 0.11	<7 ± NM	4.58 ± 0.35	0.76 ± 0.09	1.56 ± 0.23	0.51 ± 0.10	0.03 ± 0.01	C-KD
RKS1312-0215	5082 ± 38	0.14 ± 0.07	4.47 ± 0.10	<7 ± NM	3.68 ± 0.27	0.98 ± 0.11	1.48 ± 0.22	0.60 ± 0.12	0.03 ± 0.01	C-KD
RKS1316+1701	5007 ± 57	-0.14 ± 0.07	4.56 ± 0.10	<7 ± NM	3.28 ± 0.22	0.83 ± 0.09	1.48 ± 0.22	0.49 ± 0.09	0.03 ± 0.01	C-KD
RKS1318-1446	3951 ± 61	-0.30 ± 0.05	4.70 ± 0.09	<7 ± NM	5.79 ± 0.59	0.62 ± 0.07	1.45 ± 0.22	0.57 ± 0.11	0.04 ± 0.01	C-KD
RKS1320+0407	4981 ± 32	0.12 ± 0.07	4.50 ± 0.09	<7 ± NM	3.99 ± 0.30	0.95 ± 0.08	1.43 ± 0.21	0.61 ± 0.12	0.03 ± 0.01	C-KD
RKS1323+0243	5204 ± 52	-0.49 ± 0.09	4.54 ± 0.10	<7 ± NM	2.30 ± 0.14	1.03 ± 0.10	1.66 ± 0.25	0.54 ± 0.10	0.03 ± 0.01	C-KD
RKS1327-2417	5006 ± 35	-0.16 ± 0.06	4.56 ± 0.10	<7 ± NM	3.47 ± 0.24	0.95 ± 0.09	1.51 ± 0.23	0.57 ± 0.11	0.03 ± 0.01	C-KD
RKS1331-0219	5280 ± 41	-0.47 ± 0.08	4.43 ± 0.22	<7 ± NM	2.56 ± 0.17	1.02 ± 0.09	1.55 ± 0.23	0.57 ± 0.11	0.03 ± 0.01	SB1
RKS1333+0835	4765 ± 50	0.13 ± 0.09	4.52 ± 0.11	<7 ± NM	4.97 ± 0.42	0.86 ± 0.09	1.65 ± 0.25	0.51 ± 0.10	0.03 ± 0.01	C-KD
RKS1334-0018	5109 ± 55	0.31 ± 0.10	4.46 ± 0.12	<7 ± NM	4.24 ± 0.35	0.95 ± 0.08	1.73 ± 0.26	0.52 ± 0.10	0.03 ± 0.01	C-KD
RKS1334+0440	3931 ± 49	0.03 ± 0.09	4.68 ± 0.11	<7 ± NM	5.67 ± 0.64	0.61 ± 0.09	1.65 ± 0.25	0.51 ± 0.10	0.04 ± 0.01	C-KD
RKS1334-0820	4335 ± 43	-0.10 ± 0.12	4.65 ± 0.09	8.14 ± 1.1	5.16 ± 0.47	-0.30 ± 0.04	0.81 ± 0.12	0.35 ± 0.07	0.04 ± 0.01	A
RKS1335+0650	4805 ± 44	0.17 ± 0.07	4.50 ± 0.09	<7 ± NM	5.02 ± 0.42	0.89 ± 0.13	1.75 ± 0.26	0.53 ± 0.10	0.03 ± 0.01	C-KD
RKS1335-0023	3814 ± 59	-0.07 ± 0.14	4.70 ± 0.09	<7 ± NM	5.68 ± 0.60	0.62 ± 0.06	1.57 ± 0.24	0.53 ± 0.10	0.04 ± 0.01	C-KD
RKS1336+0746	4316 ± 55	-0.58 ± 0.07	4.68 ± 0.10	<7 ± NM	4.74 ± 0.33	0.78 ± 0.12	1.04 ± 0.16	0.72 ± 0.14	0.01 ± 0.00	C-KD
RKS1338-0614	3848 ± 41	0.06 ± 0.08	4.69 ± 0.09	<7 ± NM	5.45 ± 0.59	0.55 ± 0.06	1.50 ± 0.23	0.53 ± 0.10	0.04 ± 0.01	C-KD
RKS1340-0411	3867 ± 66	-0.16 ± 0.13	4.70 ± 0.10	<7 ± NM	5.77 ± 0.61	0.58 ± 0.06	1.52 ± 0.23	0.53 ± 0.10	0.04 ± 0.01	C-KD
RKS1341-0007	4079 ± 38	0.12 ± 0.05	4.66 ± 0.09	<7 ± NM	6.12 ± 0.69	0.75 ± 0.12	1.91 ± 0.29	0.50 ± 0.10	0.04 ± 0.01	C-KD
RKS1342-0141	4377 ± 45	0.00 ± 0.13	4.65 ± 0.10	<7 ± NM	5.87 ± 0.60	0.77 ± 0.09	1.03 ± 0.15	0.69 ± 0.13	0.02 ± 0.01	C-KD
RKS1345+1747	3762 ± 62	-0.44 ± 0.08	4.85 ± 0.11	<7 ± NM	5.62 ± 0.55	0.49 ± 0.06	1.55 ± 0.23	0.56 ± 0.11	0.03 ± 0.01	C-KD

Continued on next page

Table A.3 – continued from previous page

RKSTAR ID	$T_{eff} \pm \sigma$ (K)	[Fe/H] $\pm\sigma$ (dex)	$\log g \pm \sigma$ (dex)	$v \sin i \pm \sigma$ (km s^{-1})	EW[Na I D] $\pm\sigma$ (Å)	EW[Hα] $\pm\sigma$ (Å)	EW[CaII] $\pm\sigma$ (Å)	EW[CaII]$_{ratio}\pm\sigma$ (Å)	EW[Li I] $\pm\sigma$ (Å)	Status
RKS1345-0437	4018 ± 48	-0.17 ± 0.11	4.68 ± 0.10	<7 ± NM	6.00 ± 0.64	0.64 ± 0.07	1.41 ± 0.21	0.56 ± 0.11	0.04 ± 0.01	C-KD
RKS1345+0850	4739 ± 57	0.06 ± 0.07	4.53 ± 0.10	<7 ± NM	4.77 ± 0.40	0.80 ± 0.11	1.16 ± 0.17	0.53 ± 0.10	0.05 ± 0.01	C-KD
RKS1347+0618	4252 ± 45	-0.20 ± 0.10	4.66 ± 0.11	<7 ± NM	5.96 ± 0.58	0.78 ± 0.08	1.71 ± 0.26	0.55 ± 0.11	0.03 ± 0.01	C-KD
RKS1349-2206	4302 ± 48	0.15 ± 0.10	4.64 ± 0.09	<7 ± NM	6.17 ± 0.66	0.77 ± 0.09	1.39 ± 0.21	0.61 ± 0.12	0.02 ± 0.01	C-KD
RKS1353+2748	5138 ± 36	-0.44 ± 0.06	4.55 ± 0.09	<7 ± NM	2.34 ± 0.11	1.01 ± 0.11	1.72 ± 0.26	0.53 ± 0.10	0.03 ± 0.01	C-KD
RKS1353+1256	3957 ± 37	0.12 ± 0.10	4.68 ± 0.10	<7 ± NM	5.78 ± 0.68	0.65 ± 0.08	1.25 ± 0.19	0.60 ± 0.12	0.05 ± 0.01	CB
RKS1359+2252	4386 ± 34	0.09 ± 0.07	4.64 ± 0.09	<7 ± NM	5.86 ± 0.57	0.80 ± 0.11	1.28 ± 0.19	0.65 ± 0.12	0.02 ± 0.00	C-KD
RKS1411-1236	5119 ± 43	-0.11 ± 0.07	4.55 ± 0.09	<7 ± NM	3.05 ± 0.21	0.97 ± 0.08	1.51 ± 0.23	0.55 ± 0.11	0.03 ± 0.01	C-KD
RKS1412+2348	4924 ± 39	0.15 ± 0.09	4.52 ± 0.10	<7 ± NM	4.03 ± 0.31	0.73 ± 0.08	1.12 ± 0.17	0.56 ± 0.11	0.04 ± 0.01	C-KD
RKS1413-0657	3857 ± 43	-0.11 ± 0.14	4.70 ± 0.10	<7 ± NM	5.65 ± 0.59	0.55 ± 0.09	1.43 ± 0.22	0.54 ± 0.10	0.03 ± 0.01	C-KD
RKS1414-1521	NM ±	NM ±	NM ± NM	NM ± NM	NM ± NM	NM ± NM	NM ± NM	NM ± NM	NM ± NM	NM
RKS1418-0636	4097 ± 54	-0.17 ± 0.14	4.69 ± 0.09	<7 ± NM	5.81 ± 0.60	0.66 ± 0.10	1.64 ± 0.25	0.52 ± 0.10	0.02 ± 0.01	SB1
RKS1419-0509	5195 ± 74	-0.13 ± 0.06	4.57 ± 0.09	<7 ± NM	3.01 ± 0.21	1.00 ± 0.10	1.45 ± 0.22	0.58 ± 0.11	0.03 ± 0.01	C-KD
RKS1421+2937	4193 ± 52	-0.04 ± 0.07	4.67 ± 0.09	<7 ± NM	5.97 ± 0.63	0.67 ± 0.08	1.56 ± 0.23	0.51 ± 0.10	0.02 ± 0.01	C-KD
RKS1430-0838	3931 ± 61	-0.06 ± 0.15	4.69 ± 0.10	<7 ± NM	5.73 ± 0.64	0.62 ± 0.08	1.54 ± 0.23	0.55 ± 0.10	0.03 ± 0.01	C-KD
RKS1432+1121	4193 ± 46	-0.19 ± 0.08	4.68 ± 0.09	<7 ± NM	5.64 ± 0.57	0.73 ± 0.10	1.40 ± 0.21	0.58 ± 0.11	0.03 ± 0.01	C-KD
RKS1433+0920	4977 ± 34	-0.02 ± 0.08	4.51 ± 0.09	<7 ± NM	3.64 ± 0.23	0.94 ± 0.13	1.91 ± 0.29	0.50 ± 0.10	0.03 ± 0.01	C-KD
RKS1436+0944	4915 ± 62	0.16 ± 0.07	4.52 ± 0.09	<7 ± NM	4.14 ± 0.33	0.83 ± 0.07	1.30 ± 0.20	0.52 ± 0.10	0.03 ± 0.01	C-KD
RKS1437-2548	4906 ± 109	0.22 ± 0.14	4.50 ± 0.13	<7 ± NM	4.75 ± 0.39	0.91 ± 0.08	1.86 ± 0.28	0.52 ± 0.10	0.04 ± 0.01	C-KD
RKS1442+1930	4043 ± 57	-0.10 ± 0.07	4.68 ± 0.09	<7 ± NM	5.88 ± 0.63	0.61 ± 0.06	1.44 ± 0.22	0.55 ± 0.11	0.03 ± 0.01	C-KD
RKS1444+2211	4233 ± 37	-0.29 ± 0.06	4.67 ± 0.09	<7 ± NM	5.71 ± 0.53	0.74 ± 0.11	1.53 ± 0.23	0.57 ± 0.11	0.03 ± 0.01	C-KD

Continued on next page

Table A.3 – continued from previous page

RKSTAR ID	$T_{eff} \pm \sigma$ (K)	[Fe/H] $\pm\sigma$ (dex)	$\log g \pm \sigma$ (dex)	$v \sin i \pm \sigma$ (km s^{-1})	EW[Na I D] $\pm\sigma$ (Å)	EW[Hα] $\pm\sigma$ (Å)	EW[CaII] $\pm\sigma$ (Å)	EW[CaII]$_{ratio}\pm\sigma$ (Å)	EW[Li I] $\pm\sigma$ (Å)	Status
RKS1444-2215	4450 ± 34	0.24 ± 0.05	4.59 ± 0.09	<7 ± NM	6.12 ± 0.64	0.83 ± 0.12	1.70 ± 0.25	0.55 ± 0.11	0.04 ± 0.01	C-KD
RKS1445+1350	4932 ± 51	-0.30 ± 0.07	4.56 ± 0.10	<7 ± NM	3.55 ± 0.25	0.94 ± 0.10	1.44 ± 0.22	0.58 ± 0.11	0.02 ± 0.01	C-KD
RKS1446+2730	5181 ± 30	0.16 ± 0.07	4.48 ± 0.10	<7 ± NM	3.14 ± 0.24	0.98 ± 0.08	1.32 ± 0.20	0.57 ± 0.11	0.03 ± 0.01	C-KD
RKS1446+1629	4187 ± 99	-0.33 ± 0.11	4.68 ± 0.10	<7 ± NM	5.84 ± 0.58	0.69 ± 0.11	1.85 ± 0.28	0.49 ± 0.09	0.03 ± 0.01	C-KD
RKS1447+0242	4994 ± 54	-0.19 ± 0.08	4.55 ± 0.10	<7 ± NM	3.26 ± 0.22	0.92 ± 0.09	1.51 ± 0.23	0.52 ± 0.10	0.03 ± 0.01	C-KD
RKS1450+0648	4837 ± 37	-0.20 ± 0.05	4.50 ± 0.10	<7 ± NM	4.03 ± 0.28	0.90 ± 0.12	1.40 ± 0.21	0.61 ± 0.12	0.02 ± 0.01	C-KD
RKS1451-2418	4735 ± 61	-0.05 ± 0.06	4.54 ± 0.11	<7 ± NM	4.62 ± 0.36	0.89 ± 0.09	1.74 ± 0.26	0.52 ± 0.10	0.03 ± 0.01	C-KD
RKS1453+2320	4810 ± 33	-0.38 ± 0.06	4.53 ± 0.10	<7 ± NM	4.02 ± 0.28	0.88 ± 0.14	1.38 ± 0.21	0.56 ± 0.11	0.03 ± 0.01	CB
RKS1455-2707	4765 ± 34	-0.05 ± 0.06	4.50 ± 0.11	<7 ± NM	4.36 ± 0.32	0.77 ± 0.07	1.82 ± 0.27	0.46 ± 0.09	0.03 ± 0.01	C-KD
RKS1457-2124	4596 ± 110	0.06 ± 0.14	4.57 ± 0.21	NM ± NM	5.39 ± 0.48	0.86 ± 0.09	1.94 ± 0.29	0.50 ± 0.10	0.03 ± 0.01	C-KD
RKS1500-2905	3790 ± 52	-0.03 ± 0.05	4.71 ± 0.11	<7 ± NM	5.63 ± 0.61	0.21 ± 0.02	1.52 ± 0.23	0.48 ± 0.09	0.04 ± 0.01	A
RKS1500-2427	4170 ± 39	-0.10 ± 0.08	4.67 ± 0.09	<7 ± NM	5.90 ± 0.59	0.67 ± 0.09	1.40 ± 0.21	0.55 ± 0.10	0.02 ± 0.01	C-KD
RKS1500-1108	4009 ± 68	0.00 ± 0.12	4.67 ± 0.10	<7 ± NM	5.83 ± 0.67	0.65 ± 0.10	1.76 ± 0.26	0.48 ± 0.09	0.04 ± 0.01	C-KD
RKS1501+1341	3953 ± 40	-0.11 ± 0.07	4.70 ± 0.09	<7 ± NM	5.60 ± 0.59	0.49 ± 0.06	1.04 ± 0.16	0.58 ± 0.11	0.02 ± 0.01	C-KD
RKS1501+1552	4712 ± 53	0.04 ± 0.08	4.55 ± 0.10	<7 ± NM	4.85 ± 0.40	0.83 ± 0.09	1.73 ± 0.26	0.47 ± 0.09	0.03 ± 0.01	C-KD
RKS1504+0538	3901 ± 41	-0.32 ± 0.14	4.73 ± 0.13	<7 ± NM	5.24 ± 0.47	0.63 ± 0.09	1.25 ± 0.19	0.61 ± 0.12	0.00 ± 0.00	C-KD
RKS1504-1835	4311 ± 184	-0.17 ± 0.08	4.66 ± 0.11	<7 ± NM	5.88 ± 0.60	0.75 ± 0.11	1.36 ± 0.20	0.59 ± 0.11	0.02 ± 0.01	C-KD
RKS1507+2456	3848 ± 79	-0.14 ± 0.15	4.70 ± 0.09	6.69 ± 1.34	5.27 ± 0.54	0.52 ± 0.07	0.81 ± 0.12	0.67 ± 0.13	0.03 ± 0.01	C-KD
RKS1509+2400	4653 ± 40	0.05 ± 0.08	4.57 ± 0.11	<7 ± NM	5.17 ± 0.44	0.85 ± 0.11	1.35 ± 0.20	0.60 ± 0.12	0.03 ± 0.01	C-KD
RKS1510-1622	NM ±	NM ±	NM ±	NM ± NM	1.15 ± 0.07	1.04 ±	1.48 ± 0.22	0.60 ± 0.11	0.02 ± 0.01	HALO-CKD
RKS1513-0347	4292 ± 70	-0.57 ± 0.14	4.69 ± 0.21	NM ± NM	4.57 ± 0.28	0.75 ± 0.08	0.62 ± 0.09	1.08 ± 0.21	NM ± NM	C-KD

Continued on next page

Table A.3 – continued from previous page

RKSTAR ID	$T_{eff} \pm \sigma$ (K)	[Fe/H] $\pm\sigma$ (dex)	$\log g \pm \sigma$ (dex)	$v \sin i \pm \sigma$ (km s^{-1})	EW[Na I D] $\pm\sigma$ (Å)	EW[Hα] $\pm\sigma$ (Å)	EW[CaII] $\pm\sigma$ (Å)	EW[CaII]$_{ratio}\pm\sigma$ (Å)	EW[Li I] $\pm\sigma$ (Å)	Status
RKS1515+0735	4049 ± 100	-0.26 ± 0.05	4.68 ± 0.10	<7 ± NM	5.95 ± 0.61	0.66 ± 0.08	1.63 ± 0.24	0.53 ± 0.10	0.03 ± 0.01	C-KD
RKS1515+0047	5226 ± 73	-0.04 ± 0.11	4.54 ± 0.10	<7 ± NM	2.67 ± 0.18	0.94 ± 0.11	1.61 ± 0.24	0.48 ± 0.09	0.03 ± 0.01	C-KD
RKS1518-1837	4379 ± 37	0.01 ± 0.05	4.64 ± 0.09	<7 ± NM	5.66 ± 0.52	0.73 ± 0.10	1.57 ± 0.24	0.51 ± 0.10	0.03 ± 0.01	CB
RKS1519+0146	NM ± NM	NM ± NM	NM ± NM	NM ± NM	NM ± NM	NM ± NM	NM ± NM	NM ± NM	NM ± NM	C-KD
RKS1519+2912	4176 ± 76	-0.44 ± 0.14	4.69 ± 0.10	<7 ± NM	5.70 ± 0.54	0.67 ± 0.07	1.50 ± 0.23	0.53 ± 0.10	0.03 ± 0.01	C-KD
RKS1519+1155	4291 ± 40	-0.07 ± 0.12	4.66 ± 0.09	<7 ± NM	5.52 ± 0.51	0.76 ± 0.09	1.52 ± 0.23	0.49 ± 0.10	0.03 ± 0.01	C-KD
RKS1520+1522	4934 ± 34	-0.51 ± 0.06	4.55 ± 0.09	<7 ± NM	3.78 ± 0.26	0.87 ± 0.07	1.39 ± 0.21	0.60 ± 0.11	0.03 ± 0.01	C-KD
RKS1522-0446	4150 ± 51	-0.17 ± 0.09	4.67 ± 0.10	<7 ± NM	5.92 ± 0.62	0.66 ± 0.10	1.40 ± 0.21	0.55 ± 0.11	0.03 ± 0.01	C-KD
RKS1522-1039	4991 ± 37	0.25 ± 0.06	4.49 ± 0.11	<7 ± NM	4.66 ± 0.37	0.93 ± 0.11	1.77 ± 0.27	0.51 ± 0.10	0.04 ± 0.01	C-KD
RKS1522+0125	4950 ± 65	0.22 ± 0.10	4.50 ± 0.12	<7 ± NM	4.77 ± 0.39	0.92 ± 0.10	1.81 ± 0.27	0.53 ± 0.10	0.03 ± 0.01	C-KD
RKS1525-2642	4563 ± 59	-0.26 ± 0.09	4.59 ± 0.09	<7 ± NM	4.93 ± 0.38	0.84 ± 0.13	0.87 ± 0.13	0.76 ± 0.15	0.00 ± 0.00	C-KD
RKS1527+1035	4119 ± 37	0.16 ± 0.05	4.66 ± 0.09	<7 ± NM	6.20 ± 0.70	0.73 ± 0.08	1.49 ± 0.22	0.58 ± 0.11	0.03 ± 0.01	C-KD
RKS1527+0235	4116 ± 31	0.02 ± 0.10	4.66 ± 0.09	<7 ± NM	6.03 ± 0.68	0.69 ± 0.09	1.25 ± 0.19	0.60 ± 0.12	0.03 ± 0.01	C-KD
RKS1528-0920	NM ± NM	NM ± NM	NM ± NM	NM ± NM	NM ± NM	NM ± NM	NM ± NM	NM ± NM	NM ± NM	SB2
RKS1540-1802	4143 ± 38	-0.05 ± 0.12	4.67 ± 0.10	<7 ± NM	6.04 ± 0.65	0.68 ± 0.08	1.58 ± 0.24	0.52 ± 0.10	0.03 ± 0.01	C-KD
RKS1552+1052	3939 ± 44	-0.16 ± 0.08	4.71 ± 0.09	<7 ± NM	6.02 ± 0.67	0.62 ± 0.10	1.49 ± 0.22	0.54 ± 0.10	0.04 ± 0.01	SB2
RKS1554-2600	4349 ± 39	0.22 ± 0.07	4.63 ± 0.09	<7 ± NM	6.33 ± 0.72	0.79 ± 0.12	1.83 ± 0.27	0.49 ± 0.09	0.03 ± 0.00	C-KD
RKS1555+1602	5143 ± 110	-0.28 ± 0.14	4.54 ± 0.21	NM ± NM	3.95 ± 0.30	0.81 ± 0.08	1.09 ± 0.16	0.60 ± 0.12	NM ± NM	SB1
RKS1600-0147	4207 ± 49	-0.22 ± 0.10	4.67 ± 0.09	<7 ± NM	5.86 ± 0.56	0.72 ± 0.09	1.67 ± 0.25	0.52 ± 0.10	0.03 ± 0.01	C-KD
RKS1601-2625	3801 ± 53	0.08 ± 0.12	4.68 ± 0.12	<7 ± NM	5.46 ± 0.58	0.54 ± 0.08	1.17 ± 0.18	0.62 ± 0.12	0.03 ± 0.01	C-KD
RKS1604-1126	5276 ± 49	0.09 ± 0.07	4.52 ± 0.12	<7 ± NM	3.00 ± 0.22	1.01 ± 0.11	1.35 ± 0.20	0.58 ± 0.11	0.03 ± 0.01	C-KD

Continued on next page

Table A.3 – continued from previous page

RKSTAR ID	$T_{eff} \pm \sigma$ (K)	[Fe/H] $\pm\sigma$ (dex)	$\log g \pm \sigma$ (dex)	$v \sin i \pm \sigma$ (km s^{-1})	EW[Na I D] $\pm\sigma$ (Å)	EW[Hα] $\pm\sigma$ (Å)	EW[CaII] $\pm\sigma$ (Å)	EW[CaII]$_{ratio}\pm\sigma$ (Å)	EW[Li I] $\pm\sigma$ (Å)	Status
RKS1605-2027	NM ± NM	NM ± NM	NM ± NM	NM ± NM	NM ± NM	NM ± NM	NM ± NM	NM ± NM	NM ± NM	SB2
RKS1607-0542	4094 ± 31	0.19 ± 0.06	4.66 ± 0.09	<7 ± NM	6.02 ± 0.69	0.71 ± 0.11	1.45 ± 0.22	0.58 ± 0.11	0.03 ± 0.01	C-KD
RKS1608+1713	4859 ± 32	0.02 ± 0.05	4.50 ± 0.10	<7 ± NM	4.31 ± 0.32	0.86 ± 0.12	1.57 ± 0.24	0.53 ± 0.10	0.03 ± 0.01	C-KD
RKS1608-1308	4862 ± 50	-0.03 ± 0.13	4.47 ± 0.10	<7 ± NM	4.29 ± 0.32	0.93 ± 0.09	1.57 ± 0.24	0.58 ± 0.11	0.03 ± 0.01	C-KD
RKS1613+1331	5449 ± 61	-0.08 ± 0.06	4.47 ± 0.09	<7 ± NM	2.14 ± 0.14	1.04 ± 0.13	1.52 ± 0.23	0.54 ± 0.10	0.04 ± 0.01	C-KD
RKS1615+0721	4316 ± 38	-0.17 ± 0.12	4.66 ± 0.09	<7 ± NM	5.67 ± 0.52	0.73 ± 0.08	1.90 ± 0.28	0.48 ± 0.09	0.02 ± 0.01	C-KD
RKS1620-0416	3978 ± 70	0.37 ± 0.14	4.67 ± 0.21	NM ± NM	4.35 ± 0.36	0.67 ± 0.08	0.35 ± 0.05	1.62 ± 0.31	NM ± NM	C-KD
RKS1621+1713	3977 ± 43	-0.26 ± 0.07	4.71 ± 0.10	<7 ± NM	5.74 ± 0.58	0.67 ± 0.10	2.05 ± 0.31	0.46 ± 0.09	0.03 ± 0.01	C-KD
RKS1624-1338	4819 ± 33	-0.37 ± 0.06	4.53 ± 0.09	<7 ± NM	3.88 ± 0.26	0.90 ± 0.12	1.43 ± 0.21	0.59 ± 0.11	0.03 ± 0.01	C-KD
RKS1625-2156	3794 ± 68	-0.19 ± 0.12	4.75 ± 0.12	<7 ± NM	4.78 ± 0.45	0.51 ± 0.08	1.03 ± 0.15	0.62 ± 0.12	0.01 ± 0.00	C-KD
RKS1626+1539	3958 ± 62	-0.23 ± 0.17	4.71 ± 0.09	<7 ± NM	5.64 ± 0.56	0.64 ± 0.08	1.01 ± 0.15	0.62 ± 0.12	0.03 ± 0.01	C-KD
RKS1627+0055	4088 ± 43	0.16 ± 0.11	4.66 ± 0.09	<7 ± NM	6.01 ± 0.67	0.74 ± 0.08	1.38 ± 0.21	0.60 ± 0.12	0.03 ± 0.01	C-KD
RKS1627+0718	4227 ± 53	-0.15 ± 0.08	4.67 ± 0.10	<7 ± NM	6.04 ± 0.61	0.76 ± 0.07	1.69 ± 0.25	0.53 ± 0.10	0.03 ± 0.01	C-KD
RKS1628+1824	5085 ± 59	-0.43 ± 0.06	4.55 ± 0.09	<7 ± NM	2.83 ± 0.18	0.95 ± 0.10	1.50 ± 0.23	0.54 ± 0.10	0.03 ± 0.01	C-KD
RKS1629+2346	4297 ± 39	0.04 ± 0.11	4.65 ± 0.09	<7 ± NM	6.10 ± 0.64	0.78 ± 0.09	1.29 ± 0.19	0.62 ± 0.12	0.03 ± 0.01	SB1
RKS1630-0359	4306 ± 52	0.18 ± 0.09	4.64 ± 0.10	<7 ± NM	6.34 ± 0.71	0.77 ± 0.11	1.75 ± 0.26	0.54 ± 0.10	0.03 ± 0.01	C-KD
RKS1631-0718	NM ±	NM ±	NM ± NM	NM ± NM	2.89 ± 0.22	1.08 ± 0.17	1.72 ± 0.26	0.57 ± 0.11	0.08 ± 0.01	Y
RKS1632-1235	4000 ± 35	-0.11 ± 0.08	4.69 ± 0.09	<7 ± NM	5.84 ± 0.63	0.63 ± 0.07	1.46 ± 0.22	0.54 ± 0.10	0.02 ± 0.01	C-KD
RKS1633-0933	3909 ± 59	0.20 ± 0.15	4.67 ± 0.10	<7 ± NM	5.39 ± 0.57	-0.76 ± 0.09	0.82 ± 0.12	0.33 ± 0.06	0.03 ± 0.01	A
RKS1647-0111	3931 ± 106	-0.24 ± 0.23	4.70 ± 0.10	<7 ± NM	5.55 ± 0.56	0.61 ± 0.07	1.44 ± 0.22	0.53 ± 0.10	0.05 ± 0.01	C-KD
RKS1649-2426	4579 ± 31	0.10 ± 0.07	4.56 ± 0.10	<7 ± NM	5.68 ± 0.53	0.84 ± 0.09	1.63 ± 0.24	0.54 ± 0.10	0.03 ± 0.01	C-KD

Continued on next page

Table A.3 – continued from previous page

RKSTAR ID	$T_{eff} \pm \sigma$ (K)	[Fe/H] $\pm\sigma$ (dex)	$\log g \pm \sigma$ (dex)	$v \sin i \pm \sigma$ (km s^{-1})	EW[Na I D] $\pm\sigma$ (Å)	EW[Hα] $\pm\sigma$ (Å)	EW[CaII] $\pm\sigma$ (Å)	EW[CaII]$_{ratio}\pm\sigma$ (Å)	EW[Li I] $\pm\sigma$ (Å)	Status
RKS1650+1854	4685 ± 49	-0.06 ± 0.06	4.55 ± 0.11	<7 ± NM	4.77 ± 0.37	0.86 ± 0.13	1.46 ± 0.22	0.54 ± 0.10	0.04 ± 0.01	C-KD
RKS1654+1154	3692 ± 43	-0.43 ± 0.06	4.82 ± 0.10	<7 ± NM	4.92 ± 0.48	0.53 ± 0.07	0.93 ± 0.14	0.70 ± 0.13	0.01 ± 0.01	C-KD
RKS1659-2616	4015 ± 43	0.07 ± 0.16	4.67 ± 0.09	<7 ± NM	5.93 ± 0.68	0.68 ± 0.09	1.66 ± 0.25	0.53 ± 0.10	0.04 ± 0.01	CB
RKS1701+2256	4763 ± 44	0.08 ± 0.09	4.56 ± 0.10	<7 ± NM	4.57 ± 0.36	0.88 ± 0.10	1.63 ± 0.24	0.52 ± 0.10	0.03 ± 0.01	C-KD
RKS1705-0503	4273 ± 43	-0.52 ± 0.10	4.69 ± 0.10	<7 ± NM	5.33 ± 0.44	0.76 ± 0.08	1.82 ± 0.27	0.51 ± 0.10	0.03 ± 0.01	C-KD
RKS1705-0147	4835 ± 74	0.01 ± 0.11	4.50 ± 0.11	6.19 ± 0.8	4.09 ± 0.32	0.24 ± 0.04	1.30 ± 0.19	0.38 ± 0.07	0.26 ± 0.01	Y+A
RKS1706-0610	4846 ± 93	0.16 ± 0.10	4.52 ± 0.11	<7 ± NM	4.90 ± 0.41	0.91 ± 0.09	1.60 ± 0.24	0.55 ± 0.11	0.02 ± 0.01	C-KD
RKS1712+1821	4955 ± 31	-0.11 ± 0.06	4.54 ± 0.09	<7 ± NM	3.65 ± 0.24	0.93 ± 0.11	1.73 ± 0.26	0.50 ± 0.10	0.04 ± 0.01	C-KD
RKS1714-0824	5072 ± 42	-0.09 ± 0.07	4.57 ± 0.10	<7 ± NM	3.13 ± 0.22	0.86 ± 0.08	1.11 ± 0.17	0.57 ± 0.11	0.02 ± 0.01	C-KD
RKS1715-2636	5077 ± 60	-0.25 ± 0.09	4.56 ± 0.10	<7 ± NM	2.87 ± 0.18	0.94 ± 0.08	1.54 ± 0.23	0.52 ± 0.10	0.03 ± 0.01	C-KD
RKS1716-1210	4002 ± 39	-0.02 ± 0.08	4.68 ± 0.10	<7 ± NM	5.77 ± 0.62	0.54 ± 0.07	1.59 ± 0.24	0.45 ± 0.09	0.09 ± 0.01	Y
RKS1717+2913	4778 ± 48	0.00 ± 0.11	4.52 ± 0.11	<7 ± NM	4.47 ± 0.35	0.89 ± 0.13	1.49 ± 0.22	0.60 ± 0.12	0.03 ± 0.01	C-KD
RKS1722-1457	3905 ± 70	0.07 ± 0.14	4.66 ± 0.21	NM ± NM	5.17 ± 0.51	0.55 ± 0.06	0.59 ± 0.09	0.89 ± 0.17	NM ± NM	C-KD
RKS1725+0206	4049 ± 58	0.06 ± 0.13	4.66 ± 0.10	<7 ± NM	5.96 ± 0.67	0.65 ± 0.07	1.67 ± 0.25	0.50 ± 0.10	0.03 ± 0.01	C-KD
RKS1729-2350	4041 ± 56	-0.45 ± 0.11	4.71 ± 0.09	<7 ± NM	5.66 ± 0.53	0.66 ± 0.10	1.41 ± 0.21	0.57 ± 0.11	0.02 ± 0.01	C-KD
RKS1733+0914	4515 ± 50	0.03 ± 0.07	4.62 ± 0.11	<7 ± NM	5.33 ± 0.46	0.75 ± 0.12	1.46 ± 0.22	0.52 ± 0.10	0.03 ± 0.01	C-KD
RKS1737-1314	NM ±	NM ±	NM ± NM	NM ± NM	NM ± NM	NM ± NM	NM ± NM	NM ± NM	NM ± NM	NM
RKS1737+2257	4021 ± 55	-0.14 ± 0.06	4.69 ± 0.10	<7 ± NM	5.96 ± 0.66	0.62 ± 0.08	1.63 ± 0.24	0.48 ± 0.09	0.04 ± 0.01	C-KD
RKS1739+0333	4904 ± 50	0.01 ± 0.07	4.50 ± 0.11	<7 ± NM	3.93 ± 0.26	0.92 ± 0.10	1.93 ± 0.29	0.51 ± 0.10	0.03 ± 0.01	SB1
RKS1750-0603	3951 ± 47	0.27 ± 0.07	4.66 ± 0.10	<7 ± NM	5.64 ± 0.64	0.64 ± 0.07	1.65 ± 0.25	0.51 ± 0.10	0.05 ± 0.01	C-KD
RKS1752-0733	4292 ± 50	-0.36 ± 0.11	4.67 ± 0.10	<7 ± NM	5.74 ± 0.53	0.78 ± 0.10	1.82 ± 0.27	0.55 ± 0.11	0.02 ± 0.01	C-KD

Continued on next page

Table A.3 – continued from previous page

RKSTAR ID	$T_{eff} \pm \sigma$ (K)	[Fe/H] $\pm\sigma$ (dex)	$\log g \pm \sigma$ (dex)	$v \sin i \pm \sigma$ (km s^{-1})	EW[Na I D] $\pm\sigma$ (Å)	EW[Hα] $\pm\sigma$ (Å)	EW[CaII] $\pm\sigma$ (Å)	EW[CaII]$_{ratio}\pm\sigma$ (Å)	EW[Li I] $\pm\sigma$ (Å)	Status
RKS1753+2119	4901 ± 45	-0.13 ± 0.13	4.52 ± 0.10	<7 ± NM	3.66 ± 0.25	0.82 ± 0.08	1.19 ± 0.18	0.54 ± 0.10	0.04 ± 0.01	C-KD
RKS1754-2649	4249 ± 152	-0.32 ± 0.19	4.68 ± 0.10	NM ± NM	4.65 ± 0.43	-2.31 ± 0.23	0.61 ± 0.09	0.09 ± 0.02	0.09 ± 0.01	Y+A
RKS1755+0345	4085 ± 43	-0.11 ± 0.06	4.68 ± 0.10	<7 ± NM	5.87 ± 0.62	0.67 ± 0.10	1.37 ± 0.21	0.56 ± 0.11	0.04 ± 0.01	C-KD
RKS1755+1830	4310 ± 41	-0.14 ± 0.12	4.66 ± 0.10	<7 ± NM	5.45 ± 0.50	0.70 ± 0.07	1.43 ± 0.21	0.50 ± 0.10	0.02 ± 0.01	C-KD
RKS1757-2143	4113 ± 68	0.13 ± 0.06	4.66 ± 0.10	<7 ± NM	6.01 ± 0.67	0.72 ± 0.10	1.27 ± 0.19	0.61 ± 0.12	0.04 ± 0.01	C-KD
RKS1803+2545	3939 ± 47	0.24 ± 0.06	4.66 ± 0.11	<7 ± NM	5.52 ± 0.63	0.63 ± 0.08	1.15 ± 0.17	0.60 ± 0.12	0.04 ± 0.01	C-KD
RKS1804+0149	5316 ± 49	-0.40 ± 0.06	4.53 ± 0.10	<7 ± NM	2.71 ± 0.20	0.91 ± 0.10	1.51 ± 0.23	0.50 ± 0.10	0.03 ± 0.01	C-KD
RKS1809-0019	4832 ± 41	0.12 ± 0.05	4.51 ± 0.11	<7 ± NM	4.45 ± 0.33	0.83 ± 0.10	1.08 ± 0.16	0.60 ± 0.12	0.02 ± 0.00	C-KD
RKS1809-1202	3970 ± 59	0.04 ± 0.07	4.68 ± 0.10	<7 ± NM	5.77 ± 0.64	0.63 ± 0.07	1.41 ± 0.21	0.56 ± 0.11	0.03 ± 0.01	C-KD
RKS1815+1829	4137 ± 59	0.20 ± 0.05	4.66 ± 0.09	<7 ± NM	6.10 ± 0.71	0.73 ± 0.11	1.65 ± 0.25	0.55 ± 0.11	0.03 ± 0.01	C-KD
RKS1816+1354	3812 ± 57	-0.05 ± 0.11	4.70 ± 0.09	<7 ± NM	5.47 ± 0.57	0.54 ± 0.06	1.41 ± 0.21	0.55 ± 0.11	0.03 ± 0.01	C-KD
RKS1817+2640	4591 ± 62	-0.54 ± 0.07	4.62 ± 0.09	<7 ± NM	4.29 ± 0.29	0.85 ± 0.11	1.33 ± 0.20	0.62 ± 0.12	0.02 ± 0.01	C-KD
RKS1818-0642	4673 ± 31	0.02 ± 0.06	4.58 ± 0.10	<7 ± NM	4.55 ± 0.34	0.76 ± 0.09	1.30 ± 0.20	0.55 ± 0.11	0.04 ± 0.01	C-KD
RKS1819-0156	3983 ± 40	-0.24 ± 0.09	4.70 ± 0.10	<7 ± NM	5.85 ± 0.61	0.64 ± 0.09	1.36 ± 0.20	0.57 ± 0.11	0.02 ± 0.01	C-KD
RKS1822+0142	4129 ± 41	-0.07 ± 0.10	4.67 ± 0.09	<7 ± NM	5.46 ± 0.55	-0.22 ± 0.03	0.90 ± 0.14	0.39 ± 0.08	0.03 ± 0.01	A
RKS1829-2758	4361 ± 33	0.24 ± 0.07	4.63 ± 0.09	<7 ± NM	6.27 ± 0.69	0.78 ± 0.11	1.57 ± 0.24	0.57 ± 0.11	0.03 ± 0.01	C-KD
RKS1829+0903	4919 ± 45	0.13 ± 0.08	4.51 ± 0.10	<7 ± NM	4.29 ± 0.32	0.92 ± 0.13	1.53 ± 0.23	0.57 ± 0.11	0.03 ± 0.01	C-KD
RKS1829-0149	4666 ± 76	0.14 ± 0.08	4.53 ± 0.13	<7 ± NM	5.58 ± 0.52	0.85 ± 0.07	1.30 ± 0.19	0.59 ± 0.11	0.03 ± 0.01	C-KD
RKS1831-1854	5045 ± 53	-0.18 ± 0.07	4.56 ± 0.09	<7 ± NM	3.16 ± 0.21	0.97 ± 0.08	1.59 ± 0.24	0.53 ± 0.10	0.03 ± 0.01	C-KD
RKS1833+2218	4452 ± 59	-0.10 ± 0.13	4.64 ± 0.10	<7 ± NM	5.26 ± 0.44	0.77 ± 0.10	1.58 ± 0.24	0.50 ± 0.10	0.03 ± 0.01	C-KD
RKS1833-1626	NM ± NM	NM ± NM	NM ± NM	NM ± NM	NM ± NM	NM ± NM	NM ± NM	NM ± NM	NM ± NM	New SB2

Continued on next page

Table A.3 – continued from previous page

RKSTAR ID	$T_{eff} \pm \sigma$ (K)	[Fe/H] $\pm\sigma$ (dex)	$\log g \pm \sigma$ (dex)	$v \sin i \pm \sigma$ (km s^{-1})	EW[Na I D] $\pm\sigma$ (Å)	EW[Hα] $\pm\sigma$ (Å)	EW[CaII] $\pm\sigma$ (Å)	EW[CaII]$_{ratio}\pm\sigma$ (Å)	EW[Li I] $\pm\sigma$ (Å)	Status
RKS1833-1138	4162 ± 98	-0.26 ± 0.08	4.69 ± 0.10	<7 ± NM	5.83 ± 0.57	0.72 ± 0.10	1.28 ± 0.19	0.60 ± 0.11	0.02 ± 0.00	C-KD
RKS1847-0338	4106 ± 84	-0.33 ± 0.14	4.69 ± 0.11	<7 ± NM	5.93 ± 0.61	0.66 ± 0.07	1.73 ± 0.26	0.48 ± 0.09	0.02 ± 0.01	C-KD
RKS1848-1008	5023 ± 60	-0.42 ± 0.09	4.55 ± 0.09	<7 ± NM	3.18 ± 0.21	0.92 ± 0.09	1.76 ± 0.26	0.52 ± 0.10	0.03 ± 0.01	C-KD
RKS1848+1044	4657 ± 59	0.12 ± 0.07	4.54 ± 0.11	<7 ± NM	5.23 ± 0.45	0.81 ± 0.08	1.71 ± 0.26	0.48 ± 0.09	0.03 ± 0.01	C-KD
RKS1848+1726	4009 ± 62	-0.28 ± 0.13	4.69 ± 0.11	<7 ± NM	5.84 ± 0.61	0.69 ± 0.08	1.56 ± 0.23	0.56 ± 0.11	0.02 ± 0.01	C-KD
RKS1850-2655	3947 ± 35	-0.14 ± 0.09	4.70 ± 0.10	<7 ± NM	5.89 ± 0.64	0.64 ± 0.10	1.82 ± 0.27	0.50 ± 0.10	0.04 ± 0.01	C-KD
RKS1854+2844	3839 ± 41	-0.07 ± 0.06	4.69 ± 0.09	<7 ± NM	5.31 ± 0.57	0.52 ± 0.08	1.41 ± 0.21	0.55 ± 0.10	0.03 ± 0.01	C-KD
RKS1854+0051	3904 ± 41	-0.11 ± 0.16	4.70 ± 0.10	<7 ± NM	5.60 ± 0.63	0.55 ± 0.08	1.99 ± 0.30	0.45 ± 0.09	0.04 ± 0.01	C-KD
RKS1854+1058	4089 ± 49	0.33 ± 0.14	4.65 ± 0.09	<7 ± NM	6.03 ± 0.69	0.70 ± 0.08	1.79 ± 0.27	0.52 ± 0.10	0.04 ± 0.01	C-KD
RKS1855+2333	5123 ± 95	0.01 ± 0.11	4.54 ± 0.11	14.82 ± 1.06	3.29 ± 0.25	0.03 ± 0.00	0.86 ± 0.13	0.35 ± 0.07	0.03 ± 0.01	A+SB1
RKS1858-1014	4402 ± 30	0.04 ± 0.05	4.64 ± 0.09	<7 ± NM	5.69 ± 0.54	0.74 ± 0.08	1.39 ± 0.21	0.56 ± 0.11	0.02 ± 0.01	C-KD
RKS1858-0030	5248 ± 31	-0.05 ± 0.05	4.56 ± 0.09	<7 ± NM	2.73 ± 0.17	1.01 ± 0.09	1.64 ± 0.25	0.54 ± 0.10	0.03 ± 0.01	C-KD
RKS1859+0759	4341 ± 40	0.05 ± 0.15	4.63 ± 0.10	<7 ± NM	4.19 ± 0.47	0.55 ± 0.06	1.17 ± 0.18	0.52 ± 0.10	0.02 ± 0.01	C-KD
RKS1859+1107	4663 ± 76	0.09 ± 0.09	4.55 ± 0.15	<7 ± NM	5.16 ± 0.45	0.82 ± 0.09	1.51 ± 0.23	0.51 ± 0.10	0.02 ± 0.01	C-KD
RKS1901+0328	4426 ± 31	0.05 ± 0.05	4.64 ± 0.09	<7 ± NM	5.61 ± 0.53	0.74 ± 0.11	1.27 ± 0.19	0.55 ± 0.11	0.02 ± 0.01	C-KD
RKS1903-1102	4992 ± 78	0.13 ± 0.16	4.50 ± 0.11	<7 ± NM	3.88 ± 0.27	0.96 ± 0.13	1.75 ± 0.26	0.52 ± 0.10	0.04 ± 0.01	C-KD
RKS1907+0736	4358 ± 179	-0.56 ± 0.10	4.67 ± 0.12	<7 ± NM	4.82 ± 0.38	0.76 ± 0.12	1.30 ± 0.19	0.52 ± 0.10	0.02 ± 0.01	C-KD
RKS1908+1627	4187 ± 44	-0.06 ± 0.09	4.67 ± 0.09	<7 ± NM	5.81 ± 0.60	0.68 ± 0.09	0.65 ± 0.10	0.85 ± 0.16	0.02 ± 0.01	C-KD
RKS1908-1640	3958 ± 64	-0.34 ± 0.10	4.69 ± 0.11	<7 ± NM	6.02 ± 0.62	0.64 ± 0.08	1.38 ± 0.21	0.62 ± 0.12	0.02 ± 0.01	C-KD
RKS1910+2145	3931 ± 37	0.07 ± 0.09	4.67 ± 0.10	<7 ± NM	5.09 ± 0.54	-0.39 ± 0.05	0.77 ± 0.12	0.46 ± 0.09	0.04 ± 0.01	A
RKS1914+0209	NM ±	NM ±	NM ±	NM ± NM	4.70 ± 0.33	0.50 ± 0.07	0.97 ± 0.15	0.75 ± 0.14	NM ± NM	C-KD

Continued on next page

Table A.3 – continued from previous page

RKSTAR ID	$T_{eff} \pm \sigma$ (K)	[Fe/H] $\pm\sigma$ (dex)	$\log g \pm \sigma$ (dex)	$v \sin i \pm \sigma$ (km s^{-1})	EW[Na I D] $\pm\sigma$ (Å)	EW[Hα] $\pm\sigma$ (Å)	EW[CaII] $\pm\sigma$ (Å)	EW[CaII]$_{ratio}\pm\sigma$ (Å)	EW[Li I] $\pm\sigma$ (Å)	Status
RKS1915+2453	3953 ± 53	-0.28 ± 0.08	4.71 ± 0.11	6.51 ± 2.02	5.89 ± 0.61	0.67 ± 0.09	1.00 ± 0.15	0.71 ± 0.14	0.00 ± 0.00	CB
RKS1915+1133	5133 ± 41	0.31 ± 0.07	4.48 ± 0.10	<7 ± NM	3.89 ± 0.29	0.97 ± 0.09	1.09 ± 0.16	0.66 ± 0.13	0.02 ± 0.00	C-KD
RKS1923-0635	4521 ± 41	-0.35 ± 0.06	4.62 ± 0.10	<7 ± NM	5.10 ± 0.41	0.80 ± 0.11	1.70 ± 0.25	0.52 ± 0.10	0.02 ± 0.01	C-KD
RKS1924+2525	3954 ± 45	-0.20 ± 0.15	4.70 ± 0.09	<7 ± NM	5.72 ± 0.64	0.61 ± 0.07	1.14 ± 0.17	0.62 ± 0.12	0.03 ± 0.01	C-KD
RKS1924-2203	4209 ± 111	0.13 ± 0.09	4.64 ± 0.11	<7 ± NM	4.63 ± 0.50	0.51 ± 0.07	1.45 ± 0.22	0.43 ± 0.08	0.01 ± 0.00	C-KD
RKS1928+1232	4668 ± 39	0.01 ± 0.05	4.58 ± 0.09	<7 ± NM	4.95 ± 0.41	0.80 ± 0.09	1.39 ± 0.21	0.57 ± 0.11	0.03 ± 0.01	C-KD
RKS1928+2854	3839 ± 60	-0.03 ± 0.09	4.69 ± 0.11	<7 ± NM	5.36 ± 0.57	0.52 ± 0.06	1.48 ± 0.22	0.53 ± 0.10	0.03 ± 0.01	C-KD
RKS1929+0709	4005 ± 49	-0.36 ± 0.16	4.70 ± 0.10	<7 ± NM	6.07 ± 0.65	0.60 ± 0.07	1.65 ± 0.25	0.52 ± 0.10	0.04 ± 0.01	C-KD
RKS1930+2140	4391 ± 63	-0.50 ± 0.07	4.67 ± 0.09	<7 ± NM	5.41 ± 0.47	0.77 ± 0.12	1.56 ± 0.23	0.55 ± 0.11	0.03 ± 0.01	C-KD
RKS1932-1116	4997 ± 50	-0.02 ± 0.06	4.54 ± 0.12	<7 ± NM	3.47 ± 0.25	0.88 ± 0.10	1.59 ± 0.24	0.48 ± 0.09	0.03 ± 0.01	C-KD
RKS1932+0034	3864 ± 38	0.08 ± 0.06	4.68 ± 0.10	<7 ± NM	5.15 ± 0.56	0.46 ± 0.07	1.39 ± 0.21	0.49 ± 0.09	0.03 ± 0.01	C-KD
RKS1934+0434	3960 ± 58	-0.32 ± 0.10	4.70 ± 0.10	<7 ± NM	5.48 ± 0.53	0.64 ± 0.07	1.18 ± 0.18	0.63 ± 0.12	0.01 ± 0.00	C-KD
RKS1936-1026	4889 ± 35	-0.08 ± 0.06	4.49 ± 0.09	<7 ± NM	3.97 ± 0.27	0.93 ± 0.08	1.84 ± 0.28	0.52 ± 0.10	0.03 ± 0.01	C-KD
RKS1943+1005	4175 ± 48	-0.17 ± 0.06	4.67 ± 0.09	<7 ± NM	5.89 ± 0.58	0.72 ± 0.08	1.81 ± 0.27	0.50 ± 0.10	0.03 ± 0.01	C-KD
RKS1952-2356	4384 ± 44	-0.19 ± 0.08	4.65 ± 0.09	<7 ± NM	5.49 ± 0.49	0.76 ± 0.10	1.60 ± 0.24	0.51 ± 0.10	0.03 ± 0.01	C-KD
RKS1954-2356	NM ±	NM ±	NM ± NM	NM ± NM	NM ± NM	NM ± NM	NM ± NM	NM ± NM	NM ± NM	SB2
RKS1954+2013	3901 ± 31	-0.10 ± 0.12	4.68 ± 0.11	<7 ± NM	5.30 ± 0.54	0.54 ± 0.07	1.36 ± 0.20	0.55 ± 0.11	0.02 ± 0.00	C-KD
RKS1957+1313	4097 ± 41	-0.11 ± 0.12	4.68 ± 0.10	<7 ± NM	5.92 ± 0.62	0.66 ± 0.09	1.39 ± 0.21	0.54 ± 0.10	0.03 ± 0.01	C-KD
RKS2000+2242	5035 ± 110	-0.01 ± 0.14	4.54 ± 0.21	NM ± NM	3.53 ± 0.25	0.89 ± 0.07	1.58 ± 0.24	0.48 ± 0.09	NM ± NM	C-KD
RKS2002+0319	4527 ± 64	0.13 ± 0.08	4.58 ± 0.11	<7 ± NM	5.72 ± 0.54	0.81 ± 0.09	1.64 ± 0.25	0.52 ± 0.10	0.03 ± 0.01	C-KD
RKS2003+2005	4006 ± 71	-0.15 ± 0.07	4.70 ± 0.10	<7 ± NM	5.48 ± 0.53	0.57 ± 0.06	0.75 ± 0.11	0.76 ± 0.15	0.00 ± 0.00	C-KD

Continued on next page

Table A.3 – continued from previous page

RKSTAR ID	$T_{eff} \pm \sigma$ (K)	[Fe/H] $\pm\sigma$ (dex)	$\log g \pm \sigma$ (dex)	$v \sin i \pm \sigma$ (km s^{-1})	EW[Na I D] $\pm\sigma$ (Å)	EW[Hα] $\pm\sigma$ (Å)	EW[CaII] $\pm\sigma$ (Å)	EW[CaII]$_{ratio}\pm\sigma$ (Å)	EW[Li I] $\pm\sigma$ (Å)	Status
RKS2003+2320	5142 ± 72	-0.55 ± 0.10	4.54 ± 0.10	<7 ± NM	2.63 ± 0.15	0.98 ± 0.10	1.61 ± 0.24	0.55 ± 0.11	0.02 ± 0.01	C-KD
RKS2004+2547	5086 ± 42	0.22 ± 0.07	4.48 ± 0.11	<7 ± NM	3.86 ± 0.28	0.93 ± 0.11	0.85 ± 0.13	0.70 ± 0.13	0.03 ± 0.01	C-KD
RKS2008+0640	4310 ± 42	-0.29 ± 0.08	4.66 ± 0.10	<7 ± NM	5.52 ± 0.49	0.70 ± 0.09	1.47 ± 0.22	0.53 ± 0.10	0.02 ± 0.01	C-KD
RKS2009+1648	5307 ± 30	-0.16 ± 0.08	4.52 ± 0.10	<7 ± NM	2.66 ± 0.20	1.04 ± 0.15	1.37 ± 0.21	0.61 ± 0.12	0.02 ± 0.01	C-KD
RKS2009-1417	4411 ± 66	-0.21 ± 0.10	4.65 ± 0.10	<7 ± NM	5.39 ± 0.47	0.78 ± 0.09	1.83 ± 0.27	0.49 ± 0.09	0.03 ± 0.01	C-KD
RKS2009-0307	4370 ± 49	0.20 ± 0.10	4.63 ± 0.09	<7 ± NM	6.26 ± 0.68	0.81 ± 0.08	1.60 ± 0.24	0.57 ± 0.11	0.02 ± 0.01	C-KD
RKS2010-2029	4201 ± 67	-0.21 ± 0.11	4.68 ± 0.09	<7 ± NM	5.91 ± 0.60	0.65 ± 0.08	1.75 ± 0.26	0.48 ± 0.09	0.03 ± 0.01	C-KD
RKS2011+1611	5281 ± 52	-0.12 ± 0.08	4.52 ± 0.10	<7 ± NM	2.94 ± 0.20	1.00 ± 0.09	1.29 ± 0.19	0.63 ± 0.12	0.02 ± 0.01	C-KD
RKS2012-1253	3726 ± 40	-0.12 ± 0.07	4.72 ± 0.10	<7 ± NM	5.53 ± 0.59	0.53 ± 0.08	1.40 ± 0.21	0.55 ± 0.10	0.04 ± 0.01	C-KD
RKS2013-0052	4956 ± 50	0.04 ± 0.09	4.52 ± 0.10	<7 ± NM	3.82 ± 0.28	0.90 ± 0.10	1.52 ± 0.23	0.51 ± 0.10	0.03 ± 0.01	C-KD
RKS2014-0716	3867 ± 54	-0.16 ± 0.12	4.70 ± 0.09	<7 ± NM	5.59 ± 0.58	0.59 ± 0.09	1.17 ± 0.18	0.54 ± 0.10	0.05 ± 0.02	C-KD
RKS2015-2701	5078 ± 62	0.03 ± 0.06	4.49 ± 0.10	<7 ± NM	3.49 ± 0.24	0.98 ± 0.08	1.43 ± 0.21	0.61 ± 0.12	0.03 ± 0.01	C-KD
RKS2016-0204	3765 ± 38	-0.16 ± 0.06	4.76 ± 0.10	<7 ± NM	5.37 ± 0.55	0.48 ± 0.06	1.29 ± 0.19	0.57 ± 0.11	0.03 ± 0.01	C-KD
RKS2030+2650	3983 ± 65	-0.33 ± 0.12	4.71 ± 0.09	<7 ± NM	5.88 ± 0.62	0.62 ± 0.07	1.46 ± 0.22	0.55 ± 0.11	0.03 ± 0.01	C-KD
RKS2035+0607	4876 ± 31	-0.09 ± 0.06	4.50 ± 0.10	<7 ± NM	4.08 ± 0.29	0.92 ± 0.11	1.43 ± 0.21	0.59 ± 0.11	0.02 ± 0.01	C-KD
RKS2038+2346	5052 ± 31	-0.02 ± 0.05	4.56 ± 0.09	<7 ± NM	3.43 ± 0.25	0.93 ± 0.10	1.34 ± 0.20	0.55 ± 0.11	0.03 ± 0.01	C-KD
RKS2039+1004	5037 ± 36	0.01 ± 0.06	4.53 ± 0.10	<7 ± NM	3.51 ± 0.25	0.97 ± 0.08	1.31 ± 0.20	0.62 ± 0.12	0.03 ± 0.01	C-KD
RKS2041-0529	4108 ± 63	-0.08 ± 0.12	4.68 ± 0.10	<7 ± NM	5.93 ± 0.64	0.68 ± 0.10	1.57 ± 0.24	0.55 ± 0.10	0.02 ± 0.01	C-KD
RKS2041-2219	3953 ± 62	-0.16 ± 0.17	4.69 ± 0.10	<7 ± NM	4.47 ± 0.37	-1.39 ± 0.17	0.86 ± 0.13	0.31 ± 0.06	0.03 ± 0.01	A+CB
RKS2042-2116	5265 ± 55	0.17 ± 0.08	4.42 ± 0.14	<7 ± NM	3.02 ± 0.18	0.97 ± 0.11	1.79 ± 0.27	0.51 ± 0.10	0.04 ± 0.01	C-KD
RKS2042+2050	5008 ± 43	-0.15 ± 0.10	4.55 ± 0.09	<7 ± NM	3.51 ± 0.25	0.96 ± 0.14	1.54 ± 0.23	0.56 ± 0.11	0.03 ± 0.01	C-KD

Continued on next page

Table A.3 – continued from previous page

RKSTAR ID	$T_{eff} \pm \sigma$ (K)	[Fe/H] $\pm\sigma$ (dex)	$\log g \pm \sigma$ (dex)	$v \sin i \pm \sigma$ (km s^{-1})	EW[Na I D] $\pm\sigma$ (Å)	EW[Hα] $\pm\sigma$ (Å)	EW[CaII] $\pm\sigma$ (Å)	EW[CaII]$_{ratio}\pm\sigma$ (Å)	EW[Li I] $\pm\sigma$ (Å)	Status
RKS2044-2121	4108 ± 48	-0.42 ± 0.08	4.70 ± 0.09	<7 ± NM	5.61 ± 0.52	0.74 ± 0.10	1.06 ± 0.16	0.71 ± 0.14	0.00 ± 0.00	C-KD
RKS2047+1051	4493 ± 40	-0.58 ± 0.05	4.65 ± 0.09	<7 ± NM	4.64 ± 0.33	0.82 ± 0.09	1.78 ± 0.27	0.51 ± 0.10	0.03 ± 0.01	C-KD
RKS2050+2923	4716 ± 54	0.00 ± 0.11	4.55 ± 0.10	<7 ± NM	4.60 ± 0.36	0.67 ± 0.09	1.77 ± 0.27	0.44 ± 0.08	0.03 ± 0.00	C-KD
RKS2053-0245	3851 ± 80	-0.30 ± 0.22	4.77 ± 0.11	<7 ± NM	5.62 ± 0.57	0.61 ± 0.08	1.71 ± 0.26	0.51 ± 0.10	0.04 ± 0.01	C-KD
RKS2055+1310	4662 ± 31	-0.12 ± 0.13	4.57 ± 0.10	<7 ± NM	4.65 ± 0.40	0.79 ± 0.11	1.31 ± 0.20	0.48 ± 0.09	0.02 ± 0.01	SB1
RKS2059+0333	3727 ± 40	-0.46 ± 0.07	4.85 ± 0.11	<7 ± NM	5.74 ± 0.57	0.53 ± 0.08	1.80 ± 0.27	0.53 ± 0.10	0.02 ± 0.01	C-KD
RKS2059-1042	5016 ± 55	0.29 ± 0.08	4.48 ± 0.09	<7 ± NM	4.88 ± 0.41	0.92 ± 0.09	1.80 ± 0.27	0.54 ± 0.10	0.04 ± 0.01	C-KD
RKS2105+0704	4303 ± 56	0.08 ± 0.08	4.65 ± 0.09	<7 ± NM	6.07 ± 0.62	0.78 ± 0.08	1.45 ± 0.22	0.59 ± 0.11	0.02 ± 0.01	C-KD
RKS2105-1654	3820 ± 49	-0.05 ± 0.06	4.70 ± 0.10	<7 ± NM	5.38 ± 0.56	0.22 ± 0.02	1.39 ± 0.21	0.46 ± 0.09	0.03 ± 0.01	A
RKS2107-1355	5197 ± 50	0.09 ± 0.08	4.51 ± 0.12	<7 ± NM	3.05 ± 0.21	0.95 ± 0.10	1.09 ± 0.16	0.58 ± 0.11	0.03 ± 0.01	C-KD
RKS2108-0425	4566 ± 58	-0.40 ± 0.12	4.60 ± 0.12	<7 ± NM	4.67 ± 0.37	0.31 ± 0.04	1.35 ± 0.20	0.49 ± 0.09	0.03 ± 0.01	A+CB
RKS2116+0923	4732 ± 49	-0.04 ± 0.07	4.53 ± 0.10	<7 ± NM	4.45 ± 0.33	0.81 ± 0.09	1.55 ± 0.23	0.50 ± 0.10	0.03 ± 0.01	C-KD
RKS2118+0009	4732 ± 37	-0.10 ± 0.10	4.51 ± 0.10	<7 ± NM	4.43 ± 0.34	0.89 ± 0.12	1.72 ± 0.26	0.55 ± 0.11	0.03 ± 0.01	C-KD
RKS2119-2621	5582 ± 72	-0.32 ± 0.12	4.46 ± 0.18	<7 ± NM	2.08 ± 0.15	1.01 ± 0.09	1.73 ± 0.26	0.50 ± 0.10	0.03 ± 0.01	SB1
RKS2120-1951	4076 ± 69	-0.05 ± 0.14	4.66 ± 0.10	<7 ± NM	5.96 ± 0.65	0.68 ± 0.08	1.74 ± 0.26	0.49 ± 0.09	0.03 ± 0.01	C-KD
RKS2122+1052	3961 ± 44	0.01 ± 0.16	4.69 ± 0.10	<7 ± NM	5.92 ± 0.67	0.59 ± 0.07	1.72 ± 0.26	0.48 ± 0.09	0.05 ± 0.01	C-KD
RKS2125+2712	5235 ± 42	-0.14 ± 0.06	4.56 ± 0.09	<7 ± NM	2.92 ± 0.22	0.99 ± 0.14	1.71 ± 0.26	0.52 ± 0.10	0.03 ± 0.01	C-KD
RKS2126+0344	3999 ± 56	0.03 ± 0.18	4.68 ± 0.10	<7 ± NM	6.12 ± 0.70	0.68 ± 0.07	1.56 ± 0.23	0.55 ± 0.10	0.03 ± 0.01	C-KD
RKS2130-1230	4141 ± 68	-0.17 ± 0.09	4.66 ± 0.09	<7 ± NM	5.88 ± 0.59	0.72 ± 0.06	1.42 ± 0.21	0.60 ± 0.11	0.02 ± 0.01	C-KD
RKS2131+2320	NM ±	NM ±	NM ± NM	NM ± NM	NM ± NM	NM ± NM	NM ± NM	NM ± NM	NM ± NM	NM
RKS2132-2057	5033 ± 37	-0.11 ± 0.08	4.52 ± 0.10	<7 ± NM	3.27 ± 0.21	0.98 ± 0.11	1.83 ± 0.27	0.51 ± 0.10	0.03 ± 0.01	C-KD

Continued on next page

Table A.3 – continued from previous page

RKSTAR ID	$T_{eff} \pm \sigma$ (K)	[Fe/H] $\pm\sigma$ (dex)	$\log g \pm \sigma$ (dex)	$v \sin i \pm \sigma$ (km s^{-1})	EW[Na I D] $\pm\sigma$ (Å)	EW[Hα] $\pm\sigma$ (Å)	EW[CaII] $\pm\sigma$ (Å)	EW[CaII]$_{ratio}\pm\sigma$ (Å)	EW[Li I] $\pm\sigma$ (Å)	Status
RKS2141+1115	4693 ± 34	0.05 ± 0.07	4.54 ± 0.10	<7 ± NM	4.96 ± 0.40	0.87 ± 0.07	1.10 ± 0.17	0.65 ± 0.12	0.01 ± 0.00	CB
RKS2149+0543	4733 ± 55	-0.19 ± 0.08	4.53 ± 0.12	<7 ± NM	4.66 ± 0.35	0.87 ± 0.11	1.85 ± 0.28	0.50 ± 0.10	0.03 ± 0.01	C-KD
RKS2149-1140	3940 ± 39	-0.21 ± 0.09	4.70 ± 0.10	<7 ± NM	5.78 ± 0.61	0.58 ± 0.09	1.25 ± 0.19	0.59 ± 0.11	0.04 ± 0.01	C-KD
RKS2152+0154	5155 ± 45	0.14 ± 0.06	4.47 ± 0.10	<7 ± NM	3.23 ± 0.23	0.99 ± 0.10	1.33 ± 0.20	0.63 ± 0.12	0.03 ± 0.01	C-KD
RKS2153+2055	5033 ± 38	-0.07 ± 0.07	4.56 ± 0.09	<7 ± NM	3.41 ± 0.24	0.82 ± 0.07	1.59 ± 0.24	0.46 ± 0.09	0.05 ± 0.01	C-KD
RKS2153+2850	3768 ± 61	-0.35 ± 0.17	4.81 ± 0.14	<7 ± NM	5.76 ± 0.61	0.53 ± 0.07	1.37 ± 0.21	0.56 ± 0.11	0.05 ± 0.01	C-KD
RKS2153-1249	3750 ± 44	-0.11 ± 0.07	4.73 ± 0.10	<7 ± NM	5.55 ± 0.57	0.54 ± 0.09	0.79 ± 0.12	0.83 ± 0.16	0.03 ± 0.01	C-KD
RKS2155-2942	5300 ± 41	0.07 ± 0.05	4.53 ± 0.10	<7 ± NM	2.86 ± 0.20	0.96 ± 0.10	1.58 ± 0.24	0.49 ± 0.09	0.03 ± 0.01	C-KD
RKS2210+2247	4839 ± 63	-0.38 ± 0.06	4.54 ± 0.09	<7 ± NM	3.98 ± 0.28	0.91 ± 0.09	1.30 ± 0.20	0.67 ± 0.13	0.02 ± 0.01	C-KD
RKS2214+2751	3847 ± 66	-0.15 ± 0.14	4.72 ± 0.11	<7 ± NM	5.80 ± 0.63	0.60 ± 0.09	1.56 ± 0.23	0.54 ± 0.10	0.03 ± 0.01	C-KD
RKS2224+2233	4389 ± 67	-0.15 ± 0.13	4.65 ± 0.09	<7 ± NM	5.49 ± 0.50	0.76 ± 0.08	1.47 ± 0.22	0.54 ± 0.10	0.03 ± 0.01	C-KD
RKS2226-1911	4473 ± 32	0.04 ± 0.09	4.62 ± 0.11	<7 ± NM	5.43 ± 0.50	0.67 ± 0.11	1.60 ± 0.24	0.47 ± 0.09	0.03 ± 0.01	C-KD
RKS2239+0406	4922 ± 68	-0.30 ± 0.11	4.55 ± 0.10	<7 ± NM	3.50 ± 0.21	0.80 ± 0.09	1.65 ± 0.25	0.47 ± 0.09	0.04 ± 0.01	C-KD
RKS2240-2940	4453 ± 47	0.02 ± 0.08	4.64 ± 0.09	<7 ± NM	5.31 ± 0.47	0.71 ± 0.07	1.72 ± 0.26	0.46 ± 0.09	0.03 ± 0.01	C-KD
RKS2241+1849	3993 ± 36	0.03 ± 0.16	4.67 ± 0.10	<7 ± NM	5.97 ± 0.67	0.27 ± 0.04	1.52 ± 0.23	0.51 ± 0.10	0.04 ± 0.01	A
RKS2243-0624	4881 ± 33	0.03 ± 0.06	4.49 ± 0.09	<7 ± NM	4.32 ± 0.32	0.93 ± 0.11	1.74 ± 0.26	0.54 ± 0.10	0.03 ± 0.01	C-KD
RKS2247+1823	4663 ± 53	0.01 ± 0.06	4.58 ± 0.11	<7 ± NM	4.90 ± 0.40	0.83 ± 0.10	1.61 ± 0.24	0.51 ± 0.10	0.03 ± 0.01	C-KD
RKS2248+2443	3954 ± 68	-0.16 ± 0.12	4.70 ± 0.10	<7 ± NM	5.59 ± 0.58	0.60 ± 0.06	1.63 ± 0.24	0.47 ± 0.09	0.04 ± 0.01	C-KD
RKS2251+1358	5017 ± 61	-0.57 ± 0.06	4.54 ± 0.09	<7 ± NM	2.78 ± 0.16	0.95 ± 0.10	1.64 ± 0.25	0.54 ± 0.10	0.02 ± 0.01	C-KD
RKS2252+2324	4299 ± 38	-0.03 ± 0.07	4.66 ± 0.09	<7 ± NM	5.76 ± 0.57	0.71 ± 0.07	1.29 ± 0.19	0.56 ± 0.11	0.02 ± 0.01	C-KD
RKS2254+2331	3931 ± 51	0.02 ± 0.13	4.67 ± 0.11	<7 ± NM	5.19 ± 0.56	0.57 ± 0.07	1.34 ± 0.20	0.59 ± 0.11	0.02 ± 0.01	Y-MG

Continued on next page

Table A.3 – continued from previous page

RKSTAR ID	$T_{eff} \pm \sigma$ (K)	[Fe/H] $\pm\sigma$ (dex)	$\log g \pm \sigma$ (dex)	$v \sin i \pm \sigma$ (km s^{-1})	EW[Na I D] $\pm\sigma$ (Å)	EW[Hα] $\pm\sigma$ (Å)	EW[CaII] $\pm\sigma$ (Å)	EW[CaII]$_{ratio}\pm\sigma$ (Å)	EW[Li I] $\pm\sigma$ (Å)	Status
RKS2258-1338	4220 ± 40	-0.25 ± 0.07	4.68 ± 0.09	<7 ± NM	5.57 ± 0.52	0.62 ± 0.08	1.76 ± 0.26	0.47 ± 0.09	0.03 ± 0.01	C-KD
RKS2259-1122	3932 ± 63	-0.11 ± 0.14	4.68 ± 0.09	<7 ± NM	5.73 ± 0.62	0.61 ± 0.08	1.46 ± 0.22	0.52 ± 0.10	0.03 ± 0.01	C-KD
RKS2300-2231	3983 ± 67	-0.21 ± 0.09	4.69 ± 0.11	<7 ± NM	5.89 ± 0.64	0.62 ± 0.07	1.71 ± 0.26	0.49 ± 0.09	0.03 ± 0.01	C-KD
RKS2301-0350	4996 ± 56	0.20 ± 0.07	4.50 ± 0.10	<7 ± NM	4.14 ± 0.31	0.94 ± 0.09	1.65 ± 0.25	0.55 ± 0.11	0.03 ± 0.01	C-KD
RKS2307-2309	4107 ± 49	-0.11 ± 0.08	4.68 ± 0.10	<7 ± NM	5.74 ± 0.59	0.64 ± 0.09	1.77 ± 0.27	0.46 ± 0.09	0.04 ± 0.01	C-KD
RKS2308+0633	3804 ± 35	0.10 ± 0.14	4.70 ± 0.09	<7 ± NM	5.10 ± 0.54	0.07 ± 0.01	1.51 ± 0.23	0.44 ± 0.09	0.04 ± 0.01	A
RKS2309-0215	4841 ± 44	0.18 ± 0.06	4.51 ± 0.10	<7 ± NM	4.89 ± 0.40	0.89 ± 0.10	1.41 ± 0.21	0.61 ± 0.12	0.03 ± 0.01	C-KD
RKS2309+1425	4005 ± 32	-0.14 ± 0.06	4.69 ± 0.10	<7 ± NM	5.90 ± 0.63	0.63 ± 0.09	1.65 ± 0.25	0.52 ± 0.10	0.03 ± 0.01	C-KD
RKS2310-2955	4884 ± 33	0.04 ± 0.06	4.49 ± 0.09	<7 ± NM	4.15 ± 0.29	0.93 ± 0.09	1.71 ± 0.26	0.54 ± 0.10	0.03 ± 0.01	C-KD
RKS2316+0541	3920 ± 34	-0.04 ± 0.12	4.68 ± 0.11	<7 ± NM	5.76 ± 0.65	0.60 ± 0.09	1.63 ± 0.24	0.48 ± 0.09	0.04 ± 0.01	C-KD
RKS2317-2323	3776 ± 35	-0.24 ± 0.12	4.79 ± 0.12	<7 ± NM	5.12 ± 0.47	0.56 ± 0.08	1.51 ± 0.23	0.53 ± 0.10	0.05 ± 0.01	C-KD
RKS2323-1045	4956 ± 57	-0.30 ± 0.08	4.56 ± 0.10	<7 ± NM	3.19 ± 0.18	0.94 ± 0.10	1.80 ± 0.27	0.51 ± 0.10	0.03 ± 0.01	C-KD
RKS2326+0853	3855 ± 34	0.08 ± 0.11	4.67 ± 0.11	<7 ± NM	5.48 ± 0.59	0.62 ± 0.08	1.42 ± 0.21	0.56 ± 0.11	0.04 ± 0.01	C-KD
RKS2327-0117	4114 ± 44	-0.30 ± 0.05	4.69 ± 0.09	<7 ± NM	5.87 ± 0.57	0.70 ± 0.09	1.52 ± 0.23	0.56 ± 0.11	0.04 ± 0.01	C-KD
RKS2328+1604	4378 ± 37	-0.43 ± 0.06	4.66 ± 0.09	<7 ± NM	5.14 ± 0.41	0.78 ± 0.12	0.60 ± 0.09	1.00 ± 0.19	0.01 ± 0.01	C-KD
RKS2332-1650	4205 ± 49	-0.04 ± 0.08	4.67 ± 0.10	<7 ± NM	5.87 ± 0.62	0.58 ± 0.06	1.47 ± 0.22	0.46 ± 0.09	0.04 ± 0.01	C-KD
RKS2335+0136	4112 ± 31	0.05 ± 0.13	4.66 ± 0.09	<7 ± NM	5.69 ± 0.62	0.27 ± 0.03	1.28 ± 0.19	0.49 ± 0.09	0.03 ± 0.01	A
RKS2340+2021	4604 ± 68	0.15 ± 0.07	4.55 ± 0.13	<7 ± NM	5.58 ± 0.54	0.81 ± 0.11	1.46 ± 0.22	0.58 ± 0.11	0.03 ± 0.01	C-KD
RKS2342-0234	3937 ± 40	0.04 ± 0.14	4.68 ± 0.10	<7 ± NM	5.97 ± 0.72	0.51 ± 0.06	1.59 ± 0.24	0.47 ± 0.09	0.04 ± 0.01	CB
RKS2345+2933	5109 ± 46	-0.18 ± 0.05	4.56 ± 0.11	<7 ± NM	2.78 ± 0.15	0.98 ± 0.10	1.87 ± 0.28	0.50 ± 0.10	0.03 ± 0.01	CB
RKS2348-1259	4179 ± 59	-0.12 ± 0.09	4.68 ± 0.09	<7 ± NM	5.51 ± 0.54	-0.15 ± 0.02	1.38 ± 0.21	0.41 ± 0.08	0.04 ± 0.01	A

Continued on next page

Table A.3 – continued from previous page

RKSTAR ID	$T_{eff} \pm \sigma$ (K)	[Fe/H] $\pm\sigma$ (dex)	$\log g \pm \sigma$ (dex)	$v \sin i \pm \sigma$ (km s^{-1})	EW[Na I D] $\pm\sigma$ (Å)	EW[Hα] $\pm\sigma$ (Å)	EW[CaII] $\pm\sigma$ (Å)	EW[CaII]$_{ratio}\pm\sigma$ (Å)	EW[Li I] $\pm\sigma$ (Å)	Status
RKS2349+0310	4974 ± 42	-0.21 ± 0.07	4.56 ± 0.10	<7 ± NM	3.68 ± 0.25	0.93 ± 0.13	1.43 ± 0.22	0.60 ± 0.11	0.03 ± 0.01	C-KD
RKS2350-2924	5306 ± 32	0.03 ± 0.06	4.53 ± 0.09	<7 ± NM	2.79 ± 0.19	1.01 ± 0.08	1.79 ± 0.27	0.51 ± 0.10	0.03 ± 0.01	C-KD
RKS2353+2901	4029 ± 42	-0.13 ± 0.10	4.69 ± 0.10	<7 ± NM	5.82 ± 0.61	0.57 ± 0.07	1.49 ± 0.22	0.49 ± 0.09	0.03 ± 0.01	C-KD
RKS2355+2211	4805 ± 35	0.01 ± 0.07	4.51 ± 0.10	<7 ± NM	4.30 ± 0.32	0.80 ± 0.10	1.43 ± 0.21	0.51 ± 0.10	0.02 ± 0.01	C-KD
RKS2358+0949	5124 ± 47	0.26 ± 0.08	4.47 ± 0.11	<7 ± NM	3.85 ± 0.29	0.97 ± 0.08	1.66 ± 0.25	0.55 ± 0.11	0.04 ± 0.01	C-KD
RKS2359-2602	4686 ± 50	-0.05 ± 0.05	4.55 ± 0.11	<7 ± NM	4.82 ± 0.39	0.79 ± 0.11	1.48 ± 0.22	0.51 ± 0.10	0.03 ± 0.01	C-KD
RKS2359+0639	4390 ± 40	0.12 ± 0.07	4.63 ± 0.09	<7 ± NM	6.13 ± 0.63	0.80 ± 0.11	2.00 ± 0.30	0.48 ± 0.09	0.03 ± 0.01	C-KD

CHAPTER B

Spectral Library for Primary Sample K dwarfs

Additional plots can be found online at

`https://hodarijames.github.io/spectral_library/page1.html`

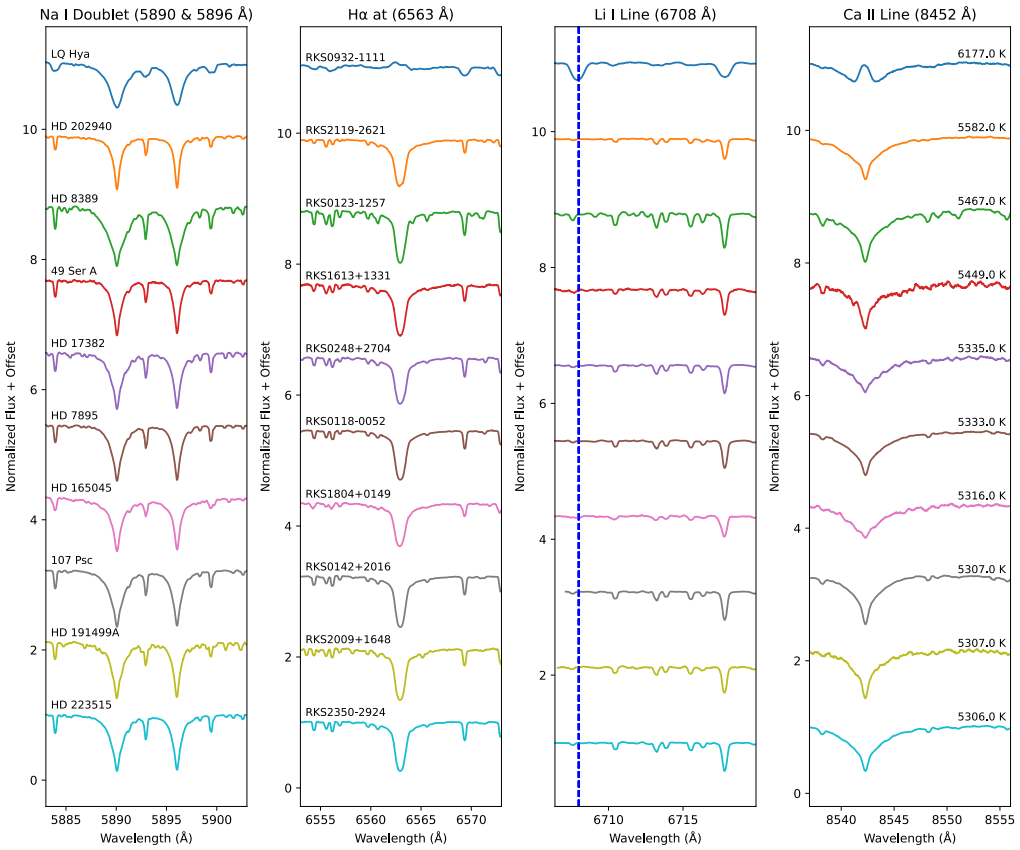

(a) Group 1: RKS Names - RKS0932-1111, RKS2119-2621, RKS0123-1257, RKS1613+1331, RKS0248+2704, RKS0118-0052, RKS1804+0149, RKS0142+2016, RKS2009+1648, RKS2350-2924

Figure B.1 Spectral Plots

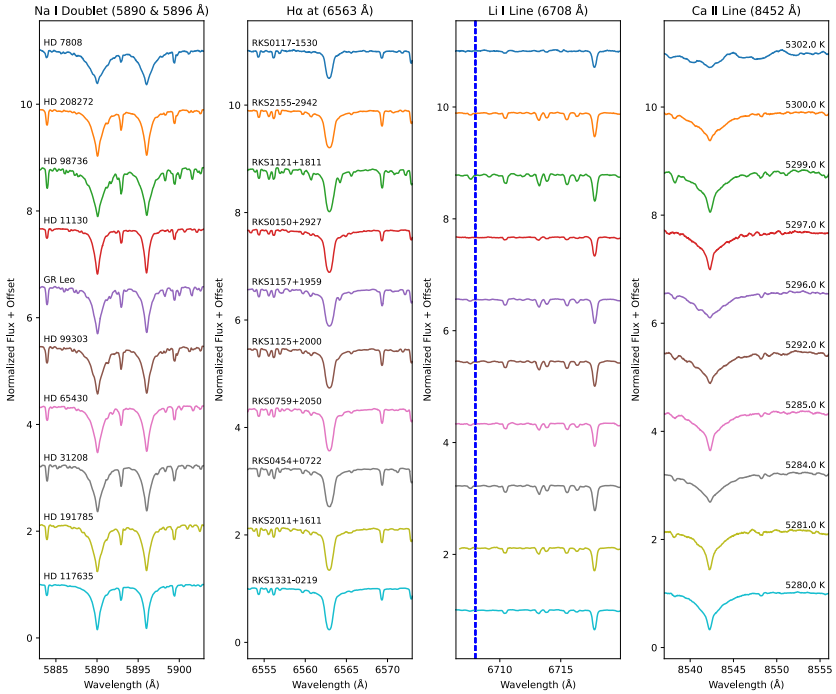

(a) Group 2: RKS Names - RKS0117-1530, RKS2155-2942, RKS1121+1811, RKS0150+2927, RKS1157+1959, RKS1125+2000, RKS0759+2050, RKS0454+0722, RKS2011+1611, RKS1331-0219

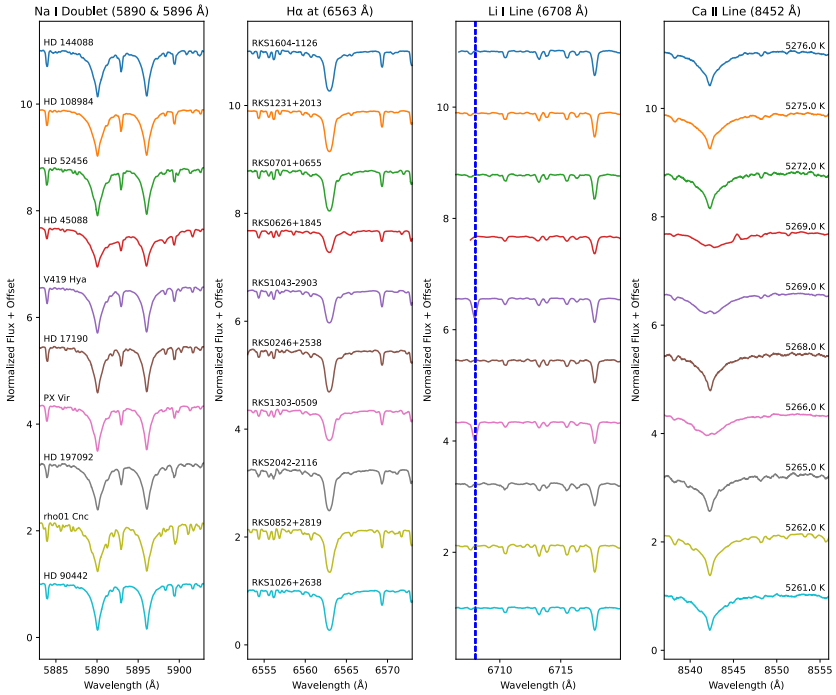

(b) Group 3: RKS Names - RKS1604-1126, RKS1231+2013, RKS0701+0655, RKS0626+1845, RKS1043-2903, RKS0246+2538, RKS1303-0509, RKS2042-2116, RKS0852+2819, RKS1026+2638

Figure B.2 Spectral Plots

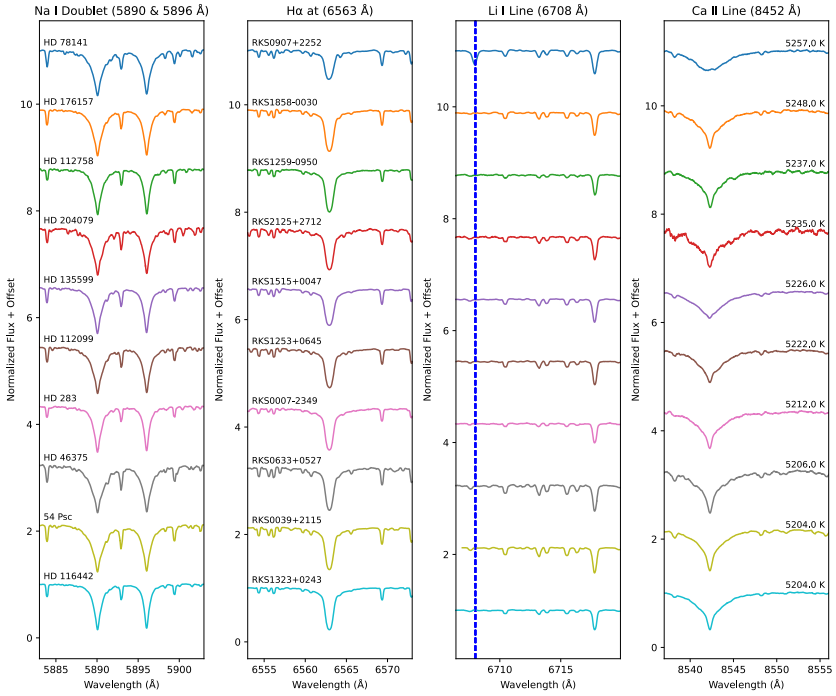

(a) Group 4: RKS Names - RKS0907+2252, RKS1858-0030, RKS1259-0950, RKS2125+2712, RKS1515+0047, RKS1253+0645, RKS0007-2349, RKS0633+0527, RKS0039+2115, RKS1323+0243

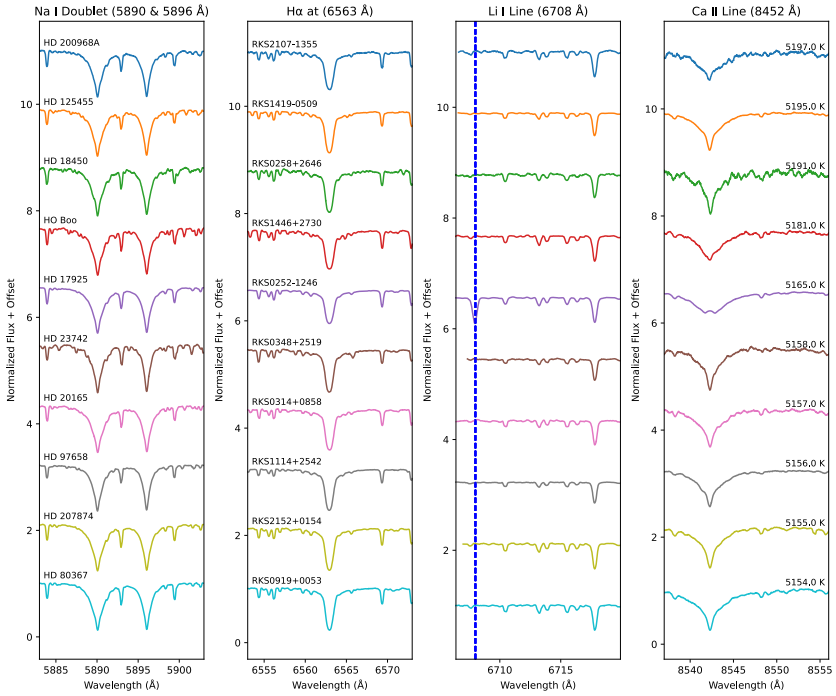

(b) Group 5: RKS Names - RKS2107-1355, RKS1419-0509, RKS0258+2646, RKS1446+2730, RKS0252-1246, RKS0348+2519, RKS0314+0858, RKS1114+2542, RKS2152+0154, RKS0919+0053

Figure B.3 Spectral Plots

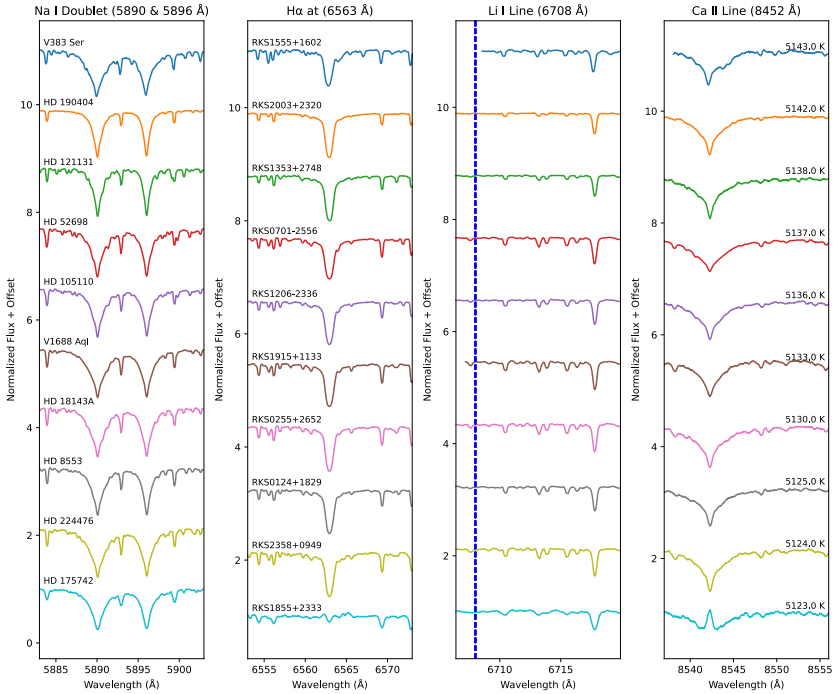

(a) Group 6: RKS Names - RKS1555+1602, RKS2003+2320, RKS1353+2748, RKS0701-2556, RKS1206-2336, RKS1915+1133, RKS0255+2652, RKS0124+1829, RKS2358+0949, RKS1855+2333

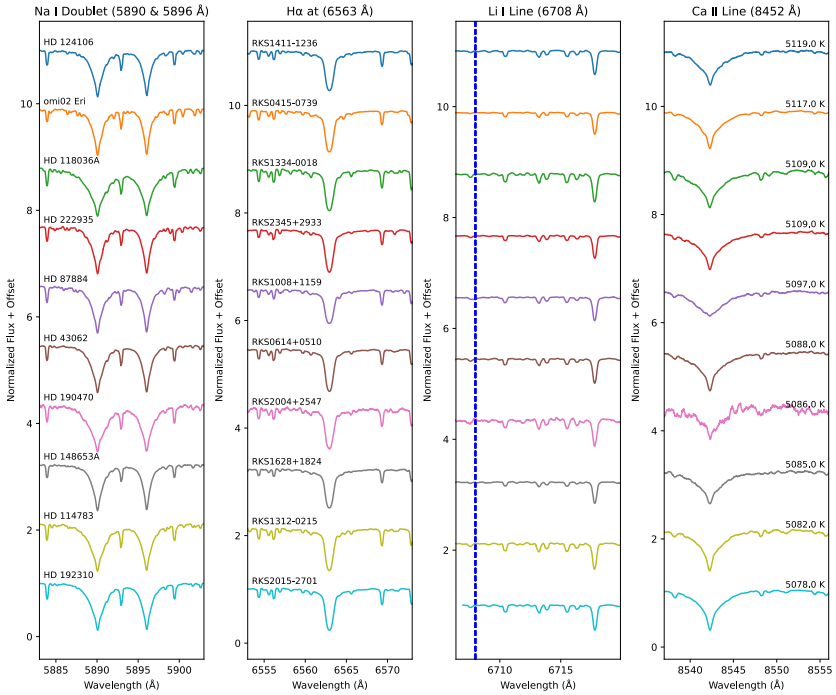

(b) Group 7: RKS Names - RKS1411-1236, RKS0415-0739, RKS1334-0018, RKS2345+2933, RKS1008+1159, RKS0614+0510, RKS2004+2547, RKS1628+1824, RKS1312-0215, RKS2015-2701

Figure B.4 Spectral Plots

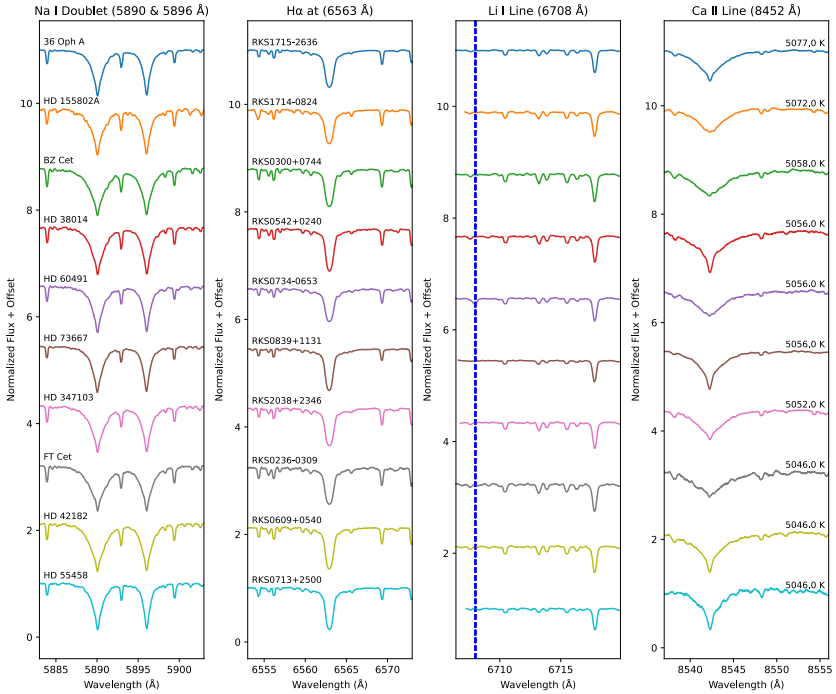

(a) Group 8: RKS Names - RKS1715-2636, RKS1714-0824, RKS0300+0744, RKS0542+0240, RKS0734-0653, RKS0839+1131, RKS2038+2346, RKS0236-0309, RKS0609+0540, RKS0713+2500

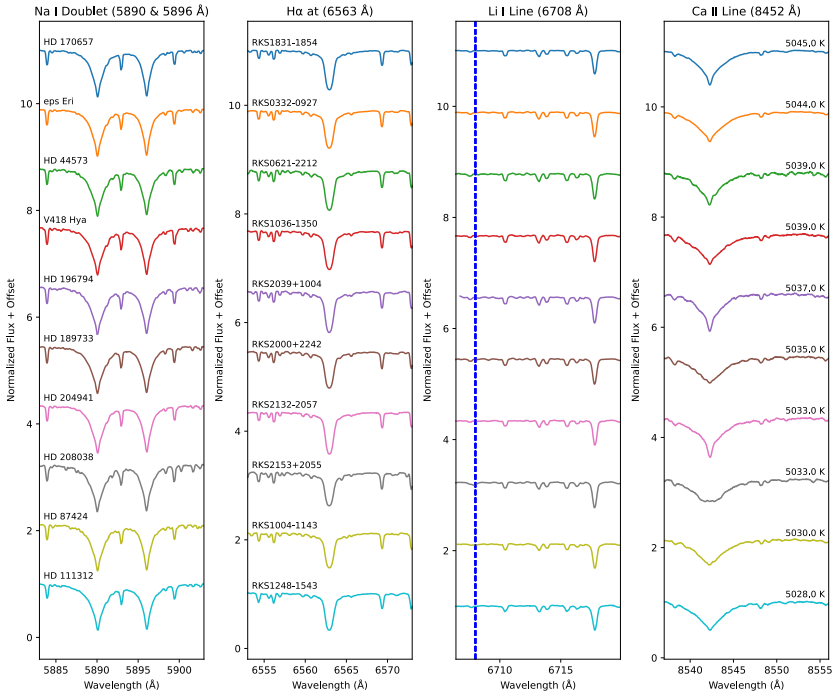

(b) Group 9: RKS Names - RKS1831-1854, RKS0332-0927, RKS0621-2212, RKS1036-1350, RKS2039+1004, RKS2000+2242, RKS2132-2057, RKS2153+2055, RKS1004-1143, RKS1248-1543

Figure B.5 Spectral Plots

CHAPTER C

Table of CHIRON Observations

Table C.1: List of Spectra Used in the Final Analysis

RKS ID	R.A.	Decl.	V	Date & Time of Obs	Exp. Time	SNR
...	(hh mm ss)	(dd mm ss)	(mag)	(UTC)	(s)	...
RKS0000+1659	00 00 48.1	+16 59 17	8.8	2021−12−06 0:34:29	900	88
RKS0001−1656	00 01 25.8	−16 56 54	10.8	2018−12−01 0:59:52	900	31
RKS0007−2349	00 07 32.5	−23 49 07	8.7	2020−12−14 1:22:54	900	71
RKS0012+2142	00 12 33.5	+21 42 48	11.8	2021−08−13 7:17:31	1200	29
RKS0012+2705	00 12 04.0	+27 05 56	8.7	2018−11−08 2:21:41	900	63
RKS0016−1435	00 16 11.0	−14 35 27	10.0	2021−08−13 6:58:21	900	55
RKS0017+2057	00 17 59.1	+20 57 24	11.0	2021−07−27 7:42:39	1800	36
RKS0019−0303	00 19 12.3	−03 03 13	10.9	2018−12−30 1:03:13	900	31
RKS0019−0957	00 19 05.5	−09 57 53	9.9	2017−08−01 8:28:07	900	38
RKS0020+1738	00 20 57.1	+17 38 15	11.3	2021−11−18 0:48:58	1200	44
RKS0021+2531	00 21 16.0	+25 31 27	9.6	2021−11−19 1:01:54	900	70
RKS0022−2701	00 22 23.5	−27 01 57	8.3	2019−10−22 3:11:29	900	40
RKS0024−2701	00 24 25.9	−27 01 36	7.9	2017−08−05 6:55:29	900	113
RKS0036−0930	00 36 00.0	−09 30 56	11.2	2020−12−30 1:41:06	1800	35
RKS0036+2610	00 36 57.9	+26 10 54	9.0	2019−10−15 4:28:21	900	36
RKS0039+2115	00 39 21.8	+21 15 01	5.9	2017−08−21 7:12:12	900	230
RKS0042+2239	00 42 56.7	+22 39 34	11.5	2020−11−06 2:26:58	1800	33
RKS0045+0147	00 45 04.8	+01 47 07	8.0	2017−07−30 9:13:22	900	38
RKS0048+0516	00 48 22.9	+05 16 50	5.7	2017−07−02 10:56:38	900	253

Continued on next page

Table C.1 −− *Continued from previous page*

RKS ID	R.A.	Decl.	V	Date & Time of Obs	Exp. Time	SNR
...	(hh mm ss)	(dd mm ss)	(mag)	(UTC)	(s)	...
RKS0051−2254	00 51 34.0	−22 54 36	9.0	2018−08−12 7:52:40	900	83
RKS0051+1844	00 51 21.7	+18 44 21	9.2	2018−08−13 7:53:46	900	32
RKS0055−2940	00 55 49.2	−29 40 33	9.4	2017−12−16 2:09:38	900	60
RKS0057+0551	00 57 44.5	+05 51 20	10.3	2018−11−06 2:44:30	900	40
RKS0102−1025	01 02 21.1	−10 25 25	10.1	2017−07−12 10:11:53	900	36
RKS0102+0503	01 02 24.5	+05 03 41	8.2	2017−08−06 9:31:01	900	102
RKS0104−2536	01 04 24.1	−25 36 18	9.8	2018−08−16 7:50:32	900	56
RKS0104+2607	01 04 32.4	+26 07 12	10.0	2019−09−20 5:19:31	900	37
RKS0105+1523	01 05 29.9	+15 23 24	8.7	2018−11−20 1:45:11	900	51
RKS0107+2257	01 07 37.8	+22 57 17	8.4	2017−07−12 10:30:30	900	52
RKS0108+1714	01 08 40.3	+17 14 33	10.5	2021−01−06 0:35:09	900	28
RKS0112−2514	01 12 46.1	−25 14 08	9.6	2017−08−03 8:42:26	900	43
RKS0113+1629	01 13 58.8	+16 29 40	9.8	2021−10−27 3:12:33	900	70
RKS0116+2519	01 16 39.3	+25 19 53	10.1	2017−07−17 9:58:20	900	32
RKS0117−1530	01 17 34.0	−15 30 11	9.8	2018−12−02 1:33:19	900	44
RKS0118−0052	01 18 41.0	−00 52 03	8.0	2021−11−30 0:51:40	900	135
RKS0121+2419	01 21 29.3	+24 19 50	10.7	2018−11−05 3:19:20	900	31
RKS0122−2653	01 22 07.6	−26 53 35	8.8	2017−07−21 10:00:54	900	69
RKS0123−1257	01 23 02.6	−12 57 57	7.9	2020−11−01 3:40:06	900	115
RKS0124+1829	01 24 53.9	+18 29 59	8.5	2021−01−10 0:37:58	900	68
RKS0125−0103	01 25 09.4	−01 03 34	9.5	2018−11−21 3:40:26	900	46

Continued on next page

Table C.1 −− *Continued from previous page*

RKS ID	R.A.	Decl.	V	Date & Time of Obs	Exp. Time	SNR
...	(hh mm ss)	(dd mm ss)	(mag)	(UTC)	(s)	...
RKS0129+2143	01 29 04.8	+21 43 23	7.7	2018−09−18 7:03:32	900	52
RKS0135−2046	01 35 45.6	−20 46 13	10.2	2021−08−27 7:02:59	900	42
RKS0139+1515	01 39 56.1	+15 15 33	8.7	2019−10−20 4:53:06	900	32
RKS0142+2016	01 42 29.7	+20 16 06	5.3	2017−07−18 10:20:17	900	245
RKS0146+1224	01 46 38.7	+12 24 42	8.9	2017−07−13 10:29:10	900	34
RKS0150+1817	01 50 28.0	+18 17 46	10.9	2021−08−13 8:22:23	1200	36
RKS0150+2927	01 50 07.8	+29 27 52	8.1	2018−11−18 2:51:35	900	69
RKS0200+2636	02 00 20.1	+26 36 00	11.0	2021−08−17 8:59:19	1200	29
RKS0205−2804	02 05 23.6	−28 04 11	10.9	2020−12−23 0:59:24	900	32
RKS0209−1620	02 09 10.9	−16 20 22	10.9	2020−12−05 3:11:14	900	31
RKS0213−2111	02 13 12.1	−21 11 47	9.8	2017−07−17 10:17:21	900	37
RKS0214−0338	02 14 13.5	−03 38 06	8.6	2017−07−18 10:38:38	900	66
RKS0215−1814	02 15 46.1	−18 14 17	9.1	2018−09−20 8:37:49	900	38
RKS0221−0652	02 21 44.4	−06 52 46	9.1	2019−10−02 5:19:19	900	40
RKS0229−1958	02 29 01.7	−19 58 45	8.8	2018−08−12 9:25:25	900	90
RKS0231−1516	02 31 42.4	−15 16 24	8.7	2017−12−16 2:46:43	900	81
RKS0231−2001	02 31 30.8	−20 01 41	10.2	2019−10−26 4:13:30	900	31
RKS0236−0309	02 36 41.7	−03 09 22	8.1	2017−07−15 10:43:21	900	43
RKS0236−2331	02 36 00.7	−23 31 16	8.3	2017−07−18 10:01:34	900	66
RKS0236−2710	02 36 00.7	−27 10 42	9.5	2019−10−02 5:37:32	900	38
RKS0236+0653	02 36 04.9	+06 53 12	5.8	2019−10−11 6:17:02	900	216

Continued on next page

Table C.1 −− *Continued from previous page*

RKS ID	R.A.	Decl.	V	Date & Time of Obs	Exp. Time	SNR
...	(hh mm ss)	(dd mm ss)	(mag)	(UTC)	(s)	...
RKS0240+0111	02 40 42.8	+01 11 55	9.5	2021−02−17 0:12:25	900	39
RKS0242+0322	02 42 32.5	+03 22 26	10.1	2019−10−20 6:12:14	900	31
RKS0243+1925	02 43 20.8	+19 25 45	8.2	2018−10−02 6:49:04	900	81
RKS0246−2305	02 46 42.8	−23 05 11	10.3	2017−08−04 10:16:27	900	31
RKS0246+1146	02 46 17.2	+11 46 30	8.6	2019−10−02 5:55:58	900	62
RKS0246+2538	02 46 15.2	+25 38 59	7.9	2019−09−26 5:53:45	900	56
RKS0247+2842	02 47 55.8	+28 42 44	11.1	2018−11−08 4:43:00	900	31
RKS0248−1145	02 48 06.5	−11 45 47	10.8	2017−12−15 2:51:21	900	33
RKS0248+2704	02 48 09.1	+27 04 07	7.6	2019−01−03 1:13:26	900	77
RKS0250+1542	02 50 36.8	+15 42 35	8.9	2018−09−29 7:32:22	900	38
RKS0251−0816	02 51 44.4	−08 16 09	9.8	2019−10−15 6:59:33	900	33
RKS0251+1038	02 51 42.8	+10 38 42	10.0	2019−10−15 6:37:50	900	35
RKS0252−1246	02 52 32.1	−12 46 10	6.1	2019−10−02 6:14:44	900	191
RKS0255+2652	02 55 39.0	+26 52 23	7.5	2020−12−20 1:36:05	900	81
RKS0255+2807	02 55 41.2	+28 07 47	11.1	2018−10−07 5:50:56	900	30
RKS0257−2458	02 57 13.1	−24 58 30	7.8	2020−10−31 4:35:33	900	119
RKS0258+2646	02 58 52.4	+26 46 26	8.2	2019−10−01 6:22:13	900	37
RKS0300+0744	03 00 02.8	+07 44 59	8.0	2017−08−05 9:52:44	900	83
RKS0303+2006	03 03 49.0	+20 06 39	8.6	2019−11−21 4:16:57	900	52
RKS0306+0157	03 06 26.7	+01 57 54	9.1	2020−10−27 5:34:33	900	81
RKS0308−2410	03 08 25.6	−24 10 03	10.1	2021−08−18 8:26:05	900	46

Continued on next page

Table C.1 −− *Continued from previous page*

RKS ID	R.A.	Decl.	V	Date & Time of Obs	Exp. Time	SNR
...	(hh mm ss)	(dd mm ss)	(mag)	(UTC)	(s)	...
RKS0308−2445	03 08 06.6	−24 45 34	10.2	...	...	...
RKS0310+1203	03 10 15.1	+12 03 01	9.4	2020−11−03 4:38:29	900	56
RKS0314−2626	03 14 44.6	−26 26 46	9.2	2018−10−02 8:02:24	900	68
RKS0314+0858	03 14 47.2	+08 58 50	7.8	2019−10−21 4:47:01	900	63
RKS0320+0827	03 20 29.1	+08 27 16	9.6	2019−10−08 7:06:54	900	37
RKS0322+2709	03 22 28.1	+27 09 21	11.0	2020−12−06 3:23:24	900	28
RKS0324−0521	03 24 59.7	−05 21 49	7.9	2019−09−18 7:52:13	900	88
RKS0329−1140	03 29 19.7	−11 40 42	10.0	2018−08−14 10:10:03	900	43
RKS0329−2406	03 29 22.8	−24 06 03	9.2	2018−08−16 9:36:04	900	67
RKS0332−0927	03 32 55.8	−09 27 29	3.7	2017−08−02 10:24:15	404	344
RKS0341+0336	03 41 10.5	+03 36 40	9.6	2021−11−12 4:03:36	900	82
RKS0342−2427	03 42 44.6	−24 27 58	9.2	2019−10−05 6:45:05	900	51
RKS0343−1253	03 43 06.1	−12 53 39	10.9	2019−10−10 7:09:44	900	27
RKS0343−1906	03 43 55.3	−19 06 39	7.1	2019−09−18 8:10:39	900	112
RKS0343+1640	03 43 52.5	+16 40 19	10.0	2019−03−06 0:00:20	900	46
RKS0344+1155	03 44 51.1	+11 55 12	9.2	2018−10−03 6:46:19	900	42
RKS0345−2751	03 45 24.1	−27 51 44	8.2	2019−12−16 2:06:56	900	60
RKS0348+1512	03 48 32.9	+15 12 07	9.5	2020−12−02 3:48:15	900	46
RKS0348+2519	03 48 26.3	+25 19 23	8.6	2019−11−20 4:19:05	900	55
RKS0349−1329	03 49 15.9	−13 29 29	11.1	2021−11−20 3:05:47	1200	51
RKS0349+0120	03 49 35.6	+01 20 53	8.6	...	...	...

Continued on next page

Table C.1 −− *Continued from previous page*

RKS ID	R.A.	Decl.	V	Date & Time of Obs	Exp. Time	SNR
...	(hh mm ss)	(dd mm ss)	(mag)	(UTC)	(s)	...
RKS0350−2349	03 50 19.5	−23 49 44	9.9	2019−10−10 7:45:00	900	37
RKS0354−0649	03 54 35.4	−06 49 33	9.0	2019−10−10 6:51:39	900	59
RKS0357−0109	03 57 28.6	−01 09 34	8.1	2019−09−19 8:17:34	900	61
RKS0404+2634	04 04 15.2	+26 34 24	11.2	2021−11−18 4:22:50	1200	38
RKS0406−2051	04 06 34.8	−20 51 11	9.7	2020−01−21 0:36:01	900	36
RKS0407+1413	04 07 43.9	+14 13 24	10.8	2021−11−23 4:32:57	1200	47
RKS0408+1220	04 08 30.8	+12 20 16	8.6	2020−02−09 0:23:08	900	44
RKS0414+0301	04 14 30.2	+03 01 19	8.8	2020−02−01 0:27:55	900	43
RKS0415−0739	04 15 16.3	−07 39 10	4.4	2020−01−31 0:30:40	900	362
RKS0417+2033	04 17 26.9	+20 33 17	9.6	2021−11−29 3:00:29	900	72
RKS0417+2240	04 17 06.8	+22 40 23	9.8	2020−01−20 1:06:03	900	33
RKS0419−0408	04 19 05.7	−04 08 55	10.5	2020−02−11 0:42:20	900	33
RKS0420−1445	04 20 10.5	−14 45 39	9.8	2020−10−27 5:58:01	900	54
RKS0421−1945	04 21 31.6	−19 45 23	10.4	2018−10−03 7:25:48	900	30
RKS0427+2426	04 27 52.9	+24 26 41	9.4	2018−10−07 7:34:38	900	40
RKS0429+2155	04 29 00.1	+21 55 21	8.3	2020−02−07 0:42:09	900	66
RKS0430+0058	04 30 16.7	+00 58 47	10.5	2018−12−17 3:48:55	900	32
RKS0436+2707	04 36 48.2	+27 07 55	8.1	2020−10−30 6:01:20	900	102
RKS0439+0952	04 39 42.6	+09 52 19	9.2	...	...	...
RKS0441+2054	04 41 18.8	+20 54 05	8.1	2021−03−01 23:57:47	900	97
RKS0443+2741	04 43 35.4	+27 41 14	8.0	2020−02−03 0:42:31	900	61

Continued on next page

Table C.1 −− *Continued from previous page*

RKS ID	R.A.	Decl.	V	Date & Time of Obs	Exp. Time	SNR
...	(hh mm ss)	(dd mm ss)	(mag)	(UTC)	(s)	...
RKS0445+0938	04 45 27.2	+09 38 27	11.2	2021−11−29 2:37:47	1200	44
RKS0448−1056	04 48 01.1	−10 56 01	9.5	2020−02−02 3:06:08	900	42
RKS0449−1447	04 49 32.7	−14 47 22	10.9	2018−10−10 6:18:24	900	38
RKS0451+2837	04 51 33.3	+28 37 49	9.6	2021−12−12 3:57:24	900	61
RKS0453+2214	04 53 04.7	+22 14 06	8.8	2017−12−15 3:46:03	900	59
RKS0454+0722	04 54 16.6	+07 22 22	8.2	2021−11−30 4:05:02	900	129
RKS0455−2833	04 55 41.9	−28 33 50	8.1	2020−01−31 0:49:08	900	76
RKS0500−0545	05 00 48.9	−05 45 13	6.2	2020−01−31 1:09:56	889	176
RKS0503−2315	05 03 21.8	−23 15 01	9.3	2020−01−24 1:32:07	900	40
RKS0503+0322	05 03 32.1	+03 22 56	11.1	2021−12−08 3:41:03	1200	39
RKS0506−1102	05 06 30.0	−11 02 34	9.6	2021−11−30 4:40:27	900	77
RKS0506+1426	05 06 42.2	+14 26 46	7.7	...	...	...
RKS0512+1943	05 12 53.4	+19 43 19	9.9	2020−02−15 0:43:19	900	30
RKS0513−2158	05 13 59.1	−21 58 24	10.5	2021−01−15 4:31:46	900	30
RKS0514+0039	05 14 48.1	+00 39 43	10.0	2018−11−21 5:24:08	900	39
RKS0514+1952	05 14 17.0	+19 52 58	9.5	2021−11−27 4:31:19	900	67
RKS0518−2123	05 18 47.1	−21 23 37	9.4	2018−10−10 6:54:11	900	38
RKS0519−0304	05 19 12.6	−03 04 25	7.8	2019−03−05 0:49:27	753	104
RKS0519−1550	05 19 59.5	−15 50 22	8.7	2018−10−10 7:29:20	900	49
RKS0522+0236	05 22 37.4	+02 36 11	7.8	2020−11−28 5:49:26	900	118
RKS0523+1719	05 23 38.3	+17 19 26	7.9	2020−02−01 0:46:07	900	67

Continued on next page

Table C.1 −− *Continued from previous page*

RKS ID	R.A.	Decl.	V	Date & Time of Obs	Exp. Time	SNR
...	(hh mm ss)	(dd mm ss)	(mag)	(UTC)	(s)	...
RKS0528−0329	05 28 26.0	−03 29 58	7.7	2020−02−08 2:18:54	900	93
RKS0533−2643	05 33 04.6	−26 43 28	9.1	2020−02−28 0:10:36	900	47
RKS0534−2328	05 34 48.6	−23 28 08	8.8	2018−11−08 8:25:57	900	74
RKS0535+2805	05 35 00.8	+28 05 54	10.1	2021−01−10 2:39:13	900	30
RKS0536+1119	05 36 30.9	+11 19 40	8.9	2020−02−29 0:00:51	900	58
RKS0542+0240	05 42 45.8	+02 40 44	8.6	2018−11−22 7:08:38	900	69
RKS0544−2225	05 44 26.5	−22 25 18	6.2	2020−10−26 8:04:39	422	181
RKS0549−1734	05 49 22.5	−17 34 44	8.5	2021−12−17 2:49:25	900	105
RKS0552−2246	05 52 31.9	−22 46 36	10.6	2021−12−18 3:48:04	1200	52
RKS0553−0559	05 53 00.2	−05 59 41	9.7	2020−03−01 23:59:13	900	40
RKS0554−1942	05 54 30.4	−19 42 05	10.6	2019−10−26 8:58:34	720	28
RKS0554+0208	05 54 28.5	+02 08 32	8.8	2020−02−29 0:19:16	900	50
RKS0600+2101	06 00 53.9	+21 01 15	10.0	2018−11−21 6:32:48	900	37
RKS0602+0848	06 02 44.2	+08 48 30	10.8	2021−01−24 2:44:54	900	32
RKS0608+2630	06 08 13.2	+26 30 08	9.4	2019−11−26 5:26:26	900	40
RKS0609+0009	06 09 46.1	+00 09 32	10.9	2019−12−03 7:09:31	900	32
RKS0609+0540	06 09 35.9	+05 40 08	8.5	2018−11−22 7:43:29	900	71
RKS0612+1023	06 12 08.4	+10 23 39	9.7	2019−12−08 6:12:33	900	39
RKS0614+0510	06 14 24.4	+05 10 05	8.4	2020−11−27 6:07:56	900	86
RKS0616+2512	06 16 39.5	+25 12 21	9.4	2020−10−30 7:23:03	900	62
RKS0617+1759	06 17 25.8	+17 59 21	10.3	2018−01−31 2:32:04	900	34

Continued on next page

Table C.1 −− *Continued from previous page*

RKS ID	R.A.	Decl.	V	Date & Time of Obs	Exp. Time	SNR
...	(hh mm ss)	(dd mm ss)	(mag)	(UTC)	(s)	...
RKS0618−1352	06 18 22.1	−13 52 07	9.9	2020−03−02 0:16:55	900	34
RKS0620+0215	06 20 13.2	+02 15 32	9.8	2020−02−19 0:46:02	900	37
RKS0621−2212	06 21 33.1	−22 12 53	8.5	2020−03−02 0:34:34	900	61
RKS0626+1845	06 26 10.2	+18 45 24	6.8	2019−11−08 7:23:41	900	148
RKS0629+2700	06 29 05.5	+27 00 31	8.6	2018−11−19 6:49:22	900	62
RKS0630−1148	06 30 07.3	−11 48 32	9.1	2020−03−03 0:06:12	900	47
RKS0630+2104	06 30 24.9	+21 04 17	11.3	2021−10−19 7:41:16	1800	27
RKS0632−2701	06 32 08.8	−27 01 58	11.4	2020−12−27 3:36:41	1800	35
RKS0633+0527	06 33 12.6	+05 27 46	7.9	2020−02−05 2:22:59	900	76
RKS0637+1945	06 37 05.2	+19 45 10	10.2	2020−02−28 0:41:02	900	36
RKS0641+2357	06 41 15.7	+23 57 27	8.1	2020−02−15 1:43:55	900	62
RKS0647−1815	06 47 15.7	−18 15 31	10.6	2018−11−21 7:27:14	900	32
RKS0652−0510	06 52 18.0	−05 10 25	6.6	2020−03−03 0:23:39	900	150
RKS0652−2306	06 52 59.6	−23 06 27	9.0	2020−02−07 3:18:19	900	46
RKS0658−1259	06 58 26.0	−12 59 30	9.1	2018−02−28 3:20:36	900	38
RKS0700−2847	07 00 09.4	−28 47 02	10.8	2020−03−15 23:55:04	900	30
RKS0701−2556	07 01 13.7	−25 56 55	6.7	2021−01−24 3:20:56	900	179
RKS0701+0655	07 01 35.5	+06 55 36	8.2	2020−02−28 0:58:55	900	57
RKS0702−0647	07 02 42.9	−06 47 57	8.4	2020−02−19 1:05:02	900	73
RKS0705+2728	07 05 42.2	+27 28 14	10.1	2020−01−24 3:40:45	900	31
RKS0706+2358	07 06 52.1	+23 58 08	10.1	2018−02−10 1:41:33	900	39

Continued on next page

Table C.1 −− *Continued from previous page*

RKS ID	R.A.	Decl.	V	Date & Time of Obs	Exp. Time	SNR
...	(hh mm ss)	(dd mm ss)	(mag)	(UTC)	(s)	...
RKS0707+0326	07 07 09.3	+03 26 50	9.8	2020−10−30 7:40:51	900	54
RKS0708−0958	07 08 09.3	−09 58 07	8.9	2018−12−20 5:55:09	900	63
RKS0708+2950	07 08 04.2	+29 50 04	8.3	2018−12−16 6:07:45	900	58
RKS0710−1425	07 10 49.5	−14 25 58	10.0	2018−12−17 4:42:05	900	41
RKS0712−2453	07 12 04.8	−24 53 31	10.4	2020−03−07 3:10:36	900	29
RKS0713+2500	07 13 53.1	+25 00 40	8.4	2018−12−19 5:27:33	900	59
RKS0716−0339	07 16 10.6	−03 39 57	9.0	2020−03−05 0:34:50	900	46
RKS0723−2001	07 23 29.2	−20 01 24	9.9	2018−12−30 3:45:00	900	42
RKS0723+1257	07 23 47.0	+12 57 52	8.2	2018−12−29 4:38:01	900	59
RKS0723+2024	07 23 43.5	+20 24 58	10.0	2020−02−07 2:47:35	900	38
RKS0724−1753	07 24 34.2	−17 53 31	10.3	2020−02−18 1:29:50	900	35
RKS0725−1041	07 25 29.8	−10 41 59	11.6	2021−12−12 6:17:52	1200	37
RKS0726−1546	07 26 26.5	−15 46 13	9.2	2022−10−15 8:59:55	900	80
RKS0730−0340	07 30 17.5	−03 40 24	10.4	2020−03−16 0:12:54	900	37
RKS0731+1436	07 31 07.7	+14 36 50	8.9	...	...	...
RKS0732+1719	07 32 02.8	+17 19 09	11.0	2022−03−20 1:00:04	900	38
RKS0734−0653	07 34 26.1	−06 53 48	8.2	2020−03−03 0:41:07	900	68
RKS0739−0335	07 39 59.3	−03 35 51	7.2	2020−02−20 3:31:17	900	118
RKS0741−2921	07 41 17.4	−29 21 32	10.7	2020−02−19 1:48:22	900	30
RKS0745+0208	07 45 01.1	+02 08 14	10.2	2020−03−02 1:10:25	900	29
RKS0752+2555	07 52 47.4	+25 55 35	8.6	2020−03−16 0:31:00	900	47

Continued on next page

Table C.1 −− *Continued from previous page*

RKS ID	R.A.	Decl.	V	Date & Time of Obs	Exp. Time	SNR
...	(hh mm ss)	(dd mm ss)	(mag)	(UTC)	(s)	...
RKS0754−0124	07 54 34.1	−01 24 44	7.4	...	...	...
RKS0754−2518	07 54 10.8	−25 18 11	9.8	2020−02−05 5:16:11	900	40
RKS0754+1914	07 54 54.0	+19 14 10	7.8	2020−03−01 1:46:05	900	67
RKS0757−0048	07 57 57.7	−00 48 51	8.1	2020−03−09 1:03:21	900	79
RKS0758−1501	07 58 25.5	−15 01 13	9.3	2018−11−19 6:31:22	900	54
RKS0758−2537	07 58 04.3	−25 37 35	8.4	2020−03−10 0:55:32	900	68
RKS0759+2050	07 59 33.9	+20 50 38	7.7	2020−03−03 1:49:45	900	85
RKS0808+2106	08 08 13.1	+21 06 18	9.4	2019−01−13 5:11:19	900	56
RKS0813−1355	08 13 08.4	−13 55 01	9.4	2020−01−07 6:54:28	900	43
RKS0814+1301	08 14 35.9	+13 01 22	8.8	2020−03−05 2:11:58	900	55
RKS0815−2600	08 15 40.0	−26 00 35	10.1	2020−03−10 1:13:08	900	32
RKS0817+1717	08 17 08.0	+17 17 56	9.4	2020−03−15 0:54:59	900	41
RKS0819+0120	08 19 19.0	+01 20 19	8.4	2020−03−11 0:33:04	900	55
RKS0820+1404	08 20 55.3	+14 04 16	9.8	2020−03−11 0:50:51	900	33
RKS0823+2150	08 23 30.9	+21 50 57	9.5	2020−03−11 1:08:36	900	33
RKS0827+2855	08 27 11.4	+28 55 53	9.6	2020−03−12 1:38:11	900	30
RKS0832−2323	08 32 33.3	−23 23 06	10.2	2020−03−12 3:24:58	900	33
RKS0838−0415	08 38 19.2	−04 15 29	11.3	2021−01−27 5:29:16	1800	36
RKS0838−1315	08 38 45.2	−13 15 24	9.7	2020−03−13 2:26:36	900	36
RKS0839+0657	08 39 00.2	+06 57 19	7.9	2020−03−13 2:44:26	900	81
RKS0839+1131	08 39 50.7	+11 31 21	7.6	2020−11−28 8:14:25	900	126

Continued on next page

Table C.1 −− *Continued from previous page*

RKS ID	R.A.	Decl.	V	Date & Time of Obs	Exp. Time	SNR
...	(hh mm ss)	(dd mm ss)	(mag)	(UTC)	(s)	...
RKS0840−0628	08 40 00.2	−06 28 33	9.9	2021−11−01 8:12:41	900	64
RKS0848+0628	08 48 26.1	+06 28 06	10.4	2017−12−15 7:31:57	900	32
RKS0850+0751	08 50 42.2	+07 51 52	9.8	2021−03−01 2:41:10	900	74
RKS0852+2819	08 52 35.8	+28 19 50	6.0	2021−01−20 5:14:32	900	230
RKS0855+0132	08 55 07.6	+01 32 47	10.0	2021−01−29 3:58:50	900	52
RKS0900+2127	09 00 47.4	+21 27 13	8.8	...	...	...
RKS0901+1515	09 01 17.4	+15 15 56	9.3	2020−12−11 6:39:14	900	69
RKS0904−1554	09 04 20.6	−15 54 51	8.8	2018−03−25 1:21:12	900	81
RKS0905+2517	09 05 18.4	+25 17 52	10.4	2021−01−12 5:55:35	900	35
RKS0907+2252	09 07 18.0	+22 52 21	8.0	2021−03−24 2:28:12	900	105
RKS0909+0512	09 09 54.1	+05 12 12	8.4	2021−01−12 6:13:22	900	97
RKS0914+0426	09 14 53.6	+04 26 34	7.9	2018−01−31 5:32:52	900	113
RKS0917−0323	09 17 55.3	−03 23 14	7.8	2020−12−22 8:31:34	900	110
RKS0918+2718	09 18 21.5	+27 18 41	9.5	2021−02−23 3:25:22	900	36
RKS0919+0053	09 19 28.3	+00 53 49	8.2	2021−01−03 7:05:29	900	80
RKS0920−0545	09 20 44.3	−05 45 14	9.1	2021−01−26 5:31:03	900	69
RKS0929−0522	09 29 35.0	−05 22 21	9.7	2018−12−17 6:34:39	900	41
RKS0929+0539	09 29 54.8	+05 39 18	7.2	2020−03−14 2:41:45	900	36
RKS0932−1111	09 32 25.5	−11 11 04	7.8	2020−03−02 4:12:42	900	89
RKS0932+2909	09 32 11.1	+29 09 25	11.4	2020−12−05 8:25:14	900	28
RKS0937+2231	09 37 58.3	+22 31 23	9.9	2018−03−26 1:23:09	900	44

Continued on next page

Table C.1 −− *Continued from previous page*

RKS ID	R.A.	Decl.	V	Date & Time of Obs	Exp. Time	SNR
...	(hh mm ss)	(dd mm ss)	(mag)	(UTC)	(s)	...
RKS0937+2241	09 37 11.3	+22 41 38	9.5	2019−01−31 5:09:42	900	39
RKS0938+0240	09 38 23.9	+02 40 36	11.9	2021−01−17 5:57:26	1800	32
RKS0947+0134	09 47 16.6	+01 34 36	11.0	2019−02−17 4:24:35	900	32
RKS0952+0307	09 52 39.1	+03 07 48	10.6	2018−02−12 4:00:32	900	40
RKS0952+0313	09 52 11.3	+03 13 18	8.9	...	...	...
RKS0959−0911	09 59 11.3	−09 11 00	9.9	2020−12−16 7:18:24	900	49
RKS1000+2433	10 00 01.7	+24 33 10	7.9	...	...	...
RKS1001−1525	10 01 37.2	−15 25 29	8.7	2018−02−12 4:38:50	900	86
RKS1004−1143	10 04 37.6	−11 43 46	8.2	2021−01−05 7:55:34	900	98
RKS1005+2629	10 05 26.5	+26 29 16	9.1	2018−02−11 5:02:18	900	62
RKS1006+0257	10 06 56.8	+02 57 51	10.0	2019−03−03 4:12:52	900	31
RKS1008+1159	10 08 12.7	+11 59 49	8.1	2021−02−17 5:26:58	900	78
RKS1011−2425	10 11 45.0	−24 25 33	11.0	2021−01−12 8:17:05	900	31
RKS1020−0128	10 20 43.4	−01 28 11	9.4	2018−03−11 3:14:34	900	61
RKS1024−1024	10 24 14.9	−10 24 21	10.0	2020−02−05 6:23:19	900	33
RKS1026−0631	10 26 41.2	−06 31 34	9.8	2022−03−01 4:18:08	900	62
RKS1026+2638	10 26 59.5	+26 38 29	8.2	2018−03−11 3:32:22	894	81
RKS1028+0644	10 28 10.4	+06 44 06	8.5	2018−03−11 3:49:53	900	86
RKS1030−2114	10 30 21.9	−21 14 12	9.6	2020−03−12 5:58:34	900	40
RKS1032+0830	10 32 00.6	+08 30 38	10.8	2021−01−20 6:54:24	900	31
RKS1036−1350	10 36 30.7	−13 50 35	8.7	2018−03−13 4:11:25	900	80

Continued on next page

Table C.1 −− *Continued from previous page*

RKS ID	R.A.	Decl.	V	Date & Time of Obs	Exp. Time	SNR
...	(hh mm ss)	(dd mm ss)	(mag)	(UTC)	(s)	...
RKS1043−2903	10 43 28.2	−29 03 51	7.7	2020−12−28 8:02:13	900	114
RKS1046−2435	10 46 36.9	−24 35 07	9.4	2019−01−29 6:46:05	900	47
RKS1053−1422	10 53 22.5	−14 22 28	9.3	2021−01−16 8:22:41	900	54
RKS1054−0432	10 54 49.1	−04 32 30	10.4	2020−02−20 7:01:58	900	37
RKS1056+0723	10 56 30.7	+07 23 18	7.4	2019−03−05 4:08:17	570	94
RKS1057+2856	10 57 11.4	+28 56 16	8.9	2019−04−11 2:05:02	900	60
RKS1059+2526	10 59 38.3	+25 26 15	8.5	2021−03−03 4:42:49	900	61
RKS1102−0919	11 02 50.1	−09 19 49	9.0	2018−02−27 4:37:26	900	71
RKS1108−2816	11 08 06.3	−28 16 04	9.3	2021−11−20 8:13:14	900	87
RKS1108+1546	11 08 31.7	+15 46 03	9.8	2021−04−01 3:05:01	900	45
RKS1111−1057	11 11 10.7	−10 57 03	9.2	2018−03−12 3:51:56	900	70
RKS1111−1459	11 11 33.1	−14 59 28	9.1	2018−07−01 23:10:50	900	37
RKS1113+0428	11 13 13.2	+04 28 56	8.7	2018−02−26 5:40:12	900	87
RKS1114−2306	11 14 48.1	−23 06 17	9.0	...	...	...
RKS1114+2542	11 14 33.1	+25 42 37	7.8	2021−02−03 5:51:50	1800	108
RKS1115−1808	11 15 20.7	−18 08 37	10.2	2021−01−07 8:05:18	900	48
RKS1116−1441	11 16 22.1	−14 41 36	10.0	2018−03−13 5:22:10	900	55
RKS1117−0158	11 17 13.6	−01 58 54	9.7	2020−02−29 5:57:50	900	36
RKS1117−2748	11 17 07.5	−27 48 48	9.8	2018−03−13 5:40:16	900	63
RKS1121−2027	11 21 26.6	−20 27 13	8.6	2018−02−26 6:20:21	900	103
RKS1121+1811	11 21 49.3	+18 11 24	7.9	2021−03−14 4:36:16	900	99

Continued on next page

Table C.1 −− *Continued from previous page*

RKS ID	R.A.	Decl.	V	Date & Time of Obs	Exp. Time	SNR
...	(hh mm ss)	(dd mm ss)	(mag)	(UTC)	(s)	...
RKS1125+2000	11 25 39.9	+20 00 07	8.3	2018−03−29 2:51:50	900	85
RKS1126+1517	11 26 49.9	+15 17 38	10.5	2022−04−03 3:26:47	900	45
RKS1127+0358	11 27 38.5	+03 58 35	10.6	2021−07−08 22:43:40	900	39
RKS1128+0731	11 28 27.7	+07 31 02	10.2	2018−06−19 23:40:18	900	38
RKS1134−1314	11 34 50.4	−13 14 31	10.4	2020−12−18 8:21:25	900	33
RKS1135+1658	11 35 59.1	+16 58 05	9.5	2019−04−07 3:27:11	900	52
RKS1139−2741	11 39 08.1	−27 41 46	10.0	2019−02−18 3:18:19	900	45
RKS1141+0508	11 41 49.5	+05 08 26	9.6	2019−07−05 23:30:28	900	53
RKS1147−1149	11 47 03.8	−11 49 26	9.0	2021−01−10 8:17:24	900	71
RKS1152+1845	11 52 08.3	+18 45 18	8.4	2018−06−19 23:02:16	900	67
RKS1154+2844	11 54 57.4	+28 44 15	10.5	2022−03−13 4:35:11	900	46
RKS1157−2608	11 57 16.2	−26 08 29	8.9	2019−04−21 5:00:51	900	75
RKS1157−2742	11 57 56.2	−27 42 25	7.0	2021−03−04 3:17:50	900	199
RKS1157+1959	11 57 28.9	+19 59 02	8.1	2021−03−10 5:17:11	900	98
RKS1158−2355	11 58 11.7	−23 55 25	8.7	2019−05−05 4:15:09	900	80
RKS1159−2021	11 59 10.0	−20 21 13	7.9	2020−03−06 6:56:56	900	74
RKS1204−0013	12 04 47.8	−00 13 36	10.8	2021−02−08 7:29:38	900	35
RKS1204+0911	12 04 17.4	+09 11 35	9.9	2019−02−18 5:06:34	900	36
RKS1205−1852	12 05 50.6	−18 52 30	10.0	2017−07−05 1:14:00	900	36
RKS1206−2336	12 06 09.0	−23 36 08	8.6	2021−01−18 8:05:10	900	78
RKS1208−0028	12 08 22.2	−00 28 57	11.3	2023−03−07 4:20:11	1800	41

Continued on next page

Table C.1 −− *Continued from previous page*

RKS ID	R.A.	Decl.	V	Date & Time of Obs	Exp. Time	SNR
...	(hh mm ss)	(dd mm ss)	(mag)	(UTC)	(s)	...
RKS1209−2646	12 09 23.4	−26 46 46	11.0	2021−01−11 7:24:16	900	31
RKS1210−1126	12 10 33.6	−11 26 59	11.3	2023−03−12 4:29:26	1800	41
RKS1220−1953	12 20 46.8	−19 53 45	9.0	2018−03−28 3:18:27	900	72
RKS1222+2736	12 22 34.0	+27 36 16	10.9	2019−02−18 6:54:13	900	30
RKS1223+2754	12 23 34.7	+27 54 47	11.3	2022−03−02 5:54:55	1800	43
RKS1227+2701	12 27 13.7	+27 01 28	8.9	2021−02−16 7:12:30	900	54
RKS1228−1654	12 28 19.1	−16 54 39	9.5	2020−03−06 7:14:19	900	40
RKS1228−1817	12 28 31.5	−18 17 50	9.2	2020−02−28 7:21:14	900	49
RKS1231+2013	12 31 18.2	+20 13 04	7.9	2021−06−27 0:40:33	900	96
RKS1233−1438	12 33 59.7	−14 38 19	9.1	2018−03−26 3:55:21	900	72
RKS1241+1522	12 41 06.4	+15 22 35	7.9	2019−03−21 5:01:58	764	102
RKS1241+1951	12 41 37.0	+19 51 05	9.1	2019−07−05 23:49:11	900	56
RKS1248−1543	12 48 32.2	−15 43 09	7.9	2017−07−14 0:54:08	900	98
RKS1248−2448	12 48 10.7	−24 48 23	8.9	2017−07−14 0:34:39	900	67
RKS1250−0046	12 50 43.5	−00 46 05	8.5	2020−03−14 5:26:16	900	52
RKS1253+0645	12 53 54.4	+06 45 46	8.2	2018−03−26 4:44:59	838	90
RKS1256−2455	12 56 30.0	−24 55 31	10.0	2020−01−23 8:38:50	900	32
RKS1257−1427	12 57 43.9	−14 27 48	9.1	2018−03−23 6:28:11	900	71
RKS1259−0950	12 59 01.5	−09 50 02	7.5	2017−07−08 23:54:29	900	57
RKS1300−0242	13 00 16.9	−02 42 17	9.8	2019−03−07 6:44:36	900	48
RKS1302−2647	13 02 20.6	−26 47 13	8.4	...	...	...

Continued on next page

Table C.1 −− *Continued from previous page*

RKS ID	R.A.	Decl.	V	Date & Time of Obs	Exp. Time	SNR
...	(hh mm ss)	(dd mm ss)	(mag)	(UTC)	(s)	...
RKS1303−0509	13 03 49.7	−05 09 42	7.7	2018−04−12 2:59:09	707	93
RKS1306+2043	13 06 15.3	+20 43 45	9.4	2018−03−28 5:12:45	900	54
RKS1310+0932	13 10 16.9	+09 32 09	9.3	2021−02−18 7:30:12	900	47
RKS1312−0215	13 12 43.7	−02 15 54	7.6	2020−03−15 5:14:46	900	96
RKS1316+1701	13 16 51.0	+17 01 01	6.5	2020−03−15 5:33:28	900	147
RKS1318−1446	13 18 05.8	−14 46 48	10.9	2021−02−22 5:59:56	900	31
RKS1320+0407	13 20 43.7	+04 07 58	8.6	2021−02−25 9:02:24	900	80
RKS1323+0243	13 23 39.1	+02 43 23	7.1	2021−02−07 7:37:05	900	157
RKS1327−2417	13 27 02.9	−24 17 25	8.7	2021−02−11 7:12:32	900	77
RKS1331−0219	13 31 39.9	−02 19 02	7.3	2019−07−10 0:27:53	900	128
RKS1333+0835	13 33 32.4	+08 35 12	8.0	2021−02−18 7:47:43	900	98
RKS1334−0018	13 34 16.2	−00 18 49	7.4	2019−07−05 1:29:23	900	110
RKS1334−0820	13 34 43.2	−08 20 31	9.2	2021−02−20 7:26:25	900	62
RKS1334+0440	13 34 21.5	+04 40 02	10.0	2021−03−08 7:50:48	900	47
RKS1335−0023	13 35 24.7	−00 23 20	10.3	2019−03−15 8:51:23	900	44
RKS1335+0650	13 35 06.3	+06 50 27	8.9	2021−02−19 7:31:22	900	62
RKS1336+0746	13 36 56.6	+07 46 01	10.0	2021−03−08 6:03:03	900	36
RKS1338−0614	13 38 58.6	−06 14 12	10.7	2019−03−16 6:04:21	900	35
RKS1340−0411	13 40 07.1	−04 11 09	9.6	2018−03−29 4:25:57	900	64
RKS1341−0007	13 41 55.6	−00 07 44	9.8	2021−02−26 6:59:33	900	45
RKS1342−0141	13 42 26.0	−01 41 10	9.2	2021−02−26 6:38:59	900	30

Continued on next page

Table C.1 −− *Continued from previous page*

RKS ID	R.A.	Decl.	V	Date & Time of Obs	Exp. Time	SNR
...	(hh mm ss)	(dd mm ss)	(mag)	(UTC)	(s)	...
RKS1345−0437	13 45 05.3	−04 37 13	10.5	2019−04−11 5:48:26	900	37
RKS1345+0850	13 45 14.7	+08 50 09	8.5	2019−05−08 5:57:52	900	34
RKS1345+1747	13 45 05.0	+17 47 07	9.8	2019−03−16 6:27:16	900	50
RKS1347+0618	13 47 28.7	+06 18 56	10.0	2019−06−01 4:25:25	900	39
RKS1349−2206	13 49 44.8	−22 06 39	8.2	2021−02−08 8:25:04	900	121
RKS1353+1256	13 53 27.5	+12 56 32	9.8	2017−06−25 0:07:53	900	29
RKS1353+2748	13 53 05.2	+27 48 24	8.4	2019−04−07 5:23:17	900	70
RKS1359+2252	13 59 19.4	+22 52 11	9.1	2021−02−11 9:00:01	900	69
RKS1411−1236	14 11 46.1	−12 36 42	7.9	2020−03−15 5:52:00	900	80
RKS1412+2348	14 12 41.5	+23 48 51	8.9	2018−02−26 8:10:45	900	66
RKS1413−0657	14 13 31.1	−06 57 32	10.1	2019−04−11 6:06:03	900	47
RKS1414−1521	14 14 21.3	−15 21 22	10.2	...	...	...
RKS1418−0636	14 18 58.2	−06 36 12	9.1	2018−04−24 5:32:51	900	29
RKS1419−0509	14 19 34.8	−05 09 04	7.6	2021−01−05 8:38:10	900	121
RKS1421+2937	14 21 57.2	+29 37 46	8.6	2019−06−02 2:18:44	900	81
RKS1430−0838	14 30 47.7	−08 38 46	9.4	2018−05−04 4:01:42	900	68
RKS1432+1121	14 32 13.1	+11 21 11	9.7	2019−09−01 23:06:08	900	31
RKS1433+0920	14 33 34.9	+09 20 03	8.8	2021−06−14 2:27:03	900	69
RKS1436+0944	14 36 00.5	+09 44 47	7.5	2021−02−10 8:54:54	900	130
RKS1437−2548	14 37 04.8	−25 48 09	8.3	2021−02−02 7:44:04	900	83
RKS1442+1930	14 42 26.2	+19 30 12	10.1	2019−03−22 6:53:48	900	38

Continued on next page

Table C.1 −− *Continued from previous page*

RKS ID	R.A.	Decl.	V	Date & Time of Obs	Exp. Time	SNR
...	(hh mm ss)	(dd mm ss)	(mag)	(UTC)	(s)	...
RKS1444−2215	14 44 35.5	−22 15 11	9.3	2019−05−21 6:05:04	900	51
RKS1444+2211	14 44 11.9	+22 11 07	9.9	2019−04−21 5:42:06	900	46
RKS1445+1350	14 45 24.1	+13 50 46	7.9	2021−02−04 9:10:21	900	92
RKS1446+1629	14 46 23.2	+16 29 48	9.3	2018−03−28 6:06:14	900	67
RKS1446+2730	14 46 03.0	+27 30 44	8.0	2019−04−07 6:25:28	900	82
RKS1447+0242	14 47 16.1	+02 42 11	7.8	2020−03−15 6:27:11	900	88
RKS1450+0648	14 50 20.9	+06 48 53	9.1	2021−02−17 9:07:27	900	59
RKS1451−2418	14 51 40.4	−24 18 14	7.8	2017−08−07 0:39:09	900	97
RKS1453+2320	14 53 41.5	+23 20 42	8.7	2017−07−07 0:43:04	900	34
RKS1455−2707	14 55 55.0	−27 07 38	9.0	2017−07−02 2:35:28	900	70
RKS1457−2124	14 57 28.0	−21 24 55	5.7	2021−05−01 4:47:50	385	171
RKS1500−1108	15 00 43.4	−11 08 06	9.5	2018−05−23 4:56:52	900	64
RKS1500−2427	15 00 19.3	−24 27 14	9.9	2021−02−10 9:13:00	900	48
RKS1500−2905	15 00 09.5	−29 05 27	11.5	2022−08−03 23:56:44	1200	34
RKS1501+1341	15 01 06.5	+13 41 39	11.0	2021−02−24 8:25:10	900	36
RKS1501+1552	15 01 29.9	+15 52 07	9.1	2021−07−17 0:43:36	900	66
RKS1504−1835	15 04 53.9	−18 35 27	9.5	2020−03−15 6:44:59	900	45
RKS1504+0538	15 04 53.5	+05 38 17	9.8	2018−03−26 6:10:10	900	55
RKS1507+2456	15 07 23.5	+24 56 07	10.2	2019−07−18 1:10:39	900	41
RKS1509+2400	15 09 04.2	+24 00 57	9.3	2019−06−06 3:08:12	900	46
RKS1510−1622	15 10 13.0	−16 22 45	9.1	2020−03−15 7:04:28	900	46

Continued on next page

Table C.1 −− *Continued from previous page*

RKS ID	R.A.	Decl.	V	Date & Time of Obs	Exp. Time	SNR
...	(hh mm ss)	(dd mm ss)	(mag)	(UTC)	(s)	...
RKS1513−0347	15 13 59.6	−03 47 52	9.8	2018−04−24 5:52:59	900	31
RKS1515+0047	15 15 59.1	+00 47 46	6.9	2017−08−07 0:20:08	900	144
RKS1515+0735	15 15 45.4	+07 35 52	10.7	2021−02−24 8:58:11	900	34
RKS1518−1837	15 18 39.5	−18 37 35	10.4	2018−08−30 0:05:48	900	45
RKS1519+0146	15 19 19.2	+01 46 04	9.9	2019−07−06 2:10:36	900	326
RKS1519+1155	15 19 35.3	+11 55 19	9.9	2019−08−11 23:19:48	900	34
RKS1519+2912	15 19 21.1	+29 12 22	10.3	2021−06−13 2:51:04	900	38
RKS1520+1522	15 20 38.9	+15 22 48	8.8	2021−06−13 3:28:07	900	74
RKS1522−0446	15 22 04.1	−04 46 38	9.5	2018−04−07 9:30:19	900	61
RKS1522−1039	15 22 36.6	−10 39 40	8.0	2017−07−05 2:51:45	900	81
RKS1522+0125	15 22 42.5	+01 25 07	8.3	2017−07−14 2:18:23	900	63
RKS1525−2642	15 25 58.5	−26 42 20	8.8	2017−08−07 1:53:14	900	56
RKS1527+0235	15 27 42.6	+02 35 51	10.2	2018−04−21 5:35:19	900	39
RKS1527+1035	15 27 38.0	+10 35 39	9.9	2018−05−23 4:22:00	900	44
RKS1528−0920	15 28 09.6	−09 20 52	6.9	2019−06−20 4:39:56	900	117
RKS1540−1802	15 40 34.5	−18 02 56	8.9	2018−03−23 8:10:23	900	83
RKS1552+1052	15 52 08.2	+10 52 28	9.4	2018−05−15 4:12:41	900	34
RKS1554−2600	15 54 38.4	−26 00 15	9.2	2017−06−25 1:57:44	900	37
RKS1555+1602	15 55 19.0	+16 02 39	8.7	2021−03−14 7:41:00	900	65
RKS1600−0147	16 00 16.4	−01 47 55	10.3	2021−03−14 8:10:03	900	30
RKS1601−2625	16 01 39.7	−26 25 15	10.8	2019−03−20 9:44:38	900	31

Continued on next page

Table C.1 −− *Continued from previous page*

RKS ID	R.A.	Decl.	V	Date & Time of Obs	Exp. Time	SNR
...	(hh mm ss)	(dd mm ss)	(mag)	(UTC)	(s)	...
RKS1604−1126	16 04 26.7	−11 26 59	8.0	2021−05−07 5:08:03	900	78
RKS1605−2027	16 05 40.4	−20 27 00	7.4	2021−02−13 9:23:53	900	148
RKS1607−0542	16 07 34.3	−05 42 25	10.3	2021−03−16 9:05:18	900	29
RKS1608−1308	16 08 24.4	−13 08 07	8.7	2018−05−24 5:35:13	900	78
RKS1608+1713	16 08 05.3	+17 13 44	9.1	2019−07−10 2:19:30	900	52
RKS1613+1331	16 13 18.4	+13 31 36	6.7	2019−08−05 1:20:40	900	36
RKS1615+0721	16 15 57.0	+07 21 25	8.7	2018−04−12 7:45:18	900	51
RKS1620−0416	16 20 24.7	−04 16 02	10.7	2020−03−15 8:11:20	1500	35
RKS1621+1713	16 21 38.0	+17 13 33	10.8	2019−08−12 0:45:19	900	29
RKS1624−1338	16 24 19.8	−13 38 29	8.4	2018−05−13 6:51:58	900	70
RKS1625−2156	16 25 13.0	−21 56 14	10.3	2021−02−11 8:46:46	900	34
RKS1626+1539	16 26 33.4	+15 39 53	10.5	2018−04−21 6:19:28	900	30
RKS1627+0055	16 27 20.3	+00 55 29	10.0	2018−04−21 6:01:35	900	42
RKS1627+0718	16 27 56.9	+07 18 19	8.8	2017−07−03 3:03:36	900	71
RKS1628+1824	16 28 52.6	+18 24 50	7.0	2019−08−10 1:01:45	900	77
RKS1629+2346	16 29 14.3	+23 46 34	10.1	2020−03−16 8:22:33	900	31
RKS1630−0359	16 30 43.0	−03 59 21	9.6	2019−07−06 3:08:15	900	51
RKS1631−0718	16 31 52.3	−07 18 18	11.0	2021−04−09 6:06:41	1800	37
RKS1632−1235	16 32 57.8	−12 35 30	10.6	2019−08−06 0:44:08	900	32
RKS1633−0933	16 33 41.6	−09 33 11	11.3	2020−02−29 8:57:48	1500	25
RKS1647−0111	16 47 17.5	−01 11 20	10.8	2019−08−07 2:38:19	900	35

Continued on next page

Table C.1 −− *Continued from previous page*

RKS ID	R.A.	Decl.	V	Date & Time of Obs	Exp. Time	SNR
...	(hh mm ss)	(dd mm ss)	(mag)	(UTC)	(s)	...
RKS1649−2426	16 49 53.1	−24 26 48	9.6	2017−06−29 3:05:30	900	46
RKS1650+1854	16 50 05.2	+18 54 01	8.9	2017−07−10 2:14:54	900	46
RKS1654+1154	16 54 12.0	+11 54 52	10.7	2019−09−20 23:45:42	900	32
RKS1659−2616	16 59 33.2	−26 16 04	10.4	2018−08−15 1:48:27	900	45
RKS1701+2256	17 01 59.8	+22 56 09	8.8	2021−07−09 1:47:55	900	77
RKS1705−0147	17 05 08.5	−01 47 09	9.5	2022−08−16 0:25:28	900	65
RKS1705−0503	17 05 03.3	−05 03 59	7.7	2019−09−19 23:55:29	900	86
RKS1706−0610	17 06 08.2	−06 10 02	8.8	2018−06−02 4:01:07	900	62
RKS1712+1821	17 12 37.6	+18 21 04	8.0	2017−07−30 1:22:35	900	50
RKS1714−0824	17 14 08.0	−08 24 13	8.5	2022−03−17 8:30:26	900	110
RKS1715−2636	17 15 20.7	−26 36 06	4.3	2019−05−21 7:58:24	900	132
RKS1716−1210	17 16 20.2	−12 10 41	10.5	2018−06−29 3:00:30	900	39
RKS1717+2913	17 17 40.4	+29 13 38	8.4	2017−07−07 2:46:21	900	37
RKS1722−1457	17 22 42.9	−14 57 37	10.9	2019−03−06 9:22:34	900	31
RKS1725+0206	17 25 45.2	+02 06 41	7.5	2017−08−17 23:58:47	900	144
RKS1729−2350	17 29 06.5	−23 50 10	9.6	2018−05−23 7:52:01	900	59
RKS1733+0914	17 33 07.2	+09 14 37	9.6	2019−07−10 3:37:30	900	45
RKS1737−1314	17 37 46.4	−13 14 46	10.1	...	...	...
RKS1737+2257	17 37 48.7	+22 57 20	9.9	2017−07−05 3:12:27	900	38
RKS1739+0333	17 39 16.9	+03 33 18	6.5	2017−08−05 1:36:56	900	186
RKS1750−0603	17 50 34.0	−06 03 01	10.1	2017−08−01 1:27:36	900	36

Continued on next page

Table C.1 −− *Continued from previous page*

RKS ID	R.A.	Decl.	V	Date & Time of Obs	Exp. Time	SNR
...	(hh mm ss)	(dd mm ss)	(mag)	(UTC)	(s)	...
RKS1752−0733	17 52 16.6	−07 33 37	9.9	2021−06−11 3:53:25	900	46
RKS1753+2119	17 53 29.9	+21 19 31	8.5	2017−07−27 2:16:23	900	42
RKS1754−2649	17 54 54.1	−26 49 41	10.3	2022−08−17 2:26:38	920	43
RKS1755+0345	17 55 24.7	+03 45 16	10.1	2018−06−19 6:12:34	900	38
RKS1755+1830	17 55 44.8	+18 30 01	9.2	2019−09−30 23:29:43	900	31
RKS1757−2143	17 57 40.9	−21 43 10	10.0	2018−04−08 9:30:29	900	53
RKS1803+2545	18 03 47.7	+25 45 20	10.8	2021−03−22 9:08:50	900	30
RKS1804+0149	18 04 01.8	+01 49 56	8.1	2019−09−08 0:41:10	900	65
RKS1809−0019	18 09 32.2	−00 19 37	8.9	2019−05−03 5:41:32	900	68
RKS1809−1202	18 09 33.2	−12 02 19	10.5	2018−06−20 6:20:22	900	37
RKS1815+1829	18 15 18.2	+18 29 59	10.1	2022−03−13 9:25:24	900	57
RKS1816+1354	18 16 02.2	+13 54 48	10.2	2018−04−08 9:48:19	900	46
RKS1817+2640	18 17 49.8	+26 40 16	9.6	2021−06−11 5:05:17	900	48
RKS1818−0642	18 18 40.6	−06 42 03	9.3	2019−04−11 8:11:40	900	60
RKS1819−0156	18 19 50.8	−01 56 19	9.7	2018−04−09 9:20:08	900	57
RKS1822+0142	18 22 17.2	+01 42 25	10.1	2021−03−28 8:46:03	1200	53
RKS1829−0149	18 29 52.4	−01 49 05	8.0	2017−07−02 4:38:34	900	98
RKS1829−2758	18 29 22.3	−27 58 19	9.4	2021−06−11 5:59:48	900	65
RKS1829+0903	18 29 31.9	+09 03 43	8.7	2019−09−15 23:31:29	900	67
RKS1831−1854	18 31 18.9	−18 54 31	6.8	2017−08−06 4:16:43	900	170
RKS1833−1138	18 33 28.8	−11 38 09	10.0	2019−10−25 23:45:11	900	32

Continued on next page

Table C.1 −− *Continued from previous page*

RKS ID	R.A.	Decl.	V	Date & Time of Obs	Exp. Time	SNR
...	(hh mm ss)	(dd mm ss)	(mag)	(UTC)	(s)	...
RKS1833−1626	18 33 24.8	−16 26 39	9.1	2019−07−10 3:18:32	900	62
RKS1833+2218	18 33 17.7	+22 18 51	8.9	2017−07−13 3:43:52	900	30
RKS1847−0338	18 47 27.2	−03 38 23	8.8	2017−08−07 4:07:32	900	76
RKS1848−1008	18 48 01.4	−10 08 46	8.5	2021−06−11 6:17:26	900	89
RKS1848+1044	18 48 29.2	+10 44 43	8.0	2017−08−07 3:27:42	900	105
RKS1848+1726	18 48 51.8	+17 26 20	9.2	2018−06−19 6:48:30	900	60
RKS1850−2655	18 50 21.1	−26 55 25	9.7	2018−08−12 1:59:09	900	64
RKS1854+0051	18 54 53.2	+00 51 46	10.7	2019−11−05 23:54:32	900	31
RKS1854+1058	18 54 53.6	+10 58 40	9.6	2018−09−10 23:57:11	900	65
RKS1854+2844	18 54 43.7	+28 44 55	11.6	2022−04−23 9:16:57	1200	33
RKS1855+2333	18 55 53.2	+23 33 23	8.2	2018−06−30 4:26:13	900	55
RKS1858−0030	18 58 56.4	−00 30 14	8.4	2019−05−03 10:08:10	900	86
RKS1858−1014	18 58 03.3	−10 14 37	9.8	2019−07−05 5:46:59	900	49
RKS1859+0759	18 59 38.6	+07 59 14	10.8	2020−11−03 23:56:35	1200	33
RKS1859+1107	18 59 39.2	+11 07 04	9.2	2019−07−10 4:34:24	900	55
RKS1901+0328	19 01 51.0	+03 28 14	9.7	2019−07−06 6:42:35	900	35
RKS1903−1102	19 03 05.8	−11 02 38	8.4	2017−06−24 7:17:28	900	32
RKS1907+0736	19 07 02.0	+07 36 57	9.2	2017−08−19 1:58:20	900	40
RKS1908−1640	19 08 10.7	−16 40 41	10.6	2019−05−17 8:51:25	900	30
RKS1908+1627	19 08 02.6	+16 27 37	10.2	2019−07−11 5:30:39	900	33
RKS1910+2145	19 10 32.1	+21 45 46	11.4	2021−06−01 6:07:36	1800	32

Continued on next page

Table C.1 −− *Continued from previous page*

RKS ID	R.A.	Decl.	V	Date & Time of Obs	Exp. Time	SNR
...	(hh mm ss)	(dd mm ss)	(mag)	(UTC)	(s)	...
RKS1914+0209	19 14 58.9	+02 09 54	9.9	2021−06−04 6:48:23	1800	42
RKS1915+1133	19 15 35.0	+11 33 16	8.1	2019−07−10 6:02:39	900	89
RKS1915+2453	19 15 18.8	+24 53 49	9.7	2021−04−11 9:39:07	900	55
RKS1923−0635	19 23 16.4	−06 35 07	9.7	2019−07−05 6:48:51	900	52
RKS1924−2203	19 24 34.2	−22 03 43	10.9	2019−11−06 0:50:23	900	31
RKS1924+2525	19 24 26.5	+25 25 50	10.9	2021−05−05 8:44:51	900	36
RKS1928+1232	19 28 15.3	+12 32 09	9.2	2019−06−01 8:43:02	900	58
RKS1928+2854	19 28 25.5	+28 54 10	10.9	2021−04−27 9:40:59	900	33
RKS1929+0709	19 29 05.1	+07 09 35	10.5	2019−07−06 7:10:32	900	29
RKS1930+2140	19 30 05.4	+21 40 34	10.0	2022−04−09 9:42:59	900	56
RKS1932−1116	19 32 06.7	−11 16 29	7.5	2017−08−19 1:40:18	900	123
RKS1932+0034	19 32 37.9	+00 34 39	10.4	2017−08−03 4:01:41	900	32
RKS1934+0434	19 34 39.8	+04 34 57	9.4	2018−05−16 9:31:30	900	61
RKS1936−1026	19 36 45.6	−10 26 36	8.4	2021−04−07 9:33:55	900	81
RKS1943+1005	19 43 25.3	+10 05 22	10.0	2017−07−19 4:26:42	900	38
RKS1952−2356	19 52 29.9	−23 56 57	9.5	2018−06−19 7:25:58	900	60
RKS1954−2356	19 54 17.7	−23 56 27	6.2	...	...	...
RKS1954+2013	19 54 37.5	+20 13 06	11.1	2021−04−25 8:55:50	900	30
RKS1957+1313	19 57 25.4	+13 13 24	10.1	2019−07−05 8:13:33	900	34
RKS2000+2242	20 00 43.7	+22 42 39	7.7	2017−08−05 3:22:08	900	102
RKS2002+0319	20 02 47.0	+03 19 34	7.5	2017−08−18 2:36:59	900	148

Continued on next page

Table C.1 −− *Continued from previous page*

RKS ID	R.A.	Decl.	V	Date & Time of Obs	Exp. Time	SNR
...	(hh mm ss)	(dd mm ss)	(mag)	(UTC)	(s)	...
RKS2003+2005	20 03 00.9	+20 05 49	10.9	2021−04−25 9:28:47	900	31
RKS2003+2320	20 03 52.1	+23 20 26	7.3	2017−07−19 5:04:20	900	111
RKS2004+2547	20 04 10.0	+25 47 24	7.8	2017−07−15 5:19:05	900	33
RKS2008+0640	20 08 24.3	+06 40 43	9.8	2019−04−21 9:50:39	900	47
RKS2009−0307	20 09 41.0	−03 07 44	9.6	2019−07−05 7:33:04	900	55
RKS2009−1417	20 09 36.4	−14 17 12	9.8	2019−09−08 3:24:02	900	39
RKS2009+1648	20 09 34.3	+16 48 20	7.6	2017−07−07 6:22:34	900	56
RKS2010−2029	20 10 19.5	−20 29 36	8.9	2017−08−05 4:00:04	900	69
RKS2011+1611	20 11 06.0	+16 11 16	7.4	2017−08−08 5:18:09	900	76
RKS2012−1253	20 12 09.4	−12 53 35	11.3	2021−05−26 7:16:24	1800	41
RKS2013−0052	20 13 59.8	−00 52 00	7.8	2017−07−02 6:51:03	900	110
RKS2014−0716	20 14 28.1	−07 16 55	10.2	2017−07−20 5:58:36	900	28
RKS2015−2701	20 15 17.3	−27 01 58	5.7	2017−07−19 6:52:53	900	217
RKS2016−0204	20 16 22.0	−02 04 08	11.2	2021−06−07 7:15:18	1800	43
RKS2030+2650	20 30 10.6	+26 50 34	9.7	2021−04−29 9:53:55	900	50
RKS2035+0607	20 35 12.7	+06 07 37	8.9	2017−07−23 5:06:25	900	46
RKS2038+2346	20 38 26.2	+23 46 41	8.7	2022−06−11 7:40:51	900	93
RKS2039+1004	20 39 22.0	+10 04 32	8.5	2019−09−02 4:24:34	900	77
RKS2041−0529	20 41 40.6	−05 29 34	10.5	2019−07−16 5:18:38	900	34
RKS2041−2219	20 41 42.2	−22 19 20	9.8	2017−07−23 4:28:59	900	29
RKS2042−2116	20 42 05.8	−21 16 37	9.3	2020−11−06 0:55:31	900	51

Continued on next page

Table C.1 −− *Continued from previous page*

RKS ID	R.A.	Decl.	V	Date & Time of Obs	Exp. Time	SNR
...	(hh mm ss)	(dd mm ss)	(mag)	(UTC)	(s)	...
RKS2042+2050	20 42 49.3	+20 50 40	8.3	2018−09−29 1:40:48	900	47
RKS2044−2121	20 44 00.6	−21 21 20	9.8	2017−07−03 6:49:23	900	46
RKS2047+1051	20 47 16.8	+10 51 36	9.7	2018−06−19 9:37:05	900	39
RKS2050+2923	20 50 10.5	+29 23 02	8.3	2019−09−18 1:43:57	900	32
RKS2053−0245	20 53 56.9	−02 45 57	11.1	2021−04−28 9:22:31	900	30
RKS2055+1310	20 55 06.8	+13 10 36	8.8	2017−08−19 4:17:27	900	41
RKS2059−1042	20 59 14.4	−10 42 49	8.5	2021−11−25 0:12:40	900	103
RKS2059+0333	20 59 08.5	+03 33 09	12.0	2021−06−20 7:14:08	1800	36
RKS2105−1654	21 05 43.4	−16 54 49	10.5	2019−11−04 1:40:02	900	31
RKS2105+0704	21 05 19.7	+07 04 09	8.3	2017−08−21 4:57:08	900	96
RKS2107−1355	21 07 10.3	−13 55 22	7.1	2017−07−20 8:31:30	900	38
RKS2108−0425	21 08 45.4	−04 25 36	9.5	2019−09−18 2:22:03	900	37
RKS2116+0923	21 16 32.4	+09 23 37	8.0	2017−08−20 5:03:26	900	105
RKS2118+0009	21 18 02.9	+00 09 41	8.2	2019−11−12 1:15:26	900	53
RKS2119−2621	21 19 45.6	−26 21 10	6.6	2020−11−28 0:17:19	900	177
RKS2120−1951	21 20 13.8	−19 51 08	9.1	2018−11−16 0:29:42	900	72
RKS2122+1052	21 22 26.6	+10 52 25	9.9	2017−07−17 7:45:02	900	30
RKS2125+2712	21 25 29.0	+27 12 38	8.3	2018−09−29 2:26:22	900	42
RKS2126+0344	21 26 42.4	+03 44 13	10.5	2021−04−25 10:12:05	900	32
RKS2130−1230	21 30 02.7	−12 30 36	9.1	2018−08−28 4:34:51	900	70
RKS2131+2320	21 31 01.7	+23 20 07	9.2	...	...	...

Continued on next page

Table C.1 −− *Continued from previous page*

RKS ID	R.A.	Decl.	V	Date & Time of Obs	Exp. Time	SNR
...	(hh mm ss)	(dd mm ss)	(mag)	(UTC)	(s)	...
RKS2132−2057	21 32 23.5	−20 57 26	8.5	2017−07−19 7:32:19	900	75
RKS2141+1115	21 41 01.3	+11 15 46	9.2	2022−05−16 9:00:19	900	77
RKS2149−1140	21 49 45.9	−11 40 57	10.9	2020−11−17 1:27:25	900	28
RKS2149+0543	21 49 12.2	+05 43 22	8.7	2018−09−29 3:37:49	900	47
RKS2152+0154	21 52 06.5	+01 54 23	8.2	2021−05−22 9:10:17	900	100
RKS2153−1249	21 53 07.5	−12 49 40	11.0	2019−07−10 7:20:20	900	30
RKS2153+2055	21 53 05.3	+20 55 49	8.2	2021−04−29 10:11:31	900	89
RKS2153+2850	21 53 07.2	+28 50 15	11.4	2021−05−23 9:38:31	1800	33
RKS2155−2942	21 55 41.9	−29 42 22	8.5	2020−10−29 0:21:11	900	84
RKS2210+2247	22 10 31.4	+22 47 49	9.2	2017−06−25 8:58:36	900	38
RKS2214+2751	22 14 31.4	+27 51 18	10.3	2018−08−15 4:48:05	900	37
RKS2224+2233	22 24 45.5	+22 33 04	8.8	2019−11−22 0:08:57	900	35
RKS2226−1911	22 26 13.5	−19 11 18	9.3	2020−11−04 0:58:48	900	61
RKS2239+0406	22 39 50.7	+04 06 58	8.5	2020−11−02 0:38:35	900	77
RKS2240−2940	22 40 43.3	−29 40 28	7.8	2018−10−01 4:31:37	900	112
RKS2241+1849	22 41 35.0	+18 49 27	10.7	2018−11−03 0:59:03	900	29
RKS2243−0624	22 43 21.3	−06 24 02	8.1	2020−10−29 1:02:57	900	94
RKS2247+1823	22 47 13.6	+18 23 04	9.0	2020−12−13 0:29:06	900	60
RKS2248+2443	22 48 35.5	+24 43 26	11.0	2020−10−26 1:01:18	1500	36
RKS2251+1358	22 51 26.3	+13 58 11	8.3	2020−11−01 1:02:32	900	78
RKS2252+2324	22 52 02.5	+23 24 47	9.8	2018−06−05 9:59:32	900	39

Continued on next page

Table C.1 −− *Continued from previous page*

RKS ID	R.A.	Decl.	V	Date & Time of Obs	Exp. Time	SNR
...	(hh mm ss)	(dd mm ss)	(mag)	(UTC)	(s)	...
RKS2254+2331	22 54 30.8	+23 31 06	11.1	2021−07−04 8:41:32	1850	29
RKS2258−1338	22 58 06.2	−13 38 33	10.1	2020−11−10 3:01:16	900	35
RKS2259−1122	22 59 53.6	−11 22 54	10.6	2020−11−11 3:24:39	900	34
RKS2300−2231	23 00 16.1	−22 31 27	7.9	2018−11−06 2:29:47	727	124
RKS2301−0350	23 01 51.5	−03 50 55	7.5	2020−11−01 1:20:25	900	125
RKS2307−2309	23 07 07.0	−23 09 34	9.6	2018−12−19 1:05:01	900	34
RKS2308+0633	23 08 52.4	+06 33 39	10.9	2020−12−17 0:26:52	900	32
RKS2309−0215	23 09 10.7	−02 15 38	8.6	2017−07−14 7:16:48	900	59
RKS2309+1425	23 09 54.9	+14 25 35	10.3	2021−08−18 6:00:22	1200	51
RKS2310−2955	23 10 48.8	−29 55 03	8.7	2020−11−06 1:13:22	900	75
RKS2316+0541	23 16 51.8	+05 41 45	10.5	2017−12−15 0:59:34	900	33
RKS2317−2323	23 17 00.2	−23 23 46	10.8	2020−11−10 3:57:41	900	31
RKS2323−1045	23 23 04.8	−10 45 51	7.8	2018−11−08 2:57:00	716	94
RKS2326+0853	23 26 12.3	+08 53 37	10.5	2020−12−12 0:28:20	900	35
RKS2327−0117	23 27 04.8	−01 17 10	10.4	2017−12−15 1:17:01	900	36
RKS2328+1604	23 28 26.1	+16 04 00	9.8	2017−06−25 9:39:11	900	30
RKS2332−1650	23 32 49.3	−16 50 44	8.6	2017−08−18 5:11:39	900	92
RKS2335+0136	23 35 00.2	+01 36 19	9.6	2017−07−27 8:02:42	900	31
RKS2340+2021	23 40 51.4	+20 21 57	8.3	2021−07−08 7:47:20	900	61
RKS2342−0234	23 42 10.6	−02 34 36	10.3	2019−09−17 3:26:25	900	29
RKS2345+2933	23 45 09.9	+29 33 42	8.4	2021−11−03 1:31:00	900	98

Continued on next page

Table C.1 −− *Continued from previous page*

RKS ID	R.A.	Decl.	V	Date & Time of Obs	Exp. Time	SNR
...	(hh mm ss)	(dd mm ss)	(mag)	(UTC)	(s)	...
RKS2348−1259	23 48 25.6	−12 59 14	9.6	2021−12−07 0:20:16	900	59
RKS2349+0310	23 49 01.1	+03 10 52	8.4	2018−09−29 4:41:28	900	37
RKS2350−2924	23 50 14.9	−29 24 06	7.9	2021−10−28 1:16:33	900	147
RKS2353+2901	23 53 08.5	+29 01 05	9.8	2018−08−16 6:25:28	900	45
RKS2355+2211	23 55 26.5	+22 11 35	8.8	2017−07−11 9:41:29	900	60
RKS2358+0949	23 58 19.8	+09 49 50	8.3	2021−08−17 6:37:07	900	84
RKS2359−2602	23 59 13.6	−26 02 55	8.7	2017−06−29 10:25:57	900	50
RKS2359+0639	23 59 47.7	+06 39 50	8.9	2018−09−29 5:01:24	900	41

REFERENCES

Adibekyan, V. Z., Figueira, P., Santos, N. C., et al. 2013, A&A, 554, A44. doi:10.1051/0004-6361/201321520

Agueros, M. A., Anderson, S. F., Covey, K. R., et al. 2009, ApJS, 181, 444. doi:10.1088/0067-0049/181/2/444

Agueros, M. A., Bowsher, E. C., Bochanski, J. J., et al. 2018, ApJ, 862, 33. doi:10.3847/1538-4357/aac6ed

Aguilera-Gomez, C., Ramirez, I., & Chaname, J. 2018, A&A, 614, A55. doi:10.1051/0004-6361/201732209

Angus, R., Morton, T. D., Foreman-Mackey, D., et al. 2019, AJ, 158, 173. doi:10.3847/1538-3881/ab3c53

Ansdell, M., Gaidos, E., Mann, A. W., et al. 2015, ApJ, 798, 41. doi:10.1088/0004-637X/798/1/41

Arney, G. N. 2019, ApJ, 873, L7. doi:10.3847/2041-8213/ab0651

Aumer, M. & Binney, J. J. 2009, MNRAS, 397, 1286. doi:10.1111/j.1365-2966.2009.15053.x

Azulay, R., Guirado, J. C., Marcaide, J. M., et al. 2015, A&A, 578, A16. doi:10.1051/0004-6361/201525704

Bahcall, J. N., Pinsonneault, M. H., & Wasserburg, G. J. 1995, Reviews of Modern Physics, 67, 781. doi:10.1103/RevModPhys.67.781

Bailer-Jones, C. A. L. 2022, ApJ, 935, L9. doi:10.3847/2041-8213/ac816a

Barnes, S. A. 2003, ApJ, 586, 464. doi:10.1086/367639

Barnes, S. A. 2007, ApJ, 669, 1167. doi:10.1086/519295

Bell, C. P. M., Mamajek, E. E., & Naylor, T. 2015, MNRAS, 454, 593. doi:10.1093/mnras/stv1981

Bensby, T., Feltzing, S., & Lundström, I. 2003, A&A, 410, 527. doi:10.1051/0004-6361:20031213

Binks, A. S. & Jeffries, R. D. 2014, MNRAS, 438, L11. doi:10.1093/mnrasl/slt141

Binney, J. & Tremaine, S. 1987, Princeton, N.J. : Princeton University Press, c1987.

Boley, K. M., Wang, J., Zinn, J. C., et al. 2021, AJ, 162, 85. doi:10.3847/1538-3881/ac0e2d

Bonanno, A., Schlattl, H., & Paternbonanno02, L. 2002, A&A, 390, 1115. doi:10.1051/0004-6361:20020749

Bonfils, X., Delfosse, X., Udry, S., et al. 2013, A&A, 549, A109. doi:10.1051/0004-6361/201014704

Bouvier, J., Barrado, D., Moraux, E., et al. 2018, A&A, 613, A63. doi:10.1051/0004-6361/201731881

Brandt, T. D. & Huang, C. X. 2015, ApJ, 807, 24. doi:10.1088/0004-637X/807/1/24

Butler, R. P., Marcy, G. W., Williams, E., et al. 1997, ApJ, 474, L115. doi:10.1086/310444

Cayrel de Strobel, G. & Cayrel, R. 1989, A&A, 218, L9

Cuntz, M. & Guinan, E. F. 2016, ApJ, 827, 79. doi:10.3847/0004-637X/827/1/79

Curtis, J. L., Agueros, M. A., Matt, S. P., et al. 2020, ApJ, 904, 140. doi:10.3847/1538-4357/abbf58

Davenport, J. R. A., Covey, K. R., Clarke, R. W., et al. 2019, ApJ, 871, 241. doi:10.3847/1538-4357/aafb76

de la Fuente Marcos, R. & de la Fuente Marcos, C. 2018, Research Notes of the American Astronomical Society, 2, 30. doi:10.3847/2515-5172/aac2d0

Douglas, S. T., Agueros, M. A., Covey, K. R., et al. 2017, ApJ, 842, 83. doi:10.3847/1538-4357/aa6e52

Dressing, C. D. & Charbonneau, D. 2015, ApJ, 807, 45. doi:10.1088/0004-637X/807/1/45

Earl, N., Tollerud, E., Jones, C., et al. 2020, Zenodo

Edwards, B., Rice, M., Zingales, T., et al. 2019, Experimental Astronomy, 47, 29. doi:10.1007/s10686-018-9611-4

Ehrenfreund, P., Irvine, W., Becker, L., et al. 2002, Exo-Astrobiology, 518, 9

Erkaev, N. V., Lammer, H., Odert, P., et al. 2013, Astrobiology, 13, 1011. doi:10.1089/ast.2012.0957

Faherty, J. K., Bochanski, J. J., Gagne, J., et al. 2018, ApJ, 863, 91. doi:10.3847/1538-4357/aac76e

Fekel, F. C., Bopp, B. W., Africano, J. L., et al. 1986, AJ, 92, 1150. doi:10.1086/114246

Feltzing, S., Bensby, T., & Lundström, I. 2003, A&A, 397, L1. doi:10.1051/0004-6361:20021661

Feng, F., Anglada-Escude, G., Tuomi, M., et al. 2019, MNRAS, 490, 5002. doi:10.1093/mnras/stz2912

Fischer, D. A. & Valenti, J. 2005, ApJ, 622, 1102. doi:10.1086/428383

Fischer, D. A., Marcy, G. W., Butler, R. P., et al. 2008, ApJ, 675, 790. doi:10.1086/525512

France, K., Arulanantham, N., Fossati, L., et al. 2018, ApJS, 239, 16. doi:10.3847/1538-4365/aae1a3

France, K., Arulanantham, N., Fossati, L., et al. 2018, ApJS, 239, 16. doi:10.3847/1538-4365/aae1a3

Freund, S., Czesla, S., Robrade, J., et al. 2022, A&A, 664, A105. doi:10.1051/0004-6361/202142573

Gagne, J., Mamajek, E. E., Malo, L., et al. 2018, ApJ, 856, 23. doi:10.3847/1538-4357/aaae09

Gaia Collaboration, Brown, A. G. A., Vallenari, A., et al. 2016, A&A, 595, A2. doi:10.1051/0004-6361/201629512

Gaia Collaboration, Brown, A. G. A., Vallenari, A., et al. 2018, A&A, 616, A1. doi:10.1051/0004-

6361/201833051

Gaia Collaboration, Brown, A. G. A., Vallenari, A., et al. 2021, A&A, 649, A1. doi:10.1051/0004-6361/202039657

Gaia Collaboration, Vallenari, A., Brown, A. G. A., et al. 2022, arXiv:2208.00211. doi:10.48550/arXiv.2208.00211

Gaidos, E., Fischer, D. A., Mann, A. W., et al. 2013, ApJ, 771, 18. doi:10.1088/0004-637X/771/1/18

Garcia-Alvarez, D., Lanza, A. F., Messina, S., et al. 2011, A&A, 533, A30. doi:10.1051/0004-6361/201116646

Gomes, J. I., Pinfield, D. J., Marocco, F., et al. 2013, MNRAS, 431, 2745. doi:10.1093/mnras/stt371

Gossage, S., Conroy, C., Dotter, A., et al. 2018, ApJ, 863, 67. doi:10.3847/1538-4357/aad0a0

Gray, R. O. & Corbally, C. 2009, Stellar Spectral Classification by Richard O. Gray and Christopher J. Corbally. Princeton University Press, 2009. ISBN: gray09 978-0-691-12511-4

Gray, R. O., Corbally, C. J., Garrison, R. F., et al. 2003, AJ, 126, 2048. doi:10.1086/378365

Gray, R. O., Corbally, C. J., Garrison, R. F., et al. 2006, AJ, 132, 161. doi:10.1086/504637

Gray, D. F. 2008, The Observation and Analysis of Stellar Photospheres, by David F. Gray, Cambridge, UK: Cambridge University Press, 2008

Griffin, R. F. 1994, The Observatory, 114, 294

Griffin, R. F. 2009, The Observatory, 129, 317

Griffin, R. F. 2012, Journal of Astrophysics and Astronomy, 33, 29. doi:10.1007/s12036-012-9137-5

Griffin, R. F. 2016, The Observatory, 136, 179

Halbwachs, J.-L., Mayor, M., & Udry, S. 2018, A&A, 619, A81. doi:10.1051/0004-6361/201833377

Harman, C. E., Schwieterman, E. W., Schottelkotte, J. C., et al. 2015, ApJ, 812, 137. doi:10.1088/0004-637X/812/2/137

Hartmann, L., Bopp, B. W., Dussault, M., et al. 1981, ApJ, 249, 662. doi:10.1086/159326

Hełminiak, K. G., Brahm, R., Ratajczak, M., et al. 2014, A&A, 567, A64. doi:10.1051/0004-6361/201220985

Henry, T. J. & McCarthy, D. W. 1993, AJ, 106, 773. doi:10.1086/116685

Henry, T. J., Soderblom, D. R., Donahue, R. A., et al. 1996, AJ, 111, 439. doi:10.1086/117796

Henry, T. J., Jao, W.-C., Subasavage, J. P., et al. 2006, AJ, 132, 2360. doi:10.1086/508233

Henry, T. J., Jao, W.-C., Winters, J. G., et al. 2018, AJ, 155, 265. doi:10.3847/1538-3881/aac262

Henry, T., Casetti-Dinescu, D., Horch, E., et al. 2022,

Hinkel, N. R., Timmes, F. X., Young, P. A., et al. 2014, AJ, 148, 54. doi:10.1088/0004-6256/148/3/54

Hinkel, N. R., Mamajek, E. E., Turnbull, M. C., et al. 2017, ApJ, 848, 34. doi:10.3847/1538-4357/aa8b0f

Hojjatpanah, S., Figueira, P., Santos, N. C., et al. 2019, A&A, 629, A80. doi:10.1051/0004-6361/201834729

Holmberg, J., Nordstrom, B., & Andersen, J. 2007, A&A, 475, 519. doi:10.1051/0004-6361:20077221

Horch, E. P., Veillette, D. R., Baena Gallé, R., et al. 2009, AJ, 137, 5057. doi:10.1088/0004-6256/137/6/5057

Horch, E. P., Broderick, K. G., Casetti-Dinescu, D. I., et al. 2021, AJ, 161, 295. doi:10.3847/1538-3881/abf9a8

Hubbard-James, H.-S., Lesley, D. X., Henry, T. J., et al. 2022, AJ, 164, 174. doi:10.3847/1538-3881/ac8d6a

Isaacson, H. & Fischer, D. 2010, ApJ, 725, 875. doi:10.1088/0004-637X/725/1/875

Ivezić, Ž., Sesar, B., Jurić, M., et al. 2008, ApJ, 684, 287. doi:10.1086/589678

Jeffries, R. D., Byrne, P. B., Doyle, J. G., et al. 1994, MNRAS, 270, 153. doi:10.1093/mnras/270.1.153

Johnson, D. R. H. & Soderblom, D. R. 1987, AJ, 93, 864. doi:10.1086/114370

Johnstone, C. P., Bartel, M., & Gudel, M. 2021, A&A, 649, A96. doi:10.1051/0004-6361/202038407

Kasting, J. F., Whitmire, D. P., & Reynolds, R. T. 1993, Icarus, 101, 108. doi:10.1006/icar.1993.1010

Kasting, J. F., Whittet, D. C. B., & Sheldon, W. R. 1996, Lunar and Planetary Science Conference

Kopparapu, R. K., Ramirez, R., Kasting, J. F., et al. 2013, ApJ, 765, 131. doi:10.1088/0004-637X/765/2/131

Kunimoto, M. & Matthews, J. M. 2020, AJ, 159, 248. doi:10.3847/1538-3881/ab88b0

Lammer, H., Selsis, F., Ribas, I., et al. 2003, ApJ, 598, L121. doi:10.1086/380815

Lammer, H., Lichtenegger, H. I. M., Kulikov, Y. N., et al. 2007, Astrobiology, 7, 185. doi:10.1089/ast.2006.0128

Lammer, H., Bredehoft, J. H., Coustenis, A., et al. 2009, A&A Rev., 17, 181. doi:10.1007/s00159-009-0019-z

Lehtinen, J., Jetsu, L., Hackman, T., et al. 2016, A&A, 588, A38. doi:10.1051/0004-6361/201527420

Lillo-Box, J., Santos, N. C., Santerne, A., et al. 2022, A&A, 667, A102. doi:10.1051/0004-6361/202243898

Lim, D., Koch-Hansen, A. J., Hansen, C. J., et al. 2021, A&A, 655, A26. doi:10.1051/0004-6361/202141728

Lindegren, L., Hernandez, J., Bombrun, A., et al. 2018, A&A, 616, A2. doi:10.1051/0004-6361/201832727

Lopez-Santiago, J., Montes, D., Galvez-Ortiz, M. C., et al. 2010, A&A, 514, A97. doi:10.1051/0004-6361/200913437

Lu, Y. L., Angus, R., Curtis, J. L., et al. 2021, AJ, 161, 189. doi:10.3847/1538-3881/abe4d6

Luck, R. E. & Heiter, U. 2006, AJ, 131, 3069. doi:10.1086/504080

Luck, R. E. 2017, AJ, 153, 21. doi:10.3847/1538-3881/153/1/21

Luck, R. E. 2018, AJ, 155, 111. doi:10.3847/1538-3881/aaa9b5

Luger, R. & Barnes, R. 2015, Astrobiology, 15, 119. doi:10.1089/ast.2014.1231

Luger, R., Barnes, R., Lopez, E., et al. 2015, Astrobiology, 15, 57. doi:10.1089/ast.2014.1215

Mamajek, E. E. & Bell, C. P. M. 2014, MNRAS, 445, 2169. doi:10.1093/mnras/stu1894

Mamajek, E. E. & Hillenbrand, L. A. 2008, ApJ, 687, 1264. doi:10.1086/591785

Mamajek, E. E. 2012, arXiv:1210.1616. doi:10.48550/arXiv.1210.1616

Martinez-Arnaiz, R., Maldonado, J., Montes, D., et al. 2010, A&A, 520, A79. doi:10.1051/0004-6361/200913725

Mason, B. D., Wycoff, G. L., Hartkopf, W. I., et al. 2001, AJ, 122, 3466. doi:10.1086/323920

Mason, B. D., Hartkopf, W. I., Wycoff, G. L., et al. 2006, AJ, 132, 2219. doi:10.1086/508231

Medina, A. A., Winters, J. G., Irwin, J. M., et al. 2022, ApJ, 935, 104. doi:10.3847/1538-4357/ac77f9

Melbourne, K., Youngblood, A., France, K., et al. 2020, AJ, 160, 269. doi:10.3847/1538-3881/abbf5c

Messina, S., Desidera, S., Turatto, M., et al. 2010, A&A, 520, A15. doi:10.1051/0004-6361/200913644

Miguel, Y., Kaltenegger, L., Linsky, J. L., et al. 2015, MNRAS, 446, 345. doi:10.1093/mnras/stu2107

Mishenina, T. V., Soubiran, C., Kovtyukh, V. V., et al. 2012, A&A, 547, A106. doi:10.1051/0004-6361/201118412

Molliere, P., van Boekel, R., Bouwman, J., et al. 2017, A&A, 600, A10. doi:10.1051/0004-6361/201629800

Montes, D. & Martin, E. L. 1998, A&AS, 128, 485. doi:10.1051/aas:1998159

Montes, D., López-Santiago, J., Gálvez, M. C., et al. 2001, MNRAS, 328, 45. doi:10.1046/j.1365-8711.2001.04781.x

Montes, D. 2013, Highlights of Spanish Astrophysics VII, 661

Morris, B. M., Curtis, J. L., Sakari, C., et al. 2019, AJ, 158, 101. doi:10.3847/1538-3881/ab2e04

Newville, M., Stensitzki, T., Allen, D. B., et al. 2014, Zenodo

Niraula, P., Redfield, S., Dai, F., et al. 2017, AJ, 154, 266. doi:10.3847/1538-3881/aa957c

Nisak, A. H., White, R. J., Yep, A., et al. 2022, AJ, 163, 278. doi:10.3847/1538-3881/ac63c3

Nordström, B., Mayor, M., Andersen, J., et al. 2004, A&A, 418, 989. doi:10.1051/0004-6361:20035959

Núnez, A., Agueros, M. A., Covey, K. R., et al. 2022, ApJ, 931, 45. doi:10.3847/1538-4357/ac6517

Paredes, L. A., Dissertation, Georgia State University, 2022.

Paredes, L. A., Henry, T. J., Quinn, S. N., et al. 2021, AJ, 162, 176. doi:10.3847/1538-3881/ac082a

Pecaut, M. J. & Mamajek, E. E. 2013, ApJS, 208, 9. doi:10.1088/0067-0049/208/1/9

Perryman, M. A. C., Brown, A. G. A., Lebreton, Y., et al. 1998, A&A, 331, 81. doi:10.48550/arXiv.astro-ph/9707253

Piskunov, N. E. & Valenti, J. A. 2002, A&A, 385, 1095. doi:10.1051/0004-6361:20020175

Plavchan, P., Werner, M. W., Chen, C. H., et al. 2009, ApJ, 698, 1068. doi:10.1088/0004-637X/698/2/1068

Quanz, S. P., Ottiger, M., Fontanet, E., et al. 2022, A&A, 664, A21. doi:10.1051/0004-6361/202140366

Quintana, E. V., Colon, K. D., Mosby, G., et al. 2021, arXiv:2108.06438. doi:10.48550/arXiv.2108.06438

Reddy, B. E., Lambert, D. L., & Allende Prieto, C. 2006, MNRAS, 367, 1329. doi:10.1111/j.1365-2966.2006.10148.x

Richey-Yowell, T., Shkolnik, E. L., Schneider, A. C., et al. 2019, ApJ, 872, 17. doi:10.3847/1538-4357/aafa74

Richey-Yowell, T., Shkolnik, E. L., Loyd, R. O. P., et al. 2022, ApJ, 929, 169. doi:10.3847/1538-4357/ac5f48

Riedel, A. R., Finch, C. T., Henry, T. J., et al. 2014, AJ, 147, 85. doi:10.1088/0004-6256/147/4/85

Riedel, A. R., Alam, M. K., Rice, E. L., et al. 2017, ApJ, 840, 87. doi:10.3847/1538-4357/840/2/87

Rugheimer, S., Kaltenegger, L., Segura, A., et al. 2015, ApJ, 809, 57. doi:10.1088/0004-637X/809/1/57

Schaefer, G. H., White, R. J., Baines, E. K., et al. 2018, ApJ, 858, 71. doi:10.3847/1538-4357/aaba71

Seager, S. 2010, Exoplanet Atmospheres: Physical Processes. By Sara Seager. Princeton University Press, 2010. ISBN: 978-1-4008-3530-0

Segura, A., Walkowicz, L. M., Meadows, V., et al. 2010, Astrobiology, 10, 751. doi:10.1089/ast.2009.0376

Shea, M., Hansen, C., Horch, E., et al. 2023,

Siess, L., Dufour, E., & Forestini, M. 2000, A&A, 358, 593. doi:10.48550/arXiv.astro-ph/0003477

Skoda, P., Draper, P. W., Neves, M. C., et al. 2014, Astronomy and Computing, 7, 108. doi:10.1016/j.ascom.2014.06.001

Skrutskie, M. F., Cutri, R. M., Stiening, R., et al. 2006, AJ, 131, 1163. doi:10.1086/498708

Skumanich, A. 1972, ApJ, 171, 565. doi:10.1086/151310

Skumanich, A. 1986, ApJ, 309, 858. doi:10.1086/164654

Soderblom, D. R., Jones, B. F., Balachandran, S., et al. 1993, AJ, 106, 1059. doi:10.1086/116704

Soderblom, D. R., Hillenbrand, L. A., Jeffries, R. D., et al. 2014, Protostars and Planets VI, 219. doi:10.2458/azu_uapress_9780816531240-ch010

Soderblom, D. R. 2010, ARA&A, 48, 581. doi:10.1146/annurev-astro-081309-130806

Soubiran, C., Le Campion, J.-F., Brouillet, N., et al. 2020, VizieR Online Data Catalog, B/pastel

Spada, F. & Lanzafame, A. C. 2020, A&A, 636, A76. doi:10.1051/0004-6361/201936384

Sperauskas, J., Deveikis, V., & Tokovinin, A. 2019, A&A, 626, A31. doi:10.1051/0004-6361/201935346

Spitzer, L. & Schwarzschild, M. 1951, ApJ, 114, 385. doi:10.1086/145478

Sreejith, A. G., Fossati, L., Youngblood, A., et al. 2020, A&A, 644, A67. doi:10.1051/0004-6361/202039167

Stanford-Moore, S. A., Nielsen, E. L., De Rosa, R. J., et al. 2020, ApJ, 898, 27. doi:10.3847/1538-4357/ab9a35

Strassmeier, K., Washuettl, A., Granzer, T., et al. 2000, A&AS, 142, 275. doi:10.1051/aas:2000328

Tarter, J. C., Backus, P. R., Mancinelli, R. L., et al. 2007, Astrobiology, 7, 30. doi:10.1089/ast.2006.0124

Tian, F. 2009, ApJ, 703, 905. doi:10.1088/0004-637X/703/1/905

Tian, F. 2015, Annual Review of Earth and Planetary Sciences, 43, 459. doi:10.1146/annurev-earth-060313-054834

Tokovinin, A., Fischer, D. A., Bonati, M., et al. 2013, PASP, 125, 1336. doi:10.1086/674012

Tokovinin, A., Mason, B. D., Mendez, R. A., et al. 2019, AJ, 158, 48. doi:10.3847/1538-3881/ab24e4

Torres, C. A. O., Quast, G. R., da Silva, L., et al. 2006, A&A, 460, 695. doi:10.1051/0004-6361:20065602

Ujjwal, K., Kartha, S. S., Mathew, B., et al. 2020, AJ, 159, 166. doi:10.3847/1538-3881/ab76d6

Viana Almeida, P., Santos, N. C., Melo, C., et al. 2009, A&A, 501, 965. doi:10.1051/0004-6361/200811194

Walkowicz, L. M. & Hawley, S. L. 2009, AJ, 137, 3297. doi:10.1088/0004-6256/137/2/3297

Wang, H.-J. & Wei, J.-Y. 2009, Research in Astronomy and Astrophysics, 9, 315. doi:10.1088/1674-4527/9/3/006

West, A. A., Hawley, S. L., Bochanski, J. J., et al. 2008, AJ, 135, 785. doi:10.1088/0004-6256/135/3/785

White, R. J., Gabor, J. M., & Hillenbrand, L. A. 2007, AJ, 133, 2524. doi:10.1086/514336

Wright, J. T. & Eastman, J. D. 2014, PASP, 126, 838. doi:10.1086/678541

Yee, S. W., Petigura, E. A., & von Braun, K. 2017, ApJ, 836, 77. doi:10.3847/1538-4357/836/1/77

Youngblood, A., France, K., Loyd, R. O. P., et al. 2017, ApJ, 843, 31. doi:10.3847/1538-4357/aa76dd

Youngblood, A., Pineda, J. S., Ayres, T., et al. 2022, ApJ, 926, 129. doi:10.3847/1538-4357/ac4711

Zuckerman, B., Song, I., & Bessell, M. S. 2004, ApJ, 613, L65. doi:10.1086/425036

Zúñiga-Fernández, S., Bayo, A., Elliott, P., et al. 2021, A&A, 645, A30. doi:10.1051/0004-6361/202037830